

UNCLASSIFIED

AD NUMBER

AD815529

LIMITATION CHANGES

TO:

Approved for public release; distribution is unlimited.

FROM:

Distribution authorized to U.S. Gov't. agencies and their contractors; Critical Technology; MAY 1967. Other requests shall be referred to Air Force Weapons Laboratory, Kirtland AFB, NM 87117. This document contains export-controlled technical data.

AUTHORITY

AFWL ltr, 30 Nov 1971

THIS PAGE IS UNCLASSIFIED

AD815529



SHORT-PULSED GAMMA-RADIATION EFFECTS ON DYNAMIC ELECTRONIC COMPONENTS

V. A. J. van Lint, J. H. Alexander, D. J. Burkhart,
D. K. Nichols, and P. R. Ward

Special Nuclear Effects Laboratory
General Atomic Division
General Dynamics Corporation
San Diego, California 92121
Contract AF 29(601)-7048



TECHNICAL REPORT NO. AFWL-TR-67-20

May 1967

AIR FORCE WEAPONS LABORATORY
Research and Technology Division
Air Force Systems Command
Kirtland Air Force Base
New Mexico

SHORT-PULSED GAMMA-RADIATION EFFECTS

ON DYNAMIC ELECTRONIC COMPONENTS

V. A. J. van Lint, J. H. Alexander, D. J. Burkhart,
D. K. Nichols, and P. R. Ward

Special Nuclear Effects Laboratory
General Atomic Division
General Dynamics Corporation
San Diego, California 92121
Contract AF 29(601)-7048

TECHNICAL REPORT NO. AFWL-TR-67-20

This document is subject to special export controls and each transmittal to foreign governments or foreign nationals may be made only with prior approval of AFWL (WLRE), Kirtland AFB, NM, 87117. Distribution is limited because of the technology discussed in the report.


FOREWORD

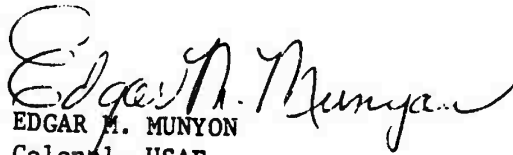
This report was prepared by the Special Nuclear Effects Laboratory, General Atomic Division, General Dynamics Corporation, San Diego, California, under Contract AF 29(601)-7048. The research was performed under Program Element 6.16.46.01.D, Project 5710, Subtask 16.020, and was funded by the Defense Atomic Support Agency (DASA).


Inclusive dates of research were August 1965 to February 1967. The report was submitted 10 April 1967 by the Air Force Weapons Laboratory Project Officer, Lt Dale Shaughnessy (WLRE). The General Atomic report number is GA-7651.

At General Atomic, the research was under the direction of V. A. J. van Lint, Associate Director of the Special Nuclear Effects Laboratory. The principal authors of the report and contributors to the research were V. A. J. van Lint, J. H. Alexander, D. J. Burkhart, S. C. Choy, D. K. Nichols, and P. R. Ward.

This technical report has been reviewed and is approved.


DALE SHAUGHNESSY
Lt, USAF
Project Officer


EDGAR M. MUNYON
Colonel, USAF
Chief, Effects Branch


CLAUDE K. STAMBAUGH
Colonel, USAF
Chief, Research Division

ABSTRACT

(Distribution Limitation Statement No. 2)

A computer code has been developed for solving the nonlinear continuity equations and Poisson's equation which describe the response of electrons and holes in semiconductor devices to ionizing radiation. The ultimate goal of the research program was to incorporate the major second-order nonlinearities given by the output of the code (and observed by experiment) into simpler circuit models for active devices. The code is presently capable of obtaining solutions for two-region diodes and three-region transistors, which can be described by a one-dimensional geometry and discontinuous p-n junctions. Trivial changes in the program are described in detail for adapting the code to solutions for graded junctions and for the epitaxial four-region transistor (NPN⁺ or PNPP⁺). Special features for representing avalanche effects, field-dependent mobility, and a recombination lifetime dependent on displacement radiation damage are included. Experiments were performed to provide data for comparison with the computer description of real diodes and transistors. The computer data are also compared with the Eber-Moll transistor model, which is typical of simpler device representations.

CONTENTS

I.	INTRODUCTION	1
II.	COMPUTER CALCULATIONS	3
2.1.	Theory.	3
2.1.1.	General Problem Statement.	5
2.1.2.	The Diode.	7
2.1.3.	Zener Field Emission.	9
2.1.4.	Transistors	10
2.1.4.1.	General Atomic Model.	10
2.1.4.2.	Ebers-Moll Model.	12
2.1.4.3.	Comparisons with Additional Simple Models. . .	15
2.2.	Description of the Codes	18
2.2.1.	The Finite Difference Scheme	18
2.2.1.1.	Restatement of the Problem	18
2.2.1.2.	Finite Differences.	19
2.2.1.3.	The Time Integration.	25
2.2.1.4.	Reduction of the System of Equations	29
2.2.1.5.	The Method of Solution of the Difference Equations.	34
2.2.1.6.	Initial Conditions	43
2.2.2.	Treatment of Special Effects	44
2.2.2.1.	The Carrier Generation Term.	44
2.2.2.2.	Saturation of Drift Velocity.	45
2.2.2.3.	Fluence-dependent Lifetimes	46
2.2.3.	Automatic Selection of Interval Sizes.	46
2.2.3.1.	Computing the Time Interval.	46
2.2.3.2.	Calculating the Spatial Intervals.	48
2.2.4.	Conservation of Charge in the Time Integration.	49
2.2.5.	Doping Profiles	51
2.3.	Results of the Computer Programs	52
2.3.1.	Computer Results for the Reference Diode	52
2.3.1.1.	Analytic Solution for No Bias, Thermal Equilibrium.	53
2.3.1.2.	Approximate Solution, No Bias, Thermal Equilibrium.	54
2.3.1.3.	Computer Solution for No Bias Solution.	57
2.3.1.4.	Computer Solution for Forward Bias	62
2.3.1.5.	Computer Solution for Reverse Bias	65
2.3.2.	Computer Results for 1N91 Diode	68
2.3.2.1.	Zero Bias	68
2.3.2.2.	Forward Bias.	74
2.3.2.3.	Reverse Bias	74

CONTENTS (cont'd)

2.3.3. Computer Results for Reference Transistor	78
2.3.4. Computer Results for 2N396A Transistor	80
2.3.5. Computer Results for High Field Effects.	84
III. EXPERIMENTAL PROGRAM	90
3.1. Experimental Techniques.	90
3.1.1. Radiation Facility.	90
3.1.2. Circuitry	92
3.1.3. Dosimetry.	98
3.2. Experimental Results and Discussion.	99
3.2.1. Tunnel Diodes	99
3.2.1.1. Summary of Theory.	99
3.2.1.2. Experimental Results.	104
3.2.2. Experimental Results and Discussion for the 1N91 Diode	105
3.2.2.1. Zero Bias	105
3.2.2.2. Forward Bias	107
3.2.2.3. Reverse Bias	107
3.2.3. Experimental Results and Discussion for 2N396A Transistor	115
IV. SUMMARY AND CONCLUSIONS	118
REFERENCES	119
Appendixes	
A. PNPP ⁺ CODE	121
B. THE DIODE CODE	123
B.1. Organization	123
B.2. Setting Up a Run on PND4	131
B.3. Input	131
B.4. Printout	139
B.5. Glossary	143
B.6. Layout of Common Variables	155
B.7. Flow Sheets.	157
C. THE TRANSISTOR CODE.	167
C.1. Organization.	167
C.2. Setting Up a Run on PNPMN.	171
C.3. Input	173
C.4. Printout	179
C.5. Glossary	183
C.6. Layout of Common Variables	197
C.7. Flow Sheets.	200

CONTENTS (cont'd)

D. COMPUTERIZED MODEL FOR RESPONSE OF DEVICES TO A PULSE OF IONIZING RADIATION. 211

Figures

1. Diode circuit (shown forward-biased)	7
2. Reference transistor (common-emitter configuration)	11
3. Circuit representation of Ebers-Moll transistor	12
4. Schematic of reference transistor	23
5. Plot showing overstability.	27
6. Progress of an unstable integration	28
7. Unconditional stability	29
8. Equilibrium zero-bias diode electric field.	55
9. Equilibrium zero-bias diode carrier densities	56
10. Zero-bias diode voltage vs time	59
11. Diode voltage decay, $R = 10^6$ ohms	61
12. Forward-biased diode voltage charge	63
13. Forward-biased diode electric field (numbers are time, in microseconds, after pulse).	64
14. Forward-biased diode carrier densities	66
15. Forward-biased diode carrier densities near junction.	67
16. Reverse-biased diode current.	69
17. No bias 1N91 Ge alloy diode	72
18. Zero-bias 1N91 diode carrier densities, $R_0 = 10^3$ ohms, dose = 10^3 rads	73
19. Forward-biased 1N91 diode, $R_0 = 10^3$ ohms, dose = 1 rad	75
20. Forward-biased 1N91 diode, $R_0 = 10^3$ ohms, dose = 10^3 rads	76
21. Reverse-biased diode current due to 0.1 rad in 10^{-13} sec, $V_0 = -10$ V, $R_0 = 10^2$ ohms	77
22. Reverse-biased 1N91 diode, $V_0 = -10$ V, $R_0 = 10^2$ ohms	79
23. Collector current of reference transistor	81
24. Transistor 2N396A primary and secondary photocurrent, dose = 1 rad.	82

25.	Electric-field profile.	85
26.	Electric-field profile (fine scale).	86
27.	Typical experimental setup.	91
28.	Block diagram of transistor test system.	93
29.	Dual cathode-follower circuit	94
30.	Transistor-diode test schematics	96
31.	Tunnel diode test schematic	96
32.	Signal monitoring system.	97
33.	Thermistor calorimeter used in dosimetry in Linac tests	98
34.	Offset voltage vs dose rate (theoretical)	102
35.	Energy-band overlap = 0.21 eV.	103
36.	No bias on 1N91 diode with 100-ohm load in series	106
37.	No bias on 1N91 diode with 10^6 -ohm load in series	108
38.	+1-V forward bias on 1N91 diode with 1000-ohm load in series	109
39.	+1-V forward bias on 1N91 diode with 1000-ohm load in series	110
40.	+10-V forward bias on 1N91 diode with 1000-ohm load in series	111
41.	+10-V forward bias on 1N91 diode with 1000-ohm load in series	112
42.	10-V reverse bias on 1N91 diode with 100-ohm load in series.	113
43.	10-V reverse bias on 1N91 diode with 100-ohm load in series.	114
44.	2N396A transistor common-emitter collector-current signal above 1 mA quiescent state.	116
45.	Primary photocurrent for 2N396A transistor (emitter open).	117

Tables

I.	Reference Silicon Diode Parameters	52
II.	Time Steps for Reverse-biased Diode.	70
III.	1N91 Ge Alloy Diode Parameters.	71
IV.	Reference Silicon Transistor Parameters	78
V.	2N396A Transistor Parameters.	83

SECTION I

INTRODUCTION

The purpose of this program has been to construct a detailed mathematical formulation of the relaxation of semiconductor devices from ionizing radiation pulses and to compare the results from mathematical calculations with experimental results and with predictions made from simpler equivalent circuit models. The ultimate goal is to determine the physical phenomena responsible for perturbation of semiconductor devices so that corrections can be made to the simpler formulations when needed, such as for high-dose radiation environments.

During a previous study under Contract AF29(601)-6374, the computer program had come close to furnishing a solution for the reference diode in an open-circuit configuration, but the solution diverged at late times because of the steep gradients in the electric field and carrier concentrations which obtain. However, the method of solution which used the quasi-linear techniques (Reference 1) demonstrated that rapid solutions were possible.

During the current research program, the diode problem was solved fully and put on a semiautomatic basis by incorporating a standard method for selecting the time increments to be used and by establishing a procedure for varying the position of the spatial mesh points to correspond with the difference in adjacent computed quantities. The diode code has been thoroughly tested for all circuit configurations (e. g., forward and reverse bias) for both the reference diode and the Type 1N91 germanium-alloy diode for which comparative experiments have been made. In addition, new physical features have been included in the equations to represent the variation in recombination lifetime due to displacement irradiation effects, to account for the change in carrier mobility in the presence of high internal electric fields, and to represent

the enhanced current caused by collisions of energetic carriers with the electrons of the lattice atoms. The code was modified for use on the AFWL CDC-6600 computer, which is used via a data link that was set up last year between General Atomic and Kirtland Air Force Base.

The solution for the linear three-region transistor was also achieved. The reference transistor solution from the General Atomic (GA) code has been compared with the Ebers-Moll model, which is typical of simpler transistor formulations. This comparison showed close agreement for the low-dose case. In addition, a few computer runs for the 2N396A transistor were performed and these are compared with experiment. The recent success of the three-region problem will enable a change of emphasis, which was previously directed toward obtaining a workable computer code, to the extraction of reasonably simple physical concepts from the numerical data.

Finally, it is worth noting that a four-region transistor of the epitaxial type (NPNN^+ or PNPP^+) can be solved by introducing change cards, which are listed in detail in Appendix A.

In the remainder of this report the theory, the computer code, significant improvements of the present contract period, and experimental results for the 1N91 diode and the 2N396A transistor are described, and the comparison between theory and experiment is discussed.

SECTION II

COMPUTER CALCULATIONS

2.1. THEORY

The goal of the computer program is to describe the behavior of semiconductor devices, such as diodes and transistors, under irradiation. At the end of this year's work, such a code is virtually complete with a complete run for a reference silicon three-region transistor and some calculations for the 2N396A transistor in the common-emitter configuration. The final achievement will be

1. To have a "production code" to test the radiation response of specific devices in any circuit configuration, and
2. To determine a simple way for including the nonlinear response to irradiation at heavy doses, as described by the GA code, into simpler circuit representations of devices given by the Ebers-Moll and Linvill models.

The calculations assume that the net effect of all radiation environments is to create an excess number of electron-hole pairs and a number of displaced atoms which may act as carrier recombination centers (flaws). The number of flaws is characterized by the recombination time for electrons and holes in each region of the device. The number of electron-hole pairs is proportional to the total ionizing radiation dosage. The behavior of the device is described by Poisson's equation and the continuity equations for each carrier (see section 2.1.1).

The basic calculation considers a one-dimensional device in any circuit configuration. At present the calculations have been confined to two or three-region devices for which the doping profile has been assumed constant except for an abrupt change at the p-n junctions, but no intrinsic difficulty in coding is presented by using additional equations for multiregion devices which can have an arbitrary doping profile. The code will accept an ionizing dose rate as a function of time, but for the

basic computer problems, the creation of electron-hole pairs instantaneously (with respect to the characteristic lifetimes) is assumed. The code has also been adapted to allow for avalanche generation of carriers in regions of high internal electric fields, to account for the time-dependence of the lifetimes with respect to integrated flux, and to compute the mobility as a function of the internal electric field. Although the above refinements to the problem may be important for several special situations, it is worth emphasizing that the greatest value of the complete code lies in its accurate description of the interplay of diffusion and drift. Since the usual simplifying assumption of quasi-neutrality is not invoked, the structure of the depletion region at the junction interfaces and the natural establishment of relations between the carriers near the junctions after heavy irradiation are obtained.

In the brief recapitulation of the basic theory included in Section 2.1.1, the three fundamental equations are written in terms of the electric field and the minority carrier for each region. In Section 2.2, the numerical method and discretization procedure are outlined. The most important improvements in the work reported herein is the adaptation of the code to describe three-region transistors and the programming of a semi-automated procedure (including remeshing of space intervals, selection of time increments, etc.) for use on the AFWL 6600 computer. In Section 2.3, some detailed results for the diode are presented along with the first runs for the transistor. At the time this report was written, the limitation on the amount of available data is due to the recent success of the transistor code and the efficiency of the automated procedure. No fundamental problems with the development of the code logic remain.

2.1.1. General Problem Statement

The fundamental equations solved by the computer are the continuity equations

$$\frac{\partial n}{\partial t} = g - R_j + A(n, p, E) + \frac{\partial}{\partial x} (nv) + D_n \frac{\partial^2 n}{\partial x^2}, \quad j = p, n, \quad (1)$$

$$\frac{\partial p}{\partial t} = g - R_j + A(n, p, E) - \frac{\partial}{\partial x} (vp) + D_p \frac{\partial^2 p}{\partial x^2} \quad (2)$$

and Poisson's equation

$$\frac{\partial E}{\partial x} = \frac{4\pi q}{K} [p(x, t) - n(x, t) + \Delta N(x)], \quad (3)$$

where q is the electronic charge, j is the region designation, n and p are the electron and hole concentrations, respectively, v is the carrier drift velocity ($v = \mu E$ in the limit of low electric fields), and E is the electric field. The form for the recombination term is

$$R_j = \frac{pn - n_0^2}{\tau_{nj}(n + n'_j) + \tau_{pj}(p + p'_j)} \quad (4)$$

The known parameters are the field-dependent electron and hole mobilities $\mu_n(E)$ and $\mu_p(E)$, the diffusion constants D_n and D_p , the dielectric constant K , the electron charge e , the rate of generation of excess carriers, g , due to an extended pulse, the generation of carriers by avalanche processes, $A(n, p, E)$, the excess number of donors to acceptors, $\Delta N(x)$, the intrinsic carrier concentration, n_0 , and the electron and hole lifetimes in each region, τ_{nj} and τ_{pj} . The quantity n' or

p' is the concentration of carriers that would exist if the Fermi level were at the energy level of the recombination center, which is usually not known. However, these quantities may be taken to be equal to n_i since they are of small importance.

The boundary conditions to be imposed at $x = -a$ and $x = b$ are

$$\frac{\partial n}{\partial x} = \frac{\partial p}{\partial x} = 0, \quad (5)$$

$$q (\mu_n n + \mu_p p) E + \frac{K}{4\pi} \frac{\partial E}{\partial t} = \frac{i}{a_0}, \quad (6)$$

where i is the current through the diode and a_0 is the area of its cross section. Equation (6) makes the current density at the boundaries consistent with the given external current i . If $i = 0$, one can simply replace Eq. (6) by

$$E = 0 \quad (7)$$

at $x = -a$ and $x = b$.

The interface conditions at $x = 0$ are

$$n^-(0, t) = n^+(0, t), \quad p^-(0, t) = p^+(0, t), \quad (8)$$

$$\left. \frac{\partial n}{\partial x} (0, t) \right|^- = \left. \frac{\partial n}{\partial x} (0, t) \right|+, \quad \left. \frac{\partial p}{\partial x} (0, t) \right|^- = \left. \frac{\partial p}{\partial x} (0, t) \right|+, \quad (9)$$

$$E^-(0, t) = E^+(0, t), \quad (10)$$

$$\left(\frac{\partial E}{\partial x} \right)^- - \frac{4\pi q}{K} \Delta N_p = \left(\frac{\partial E}{\partial x} \right)^+ - \frac{4\pi q}{K} \Delta N_n, \quad (11)$$

where the discontinuity in dE/dx is seen by substitution of Eq. (8) into Eq. (3).

2.1.2. The Diode

The diode problem consists essentially of determining the time-dependent current (or voltage) following an irradiation pulse for the single circuit shown in Figure 1.

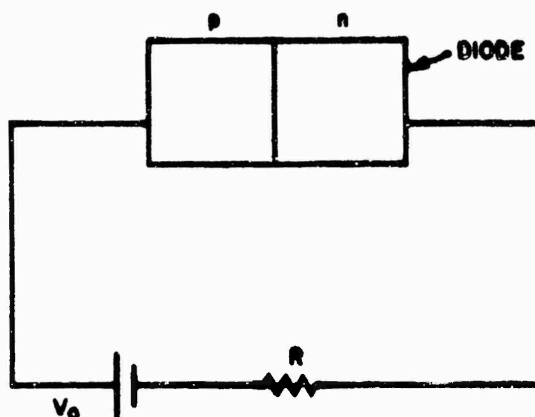


Figure 1. Diode circuit (shown forward-biased)

The relation between the current I (positive sign for flow from p region to n region) and the voltage drop across the diode, V , given by the computer output is

$$V_0 = V_{BI} - V + IR$$

where V_0 is the applied voltage (positive if forward biased) and V_{BI} is the "built in" diode voltage (e. g., 0.26 V for the 1N91 diode). The problem that has been run for both forward and reverse bias on the reference diode displays the typical response to irradiation, but of most interest is the fact that a series of "open-circuit" runs for various large values of the resistance, R , showed that the response of the diode is extremely sensitive to the small amounts of current that are present in any experimental measurement. These observations are discussed further in Section 2.3.

The new changes in the diode program for this year include:

1. Lifetime versus Integrated Flux. A routine has been included in the code to account for the fact that the recombination lifetime may decrease as increased dose creates more and more recombination centers because of the formation of permanent displaced atoms. The relation that is used is

$$1/\tau_j = 1/\tau_j(0) + K_j(\Phi) \cdot \Phi, \quad (12)$$

where τ_j is either τ_{nj} or τ_{pj} , $\tau_j(0)$ is the initial lifetime, Φ is the integrated fluence, and $K(\Phi)$ is a damage constant which is often taken to be constant in evaluating experimental data.

2. Field-dependent Mobility. The value of the mobility changes in regions of high internal electric fields ($E > 10^3$ V/cm) when it can no longer be assumed that the carriers are in thermal equilibrium with the lattice. In the limit of very high fields ($E > 10^4$ V/cm), the electron and hole velocities in silicon and germanium approach a maximum velocity of $v_{sat} \sim 10^6$ or 10^7 cm/sec. The data (and a detailed discussion of this effect) are given by Gunn (Reference 2).

3. Avalanche Breakdown. Avalanche breakdown, which arises from the ionization of lattice electrons by impact with high-velocity carriers comprising the current can cause a huge multiplication of the ordinary reverse current in heavily doped junctions operated under a high reverse bias. The multiplication M is given by

$$1 - 1/M = \int_0^l \alpha \, dx, \quad (13)$$

where l is the length of the avalanche region and α is the number of ionizations per centimeter of path length. The value of α in silicon is given by theory as

$$\alpha = 1.55 \times 10^5 \exp \left(\frac{-33 \times 10^4}{E^2} \right) \text{ cm}^{-1} \quad (14)$$

with E (in kV/cm) in reasonable agreement with experiment. However, experimental measurements involve rather crude pictures of the diode to reduce their data on current multiplication to the more fundamental parameter α , so that the theoretical expression (which is programmed) is fully justified for use in the code.* The extra ionized carriers are incorporated in the current as a generation term

$$A(n,p,E) = \alpha_n v_{sat}(n)n + \alpha_p v_{sat}(p)p, \quad (15)$$

where the saturation velocity of the electrons and holes is used since avalanche always occurs in only those high field regions where $E > 10^5$ V/cm. Data for germanium and silicon is given by Gunn in Reference 2.

2.1.3. Zener Field Emission

Historically, the question of whether electrons are ionized directly by high electric fields has been of interest, but in practice such an effect seldom occurs in p-n semiconductor junctions. Under large reverse fields, avalanche processes occur very readily if the high-field region is not confined to too short a distance about the junction interface, but in order to obtain a small region of high electric field intensity, high doping of each region is required which very often leads to the generation of tunnel currents. The most detailed argument supporting the existence of field emission is (apparently) given by the article of Chynoweth and McKay (Reference 3). They showed that in highly doped junctions, a smooth glow can be seen during a breakdown which does not have the noise or the light characteristics associated with the onset of avalanche breakdown. They attributed this new mechanism to internal field emission, but had some difficulty in reconciling this interpretation with the theoretical requirement given by Shockley, et al. (Reference 4) that the minimum internal field be 1.4×10^6 V/cm. This analysis preceded by a year the discovery

*In fact, a strong case can be made for using the GA code to determine better values of α from the data on current multiplication.

of the tunnel effect, described by Esaki (Reference 5), so Chynoweth and McKay did not attempt to correlate their observed wobble in the forward-bias current-voltage characteristic with some mixture of tunnel and avalanche current which may also have been present.

Since the question of whether field emission ever dominates the current response of p-n semiconductor junctions is not firmly resolved, and since nearly all large reverse-current characteristics are attributed to avalanche or tunnel processes, it has not been deemed worthwhile to attempt to improve on the phenomenological expression for the reverse-bias emission current given by Shockley (Reference 4):

$$I_E = a(V_{BI} - V_0) \exp \left[-n/(V_{BI} - V_0) \right] . \quad (16)$$

when a and n are constants to be evaluated from experiment. At best, Eq. (16) might be added to the calculated diode current only in an ad hoc manner since the voltage is an integral of the field distribution and the current is only "known" at the terminals.

A complete description of the code for the diode is given in Appendix B.

2.1.4. Transistors

2.1.4.1. General Atomic Model. The solution for the behavior of a transistor is accomplished in much the same manner as the solution for diodes (see Section 2.2 for details), but the code is presently limited to only three-region devices. The boundary conditions on the currents are determined by whether the external circuit is common-emitter, common-base, or common-collector (emitter-follower) configuration, and the base current is treated as a local generation of majority carriers injected midway between the base junctions.

The reference pnp silicon transistor in the common-emitter circuit* is described by Figure 2 and Section 2.3, which lists the physical input parameters for all of the devices considered in this report.

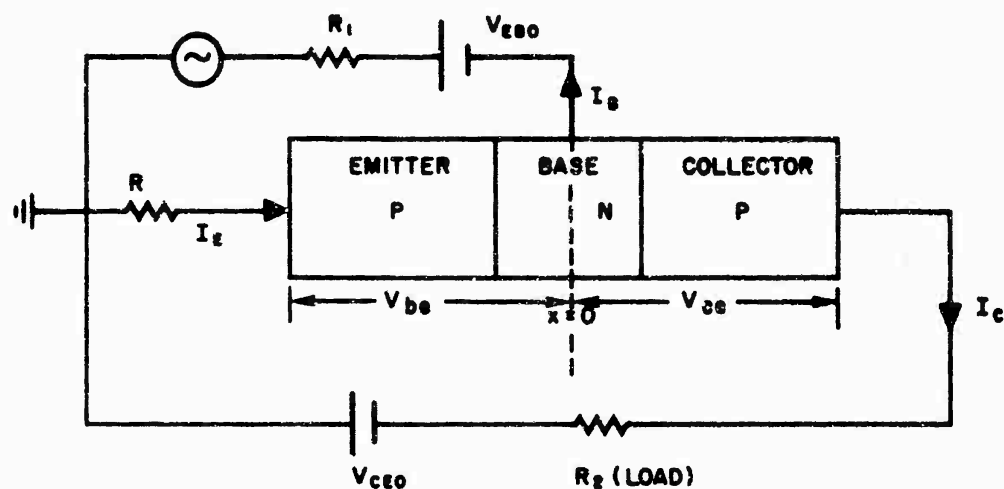


Figure 2. Reference transistor (common-emitter configuration)

The currents shown in Figure 2 are positive, as shown, and the voltage input quantities V_{EB0} and V_{CE0} are positive if applied with the polarity shown. Additional input data for a given run on the reference transistor are R_1 , R_2 , R_3 and the radiation dose (in carriers/cm³). The code prints out V_{be} , V_{ce} with a positive sign if the right side has a higher potential

*It is clear that, by suitable choice of infinite resistances, the common-emitter configuration is reduced to open-emitter and open-base configurations used for measuring transistor parameters.

than the left, I_B , and I_C ($I_E = I_B + I_C$) as a function of time.* A complete description of the code for the transistor is given in Appendix C.

The GA code can be very simply adapted to any type of existing transistor (alloy, diffused, germanium, etc.) with three regions, and only a slightly more complicated (see Appendix A and Section 2.2) set of input quantities is required to solve for epitaxial transistors of the $NPNN^+$ or $PNPP^+$ type when three connections are made to an external circuit.

2.1.4.2. Ebers-Moll Model. The reference transistor described above has also been adapted to the Ebers-Moll model, which describes the transistor in terms of various resistances and capacitances, which are connected as shown in Figure 3. The resistances R_{ee} and R_{cc}

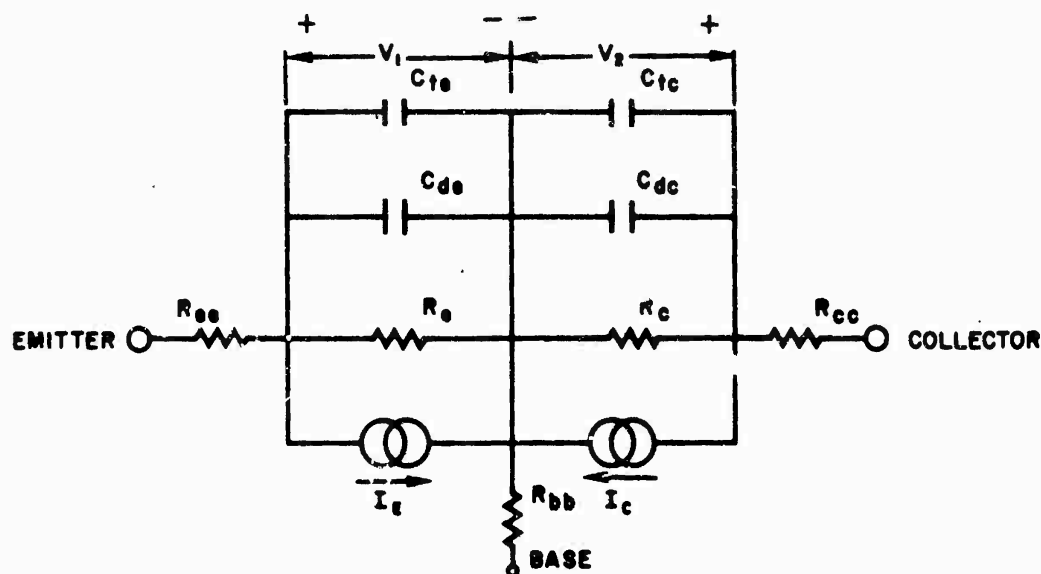


Figure 3. Circuit representation of Ebers-Moll transistor

* These output quantities are computed at the end of each iteration step also to ensure most accurate convergence, as discussed in detail in Section 2.2

and collector bulk resistance and R_{bb} is the base spreading resistance (a factor which cannot be considered in the one-dimensional GA code).

The resistances R_e and R_c are derivatives of a measured ohmic increase in current versus voltage under reverse bias, which is due (presumably) to surface effects. Since the GA code only considers bulk effects, these resistances are assumed to be infinite. The currents are given by

$$I_E = \frac{I_{E0}}{1 - \alpha_n \alpha_i} \left[\exp\left(\frac{qV_1}{kT}\right) - 1 \right] - \frac{\alpha_i I_{C0}}{1 - \alpha_n \alpha_i} \left[\exp\left(\frac{qV_2}{kT}\right) - 1 \right], \quad (17)$$

$$I_C = \frac{I_{C0}}{1 - \alpha_n \alpha_i} \left[\exp\left(\frac{qV_2}{kT}\right) - 1 \right] - \frac{\alpha_n I_{E0}}{1 - \alpha_n \alpha_i} \left[\exp\left(\frac{qV_1}{kT}\right) - 1 \right] \quad (18)$$

where I_{E0} and I_{C0} are the emitter-base and collector-base saturation currents, respectively, and α_n and α_i are the normal and inverted common-base current gain to be specified as input quantities. The voltages, V_1 and V_2 , shown on Figure 3 are calculated by the code.

The capacitances C_{te} and C_{tc} are known as the space-charge (or transition) capacitance for each junction; they are equal to the change in the local space charge for a change in the applied voltage at the junction. Thus, per unit area,

$$C_{te} = \frac{R_1}{(V_{ze} - V_1)N_e}, \quad (19)$$

$$C_{tc} = \frac{R_2}{(V_{zc} - V_2)N_c}, \quad (20)$$

where V_{ze} and V_{zc} are the "built-in" junction voltages, N_e and N_c are factors to allow for the concentration profile of the junction ($N_e = N_c = 0.5$ for a step-junction); the resistances are

$$R_{1,2} = \frac{(2\pi q\kappa)^{\frac{1}{2}}}{4\pi \left[\left(\frac{N_D}{N_A} \right)^{\frac{1}{2}} + \left(\frac{N_A}{N_D} \right)^{\frac{1}{2}} \right]}, \quad (21)$$

where N_D and N_A are the donor and acceptor concentrations at the appropriate junction and $\kappa = K\epsilon_0$, where K is the dielectric constant.

The capacitances C_{de} and C_{dc} are the diffusion capacitances which arise from the difference in the amount of charge in a diffusion profile of the minority carrier when different junction voltages are applied. The formulas are

$$C_{de} = \frac{q \left\{ \frac{I_{E0}}{1 - \alpha_n \alpha_i} \left[\exp\left(\frac{qV_1}{kT}\right) - 1 \right] + \frac{I_{E0}}{1 - \alpha_n \alpha_i} \right\}}{2\pi kTF_n},$$

$$C_{dc} = \frac{q \left\{ \frac{I_{C0}}{1 - \alpha_n \alpha_i} \left[\exp\left(\frac{qV_2}{kT}\right) - 1 \right] + \frac{I_{C0}}{1 - \alpha_n \alpha_i} \right\}}{2\pi kTF_i},$$

where F_n and F_i are the cutoff frequencies for active normal and active inverted operation. Although Hunter (Reference 6) shows that these quantities are a function of bias and current, they remain sufficiently constant to be specified by a single input number.

In order to introduce the effect of irradiation into this model, it is necessary to specify the maximum (primary) collector photocurrent, which is calculated, by using the usual simplifying assumptions, as

$$I_{PPC} = q a_0 g \sqrt{D_p \tau_c} \{ [u(t) \operatorname{erf}(\sqrt{t/\tau_c})] - [u(t - t_p) \operatorname{erf}(\sqrt{(t - t_p)/\tau_c})] \}, \quad (22)$$

where a_0 is the area between collector and base, g is the generation rate of electron hole pairs per cubic centimeter, τ_c is the collector lifetime, and t_p is the length of the pulse. The function u has the value

$$u(>0) = 1,$$

$$u(<0) = 0.$$

In the limit of short pulse times, Eq. (22) can be reduced to

$$I_{PPC} = \frac{2 q a_0 g \sqrt{D_p t_p}}{\sqrt{\pi}}, \quad (23)$$

which, it is seen, is not proportional to the total dose gt_p . Thus, for an exact comparison with the GA code, it is necessary to supply the GA code with a finite time for t_p along with the appropriate generation rate. However, of greater interest is the rate of current decay after the current is no longer limited by the external circuit resistance, as discussed in Section 2.3.2.

2.1.4.3. Comparisons with Additional Simple Models.* Two other well-known simple models which are used to describe a transistor are the charge-control model and the Linvill model. Both of these models are of equal accuracy (e.g., they have the same order of approximation) as the Ebers-Moll model, which we may consider as typical; but all of them are considerably less accurate than the solution of the difference equations given by the GA code. The advantage of the simple models is that they are easier to work with and reveal physical insights which are much more difficult to extract from the GA code. The ultimate goal of the present program will be to determine the nature of

*The following discussion is based on an excellent tutorial paper comparing the three simple models by D. J. Hamilton, F. A. Lindholm, and J. A. Narud (Reference 7).

the inaccuracies left out of the simpler models and to include them in a reasonably physical manner from the data generated by the GA code.

Basically, all three simple models are derived from Eqs. (1), (2), and (3), which are used by the GA code, but all assume that there exists a depleted space-charge region with a boundary condition connecting the p and n regions, given by the expressions

$$p = p_n \exp \left(\frac{qV}{kT} \right) \quad \text{for n region,} \quad (24)$$

$$n = n_p \exp \left(\frac{qV}{kT} \right) \quad \text{for p region,} \quad (25)$$

where V is the algebraic sum of the external and built-in voltages.

Equations (24) and (25) are the first approximation, which is only valid for small currents or small radiation doses. The second assumption is that the base region of the transistor is space-charge neutral.

The next step, which all of the simpler models require, is the elimination of the space variables in Eqs. (1), (2), and (3). For the Ebers-Moll model, the calculational procedure assumes that the forward and inverse current gain can be represented by single pole functions involving a complex frequency. This procedure has the effect of replacing the partial differential equations by simple ordinary differential equations in time. For the charge-control model, the initial mathematical simplification is to integrate the continuity equation in terms of minority-carrier charge density over the length of the base region. Thus, the total charge in the base is considered the controlling variable rather than the distribution of carrier density. An additional requirement needed to obtain a tractable solution is that the instantaneous carrier concentration is linear across the base region, as it is known to be at steady state with the foregoing assumptions. For the Linvill model, the space variable is removed by writing difference equations (just as for the GA code) for spatial

derivatives for finite number of points. Thus, a complete description is obtained by solving simultaneously a set of ordinary differential equations. The interesting feature is that if we consider a given mesh point as a node, then each equation has the form of a Kirchhoff's law equation, and the whole set of equations may be viewed as describing a circuit network with lumped elements corresponding to the coefficients of the difference equations for the minority carrier concentrations. This symbolic visualization is valuable in that it permits all of the tools for solving problems in network theory to be applied and provides some physical insights.

The Ebers-Moll and Linvill models can be made as exact as desired (within the limitations of the boundary relation between regions and the assumptions of space-charge neutrality in the base) by summing an infinite series for the Ebers-Moll model or by letting the number of mesh points approach infinity for the Linvill model. However, for the first-order approximation, all models reduce to the same pair of ordinary first-order differential equations when the proper relation between the three different dependent variables is made.

Each model serves a special use, nevertheless. The Ebers-Moll model is useful if it is sufficient to consider the transistor as a black box with four conveniently measured terminal variables described by relatively simple analytical expressions. The charge-control model is interesting in that it gives physical insight to the role of the total minority-carrier charge of the base in influencing transistor behavior, but much is lost since the relevant variable is charge density. The Linvill model is useful both for specifying the terminal behavior of the transistor and for gaining physical insight in terms of rather incomprehensible lumped parameters. In addition, the transient response can be specified naturally in terms of excess electron-hole pairs (Reference 8); it is not necessary to determine the current or voltage perturbation that is required for the other models. The main disadvantage of this model is that the lumped

parameters are measured indirectly. However, for all three models, the same four physical measurements are sufficient to specify the solution for a given transistor. For a detailed biography discussing each of these models, the reader is referred to Reference 7.

2.2. DESCRIPTION OF THE CODES

Two FORTRAN codes, PND4 and PNPMN, were written for calculating the behavior of semiconductor devices. The PND4 code, which is an extension of the previously reported code, (Reference 9) PND3, treats diodes. The extensions were of two types. First, the adjustment of the sizes of the intervals of both the temporal and spatial variables was automated so that complete problems may now be run in one pass on the computer. Second, descriptions of new phenomena, including generation of carriers by avalanche, saturation of the drift velocities of the carriers in high fields and variation in lifetimes of carriers with integrated flux, were added. Also a large variety of pulse shapes may be described and the possibility of treating devices with complex doping profiles was provided for.

The transistor code PNPMN is a parallel extension of PND3. Like PND3, PNPMN adjusts its intervals automatically and can handle the enlarged repertoire of doping profiles. However, the main advance in PNPMN is the treatment of the flow of carriers in the presence of an intermediate contact.

The following paragraphs constitute a unified description of the two codes.

2.2.1. The Finite Difference Scheme

2.2.1.1. Restatement of the Problem. Both PND4 and PNPMN solve the partial differential equations, Eqs. (1), (2) and (3), of Section 2.1 on a domain $-a \leq x \leq b$ subject to the boundary conditions (5) and (6). In the case of the transistor code, the term i_B/qa_0^2 is added to the right-hand side (RHS) of the conservation equation for electrons in a short interval of

length l around the base contact, where i_B is the base current and a_0 is the effective cross-sectional area of the device. This term has the effect of injecting electrons in a small region of volume $a_0 l$ around the base contact at a rate of i_B/e carriers per second.

Analytically, the problem is an initial-value problem, and to make the statement of the problem complete, the concentrations $n(x, t_0)$ and $p(x, t_0)$ of the carriers must be specified at some initial time $t = t_0$. The electric field at time $t = t_0$ may be obtained from Poisson's equation, Eq. (3), using the given carrier concentrations and the electric field $E(-a, t_0)$ at $x = -a$. The methods by which initial distributions of carriers may be generated are described in a later part of this section.

2.2.1.2. Finite Differences. The computer obtains a numerical solution of the problem by solving an algebraic analog of the partial difference equations in which the derivatives have been replaced by finite difference quotients. First, the domain $-a \leq x \leq b$ is divided into $I - 1$ intervals with end points x_i , where $x_i < x_{i+1}$, $1 \leq i \leq I$. The midpoint of interval i is denoted by $x_{i+\frac{1}{2}}$, so

$$x_{i+\frac{1}{2}} = \frac{x_i + x_{i+1}}{2}.$$

The midpoints of the first and last intervals are the endpoints of the device, so $x_{\frac{1}{2}} = -a$ and $x_{I-\frac{1}{2}} = b$.

If f is some function of x , then define

$$f_j = f(x_j), \quad (26)$$

$$\delta f_j = f_{j+\frac{1}{2}} - f_{j-\frac{1}{2}}, \quad (27)$$

$$\bar{f}_j = \frac{1}{2} (f_{j+\frac{1}{2}} + f_{j-\frac{1}{2}}), \quad (28)$$

where j is either an integer or half an integer.

The carrier concentrations n and p are calculated at endpoints of intervals and the electric field E is calculated at midpoints. Thus, integer subscripts are appropriate for n and p , whereas half odd-integer subscripts are appropriate for E .

The partial derivatives that appear in the conservation equations and Poisson's equation are approximated as follows:

$$\frac{\delta n_{i+\frac{1}{2}}}{\delta x_{i+\frac{1}{2}}} = \frac{n_{i+1} - n_i}{x_{i+1} - x_i} \quad \text{for } \frac{\partial n}{\partial x}(x_{i+\frac{1}{2}}),$$

$$\frac{\delta \left(\frac{\delta n_i}{\delta x_i} \right)}{\delta x_i} = \frac{\frac{\delta n_{i+\frac{1}{2}}}{\delta x_{i+\frac{1}{2}}} - \frac{\delta n_{i-\frac{1}{2}}}{\delta x_{i-\frac{1}{2}}}}{\frac{1}{2}(x_{i+1} - x_{i-1})}$$

$$= \frac{\frac{n_{i+1} - n_i}{x_{i+1} - x_i} - \frac{n_i - n_{i-1}}{x_i - x_{i-1}}}{\frac{1}{2}(x_{i+1} - x_{i-1})} \quad \text{for } \frac{\partial^2 n}{\partial x^2}(x_i),$$

$$\frac{\delta E_i}{\delta x_i} = \frac{E_{i+\frac{1}{2}} - E_{i-\frac{1}{2}}}{\frac{1}{2}(x_{i+1} - x_{i-1})} \quad \text{for } \frac{\partial E}{\partial x}(x_i),$$

$$v_{i+\frac{1}{2}} \quad \text{for } v_n(E_{i+\frac{1}{2}}),$$

$$u_{i+\frac{1}{2}} \quad \text{for } v_p(E_{i+\frac{1}{2}}),$$

$$\frac{\delta \bar{n}_i v_i}{\delta x_i} = \frac{\bar{n}_{i+\frac{1}{2}} v_{i+\frac{1}{2}} - \bar{n}_{i-\frac{1}{2}} v_{i-\frac{1}{2}}}{\frac{1}{2}(x_{i+1} - x_{i-1})}$$

$$= \frac{(n_{i+1} + n_i) v_{i+\frac{1}{2}} - (n_i + n_{i-1}) v_{i-\frac{1}{2}}}{x_{i+1} - x_{i-1}} \quad \text{for } \frac{\partial n v}{\partial x}(x_i).$$

Thus, the original partial differential equations are replaced by the coupled system of ordinary differential equations:

$$\frac{dn_i}{dt} = G_i - \frac{\delta \bar{n}_i v_i}{\delta x_i} + D_n \frac{\delta \left(\frac{\delta n_i}{\delta x_i} \right)}{\delta x_i}, \quad (29)$$

$$\frac{dp_i}{dt} = G_i - \frac{\delta \bar{p}_i u_i}{\delta x_i} + D_p \frac{\delta \left(\frac{\delta p_i}{\delta x_i} \right)}{\delta x_i}, \quad (30)$$

$$\frac{\delta E_i}{\delta x_i} = \frac{4\pi q}{\kappa} (p_i - n_i + \Delta N_i), \quad (31)$$

where $2 \leq i \leq I - 1$ and

$$G_i = g + A_i - R_i, \quad (32)$$

$$A_i = n_i \alpha_n (\bar{E}_i) + p_i \alpha_p (\bar{E}_i), \quad (33)$$

$$R_i = \frac{n_i p_i n_0^2}{d_i}, \quad (34)$$

and the quantities D_n and D_p are the diffusion constants for electrons and holes, respectively. In the codes, D_n and D_p are two input quantities and they are assumed to be independent of time and position. The velocities v_n and v_p are assumed to be proportional to the electric field until they saturate, i. e.,

$$v_n = -\mu_n E \quad \text{if } |E| < v_{ns}/\mu_n, \quad (35)$$

$$v_n = -v_{ns} E/|E| \quad \text{if } |E| \geq v_{ns}/\mu_n \quad (36)$$

and

$$v_p = \mu_p E \quad \text{if } |E| < v_{ps}/\mu_p, \quad (37)$$

$$v_p = v_{ps} E/|E| \quad \text{if } |E| \geq v_{ps}/\mu_p. \quad (38)$$

In the three-region code PNPMN, saturation is not accounted for, or, in other words, $v_{ns} = v_{ps} = \infty$ necessarily. The calculation of the functions α_n and α_p that occur in the avalanche term, Eq. (33), and in the denominator d_i of the recombination term, Eq. (34), are discussed later.

The boundary conditions are used to determine the values of n_1 , p_1 , p_I , n_I , and $E_{3/2}$. The condition $\frac{\partial n}{\partial x}(-a) = 0$ becomes simply

$$n_1 = n_2. \quad (39)$$

Similarly,

$$p_1 = p_2, \quad (40)$$

$$n_I = n_{I-1}, \quad (41)$$

and

$$p_I = p_{I-1}. \quad (42)$$

The boundary equation for E then becomes

$$\frac{dE_{3/2}}{dt} = \frac{4\pi}{\kappa} \left[\frac{i}{A_0} - q(p_2 U_{3/2} - n_2 v_{3/2}) \right], \quad (43)$$

where i is the current that passes into the device at the left end from the external circuit. It might seem as though the problem were overdetermined because $E_{I-1/2}$ must satisfy an equation such as Eq. (43) while at the same time it may be obtained from $E_{1/2}$ through the finite difference form (31) of Poisson's equation. It will become apparent, however, when the solution of the equations is discussed, that these two procedures for determining $E_{I-1/2}$ yield the same result.

The currents in the external circuit depend on input circuit parameters and potential differences between contacts. The diode circuit is a special case of the transistor circuit, so it will be expedient to discuss the latter circuit first. The transistor circuit, as shown in Figure 2 is essentially the one shown in Figure 4.

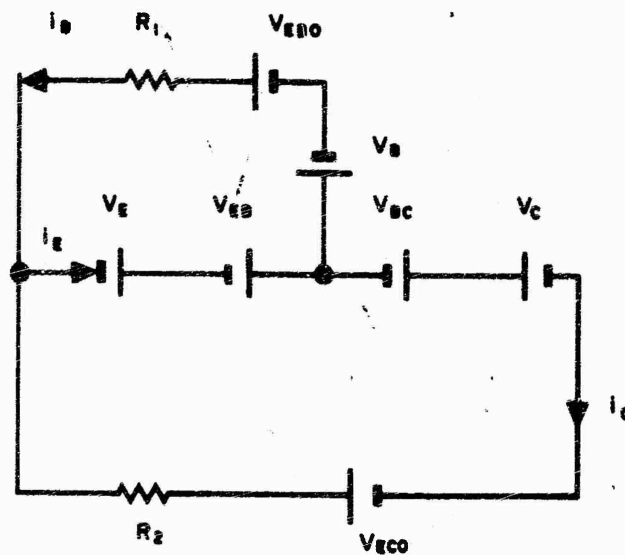


Figure 4. Schematic of reference transistor

The voltages V_E , V_B , and V_C represent the three contact potentials and V_{EB} and V_{BC} represent the rise in potential across the emitter-base and base-collector junctions, respectively. The other quantities, R_1 , R_2 , i_E , i_B , i_C , V_{EB0} , and V_{EC0} , are as discussed in Section 2.1.4.

The equations for the currents are then

$$V_{EB0} + V_{EB} + V_E - V_B = R_1 i_B, \quad (44)$$

$$V_{EC0} + V_{EB} + V_{BC} + V_E - V_C = R_2 i_C, \quad (45)$$

and

$$i_E = i_B + i_C. \quad (46)$$

The contact potentials are calculated directly from input quantities according to the formula

$$V_c = \theta \log \left[\sqrt{(\Delta N_c)^2 + 4n_0^2} + \Delta N_c \right], \quad c = E, B, \text{ or } C, \quad (47)$$

where θ is the temperature (in volts) of the semiconducting material, n_0 is the intrinsic concentration of electrons, and ΔN_c is the difference between the concentrations of donors and acceptors in the immediate neighborhood of the contact.

The potential rise generated by space charge is calculated from the electric field using a trapezoidal rule to discretize the equation

$$\Delta V = - \int_{x_1}^{x_2} E \, dx.$$

Specifically,

$$V_{EB} = - \sum_{i=2}^{i_b-1} \bar{E}_i \delta x_i - \frac{1}{2} \bar{E}_{i_b} \delta x_{i_b} \quad (48)$$

and

$$V_{EB} + V_{BC} = - \sum_{i=2}^{I-1} \bar{E}_i \delta x_i, \quad (49)$$

where x_{i_b} is the location of the base contact. As for the diode, the current is calculated from the same equations with the following interpretation:

<u>Diode</u>		<u>Transistor</u>
V_0	replaces	V_{EC0}
V	replaces	$V_{EB} + V_{BC}$
i	replaces	i_C
R	replaces	R_2
V_{BI}	replaces	$V_C - V_E$
		$R_1 = \infty$
		$i_B = 0$

2.2.1.3. The Time Integration. The numerical integration of the system of ordinary differential equations, Eqs. (29), (30), and (43), subject to the conditions imposed by Eqs. (31), (39), (40), (41), and (42) is accomplished by substituting a finite difference quotient for the time derivatives in much the same way as was done for the spatial derivatives. Thus, if t^{l-1} and t^l denote the endpoints of the interval of the l th step in the time integration, the following equations are solved

$$\frac{n_i^l - n_i^{l-1}}{t^l - t^{l-1}} = \omega \left. \frac{dn_i}{dt} \right|_t^l + (1-\omega) \left. \frac{dn_i}{dt} \right|_t^{l-1}, \quad (50)$$

$$\frac{p_i^l - p_i^{l-1}}{t^l - t^{l-1}} = \omega \left. \frac{dp_i}{dt} \right|_t^l + (1-\omega) \left. \frac{dp_i}{dt} \right|_t^{l-1}, \quad (51)$$

where ω is a weight factor that may be set anywhere in the range $0 \leq \omega \leq 1$. Before proceeding farther, let us define

$$H_i(n_{i-1}, n_i, n_{i+1}, p_i, E_{i-\frac{1}{2}}, E_{i+\frac{1}{2}}, t) = G_i(n_i, p_i, \bar{E}_i, t) - \frac{\delta \bar{n}_i v_i}{\delta x_i} + D_n \frac{\delta n_i}{\delta x_i}, \quad (52)$$

$$J_i(p_{i-1}, p_i, p_{i+1}, n_i, E_{i-\frac{1}{2}}, E_{i+\frac{1}{2}}, t) = G_i(n_i, p_i, \bar{E}_i, t) - \frac{\delta \bar{p}_i u_i}{\delta x_i} + D_p \frac{\partial \left(\frac{\delta p_i}{\delta x_i} \right)}{\delta x_i}, \quad (53)$$

$$H_i^l = H_i(n_{i-1}^l, n_i^l, n_{i+1}^l, p_i^l, E_{i-\frac{1}{2}}^l, E_{i+\frac{1}{2}}^l, t^l), \quad (54)$$

$$J_i^l = J_i(p_{i-1}^l, p_i^l, p_{i+1}^l, n_i^l, E_{i-\frac{1}{2}}^l, E_{i+\frac{1}{2}}^l, t^l). \quad (55)$$

Thus, Eqs. (50) and (51) become

$$\frac{n_i^l - n_i^{l-1}}{t^l - t^{l-1}} = \omega H_i^l + (1-\omega) H_i^{l-1}, \quad (56)$$

$$\frac{p_i^l - p_i^{l-1}}{t^l - t^{l-1}} = \omega J_i^l + (1-\omega) J_i^{l-1}. \quad (57)$$

Solving Eqs. (56) and (57) for n_i^l and p_i^l , using given values for n_i^{l-1} and p_i^{l-1} , $1 < i < I$, t^{l-1} , t^l , and $E_{3/2}^{l-1}$, constitutes a step from time t^{l-1} to time t^l in the numerical integration. The process is straightforward when $\omega = 0$. In that case, the equations become

$$n_i^l = n_i^{l-1} + (t^l - t^{l-1}) H_i^{l-1}, \quad (58)$$

$$p_i^l = p_i^{l-1} + (t^l - t^{l-1}) J_i^{l-1}, \quad (59)$$

where the RHS's can be evaluated using the given values of the carrier densities n_i^{l-1} and p_i^{l-1} at time $t = t^{l-1}$. Such a procedure is not practical, however, because small errors will become magnified from step to step unless a very small time step ($< 10^{-13}$ sec in realistic problems) is used. The reason is that in the solution of realistic problems there will usually be some point in the mesh where $\partial H_i / \partial n_i < -10^{13} n_i$.

Physically, this means that if excess electrons were injected into such a region (i. e., a region of dimensions δx_i around the point x_i) in a device of the type being modeled, they would redistribute themselves on a 10^{-13} sec time scale. Numerically, the effect is that if an error is made in n_i , the derivative dn_i/dt will adjust itself so that the error will be corrected in $< 10^{-13}$ sec. But if the change in n_i is extrapolated beyond 10^{-13} sec, the error will be overcorrected and will reappear as an error of greater magnitude and opposite sign at the end of the time step. This phenomenon of overstability is illustrated in Figure 5, where it is assumed that Eq. (58) is used at $x = x_i$ and that, somehow, exact values are used at other points.

Figure 6 shows how the error oscillates with increasing amplitude when the procedure is used for several consecutive steps with too large a value for Δt .

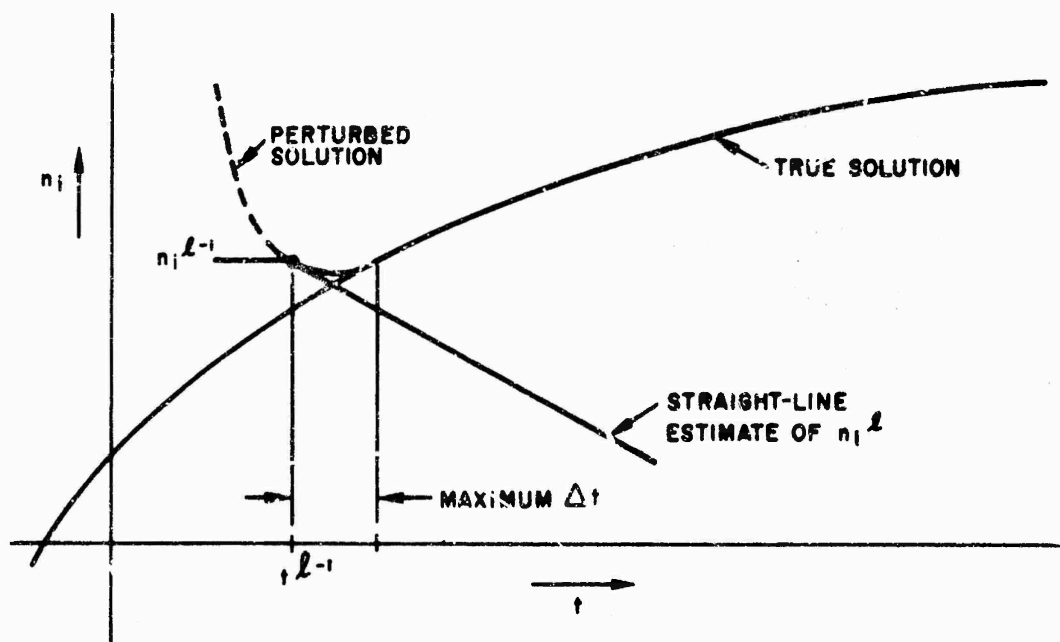


Figure 5. Plot showing overstability

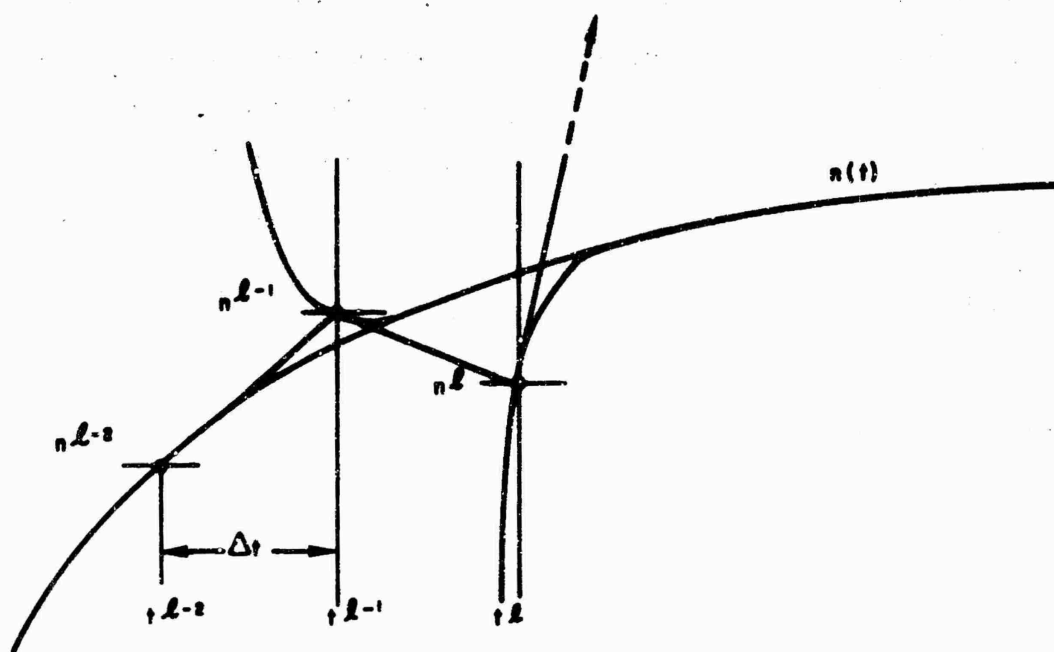


Figure 6. Progress of an unstable integration

Solving Eqs. (56) and (57) with $\omega \geq \frac{1}{2}$ is usually stable for arbitrary positive Δt . A satisfactory analysis of stability for the precise problem discussed in this report is lacking, but it can be said that in all cases that have been tried, no evidence of instability has been observed with $\omega = 1$. The reason that this might be expected to be true is illustrated by Figure 7, which shows that when the linear estimate for n_i^l is made tangent to some perturbed solution at t^l (rather than t^{l-1}), which is the effect of setting $\omega = 1$, a strong stabilizing influence is operative.

For model problems that can be fully analyzed, it has been shown (e. g., by Richtmyer, Reference 10) that a procedure like solving systems (56) and (57) is unconditionally stable when $\frac{1}{2} \leq \omega \leq 1$ and that the numerical solution converges to the solution of the differential equations most rapidly as $\Delta t \rightarrow 0$ when $\omega = \frac{1}{2}$. For real problems, however, where limitations of computing time place an effective lower limit on Δt , $\omega = 1$ appears to be more satisfactory than $\omega = \frac{1}{2}$. In fact, although the codes

were redesigned to operate with any ω and the input routines allow the user to specify ω , there are some features that have not been tested with $\omega < 1$.

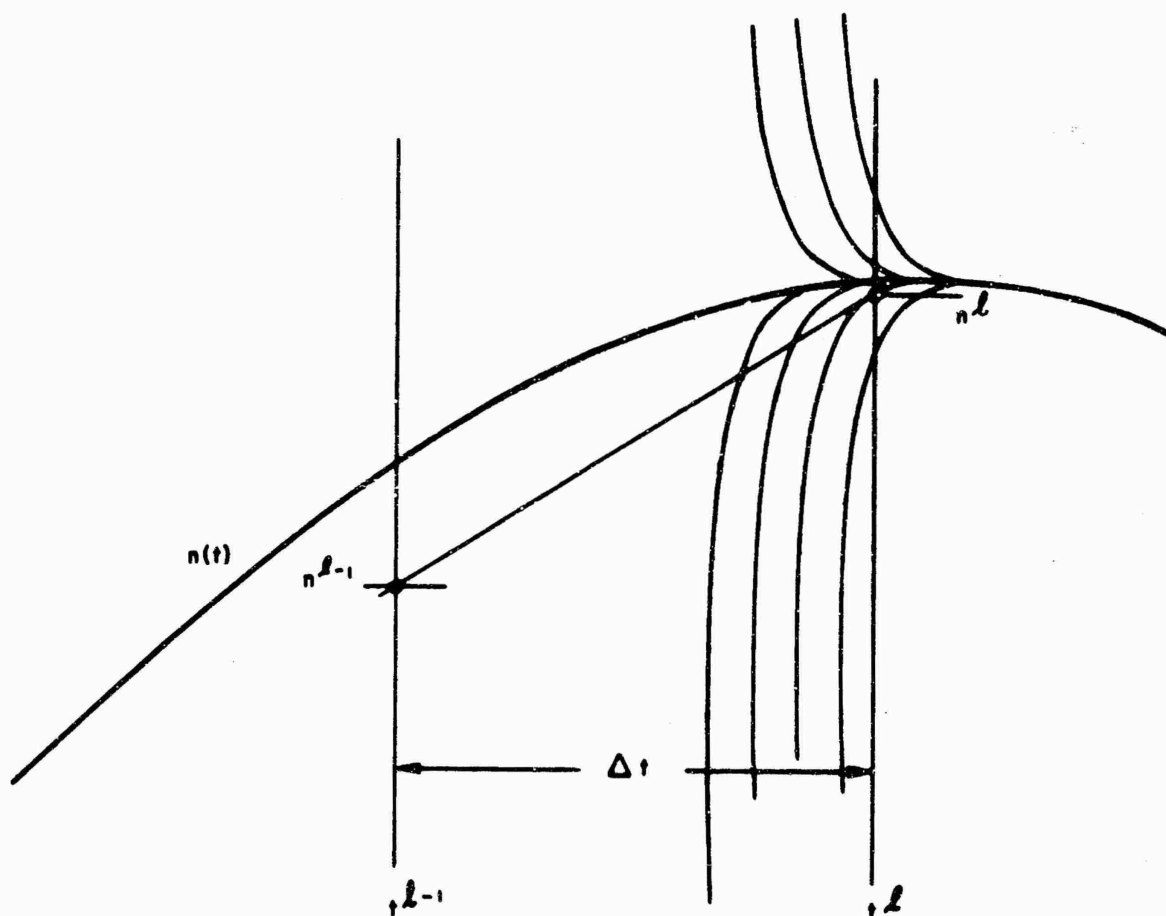


Figure 7. Unconditional stability

2.2.1.4. Reduction of the System of Equations. The finite difference equations (50) and (51) for conservation of carriers and the finite difference form of Poisson's equation (31) give us three equations per spatial interval that must be solved simultaneously when $\omega > 0$. It is possible to reduce the number of equations that must be solved to only twice the

number of intervals by eliminating one of the carrier densities. The transformations required make extensive use of the identity

$$\begin{aligned}
 \sum_{i=k}^{\ell} \delta f_i &= \delta f_k + \delta f_{k+1} + \dots + \delta f_{\ell-1} + \delta f_{\ell} \\
 &= (f_{k+\frac{1}{2}} - f_{k-\frac{1}{2}}) + (f_{k+\frac{3}{2}} - f_{k+\frac{1}{2}}) + \dots \\
 &\quad + (f_{\ell-\frac{1}{2}} - f_{\ell-\frac{3}{2}}) + (f_{\ell+\frac{1}{2}} - f_{\ell-\frac{1}{2}}) \\
 &= f_{\ell+\frac{1}{2}} - f_{k-\frac{1}{2}}.
 \end{aligned}$$

All the intermediate terms cancel each other out.

First, multiply Eq. (31) through by δx_i and sum over i . Thus,

$$E_{k+\frac{1}{2}} - E_{3/2} = \sum_{i=2}^k \delta E_i = \frac{4\pi q}{\kappa} \sum_{i=2}^k (p_i - n_i + \Delta N_i) \delta x_i.$$

Then, because $\Delta N_i = \Delta N_i^{\ell-1}$,

$$\begin{aligned}
 \frac{E_{k+\frac{1}{2}}^{\ell} - E_{k+\frac{1}{2}}^{\ell-1}}{t^{\ell} - t^{\ell-1}} - \frac{E_{3/2}^{\ell} - E_{3/2}^{\ell-1}}{t^{\ell} - t^{\ell-1}} &= \frac{4\pi q}{\kappa} \sum_{i=2}^k \frac{p_i^{\ell} - p_i^{\ell-1} - n_i^{\ell} + n_i^{\ell-1}}{t^{\ell} - t^{\ell-1}} \delta x_i \\
 &= \frac{4\pi q}{\kappa} \sum_{i=2}^k (\omega J_i^{\ell} + (1-\omega) J_i^{\ell-1} - \omega H_i^{\ell} - (1-\omega) H_i^{\ell-1}) \delta x_i
 \end{aligned} \tag{60}$$

using (56) and (57). But

$$\begin{aligned}
\sum_{i=2}^k (J_i - H_i) \delta x_i &= \sum_{i=2}^k \left(-\bar{p}_i u_i + D_p \frac{\delta p_i}{\delta x_i} + \bar{n}_i v_i - D_n \frac{\delta n_i}{\delta x_i} \right) \\
&= -\bar{p}_{k+\frac{1}{2}} u_{k+\frac{1}{2}} + D_p \frac{\delta p_{k+\frac{1}{2}}}{\delta x_{k+\frac{1}{2}}} + \bar{p}_{3/2} u_{3/2} - D_p \frac{\delta p_{3/2}}{\delta x_{3/2}} \\
&\quad + \bar{n}_{k+\frac{1}{2}} v_{k+\frac{1}{2}} - D_n \frac{\delta n_{k+\frac{1}{2}}}{\delta x_{k+\frac{1}{2}}} - \bar{n}_{3/2} v_{3/2} + D_n \frac{\delta n_{3/2}}{\delta x_{3/2}}.
\end{aligned}$$

If we set

$$\begin{aligned}
K_{k+\frac{1}{2}} = K(n_k, n_{k+1}, p_k, p_{k+1}, E_{k+\frac{1}{2}}) &= \frac{4\pi q}{\kappa} \left(-\bar{p}_{k+\frac{1}{2}} u_{k+\frac{1}{2}} + D_p \frac{\delta p_{k+\frac{1}{2}}}{\delta x_{k+\frac{1}{2}}} \right. \\
&\quad \left. + \bar{n}_{k+\frac{1}{2}} v_{k+\frac{1}{2}} - D_n \frac{\delta n_{k+\frac{1}{2}}}{\delta x_{k+\frac{1}{2}}} \right) + \frac{4\pi i_E}{\kappa a_0}, \quad (61)
\end{aligned}$$

where i_E is the emitter current (its role will become evident very soon), then

$$\frac{4\pi q}{\kappa} \sum_{i=2}^k (J_i - H_i) \delta x_i = K_{k+\frac{1}{2}} - K_{3/2}$$

and Eq. (60) becomes

$$\frac{E_{k+\frac{1}{2}}^\ell - E_{k+\frac{1}{2}}^{\ell-1}}{t^\ell - t^{\ell-1}} \omega K_{k+\frac{1}{2}}^\ell + (1 - \omega) K_{k+\frac{1}{2}}^{\ell-1} + \frac{E_{3/2}^\ell - E_{3/2}^{\ell-1}}{t^\ell - t^{\ell-1}} - \omega K_{3/2}^\ell - (1 - \omega) K_{3/2}^{\ell-1}.$$

But, by Eqs. (39) and (40), $\delta p_{3/2} = \delta n_{3/2} = 0$, $\bar{p}_{3/2} = p_2$, and $\bar{n}_{3/2} = n_2$, so

$$K_{3/2} = \frac{4\pi q}{\kappa} (-p_2 u_{3/2} + n_2 v_{3/2}) + \frac{4\pi i_E}{\kappa a_0},$$

and using the boundary equation (43), we get

$$\frac{E_{3/2}^{\ell} - E_{3/2}^{\ell-1}}{t^{\ell} - t^{\ell-1}} = \omega K_{3/2}^{\ell} + (1 - \omega) K_{3/2}^{\ell-1},$$

substituting i for k , our equation becomes

$$\frac{E_{i+\frac{1}{2}}^{\ell} - E_{i+\frac{1}{2}}^{\ell-1}}{t^{\ell} - t^{\ell-1}} = \omega K_{i+\frac{1}{2}}^{\ell} + (1 - \omega) K_{i+\frac{1}{2}}^{\ell-1}. \quad (62)$$

Thus the boundary equation for E has been extended to the interior. In the case of the diode, Eq. (62) holds over the entire range $1 \leq i < I$, showing that the right-hand boundary condition on E is automatically satisfied, as was claimed. In the transistor problem, however, a modification is required because the term $i_B / e a_0 \delta x_{i_b}$ must be added to the generation term for electrons in interval i_b , where the base contact is made. The effect of the modification is to subtract $4\pi i_B / \kappa a_0$ from $K_{i+\frac{1}{2}}$ for $i \geq i_b$. Since $i_C = i_E - i_B$, this means that the collector current replaces the emitter current in the expression for $K_{i+\frac{1}{2}}$ in intervals lying to the right of the base contact.

Equation (62) still involves both carriers. However, either carrier may be eliminated using Poisson's equation, Eq. (31), which implies that

$$p_i = P_i(n_i, E_{i-\frac{1}{2}}, E_{i+\frac{1}{2}}) \equiv n_i - \Delta N_i + \frac{\kappa}{4\pi q} \frac{\delta E_i}{\delta x_i} \quad (63)$$

and

$$n_i = N_i(p_i, E_{i-\frac{1}{2}}, E_{i+\frac{1}{2}}) \equiv p_i + \Delta N_i - \frac{\kappa}{4\pi q} \frac{\delta E_i}{\delta x_i}. \quad (64)$$

The procedure in both modes is to eliminate at each point the density of the majority carrier. At a point i where $p_i^{\ell-1} < n_i^{\ell-1}$, Eqs. (57) and (62) are solved, with Eq. (64) used to eliminate n_i , and at a point i where $n_i^{\ell-1} < p_i^{\ell-1}$, Eqs. (56) and (62) are solved, with Eq. (63) used to eliminate p_i . The reason for always eliminating the majority carrier is that it is

an easy quantity to calculate using Eq. (63) or Eq. (64), once the electric field and the density of minority carriers is known. On the other hand, serious cancellation can occur when the calculation of the density of minority carriers in terms of the density of majority carriers is attempted. For example, knowing that $n \approx \Delta N$ and $\nabla \cdot E \approx 0$ in those parts of the n region which are far from the junction is of no help whatsoever in calculating p .

If the identity of the majority carrier changes between point i and point $i+1$, then point i is a crossover point. In PND4 it is assumed that there is exactly one crossover point and in PNPMN it is assumed that there are an even number of them but not more than ten.

The process by which Eq. (62) was obtained has a direct analytical analog. Integrating Poisson's equation gives

$$E(x) - E(-a) = \frac{4\pi q}{\kappa} \int_a^x (p - n + \Delta N) dx.$$

Hence,

$$\begin{aligned} \frac{\partial E(x)}{\partial t} - \frac{\partial E(-a)}{\partial t} &= \frac{4\pi q}{\kappa} \int_{-a}^x \left[\frac{\partial p}{\partial t} - \frac{\partial n}{\partial t} \right] dx \\ &= \frac{4\pi q}{\kappa} \int_{-a}^x \left[-\frac{\partial p v}{\partial x} + D_p \frac{\partial^2 p}{\partial x^2} + \frac{\partial n v}{\partial x} - D_n \frac{\partial^2 n}{\partial x^2} \right] dx \\ &= \frac{4\pi q}{\kappa} \left[-p v_p + D_p \frac{\partial p}{\partial x} + n v_n - D_n \frac{\partial n}{\partial x} \right]_{-a}^x. \end{aligned}$$

Again,

$$\frac{\partial p}{\partial x}(-a) = \frac{\partial n}{\partial x}(-a) = 0$$

and

$$\frac{i}{a_0} = \frac{\kappa}{4\pi} \frac{\partial E(-a)}{\partial t} + q(pv_p - nv_n),$$

so

$$\frac{\partial E(x)}{\partial t} = \frac{4\pi q}{\kappa} \left[-pv_p + D_p \frac{\partial p}{\partial x} + nv_n - D_n \frac{\partial n}{\partial x} + \frac{i}{a_0 q} \right],$$

which is an analytic version of Eq. (62) asserting that the total current is the sum of the carrier current and the displacement current.

2.2.1.5. The Method of Solution of the Difference Equations. The problem has been reduced to this: Given in each interval i at time t^{l-1} the electric field strength $E_{i+\frac{1}{2}}^{l-1}$ and the density of the minority carrier, n_i^{l-1} or p_i^{l-1} , whichever is smaller, find $E_{i+\frac{1}{2}}^l$ and either n_i^l or p_i^l at time t^l using Eq. (62) and either Eq. (56) or Eq. (57). Having found the field strengths and the minority-carrier densities, use Eqs. (63) and (64) to find the majority-carrier densities. The solution is not easy to obtain because the equations are nonlinear and, when $\omega > 0$, coupled. The method that was adopted is to estimate the unknown fields and densities, make a linear approximation to the equations in the neighborhood of the estimate by means of a two-term Taylor expansion, and solve the resulting system of linear equations by direct elimination and back-substitution. The solution of the linearized equations becomes a new estimate. If it does not satisfy the nonlinear equations well enough, the procedure is repeated.

To show exactly how the linearized equations are obtained, denote the estimated values of i_c^l , n_i^l , p_i^l , and $E_{i+\frac{1}{2}}^l$ at $t = t^l$ by i_c^* , n_i^* , p_i^* , and $E_{i+\frac{1}{2}}^*$, respectively, and set

$$\iota = (i_c^l - i_c^*)/a_0, \quad (65)$$

$$\nu_i = n_i^l - n_i^*, \quad (66)$$

$$\pi_i = p_i^l - p_i^*, \quad (67)$$

$$\epsilon_{i+\frac{1}{2}} = E_{i+\frac{1}{2}}^l - E_{i+\frac{1}{2}}^* \quad (68)$$

Assume that $n_k^{l-1} < p_k^{l-1}$ for $k = i-1, i$, and $i+1$. Then Eq. (56) becomes

$$\begin{aligned} \frac{1}{\omega} \frac{\nu_i + N_i^* - N_i^{l-1}}{t^l - t^{l-1}} &= \frac{1-\omega}{\omega} H_i^{l-1} + H_i^* + \frac{\partial H_i}{\partial n_{i-1}} \nu_{i-1} + \frac{\partial H_i}{\partial n_i} \nu_i + \frac{\partial H_i}{\partial n_{i+1}} \nu_{i+1} \\ &+ \frac{\partial H_i}{\partial p_i} \left[\frac{\partial p_i}{\partial n_i} \nu_i + \frac{\partial p_i}{\partial E_{i-\frac{1}{2}}} \epsilon_{i-\frac{1}{2}} + \frac{\partial p_i}{\partial E_{i+\frac{1}{2}}} \epsilon_{i+\frac{1}{2}} \right] \\ &+ \frac{\partial H_i}{\partial E_{i-\frac{1}{2}}} \epsilon_{i-\frac{1}{2}} + \frac{\partial H_i}{\partial E_{i+\frac{1}{2}}} \epsilon_{i+\frac{1}{2}} \end{aligned}$$

or

$$\begin{aligned} \frac{1-\omega}{\omega} H_i^{l-1} + H_i^* - \frac{1}{\omega} \frac{N_i^* - N_i^{l-1}}{t^l - t^{l-1}} &= -\frac{\partial H_i}{\partial n_{i-1}} \nu_{i-1} + \left[\frac{1}{\omega(t^l - t^{l-1})} - \frac{\partial H_i}{\partial n_i} - \frac{\partial H_i}{\partial p_i} \frac{\partial p_i}{\partial n_i} \right] \nu_i \\ &- \frac{\partial H_i}{\partial n_{i+1}} \nu_{i+1} - \left(\frac{\partial H_i}{\partial E_{i-\frac{1}{2}}} + \frac{\partial H_i}{\partial p_i} \frac{\partial p_i}{\partial E_{i-\frac{1}{2}}} \right) \epsilon_{i-\frac{1}{2}} \\ &- \left(\frac{\partial H_i}{\partial E_{i+\frac{1}{2}}} + \frac{\partial H_i}{\partial p_i} \frac{\partial p_i}{\partial E_{i+\frac{1}{2}}} \right) \epsilon_{i+\frac{1}{2}} \end{aligned} \quad (69)$$

and Eq. (62) becomes

$$\begin{aligned} \frac{1}{\omega} \frac{\epsilon_{i+\frac{1}{2}} + E_{i+\frac{1}{2}}^* - E_{i+\frac{1}{2}}^{l-1}}{t^l - t^{l-1}} &= \frac{1-\omega}{\omega} K_{i+\frac{1}{2}}^{l-1} + K_{i+\frac{1}{2}}^* + \frac{\partial K_{i+\frac{1}{2}}}{\partial E_{i+\frac{1}{2}}} \epsilon_{i+\frac{1}{2}} + \frac{\partial K_{i+\frac{1}{2}}}{\partial n_i} \nu_i + \frac{\partial K_{i+\frac{1}{2}}}{\partial n_{i+1}} \nu_{i+1} \\ &+ \frac{\partial K_{i+\frac{1}{2}}}{\partial p_i} \left(\frac{\partial p_i}{\partial n_i} \nu_i + \frac{\partial p_i}{\partial E_{i-\frac{1}{2}}} \epsilon_{i-\frac{1}{2}} + \frac{\partial p_i}{\partial E_{i+\frac{1}{2}}} \epsilon_{i+\frac{1}{2}} \right) \\ &+ \frac{\partial K_{i+\frac{1}{2}}}{\partial p_{i+1}} \left(\frac{\partial p_{i+1}}{\partial n_{i+1}} \nu_{i+1} + \frac{\partial p_{i+1}}{\partial E_{i+\frac{1}{2}}} \epsilon_{i+\frac{1}{2}} + \frac{\partial p_{i+1}}{\partial E_{i+3/2}} \epsilon_{i+3/2} \right) + \frac{4\pi t}{\kappa} \end{aligned}$$

or

$$\begin{aligned}
\frac{1-\omega}{\omega} K_{i+\frac{1}{2}}^{l-1} + K_{i+\frac{1}{2}}^* - \frac{1}{\omega} \frac{E_{i+\frac{1}{2}}^* - E_{i+\frac{1}{2}}^{l-1}}{t^l - t^{l-1}} &= - \frac{4\pi\epsilon}{\kappa} - \frac{\partial K_{i+\frac{1}{2}}}{\partial p_i} \frac{\partial P_i}{\partial E_{i-\frac{1}{2}}} \epsilon_{i-\frac{1}{2}} \\
&\quad - \left(\frac{\partial K_{i+\frac{1}{2}}}{\partial n_i} + \frac{\partial K_{i+\frac{1}{2}}}{\partial p_i} \frac{\partial P_i}{\partial n_i} \right) \nu_i \\
&\quad + \left[\frac{1}{\omega(t^l - t^{l-1})} - \frac{\partial K_{i+\frac{1}{2}}}{\partial E_{i+\frac{1}{2}}} \right. \\
&\quad \left. - \frac{\partial K_{i+\frac{1}{2}}}{\partial p_i} \frac{\partial P_i}{\partial E_{i+\frac{1}{2}}} \right. \\
&\quad \left. - \frac{\partial K_{i+\frac{1}{2}}}{\partial p_{i+1}} \frac{\partial P_{i+1}}{\partial E_{i+\frac{1}{2}}} \right] \epsilon_{i+\frac{1}{2}} \\
&\quad - \left(\frac{\partial K_{i+\frac{1}{2}}}{\partial n_{i+1}} + \frac{\partial K_{i+\frac{1}{2}}}{\partial p_{i+1}} \frac{\partial P_{i+1}}{\partial n_{i+1}} \right) \nu_{i+1} \\
&\quad - \frac{\partial K_{i+\frac{1}{2}}}{\partial p_{i+1}} \frac{\partial P_{i+1}}{\partial E_{i+3/2}} \epsilon_{i+3/2}, \tag{70}
\end{aligned}$$

where P_i is defined by Eq. (63). Performing the indicated differentiations yields

$$\begin{aligned}
\frac{\partial H_i}{\partial n_i} &= \frac{\partial G_i}{\partial n_i} - \frac{\partial v_i^*}{2\delta x_i} - \frac{D_n}{\delta x_u} \left(\frac{1}{\delta x_{i+\frac{1}{2}}} + \frac{1}{\delta x_{i-\frac{1}{2}}} \right) \\
&= \alpha_n(\bar{E}_i^*) - \frac{p_i}{d_i} - \frac{\partial v_i^*}{2\delta x_i} - \frac{D_n}{\delta x_i} \left(\frac{2}{\delta x_i} \right), \tag{71}
\end{aligned}$$

$$\frac{\partial H_i}{\partial n_{i+1}} = \frac{v_{i+\frac{1}{2}}^*}{2\delta x_i} + \frac{D_n}{\delta x_i \delta x_{i+\frac{1}{2}}}, \tag{72}$$

$$\begin{aligned}
\frac{\partial H_i}{\partial E_{i+\frac{1}{2}}} &= \frac{\partial G_i}{\partial E_{i+\frac{1}{2}}} + \frac{\bar{n}_{i+\frac{1}{2}}^*}{\delta x_i} v'_n(E_{i+\frac{1}{2}}^*) \\
&= \frac{n_i^*}{2} \alpha'_n(\bar{E}_i^*) + \frac{p_i^*}{2} \alpha'_p(\bar{E}_i^*) + \frac{\bar{n}_{i+\frac{1}{2}}^*}{\delta x_i} v'_n(E_{i+\frac{1}{2}}^*), \quad (73)
\end{aligned}$$

$$\frac{\partial H_i}{\partial p_i} = \frac{\partial G_i}{\partial p_i} = \alpha'_p(\bar{E}_i^*) - \frac{n_i^*}{d_i}, \quad (74)$$

$$\frac{\partial P_i}{\partial n_i} = 1, \quad \frac{\partial P_i}{\partial E_{i+\frac{1}{2}}} = \pm \frac{\kappa}{4\pi q \delta x_i}, \quad (75)$$

$$\frac{\partial K_{i+\frac{1}{2}}}{\partial n_{i+\frac{1}{2} \pm \frac{1}{2}}} = \pm \frac{D_n}{\delta x_{i+\frac{1}{2}}}, \quad \frac{\partial K_{i+\frac{1}{2}}}{\partial p_{i+\frac{1}{2} \pm \frac{1}{2}}} = \pm \frac{D_p}{\delta x_{i+\frac{1}{2}}}, \quad (76)$$

$$\frac{\partial K_{i+\frac{1}{2}}}{\partial E_{i+\frac{1}{2}}} = -\bar{p}_{i+\frac{1}{2}}^* v'_p(E_{i+\frac{1}{2}}^*) + \bar{n}_{i+\frac{1}{2}}^* v'_n(E_{i+\frac{1}{2}}^*). \quad (77)$$

Note that majority carrier densities are only virtually eliminated; really, the technique is to regard them as auxiliary functions. As a consequence, the equations obtained at crossover points are very similar to those at regular points. If, for example, $n_k^{\ell-1} < p_k^{\ell-1}$ at $k = i - 1$ and i but not at $k = i + 1$, then Eq. (56) becomes

$$\begin{aligned}
\frac{1}{\omega} \frac{v_i + n_i^* - n_i^{\ell-1}}{t^\ell - t^{\ell-1}} &= \frac{1-\omega}{\omega} H_i^{\ell-1} + H_i^* + \frac{\partial H_i}{\partial n_{i-1}} v_{i-1} + \frac{\partial H_i}{\partial n_i} v_i \\
&+ \frac{\partial H_i}{\partial n_{i+1}} \left(\pi_{i+1} + \frac{\partial N_{i+1}}{\partial E_{i+\frac{1}{2}}} \epsilon_{i+\frac{1}{2}} + \frac{\partial N_{i+1}}{\partial E_{i+3/2}} \epsilon_{i+3/2} \right) \\
&+ \frac{\partial H_i}{\partial p_i} \left(v_i + \frac{\partial P_i}{\partial E_{i-\frac{1}{2}}} \epsilon_{i-\frac{1}{2}} + \frac{\partial P_i}{\partial E_{i+\frac{1}{2}}} \epsilon_{i+\frac{1}{2}} \right)
\end{aligned}$$

$$+ \frac{\partial H_i}{\partial E_{i-\frac{1}{2}}} \epsilon_{i-\frac{1}{2}} + \frac{\partial H_i}{\partial E_{i+\frac{1}{2}}} \epsilon_{i+\frac{1}{2}}$$

or

$$\begin{aligned} \frac{1-\omega}{\omega} H_i^{\ell-1} + H_i^* - \frac{1}{\omega} \frac{n_i^* - n_i^{\ell-1}}{t^\ell - t^{\ell-1}} &= - \frac{\partial H_i}{\partial n_{i-1}} \nu_{i-1} - \frac{\partial H_i}{\partial E_{i-\frac{1}{2}}} \epsilon_{i-\frac{1}{2}} \\ &+ \left[\frac{1}{\omega(t^\ell - t^{\ell-1})} - \frac{\partial H_i}{\partial n_i} - \frac{\partial H_i}{\partial p_i} \right] \nu_i \\ &- \left(\frac{\partial H_i}{\partial E_{i+\frac{1}{2}}} + \frac{\partial H_i}{\partial n_{i+1}} \frac{\partial N_{i+1}}{\partial E_{i+\frac{1}{2}}} \right) \epsilon_{i+\frac{1}{2}} - \frac{\partial H_i}{\partial n_{i+1}} \pi_{i+1} \\ &- \frac{\partial H_i}{\partial n_{i+1}} \frac{\partial N_{i+1}}{\partial E_{i+3/2}} \epsilon_{i+3/2}, \quad (78) \end{aligned}$$

which is the same as Eq. (69) with the addition of the terms

$$- \frac{\partial H_i}{\partial n_{i+1}} \frac{\partial N_{i+1}}{\partial E_{i+1\pm\frac{1}{2}}} \epsilon_{i+1\pm\frac{1}{2}}.$$

The equations for calculating the correction ϵ to the currents are derived from Eqs. (44), (45), (48), and (49). Thus,

$$a_0 R_1 \epsilon_B = - \sum_{i=2}^{i_b-1} \bar{\epsilon}_i \delta x_i - \frac{1}{2} \bar{\epsilon}_{i_b} \delta x_{i_b} \quad (79)$$

and

$$a_0 R_2 \epsilon_C = - \sum_{i=2}^{I-1} \bar{\epsilon}_i \delta x_i. \quad (80)$$

Since the functional form of J_i is exactly that of H_i , it would be unnecessarily redundant to exhibit its derivatives too.

In order to get a clear picture of the structure of the linearized equations, it is necessary to rename the variables. Let

$$Y_{2i} = \nu_i,$$

$$B_{2i} = \frac{1-\omega}{\omega} H_i^{\ell-1} + H_i^* - \frac{1}{\omega} \frac{n_i^* - n_i^{\ell-1}}{t^\ell - t^{\ell-1}} \quad \text{when } n_i < p_i;$$

let

$$Y_{2i} = \pi_i,$$

$$B_{2i} = \frac{1-\omega}{\omega} J_i^{\ell-1} + J_i^* - \frac{1}{\omega} \frac{p_i^* - p_i^{\ell-1}}{t^\ell - t^{\ell-1}} \quad \text{when } p_i \leq n_i;$$

let

$$Y_{2i+1} = \epsilon_{i+\frac{1}{2}},$$

$$B_{2i+1} = \frac{1-\omega}{\omega} K_{i+\frac{1}{2}}^{\ell-1} + K_{i+\frac{1}{2}}^* - \frac{1}{\omega} \frac{E_{i+\frac{1}{2}}^* - E_{i+\frac{1}{2}}^{\ell-1}}{t^\ell - t^{\ell-1}};$$

and, finally, let

$$Y_1 = \iota_B \quad \text{and} \quad Y_2 = \iota_C.$$

Then Eq. (69) may be rewritten as

$$A_{2i}^{2i-2} Y_{2i-2} + A_{2i}^{2i-1} Y_{2i-1} + A_{2i}^{2i} Y_{2i} + A_{2i}^{2i+1} Y_{2i+1} + A_{2i}^{2i+2} Y_{2i+2} = B_{2i} \quad (69a)$$

and Eq. (70) as

$$\begin{aligned} \bar{A}(Y_i + Y_2) + A_{2i+1}^{2i-1} Y_{2i-1} + A_{2i+1}^{2i} Y_{2i} + A_{2i+1}^{2i+1} Y_{2i+1} \\ + A_{2i+1}^{2i+2} Y_{2i+2} + A_{2i+1}^{2i+3} Y_{2i+3} = B_{2i+1} \quad (70a) \end{aligned}$$

where the matrix elements A_{2i}^{2i+j} are various partial derivatives of H_i (or J_i when $p_i \leq n_i$) and the matrix elements A_{2i+1}^{2i+j} are partial derivatives of

$K_{i+\frac{1}{2}}$. The term $\bar{A}(Y_1+Y_2)$ in Eq. (70a) represents $-4\pi\epsilon_E/\kappa$. This is valid only when $i < i_b$, where i_b is the index of the interval containing the base contact. When $i \geq i_b$, this term is replaced by $\bar{A}Y_2 = -4\pi\epsilon_C/\kappa$. In either case,

$$\bar{A} = -\frac{4\pi}{\kappa}.$$

In the new notation, Eqs. (79) and (80) are rewritten as

$$A_1^1 Y_1 + \sum_{i=1}^{i_b} A_1^{2i+1} Y_{2i+1} = B_1 \quad (79a)$$

and

$$A_2^2 Y_2 + \sum_{i=1}^{I-1} A_2^{2i+1} Y_{2i+1} = B_2, \quad (80a)$$

where

$$A_1^1 = a_0 R_1,$$

$$A_2^2 = a_0 R_2,$$

$$A_1^3 = A_2^3 = \frac{1}{2}(x_{5/2} - x_{3/2}),$$

$$A_i^{2i+1} = \frac{1}{2}(x_{i+3/2} - x_{i-1/2}) \quad 2 \leq i \leq i_b - 2,$$

$$A_1^{2i_b-1} = \frac{1}{2}(x_{i_b} - x_{i_b-3/2}),$$

$$A_1^{2i_b+1} = \frac{1}{2}(x_{i_b} - x_{i_b-\frac{1}{2}}),$$

$$A_2^{2i+1} = \frac{1}{2}(x_{i+3/2} - x_{i-1/2}) \quad 2 \leq i \leq I-2,$$

$$A_2^{2I-1} = \frac{1}{2}(x_{I-1/2} - x_{I-3/2}),$$

and

$$B_1 = B_2 = 0.$$

It is now easy to see that the matrix of coefficients A_n^m has the form

$$A = \begin{bmatrix} a_{11} & | & a_{12} \\ \hline a_{21} & | & a_{22} \end{bmatrix}$$

where a_{11} is a 2×2 submatrix and a_{22} is a $(2I - 3) \times (2I - 3)$ submatrix. Furthermore, the big submatrix a_{22} has only five nonzero diagonals: the main diagonal and the two closest ones on either side. Actually, a_{22} has some exceptional elements that are easily eliminated. They arise in the equations for B_{2k} and B_{2k+2} when $i = k$ is a crossover point. For example, it may be seen from Eq. (78), which is the equation for B_{2k} , that

$$A_{2k}^{2k+3} = - \frac{\partial H_k}{\partial N_{k+1}} \frac{\partial N_{k+1}}{\partial E_{k+3/2}}$$

will not generally vanish. Similarly, it can be expected that $A_{2k+2}^{2k-1} \neq 0$. However, the pattern of nonzero terms has the form

Row number

$2k - 1$	A	A	<u>A</u>	A	A			
$2k$		A	A	<u>A</u>	A	C		
$2k + 1$			Λ	A	<u>A</u>	A	A	
$2k + 2$			C	A	A	<u>A</u>	A	A
$2k + 3$					A	A	<u>A</u>	A A

where Λ = ordinary element

\underline{A} = element on main diagonal,

C = exceptional element.

and the A terms have been omitted. The coefficients A_{2k+1}^{2k-1} and A_{2k+1}^{2k+3} of row $2k+1$ lying immediately above and below the exceptional elements are, for physical reasons, large in magnitude, so subtracting the correct multiples of row $2k+1$ from the rows above and below will always suffice to eliminate the exceptional elements.

The procedure for solving the linearized equations is:

1. Eliminate the exceptional elements introduced by the cross-over points.
2. Eliminate the two diagonals below the main diagonal in rows 3 through $2J - 1$.
3. Eliminate all elements in rows 1 and 2 except for columns 1 and 2 (α_{12}).
4. Solve rows 1 and 2 for ι_B and ι_C .
5. By back substitution, solve rows $2I - 1$ back up to 3.

The process is essentially self-contained in that only an insignificant amount of storage is required beyond the storage required to hold α_{11} , α_{12} , α_{21} , and the five nonzero diagonals of α_{22} .

The criterion for convergence of the procedure, i. e., the iterative process for calculating successive estimates of n_i^l , p_i^l , $E_{i+1/2}^l$, and i_c^l , is that $|v_i/n_i|$ and $|\pi_i/p_i|$ be smaller than some input quantity ϵ_{\max} for all i . If the criterion has not been met by the time the number of iterations has reached some critical value, also specified in the input, the time step is multiplied by m_t , a small (input) factor, and the procedure is repeated. It is easy to see that as $\Delta t \rightarrow 0$, the diagonal terms of the matrix are dominated by $1/\omega\Delta t$ so that the equations can be solved with less and less round-off error, and since, in addition, the values of the variables at the beginning of the time step become good estimates of their values at the end, fewer and fewer iterations are required to meet the convergence criterion. Thus, some progress is always possible with

sufficiently small Δt . There is, however, a test, which is discussed below in connection with automatic control of the size of the time step, that aborts the run when progress is too slow.

On the first iteration of each time step, the values of the densities and fields are first estimated to be equal to their values at the previous step. When the IBM-7044 was used for running PND3, it was found that it was much more efficient to extrapolate the densities and fields from as many as five previous time steps, but the code runs so fast on the CDC-6600 that it did not seem advisable to retain that feature.

2.2.1.6. Initial Conditions. There are two kinds of problems that the codes were designed to solve: one is to find equilibrium states of semi-conducting devices and the other is to investigate their transient response to pulses of radiation. The initial condition appropriate to a problem of the second kind is the solution to a problem of the first kind. The method for solving the first type of problem is, starting with the closest available estimate to the solution, to run a transient problem to equilibrium. Nevertheless, occasionally it is necessary to start from scratch. The method used in PND3 was carried over to PND4. It amounted to estimating the concentrations and fields by functions of the form $a + b \exp(cx)$. The constants a , b , and c are adjusted to satisfy Poisson's equation and give correct values at the ends of the diode and the correct voltage across the diode. It turns out, however, that it is not always possible to satisfy all these conditions, and when it is, the result resembles reality only remotely. Since the procedure used in PND3 sometimes failed and since it was more complicated than it was worth when it worked, a simpler, safer procedure was devised for PNPMN. It is to set the electric field equal to zero everywhere and set the concentrations to the positive solution of the equations

$$n_i - p_i = \Delta N_i, \quad (81)$$

$$(n_i - r)(p_i - r) = n_0^2. \quad (82)$$

Equation (81) makes the space charge vanish and Eq. (82) is an equation that the densities satisfy immediately following the injection of r pairs per cubic centimeter into material that had been in thermal equilibrium. It is often necessary to set $r \sim 10^{-5} \Delta N$ maximum because, otherwise, the codes have difficulty handling the discontinuities in the concentrations of carriers near the junctions.

2.2.2. Treatment of Special Effects

2.2.2.1. The Carrier Generation Term. While PND3 was being developed, it was found that the simple carrier recombination term

$$\frac{np - n_0^2}{n\tau_n}$$

would not work over the whole n region of a diode in which the p side is heavily doped. One reason for the failure of that approximation to the recombination rate is that when the concentration of holes in the p region is much higher than that of electrons in the n region, the holes will diffuse into the n region and become the majority carrier over most of the depletion layer. The recombination term should, according to the Shockly-Read theory (Reference 11), be

$$R = \frac{np - n_0^2}{(n + n')\tau_n + (p + p')\tau_p}, \quad (83)$$

where n' and p' are what the concentrations of electrons and holes would be if the Fermi level were at the energy level of the recombination centers. Thus, $n'p' = n_0^2$, so one or the other must be larger than the intrinsic density n_0 . But if a junction is biased sufficiently, the field in the depletion layer can get strong enough to reduce the density of all carriers to values far below n_0 , in which case the dominant term in the denominator d_i of R becomes $n\tau_n + p\tau_p$. Consequently, it is well to use Eq. (83) in its complete form.

In both codes, the denominator

$$d_i = (n_i + n')\tau_n + (p_i + p')\tau_p$$

of R_i is calculated only once each time step, before the first iteration, and that value is used for all iterations. Since the concentrations are usually dropping, the effect is usually to make d_i too large, so the effective time constant of the recombination process comes out to be larger than the input τ 's, by just how much depends on the size of the time step.

Carriers may be injected into the transistor either at a uniform rate g or in a delta-function pulse in the PNPMN code. The PND4 code allows a delta-function pulse plus any rate $g(t)$ that is a piecewise linear function of time.

In PND4, the rate of generation of carriers by avalanche is taken to be

$$A(n, p, E) = nk_n e^{-b_n/E^2} + pk_p e^{-b_p/E^2}, \quad (84)$$

where k_n , k_p , b_n , and b_p are four input parameters. The functions $\alpha_n(E)$ and $\alpha_p(E)$ of Eqs. (33), (71), (73), and (74) are

$$\alpha_n(E) = k_n e^{-b_n/E^2}, \quad (85)$$

$$\alpha_p(E) = k_p e^{-b_p/E^2}, \quad (86)$$

so

$$\alpha'_n(E) = 2b_n \alpha_n(E)/E^3, \quad (87)$$

$$\alpha'_p(E) = 2b_p \alpha_p(E)/E^3. \quad (88)$$

2.2.2.2. Saturation of Drift Velocity. The calculation of the drift velocity has been described previously. To account for this effect (PND4 only), the usual form, μE , of the drift velocity is simply truncated

when the value v_s as saturation is reached. Also, in the calculation of derivatives, as indicated in Eq. (73), the derivative of the drift velocity, which is normally $\pm\mu$, depending on the sign of the charge of the carrier, is set to zero at saturation.

2.2.2.3. Fluence-dependent Lifetimes. As has already been mentioned, the decrease in the lifetimes of the carriers with continuing radiation damage is accounted for by setting

$$\frac{1}{\tau_j^l} = \frac{1}{\tau_j^0} + K_j \int_0^l (\partial\phi/\partial t) dt, \quad (89)$$

where j indicates a type of lifetime. The calculation of τ_j^l is performed when the denominator of the recombination term is calculated. Since τ decreases as time passes, using the final value tends to make the denominator too small (which counteracts to some extent the error caused by using the densities associated with the beginning of the time interval, as described before).

2.2.3. Automatic Selection of Interval Sizes

2.2.3.1. Computing the Time Interval. There are two not unrelated factors that must be considered in selecting the time interval. One is the accuracy of the integration, which generally increases as the time intervals are refined until they become so small that the round-off error is as large as the error caused by using finite differences quotients in place of derivatives. The other factor is the convergence of the iterative procedure for calculating densities and fields at the end of a time interval on the basis of their values at the beginning of the interval.

Basically, the method for choosing the time interval is to calculate

$$w^l = \max_{1 \leq i \leq I} \left(\frac{n_i^l - n_i^{l-1}}{n_{i-1}^l + n_i^l + n_{i+1}^l}, \frac{p_i^l - p_i^{l-1}}{p_{i-1}^l + p_i^l + p_{i+1}^l} \right) \quad (90)$$

and to set

$$t^{l+1} - t^l = \frac{w_0 (t^l - t^{l-1})}{100 w^l} \quad (91)$$

so that if the behavior of the device is not too erratic, one can expect that w^{l+1} will be about $w_0/100$. The reason for including the terms with indices $i \pm 1$ in the denominators in Eq. (90) is that there are usually one or two places in the device where the density changes by more than an order of magnitude from one mesh point to the next. It has been found that a considerably larger fractional change of density per time step can be tolerated at such locations, and averaging the denominator over several consecutive points is an automatic way of taking this into account. The code also adjusts w_0 . If the calculation proceeds for n_1 consecutive time steps without taking more than n_2 iterations, then w_1 is added to w_0 , where n_1 , n_2 , and w_1 , are fixed input numbers. However, as a control on the accuracy of the integration procedure, an upper bound, w_{\max} , which is another input parameter, is imposed on w_0 . Still another parameter, $w_2 < 1$ multiplies w_0 when negative densities appear or in case of a failure of the iterative procedure to converge. A lower limit w_{\min} can be imposed on w_0 , if desired, but this seems to be a useless facility. Rather than use w_{\min} to prevent the calculation from bogging down and wasting computing time, the user can specify that the calculation is to be discontinued if it goes for more than n_3 consecutive steps with $w^l < \epsilon_w$.

There is no analysis as yet to serve as a basis for selecting the parameters described above, but good results have been obtained with the following choices:

$n_1 = 3$	$w_1 = 10$
$n_2 = 3$	$w_2 = .5$
$n_3 = 5$	$w_{\max} = 10$
$w_0 = 10.$	$w_{\min} = 1.$
	$\epsilon_w = .001$

2.2.3.2. Calculating the Spatial Intervals. If too many spatial intervals are used, the calculation will run longer than necessary because of the increased amount of calculation per iteration and because of the rise in round-off error, especially in solving the linear system, which will result in more iterations being required to meet the convergence criterion. Consequently, it is highly desirable and often necessary to choose a rather carefully graded spatial mesh. Five not entirely unrelated automatic meshing procedures were tested in the course of the code development effort. The one that emerged is based on the idea of minimizing the maximum value of $|\log n_i/n_{i+1}|$, $|\log p_i/p_{i+1}|$ and $|\log (|E_{i+\frac{1}{2}}| + E_M)/(|E_{i-\frac{1}{2}}| + E_M)|$ subject to the following conditions: (1) that the number I of points in the mesh be between specified limits $I_{\min} \leq I \leq I_{\max}$, (2) that the endpoints of the mesh be $-a$ and b , and (3) that $\rho_x^{-1} < \delta x_i / \delta x_{i+1} \leq \rho_x$ for all i , where a , b , E_M , I_{\min} , I_{\max} , and ρ_x are all input parameters. The method that was developed for finding a mesh that satisfies these conditions proceeds by first guessing at ρ , the maximum absolute value that the above-mentioned logarithms are allowed to assume. With the given ρ , a mesh is constructed with the fewest number of intervals, subject to the conditions on the logarithms and on the ratios of successive interval lengths. A systematic search procedure is then instituted (using the rule of false position) for finding the value of ρ that produces the right number of intervals. An ordinary problem may require twenty meshes before equilibrium is obtained, but because $\Delta I / \Delta \rho$ changes only slowly, that quantity may be saved from remesh to remesh and serve as a means for estimating by how much ρ ought to be changed. Consequently, it is only while constructing the first mesh that more than two or three trials are required.

Revising the mesh is a minor catastrophe in the course of running a problem. Inevitably, the time step must be dropped below 10^{-11} sec and usually to 10^{-14} sec, and it takes from five to ten short time steps before the calculation really gets under way again. The reason is that

once a new mesh has been selected, there is no satisfactory way for determining what the densities should be at the new points. At any rate, remeshing too frequently causes erratic results and consumes much computer time. It has been found that remeshing only when the ratio of densities at adjacent mesh points exceeds 30 or 100 gives good results.

The procedure that is used for calculating densities at the new mesh points selected by a remeshing operation is the following: It is assumed that the electron concentration between $x_{i-1/2}$ and $x_{i+1/2}$ has the constant value n_i , for all i between 2 and $I-1$. If x_j^* is the new mesh, then n_j^* is taken to be the number of electrons between $x_{j-1/2}^*$ and $x_{j+1/2}^*$ divided by δx_j^* . A similar procedure is used to calculate p_j^* and ΔN_j^* , except that in the case of ΔN , reference is always made to the input data which specify constant values of ΔN over two or three large regions. The great virtue of this otherwise rather crude procedure is that it strictly conserves charge. The difficulty with any procedure that does not enjoy this property is that astronomical electric fields are likely to result.

2.2.4. Conservation of Charge in the Time Integration

Multiplying Eq. (29) through by δx_i and summing gives

$$\begin{aligned} \frac{d}{dt} \sum_{i=2}^{I-1} n_i \delta x_i &= \sum_{i=2}^{I-1} G_i \delta x_i - \sum_{i=2}^{I-1} \delta n_i v_i + D_n \sum_{i=2}^{I-1} \delta \frac{\partial n_i}{\partial x_i} \\ &= \sum_{i=2}^{I-1} G_i \delta x_i - n_{I-1} v_{I-1/2} + n_2 v_{3/2}, \end{aligned} \quad (92)$$

in which the boundary conditions $n_1 = n_2$, $n_I = n_{I-1}$ have been used. This equation states that in the finite difference approximation, the rate at which the number of electrons in the device increases is exactly equal to the rate at which they are generated plus the rate at which they flow in at the ends. When the time derivative in Eq. (92) is replaced by a difference

quotient, the equation becomes

$$\frac{n^{\ell} - n^{\ell-1}}{t^{\ell} - t^{\ell-1}} = \omega (C_n^{\ell} - R^{\ell}) + (1 - \omega) (C_n^{\ell-1} - R^{\ell-1}), \quad (93)$$

where

$$N = \sum_{i=2}^{I-1} n_i \delta x_i, \quad (94)$$

$$C_n = n_2 v_{3/2} - n_{I-1} v_{I-1/2} + \frac{i_B}{qa_0}, \quad (95)$$

and

$$R = - \sum_{i=2}^{I-1} G_i \delta x_i, \quad (96)$$

and, analogously, for holes,

$$\frac{p^{\ell} - p^{\ell-1}}{t^{\ell} - t^{\ell-1}} = \omega (C_p^{\ell} - R^{\ell}) + (1 - \omega) (C_p^{\ell-1} - R^{\ell-1}), \quad (97)$$

where

$$p = \sum_{i=2}^{I-1} p_i \delta x_i, \quad (98)$$

and

$$C_p = p_2 u_{3/2} - p_{I-1} u_{I-1/2}. \quad (99)$$

The LHS and RHS of Eqs. (93) and (97) are calculated and printed by both codes for each edited time step. Discrepancies are caused by either round-off error or by lack of convergence in the iterative solution of the difference equations and have no bearing on the question of how closely an exact solution of the difference equations would agree with the true solution of the differential equations of Section 2.1.

2.2.5. Doping Profiles

In both the PND4 and the PNPMN codes, the values of ΔN_i are entirely arbitrary, so that any doping profile is permissible. As the codes are presently constituted, however, the input routines allow ΔN to have only one value in each region of a device. The few changes required in PNPMN for treating a more realistic distribution of the dopant have been worked out in some detail but they have not been tested. They are:

1. In CFFPNP, the subroutine that calculates the geometrical coefficients of the difference equations and the array ΔN_i , the distribution is specified to be

$$\Delta N(x) = \bar{N}_{k+1} \frac{x - x_k}{x_{k+1} - x_k} + \bar{N}_k \frac{x_{k+1} - x}{x_{k+1} - x_k}$$

for $x_k \leq x \leq x_{k+1}$, and whenever a new mesh is selected, the value of ΔN_i is taken to be

$$\Delta N_i = \frac{1}{\delta x_i} \int_{x_{i-\frac{1}{2}}}^{x_{i+\frac{1}{2}}} \Delta N(x) dx,$$

where the integral is calculated simply by adding up the areas under the trapezoids between $x_{i-\frac{1}{2}}$ and $x_{i+\frac{1}{2}}$.

2. In IZPNP, the subroutine that initializes the arrays containing n_i , p_i , and $E_{i+\frac{1}{2}}$ when starting from scratch, the array $E_{i+\frac{1}{2}}$ is initialized at 0 and the quantities n_i and p_i are initialized at the positive solution of the equations

$$p_i - n_i + \Delta N_i = 0,$$

$$(p_i - r)(n_i - r) = n_0^2,$$

where r is the density of pairs generated by the initial pulse, and the

contact potentials, $V_B - V_E$ and $V_C - V_E$, which are ordinarily already calculated when IZPNP is entered, are recalculated according to Eq. (47), using values of ΔN obtained from the array $\overline{\Delta N}$ instead of from the regular input specification.

2.3. RESULTS OF THE COMPUTER PROGRAMS

The computer programs have been exercised by calculating currents and voltages in a reference diode, a germanium 1N91 diode, a reference transistor, a 2N396A transistor, and a reference Zener diode.

2.3.1. Computer Results for the Reference Diode

A reference diode was formulated to exercise the computer program and to illustrate the phenomena of carrier recombination and transport within the diode. This diode could be representative of a low-frequency diffused structure since the carrier lifetimes on both sides of the junction are fairly long. The parameters of the reference diode are listed in Table I.

Table I
REFERENCE SILICON DIODE PARAMETERS

$N_p = 2.6 \times 10^{16}/\text{cm}^3$	$D_n = 33.75 \text{ cm}^2/\text{sec}$
$N_n = 9.3 \times 10^{14}/\text{cm}^3$	$D_p = 12.0 \text{ cm}^2/\text{sec}$
$\mu_n = 1350 \text{ cm}^2/\text{V-sec}$	$n_{0p} = 8.5839 \times 10^3/\text{cm}^3$
$\mu_p = 480 \text{ cm}^2/\text{V-sec}$	$n_{0n} = 9.3 \times 10^{14}/\text{cm}^3$
Length of p region = 1.0 cm	$p_{0n} = 2.3998 \times 10^5/\text{cm}^3$
Length of n region = 1.0 cm	$K = 1.33 \times 10^{11} (K = 12)$
$\tau_p = 10^{-6} \text{ sec}$	$n' = 3.1 \times 10^{10}/\text{cm}^3$
$\tau_n = 5 \times 10^{-6} \text{ sec}$	$p' = 7.1994 \times 10^9/\text{cm}^3$
$p_{0p} = 2.6 \times 10^{16}/\text{cm}^3$	Area of junction = $2.4 \times 10^{-2} \text{ cm}^2$

The simplest problem to solve is the carrier density and electric field under no-bias thermal-equilibrium conditions. This solution can be achieved exactly analytically, it can be solved by the conventional depletion layer treatment, and it should be approached by the time-dependent computer solution as the radiation-induced excess carriers disappear in any zero-bias configuration.

2.3.1.1. Analytic Solution for No Bias, Thermal Equilibrium.

Under no-bias thermal-equilibrium conditions, the basic differential equations (1), (2), and (3) can be simplified by setting

$$\frac{\partial n}{\partial t} = \frac{\partial p}{\partial t} = 0, \quad R = 0, \quad \frac{D_n}{\mu_n} = \frac{D_p}{\mu_p} = \frac{kT}{q}.$$

The relation between mobility and diffusion constant is Einstein's relation and is a consequence of the fact that both carrier drift under the influence of an electric field and carrier diffusion under the influence of a density gradient are limited by the same scattering processes.

In this case Eqs. (1) and (2) can be integrated once. The integration constants are the electron and hole particle current densities, which must also be zero at thermal equilibrium. The resulting equations are

$$\mu_n \left(nE + \frac{kT}{q} \frac{\partial n}{\partial x} \right) = 0, \quad (100)$$

$$\mu_p \left(-pE + \frac{kT}{q} \frac{\partial p}{\partial x} \right) = 0. \quad (101)$$

A partial solution is

$$E = - \frac{kT}{q} \frac{\partial}{\partial x} (\log n), \quad (102)$$

$$p = n_0^2/n. \quad (103)$$

If we define the potential, V , as the potential difference with reference to intrinsic material,

$$V = - \int E dx, \quad (104)$$

then

$$\begin{aligned} n &= n_0 e^{+(q/kT)V} , \\ p &= n_0 e^{-(qV/kT)} . \end{aligned} \quad (105)$$

Poisson's equation can now be translated into a single equation in one unknown:

$$-\frac{\kappa}{4\pi q} \frac{\partial^2 V}{\partial x^2} = -2n_0 \sinh \frac{qV}{kT} + \Delta N \quad (106)$$

or

$$L_0^2 \frac{\partial^2 \psi}{\partial x^2} = 2 \sinh \psi - \Delta N/n_0 , \quad (107)$$

where

$$\psi = qV/kT ,$$

and

$$L_0 = \sqrt{\frac{\kappa kT}{4\pi n_0 q^2}}$$

is the Debye length in intrinsic material.

This ordinary differential equation has not been solved in closed form, but is amenable to computer integration. The results for the electric field and carrier densities for the reference diode are shown in Figures 8 and 9. Note particularly that the range of concentrations covers more than a factor of 10^{12} .

2.3.1.2. Approximate Solution, No Bias, Thermal Equilibrium.

The first step in all approximate treatments of diodes and transistors is to replace the structure by two types of regions--bulk and depletion regions. In physical terms, the bulk region is assumed to be quasi-neutral in which the fixed space charge $+\Delta N$ is canceled by the mobile charges $-q(n - p)$. Hence Eq. (3) in a quasi-neutral is replaced (not supplemented) by

$$n - p = \Delta N .$$

The depletion region is assumed to be characterized by the opposite

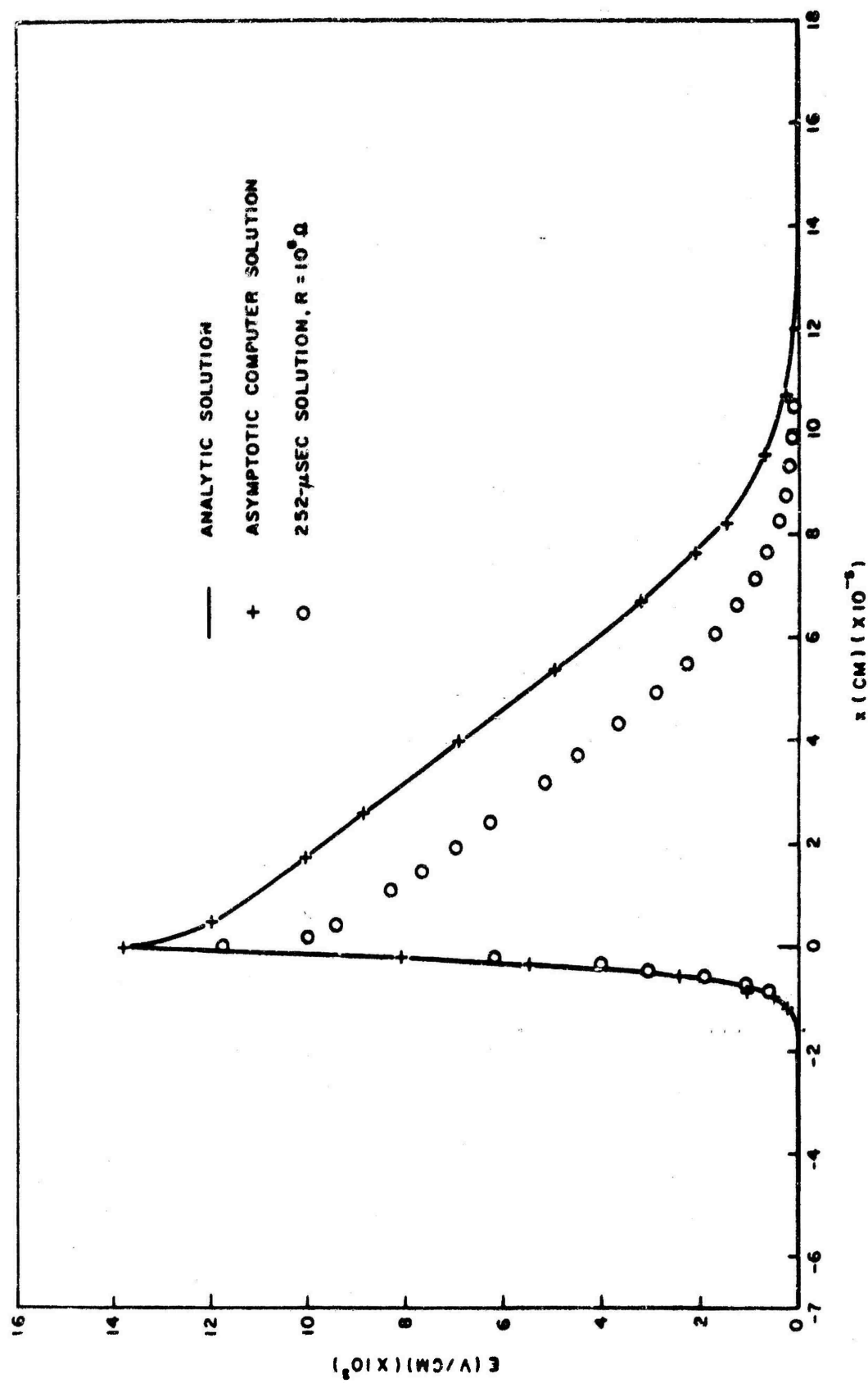


Figure 8. Equilibrium zero-bias diode electric field

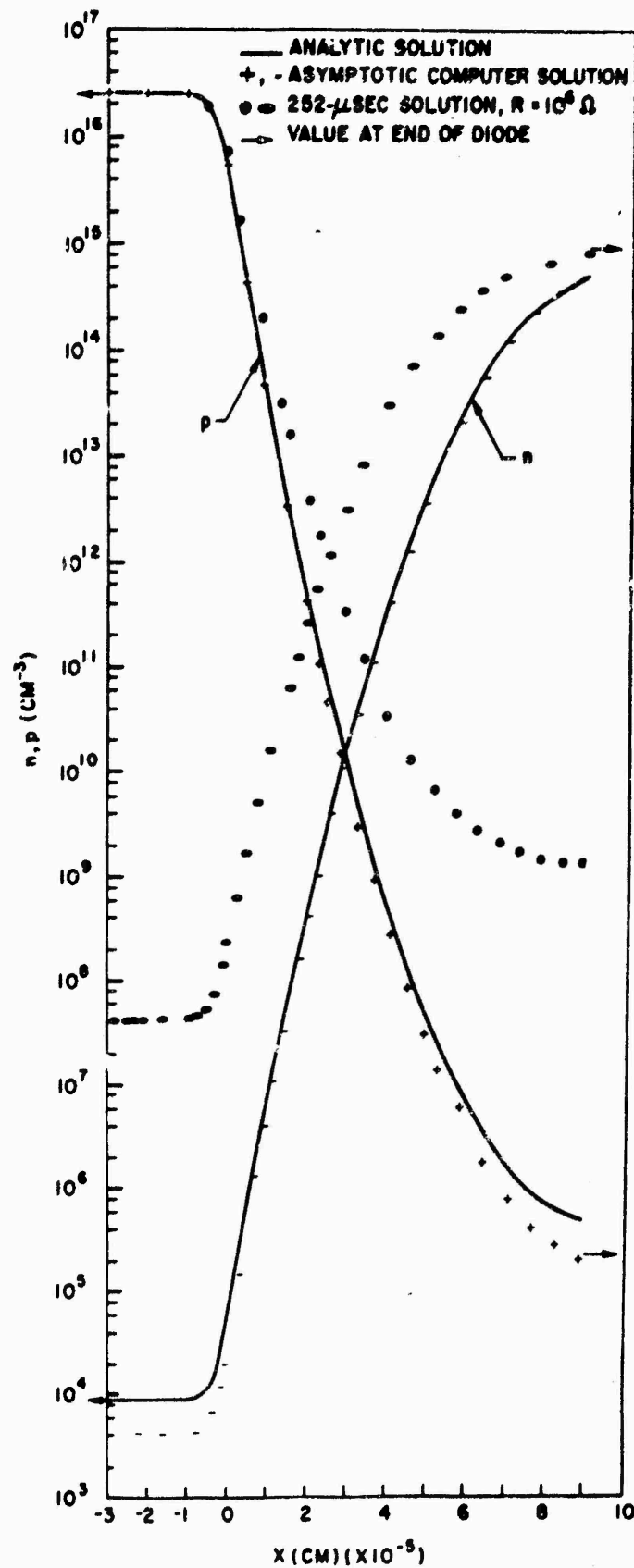


Figure 9. Equilibrium zero-bias diode carrier densities

approximation: the mobile charge is small compared to the fixed space charge. In this region, the fixed-charge approximation replaces Eq. (3) by

$$\frac{\partial E}{\partial x} = \frac{4\pi q}{\kappa} \Delta N(x) .$$

These approximations can also be translated into the form of Eq. (107). In the bulk region,

$$L_0^2 \frac{\partial^2 \psi}{\partial x^2} = - \frac{\Delta N}{n_0} .$$

This equation results in an electric field which varies linearly away from the junction with a slope proportional to ΔN . The bulk and depletion regions are joined where $E = 0$. The results of this approximation for the reference diode are also shown in Figures 8 and 9.

It is unfortunate that this simple approach is not sufficient to achieve solutions to diode problems under bias. The foregoing approximation is always made first, but it must soon be followed by the neglect of one carrier type and the assumption that minority-carrier concentrations in bulk regions are always negligible compared to majority-carrier concentrations.

2.3.1.3. Computer Solution for No-bias Solution. During the previous year's research (Reference 1), the reference diode was run in an open-circuit configuration. One of the problems encountered was that the solution stabilized in time at a nonthermal equilibrium carrier-density profile. The improved calculation methods, including the extra precision of the CDC-6600 computer and the automatic time-step and remeshing procedures, have solved this problem and the eventual solution is effectively at thermal equilibrium. The most rigorous tests of this fact are that the final product of carrier densities, $n_\infty p_\infty$, must equal N_0^2 throughout the structure. Equivalently, the carrier densities and electric field must agree with the values calculated by the analytic solution for the equilibrium zero-bias diode. Figures 8 and 9 illustrate the comparison with the asymptotic

computer solution for a run with no bias and an external circuit resistance of 10^3 ohms. The electric field agrees within the accuracy of the plotting as does the total voltage. The carrier density product near the junction appears to fall consistently low by a factor of 2. A similar run with an external resistance of 10^6 ohms produced an electron-hole density product which was low by a factor of 1.3, again with an accurate electric field. This error is possibly due to the large time steps at the end of the problem or is a consequence of the numerical methods used, but it is not serious. As a matter of fact, calculating within a factor of 2 carrier-density profile, which varies by a factor of 10^{11} , is a remarkable achievement.

The time dependencies of the diode voltage for an external resistance of 10^3 and 10^6 ohms (the latter is essentially an open circuit) are shown in Figure 10. These and all other curves will describe a transient following a pulsed injection of 10^{17} carrier pairs/cm³. The long relaxation time with the high-resistance circuit was at first thought to be due to an error in the code. Similar behavior had previously been observed experimentally, on a somewhat shorter time scale, but had been ascribed to unexpectedly large circuit capacitance. However, the circuit capacitance is not included in the code at present. Further investigation revealed that this behavior is a true consequence of the equations being solved. Figure 9 also shows the distribution of excess carriers in the depletion layer at 252 μ sec. In the lower impedance circuit, relaxation was complete at this time. Noting the logarithmic scale of the plot in Figure 9, it can be seen that the excess concentration of majority carriers (electrons) on the N side of the junction is much greater than the excess minority-carrier concentration. The effect of the resultant space-charge distribution on the electric field is shown in Figure 8. It can be shown from a numerical analysis that this configuration is relatively stable to a net carrier transport when the total current must be small and must relax primarily by carrier recombination.

The recombination rate

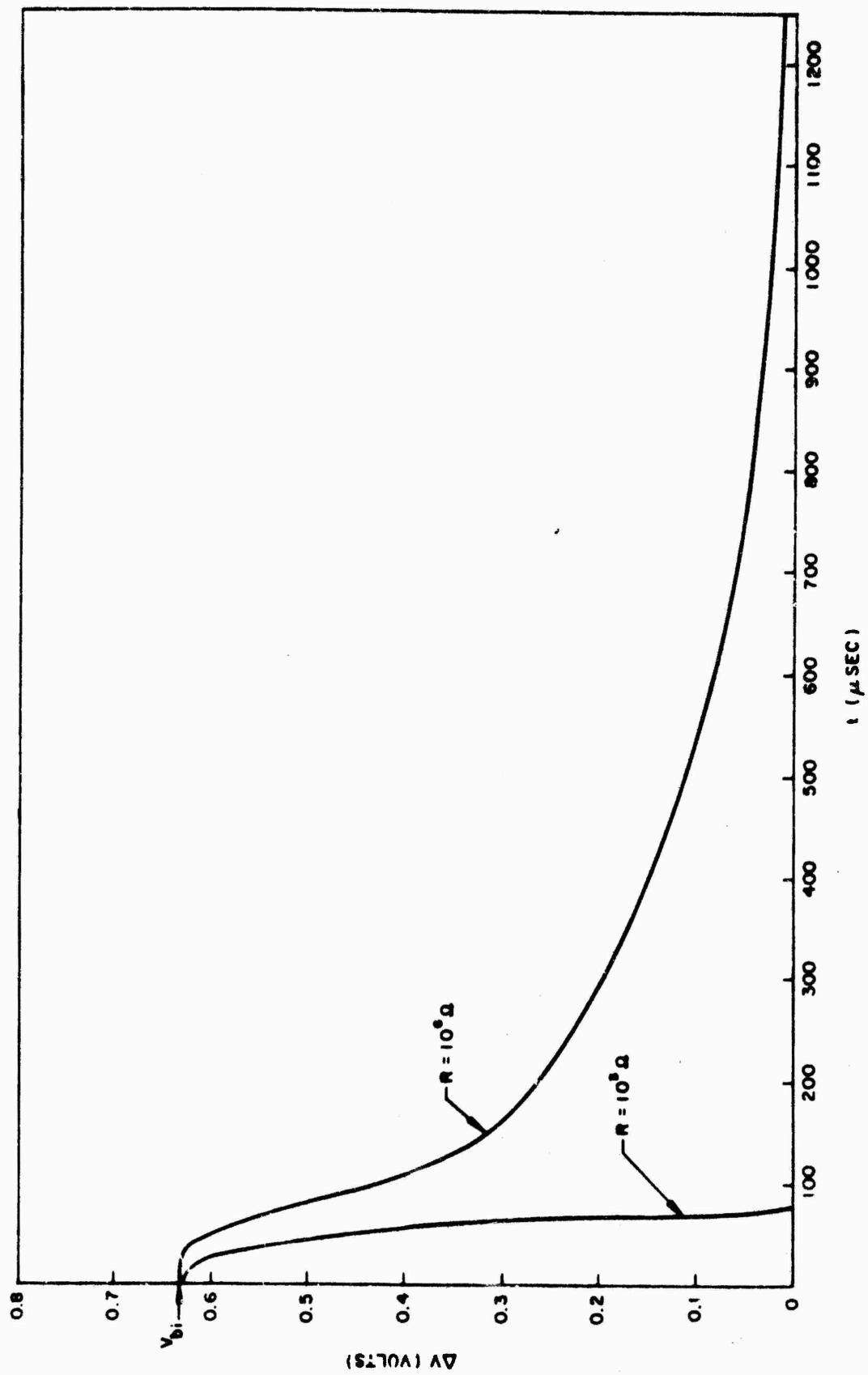


Figure 10. Zener-bias diode voltage vs time

$$R = \frac{n_p - n_0^2}{\tau_{p0}(n + n^1) + \tau_{n0}(p + p^1)}$$

In the n region holding most of the excess carriers, $n \gg p + p^1$, n^1 and $np \gg n_0^2$. Since τ_{p0} and usually τ_{n0} do not differ by more than a factor of 10, we can approximate

$$R \approx \frac{np}{\tau_{p0}n} = \frac{p}{\tau_{p0}}$$

Hence, the mean lifetime of a minority carrier is τ_{p0} . However, the rate of majority-carrier removal is equal to the rate of minority-carrier removal. Hence, the mean life of a majority carrier, defined as $\tau_{maj} = n/R$, is

$$\tau_{maj} = \tau_{p0}(n/p)$$

and is increased by the factor n/p . In the case shown in Figure 9 the factor n/p has values up to and beyond 10^5 in the region of interest.

The physical reason for this anomalous lifetime is that all the available recombination centers are already occupied by majority carriers and hence are unavailable for recombination until a minority carrier is captured. At the same time, the transport of minority carriers to this region from the other side of the junction is inhibited by the requirement for the current to remain small.

In experiments with actual diodes, such long decay times are not usually observed, or they have been attributed to circuit capacitance. In the example shown, the latter portion of the decay fits an exponential curve very well, as shown in Figure 11, with $\tau = 350 \mu\text{sec}$. If this were attributed to a shunt circuit capacitance, $C = 350 \text{ pF}$. This value, although large compared to the stray capacitance in the better test circuits, could escape notice if an appreciable length of coaxial cable were attached to the diode. This point will be discussed further in Section 3.3.

It should be added that the excess minority carriers shown at the edges of the plot in Figure 9 gradually decrease toward the ends of the diode

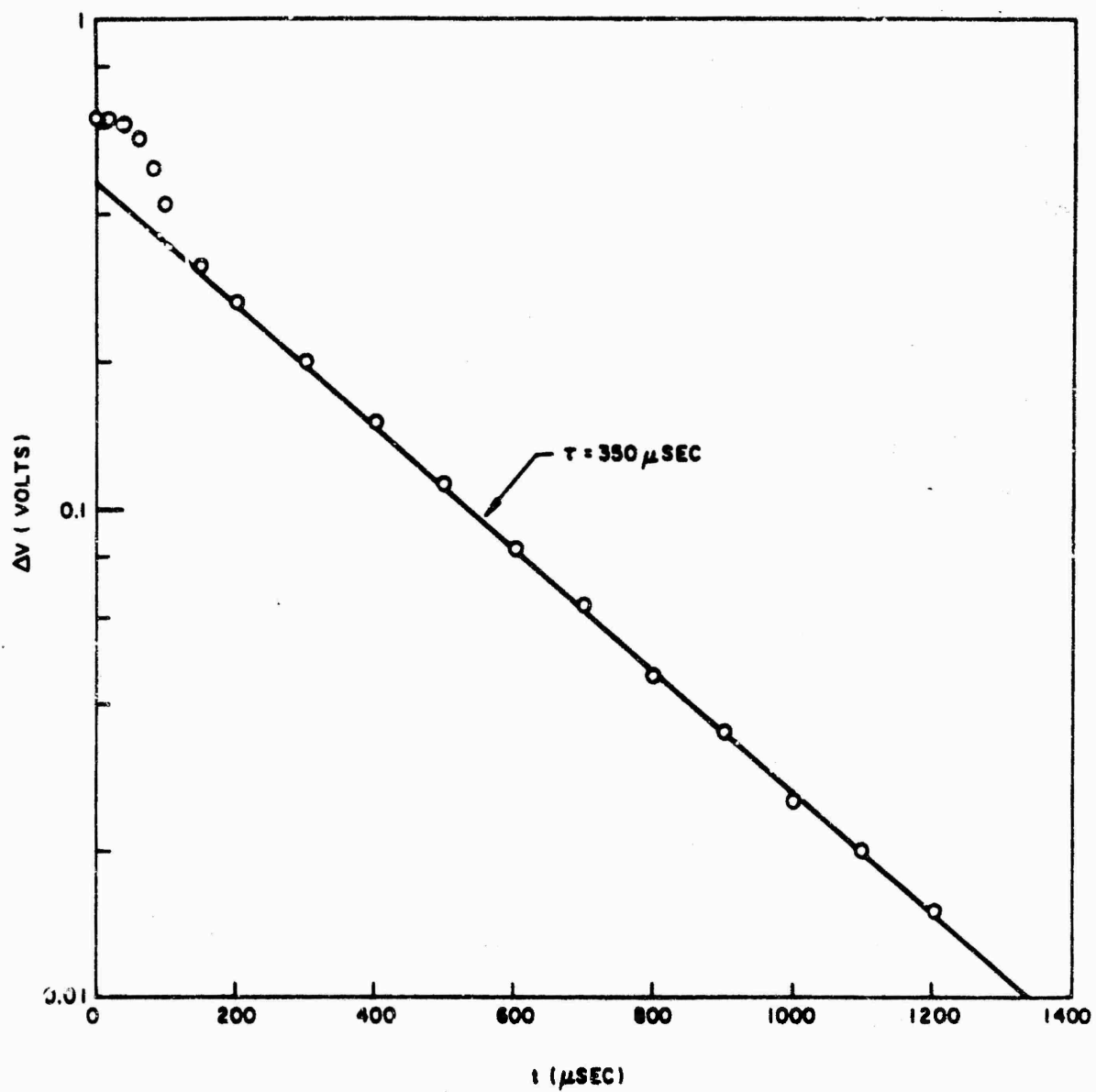


Figure 11. Diode voltage decay, $R = 10^6$ ohms

and recombination is complete at far distances from the junction, as expected. It is only in the depletion layer that carriers survive so long. However, these few carriers have a determining effect on the electric field in the depletion region and hence the diode voltage.

One unique feature of these calculations is that they present a microscopic picture of the carrier behavior in the diode. The usefulness of this information has been demonstrated in the foregoing discussion. Other examples will be apparent in subsequent sections.

2.3.1.4. Computer Solution for Forward Bias. In a diode under bias it is not possible to reduce even the equilibrium mathematical problem to a single differential equation as illustrated in Section 2.3.1.1 for the unbiased diode. However, the validity and accuracy of the asymptotic computer solution have been demonstrated in Section 2.3.1.3, and further comparisons with approximate formulations are probably unnecessary.

A simple model of ionization effects on a forward-biased diode predicts that the forward voltage drop should increase on irradiation at constant current or the forward current should decrease at constant voltage. This theory, which assumes that all the voltage drop is across the junction (no significant bulk resistance), bases the prediction on the fact that the extra diffusion current due to ionization-induced carriers flows toward and across the junction in the reverse direction. Another way of expressing this conclusion is to say that the electric field of a normal junction can be represented as a battery tending to push current in the forward direction. This battery is opposed in thermal equilibrium by an equal and opposite battery representing the contact potentials. If the junction battery voltage is decreased by radiation, the contact potentials are effective in decreasing the diode current.

The solution for the change in forward voltage shown in Figure 12 appears to be anomalous, since at first the forward voltage drop decreases and is then followed at later times by the expected increase. However, upon examination of the junction electric field in Figure 13, the expected decrease

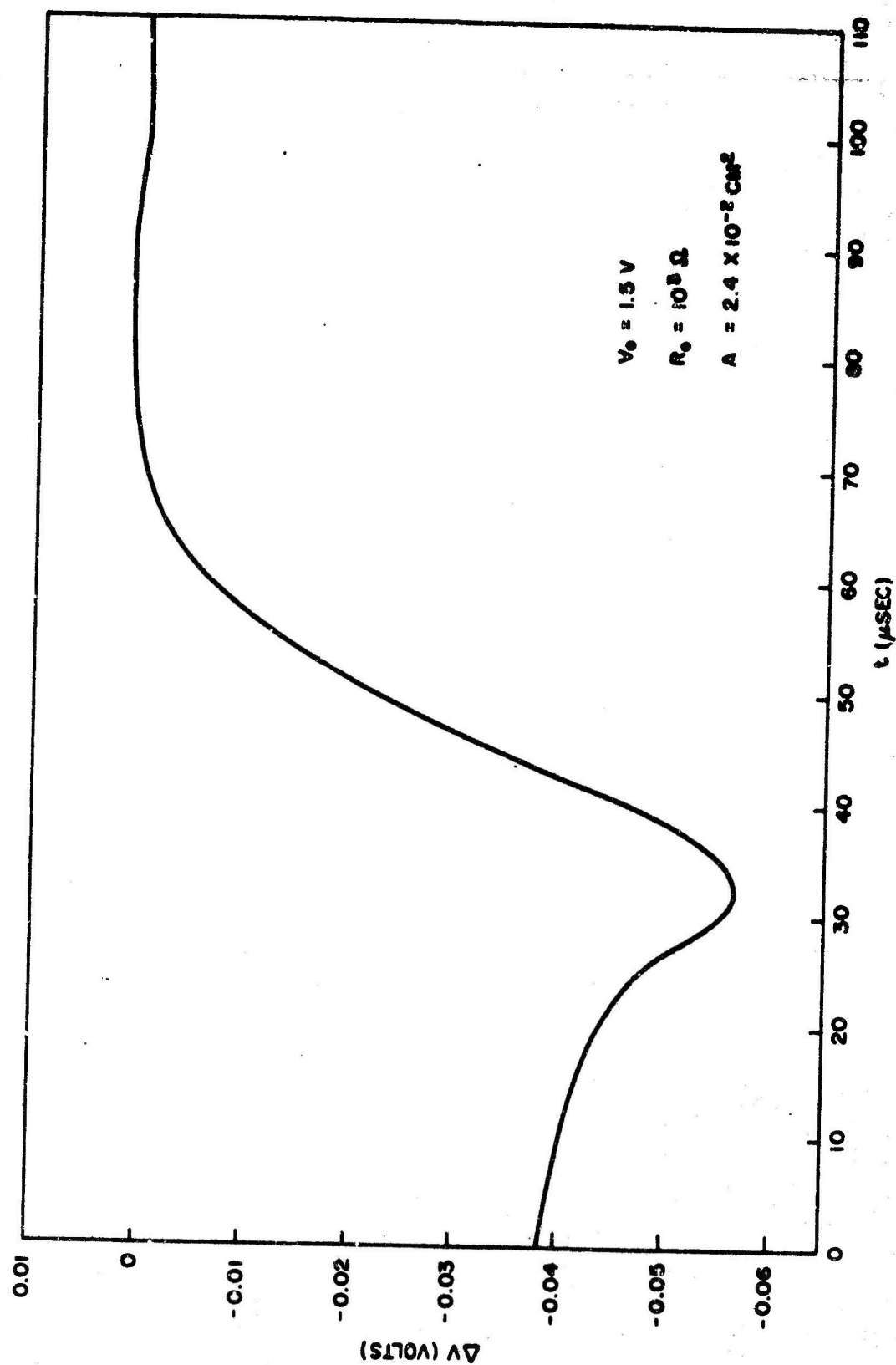


Figure 12. Forward-biased diode voltage charge

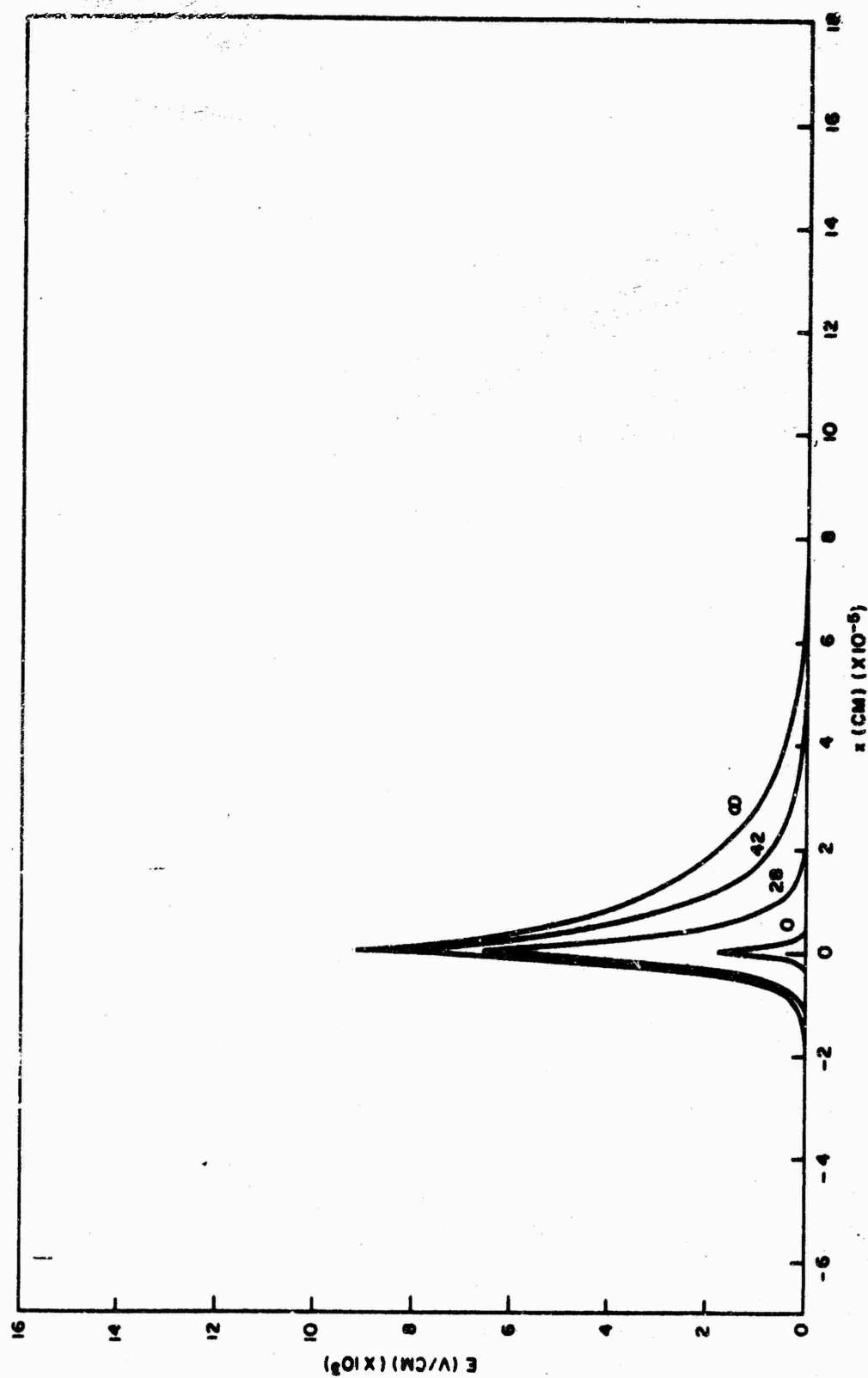


Figure 13. Forward-biased diode electric field (numbers are time, in microseconds, after pulse)

is found to be due to irradiation. The explanation is that at early times for this high ionization dose (10^{17} carriers/cm³), the increased conductivity of the bulk material has decreased the bulk voltage drop by more than the increase due to the unbalanced contact potentials. The decrease during the first 30 μ sec is not understood; it could be due to selection of inaccurate initial conditions. A similar behavior in the solution of the 1N91 diode disappeared when the initial conditions were chosen as an accurate reproduction of the asymptotic solution plus 10^{17} carrier pairs/cm³. Note also that Figures 10 and 13 are drawn to the same scale to emphasize the large drop in internal field and junction width under forward-bias conditions.

Again it is possible to display the details of the carrier-density behavior during the decay by using the computer solution as shown in Figures 14 and 15. Note the exponential dependence of minority-carrier density on distance away from the junction (as predicted by the diffusion solution) for the equilibrium solution. Notice also during the decay that both electrons and holes are diffusing toward the junction on the N side of the junction. This behavior is a consequence of the large dose, which formed a concentration of excess carriers far exceeding even the majority-carrier concentration. Therefore, the net current on the N side is being supplied by the small electric field acting on an almost intrinsic material. The simple diode theories are unable to describe such a process.

2.3.1.5. Computer Solution for Reverse Bias. Probably the most difficult solution to achieve is the reverse-biased one, because the carrier densities vary most widely and the electric fields are the largest. As a matter of experience, care must be taken to avoid introducing negative numerical densities of carriers by the approximation procedures and round-off errors. It can be shown that the differential equations used will not evolve negative densities as long as they start with positive densities, as must be required if the equations describe physical reality. However, if negative densities were introduced, there is no obvious mechanism in the equations for eliminating them. Hence, the numerical procedures must be

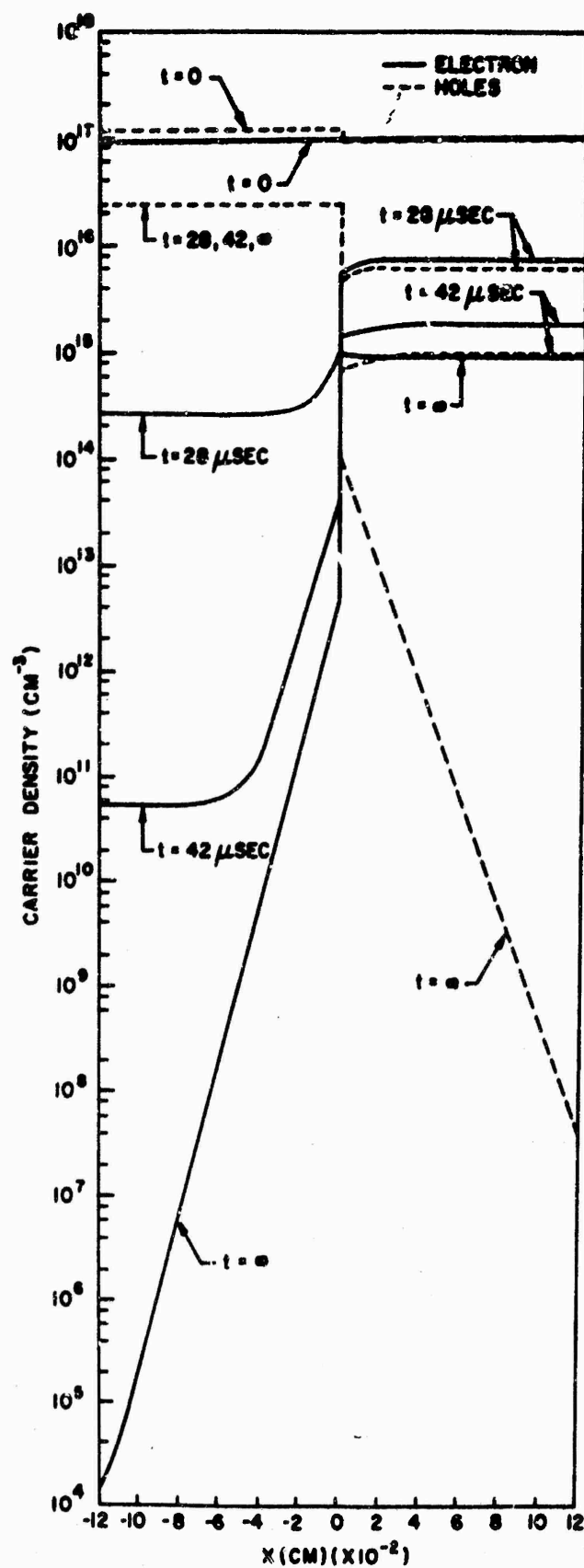


Figure 14. Forward-biased diode carrier densities

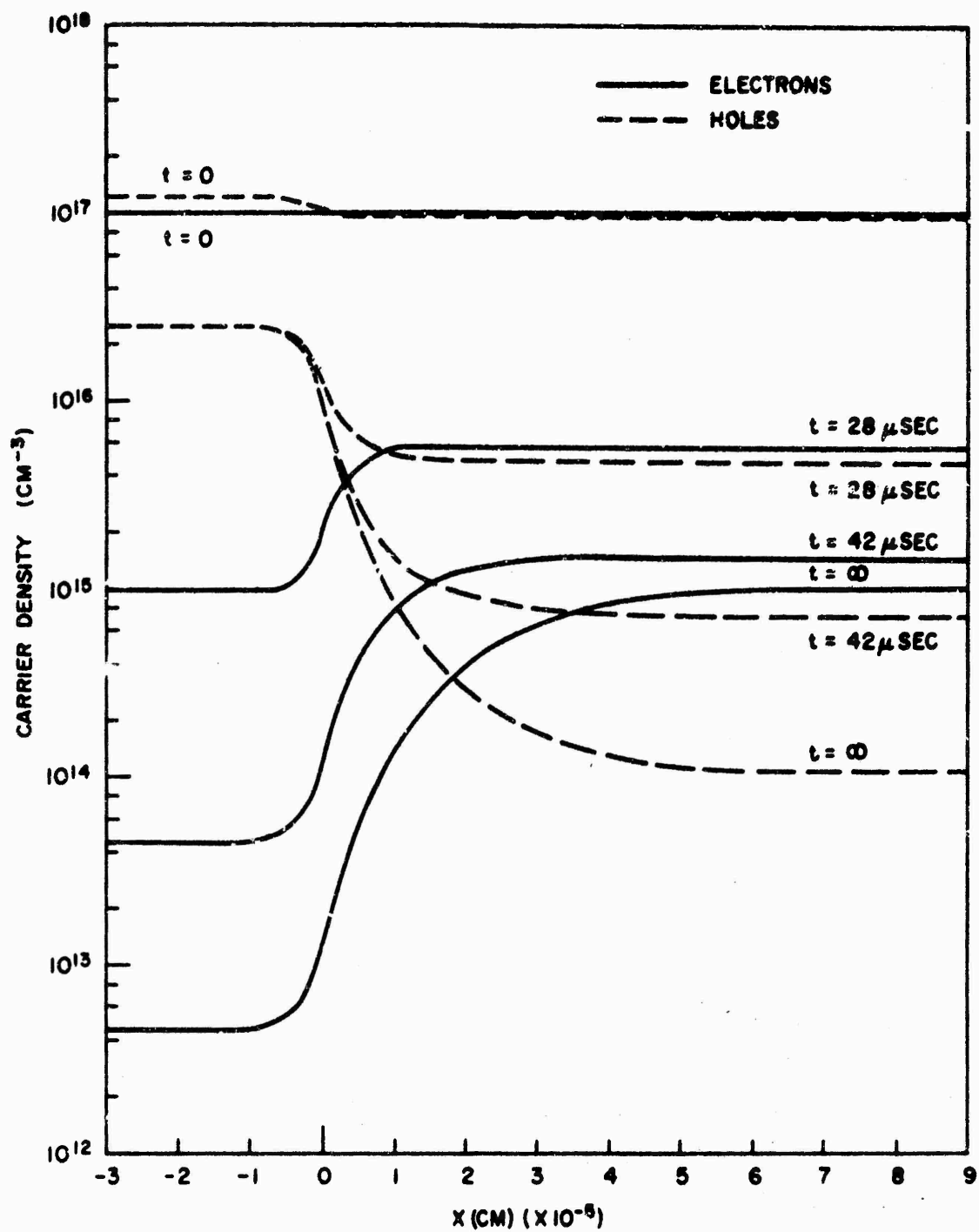


Figure 15. Forward-biased diode carrier densities near junction

accurate enough to avoid their introduction. Therefore, one of the criteria for remeshing the spatial division of the diode is the appearance of negative densities.

The reverse current as a function of time for a reverse-biased diode is shown in Figure 16. It is instructive to summarize the time steps taken by the computer in calculating this curve with associated carrier densities in the diode. Table II lists the time steps and also the diode junction voltage. Note the rapid lengthening of the time steps initially as long as the diode is in saturation. As soon as the diode starts to recover its reverse bias ($\sim 48 \mu\text{sec}$), the time step must be shortened to accommodate the rapidly changing electric field. The time step stays very small, with frequent remeshing, until the reverse voltage is fully established across the diode at $\sim 56 \mu\text{sec}$, after which the time step lengthens. In all, only 18 steps were required to get to $48 \mu\text{sec}$, whereas 135 steps and 9 remeshings were required to go from 48 to $56 \mu\text{sec}$, and only another 35 steps and one remeshing were required to complete the solution down to 0 residual current of 0.2×10^{-9} A. The need for automatic time-step and remeshing procedures is obvious for this problem.

2.3.2. Computer Results for 1N91 Diode

2.3.2.1. Zero Bias. The 1N91 germanium alloy diode was the first real diode run on the computer program. Its characteristics are described in Table III. Typical of alloy diodes, the carrier lifetime on one side of the junction (p side) is very short (10^{-9} sec was assumed) and the doping on that side is very heavy. Therefore, most of the depletion layer is in the NP region and the electric field must fall very quickly in the N region.

The results for four zero-bias runs with a low and high circuit resistance and a low and high dose are shown in Figure 17. The long decay at high resistance, discussed in Section 2.3.1.3, is again in evidence. In this case, the apparent exponential lifetime is $380 \mu\text{sec}$ at 10^3 rads and $315 \mu\text{sec}$ at 10 rads.

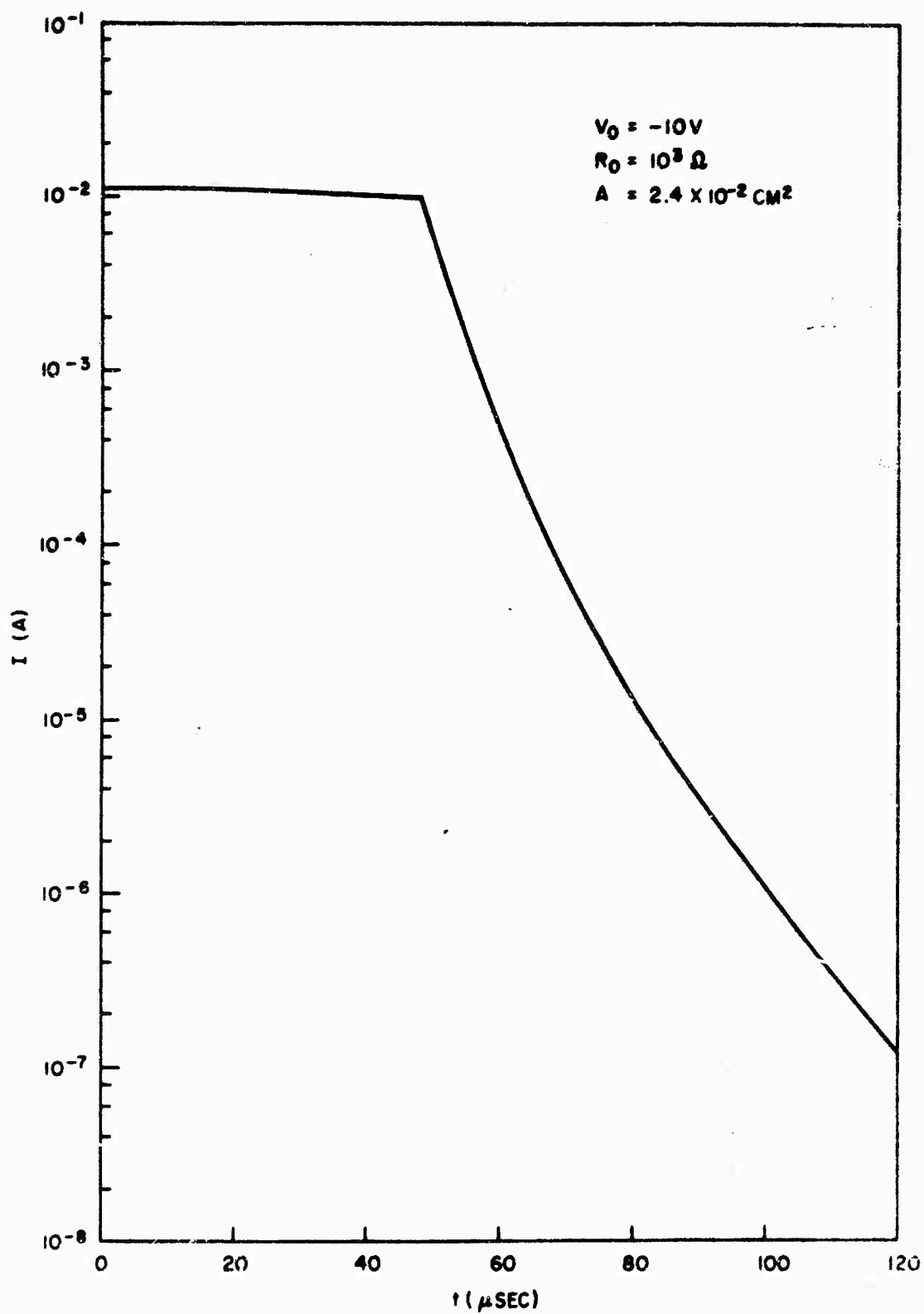


Figure 16. Reverse-biased diode current

Table II

TIME STEPS FOR REVERSE-BIASED DIODE

<u>Time</u> <u>($\times 10^{-5}$)</u>	<u>Volts</u>	<u>Time</u> <u>($\times 10^{-5}$)</u>	<u>Volts</u>	<u>Time</u> <u>($\times 10^{-5}$)</u>	<u>Volts</u>
1×10^{-9}	8.34	4.808	1.143	4.91*	4.416
1.53×10^{-8}	1.66	4.8088	1.143	4.969	5.60
8.06×10^{-8}	0.113	4.8096	1.179	(14 steps)	
9.09×10^{-7}	0.0310	4.8103	1.196	4.969*	5.594
1.39×10^{-5}	0.0309	4.811	1.215	5.06	6.886
8.22×10^{-4}	0.0309	4.81106*	1.138	(14 steps)	
1.50×10^{-2}	0.0317	4.81108	1.1409	5.06*	6.896
1.61×10^{-1}	0.0389	(5 steps)		5.218	8.209
6.39×10^{-1}	0.0616	4.819	1.367	(14 steps)	
1.24	0.104	(7 steps)		5.218*	8.215
1.85	0.177	4.829	1.778	5.579	9.557
2.94	0.331	(10 steps)		(11 steps)	
3.67	0.477	4.82928*	1.810	5.579*	9.554
4.03	0.580	4.8293	1.808	6.68	10.51
4.29	0.679	(4 steps)		(14 steps)	
4.53	0.794	4.832	1.901	9.57	10.63
4.77	0.961	(2 steps)		(7 steps)	
4.795	1.013	4.847	2.48	9.57*	10.63
4.803	1.07	(8 steps)		9.79	10.63
4.804	1.08	4.847*	2.45	(6 steps)	
4.806	1.106	4.876	3.38	10.9	10.63
4.807	1.122	(14 steps)		12.0	10.63
		4.876*	3.39	13.1	10.63
		4.91	4.41	14.3	10.63
		(14 steps)		15.4	10.63
				16.5	10.63
				17.7	10.63

* Indicates points at which remeshing was required.

Table III

1N91 Ge ALLOY DIODE PARAMETERS

$N_p = -3.4 \times 10^{17}/\text{cm}^3$	$\tau_n = 50 \times 10^{-6} \text{ sec}$
$N_p = 5.19 \times 10^{13}/\text{cm}^3$	$p_{0p} = 3.4 \times 10^{17}/\text{cm}^3$
$D_n = 95 \text{ cm}^2/\text{sec}$	$n_{0p} = 1.694 \times 10^9/\text{cm}^3$
$D_p = 45.5 \text{ cm}^2/\text{sec}$	$n_{0n} = 6.13 \times 10^{13}/\text{cm}^3$
$\mu_n = 3800 \text{ cm}^2/\text{V-sec}$	$p_{0n} = .94 \times 10^{13}/\text{cm}^3$
$\mu_p = 1820 \text{ cm}^2/\text{V-sec}$	$K = 1.78 \times 10^{-11} (K = 16)$
Length of p region = 10^{-2} cm	$n' = 2.4 \times 10^{14}/\text{cm}^3$
Length of n region = $3 \times 10^{-2} \text{ cm}$	$p' = 2.4 \times 10^{14}/\text{cm}^3$
$\tau_p = 10^{-9} \text{ sec}$	Area of junction = 0.023 cm^2

Unfortunately, the assumed characteristics of the 1N91 diode include a very long lifetime in the N region of 50 μsec . A value of 5 to 10 μsec would probably have been more reasonable, particularly for units which had been abused by the high-energy electron beam. This error was discovered too late to be corrected in the computer runs. Since most of the late decay, especially at low impedance, should scale proportionately to τ , it would not be surprising if the experimental decay times were shorter than the predicted ones by a factor of 5 to 10.

It is interesting to note that in the $R_0 = 100\text{-ohm}$ curves in Figure 17, there is an apparent straight section, as predicted by the simple single-carrier theory. The slope also agrees with the theoretical value of $dv/dt = kT/q\tau$.

The relaxation of carrier densities near the junction is illustrated in Figure 18. Initially, there is a rapid drop in carrier density on the short-lifetime P side. This drop is sufficient to cause some carriers from $\sim 2 \times 10^{-3} \text{ cm}$ of the N side to diffuse across the junction in pairs and be

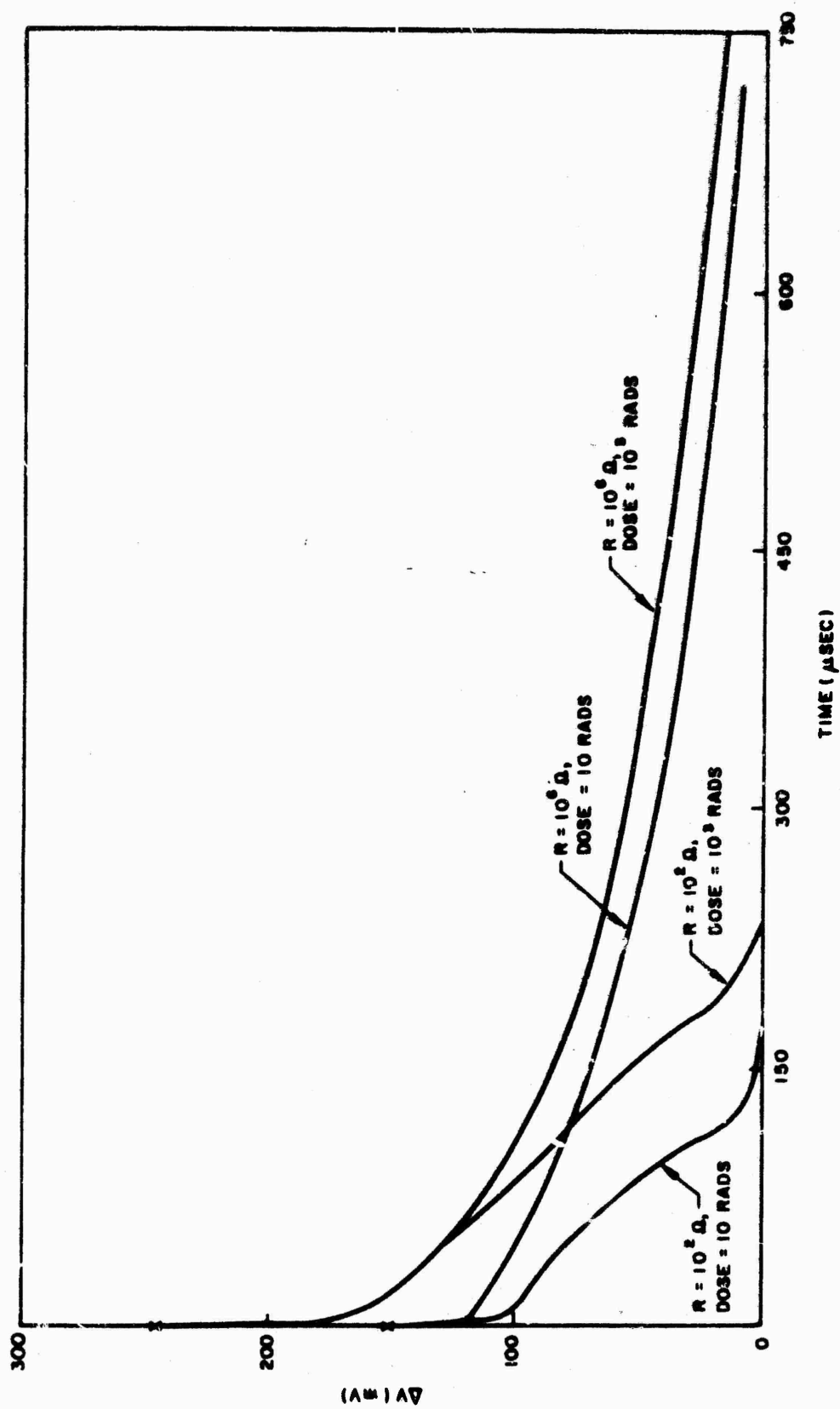


Figure 17. No bias LN91 Ge alloy diode

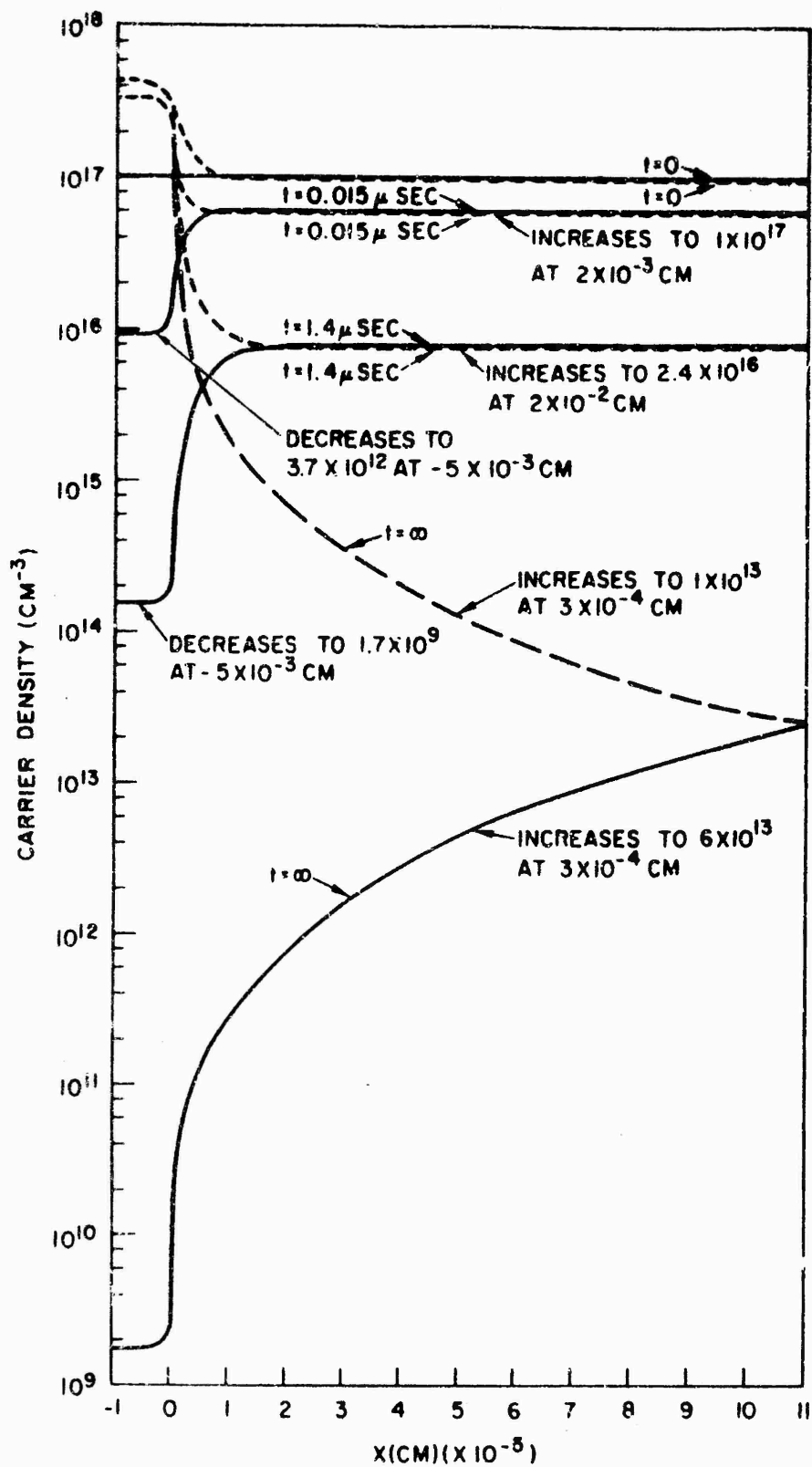


Figure 18. Zero-bias 1N91 diode carrier densities, $R_0 = 10^3$ ohms, dose = 10^3 rads

recombined on the P side. This pair diffusion is responsible for a significant portion of the carrier removal, even at $14 \mu\text{sec}$, and is probably responsible for the rapid drop in voltage at early times in Figure 17. Only at later times does carrier recombination predominate, resulting in the predicted linear curve. It is again clear that this ambipolar diffusion toward the junction cannot be analyzed with the simple diode models.

2.3.2.2. Forward Bias. The relaxation of the diode voltage in a forward-biased diode is shown in Figure 19. To get the results shown, the problem was run from a nominal -1 sec to zero time from a set of inaccurate initial conditions. At zero time, the radiation-induced excess carriers were introduced and the subsequent relaxation followed. This procedure was necessary because, contrary to the zero-bias or reverse-biased cases, the assumed initial carrier distribution has a marked effect on the answer. The reason is presumably that under forward bias the diffusion layers around the junction contain a large number of extra minority carriers and their redistribution produces voltages comparable to the effects of radiation-induced carriers.

The signal magnitudes, with the lower current effect being larger, are in agreement with the simple theory (Reference 1).

The same two problems were also run with an initial dose of 10^3 rads. Unfortunately, the initial conditions were not accurate. However, the radiation-induced excess-carrier concentrations were much larger, so the solution should be less sensitive to errors in the carrier distribution due to current flow. The results are shown in Figure 20. They are quantitatively reasonable and probably trustworthy in spite of the initial conditions.

2.3.2.3. Reverse Bias. For most of the data presented so far, the radiation-induced excess carriers were introduced instantaneously. One run on a reverse-biased 1N91 was performed with a radiation pulse 10^{-13} sec wide delivered to a diode which had achieved equilibrium. The result is shown in Figure 21. Note that the current continues to grow for 10^{-9} sec, probably because of diffusion toward the junction of electrons from the P side.

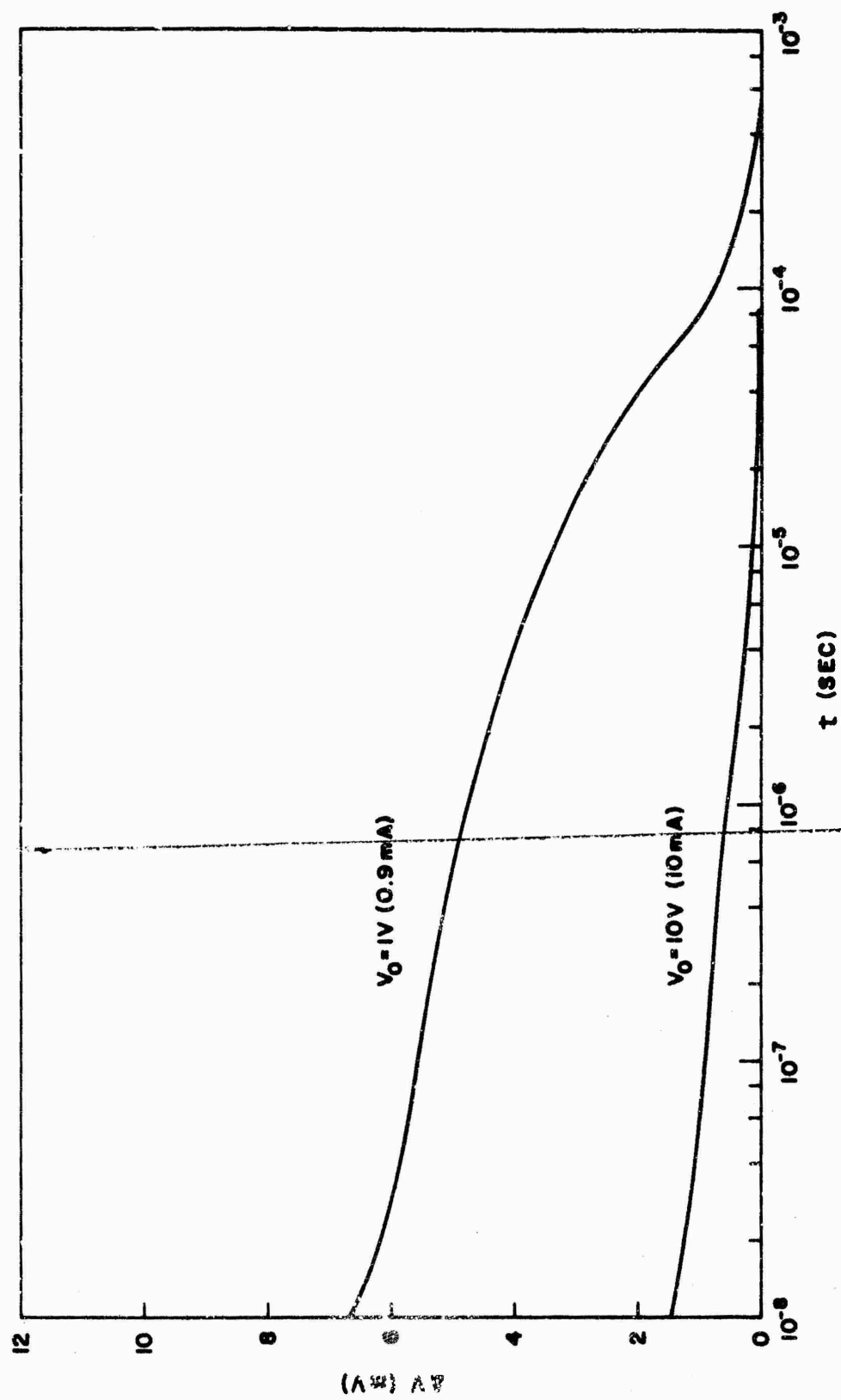


Figure 19. Forward-biased 1N91 diode, $R_0 = 10^3$ ohms, dose = 1 rad

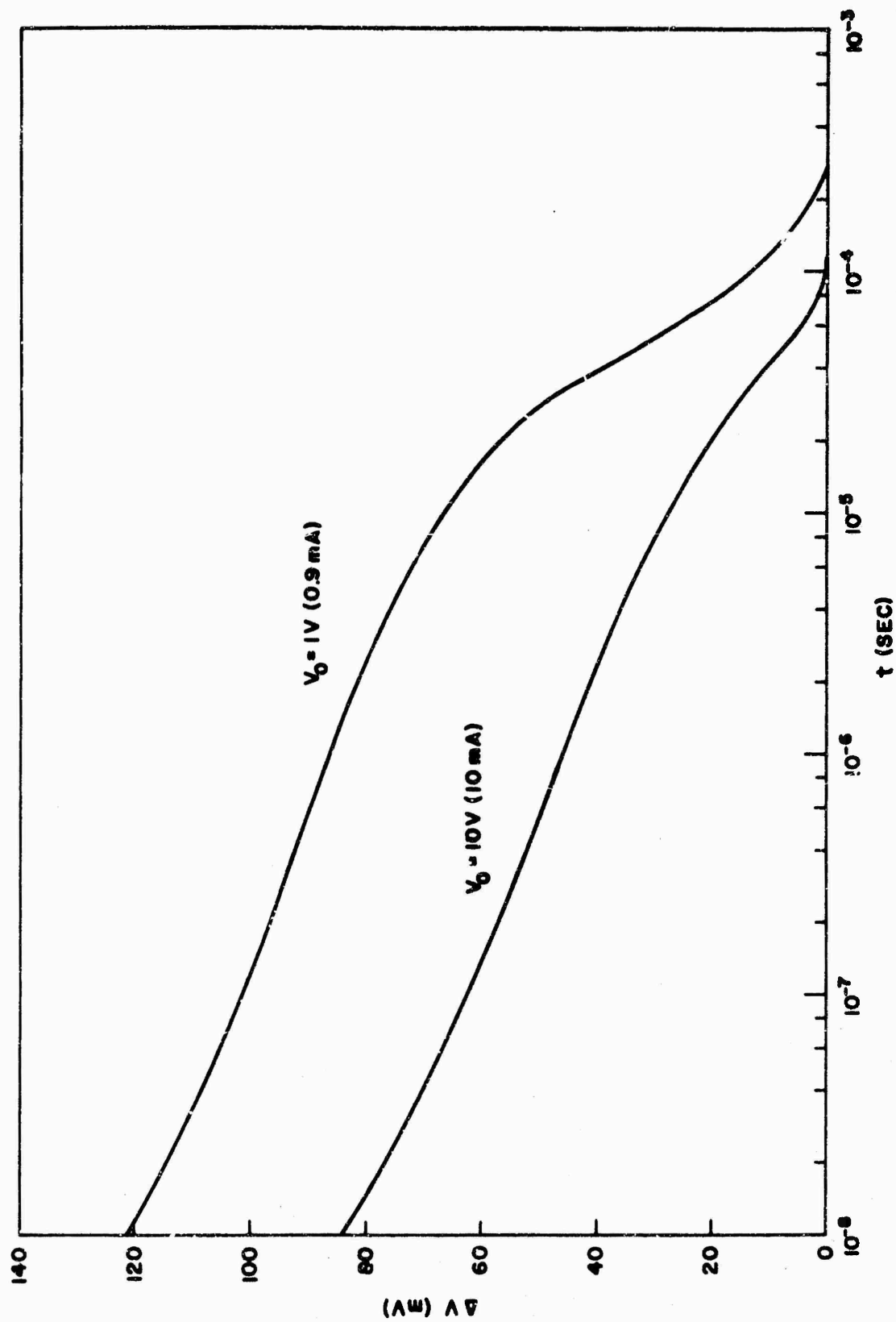


Figure 20. Forward-biased IN91 diode, $R_0 = 10^3$ ohms, dose = 10^3 rads

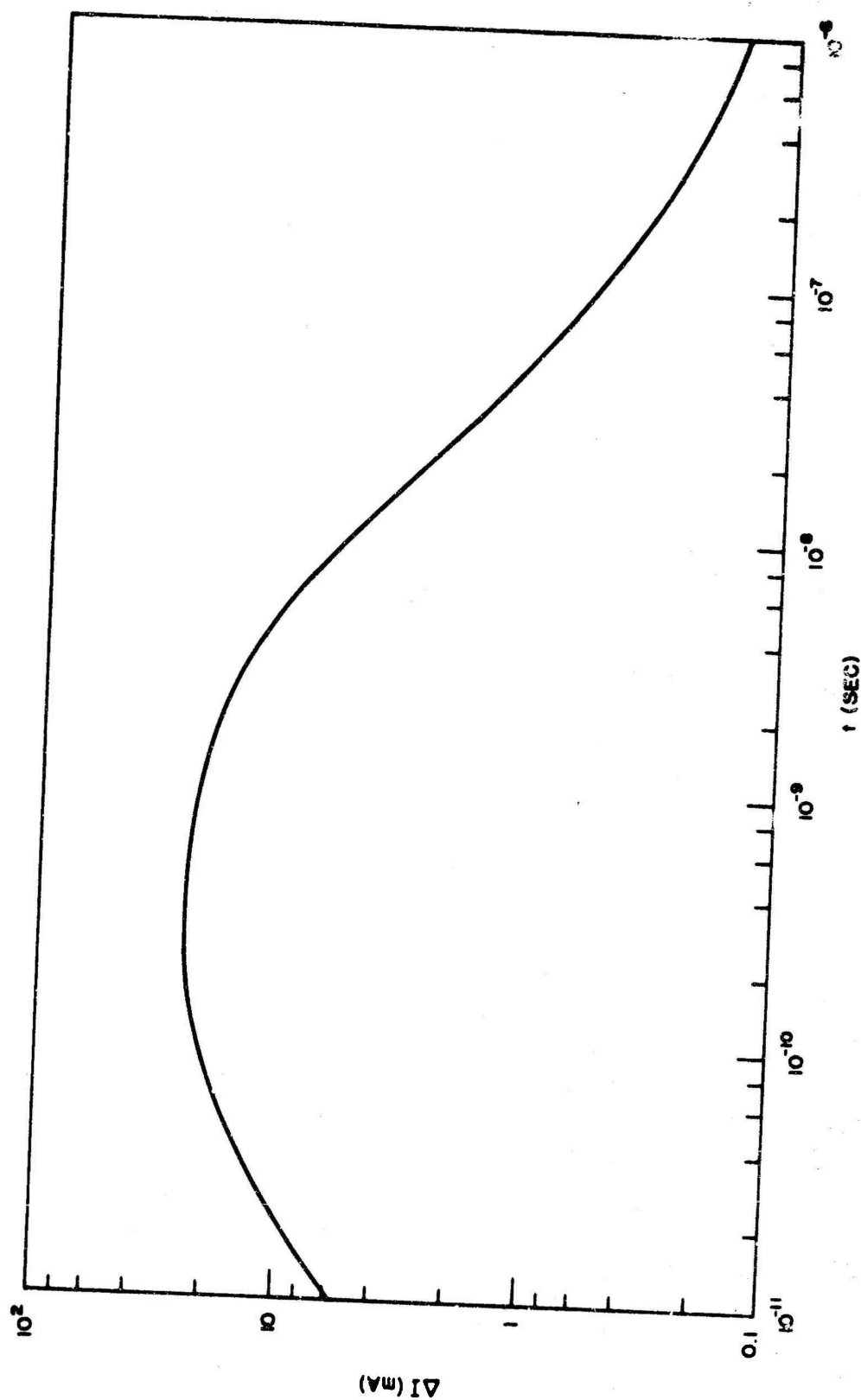


Figure 21. Reverse-biased diode current due to 0.1 rad in 10^{-13} sec, $V_0 = -10$ V, $R_0 = 10^2$ ohms

The shape and amplitude of the decay curve beyond 10^{-8} sec agrees well with the results of an instantaneous-generation run.

Figure 22 shows that with a dose of 10 rads the diode is predicted to go into saturation very briefly ($0.15 \mu\text{sec}$). At 10^3 rads, the saturation time is slightly greater than a carrier lifetime (assumed to be $50 \mu\text{sec}$). The recovery process in both cases agrees well with typical experimental shapes.

2.3.3. Computer Results for Reference Transistor

A reference transistor was formulated to check out the computer program. Its characteristics are described in Table IV. It was run in

Table IV

REFERENCE SILICON TRANSISTOR PARAMETERS

$n_0 = 1.4 \times 10^{10} / \text{cm}^3$	$n'_e = 0$
$\mu_n = 1350 \text{ cm}^2 / \text{V-sec}$	$p'_e = 0$
$\mu_p = 480 \text{ cm}^2 / \text{V-sec}$	$n'_b = 0$
$N_e = -60 \times 10^{13} / \text{cm}^3$	$p'_b = 0$
$N_b = 0.7 \times 10^{17} / \text{cm}^3$	$n'_c = 0$
$N_c = -0.2 \times 10^{17} / \text{cm}^3$	$p'_c = 0$
$kT = 0.025 \text{ eV}$	$V_{eb} = 10 \text{ V}$
$\kappa = 1.33 \times 10^{-11} (\text{K} = 12)$	$V_{ec} = 25 \text{ V}$
$\tau_{ne} = 10^{-7} \text{ sec}$	$R_{eb} = 10^5 \text{ ohms}$
$\tau_{pe} = 10^{-9} \text{ sec}$	$R_{ec} = 10^3 \text{ ohms}$
$\tau_{nb} = 10^{-7} \text{ sec}$	$a_0 = 10^{-3} \text{ cm}^2$
$\tau_{pb} = 10^{-7} \text{ sec}$	$x_e = -10^{-2} \text{ cm}$
$\tau_{nc} = 10^{-7} \text{ sec}$	$x_{eb} = -1.5 \times 10^{-4} \text{ cm}$
$\tau_{pc} = 10^{-6} \text{ sec}$	$x_{bc} = 1.5 \times 10^{-4} \text{ cm}$
	$x_c = 10^{-2} \text{ cm}$

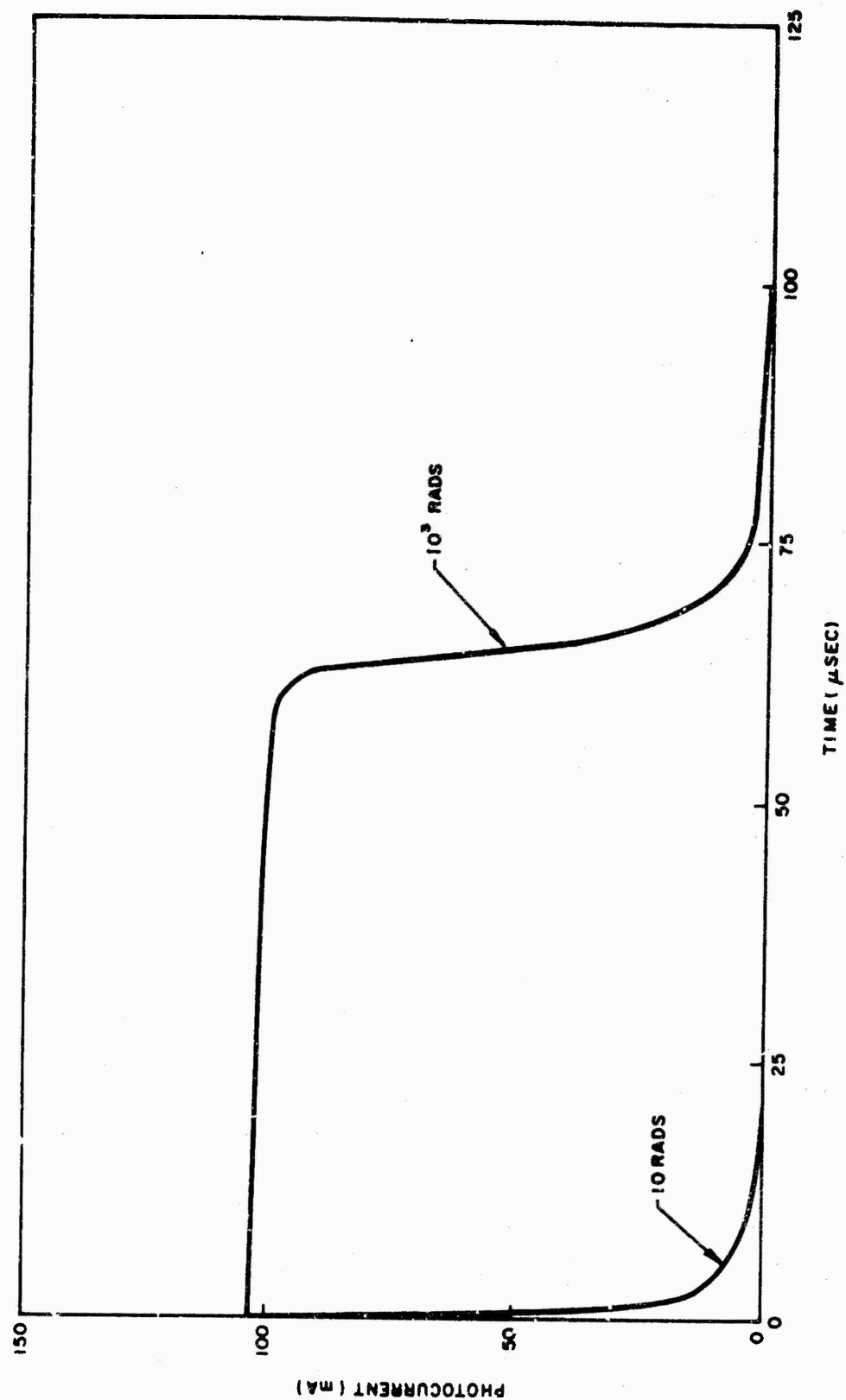


Figure 22. Reverse-biased 1N91 diode, $V_0 = -10$ V, $R_0 = 10^2$ ohms

a grounded emitter configuration with a 10^5 -ohm base resistor and a 10^3 -ohm collector resistor. The collector current following injection of 10^{17} carrier pairs/cm³ is shown in Figure 23. Saturation occurs for almost 1 μ sec and is then followed by recovery with a lifetime of ~ 1 μ sec.

A computer run was performed for the same transistor with the NET-1 computer code incorporating the Ebers-Moll Model transistor. The agreement shown in Figure 23 may be somewhat fortuitous, because the response in the Ebers-Moll model depends slightly on the assumption of a finite radiation-pulse width. Nevertheless, it is clear that the duration of saturation and shape of the recovery phase is similar in the two predictions.

2.3.4. Computer Results for 2N396A Transistor

The 2N396A PNP germanium alloy transistor was the first real transistor chosen for the computer run because of its similarity in construction, doping, and lifetime to the 1N91 diode. The properties of this transistor are given in Table V. As it is an alloy, the collector and emitter dopings are high and lifetimes are short.

There are two limiting cases of a transistor bias circuit: open emitter and open base, both of which were run on the computer code. For the open-emitter problem, a 100-ohm load resistor and a -10 V bias were assumed to be in the base-collector circuit. In this configuration of an alloy device, most of the effective excess carriers are generated in the base and base-collector depletion layer because the collector diffusion length is very short. Therefore, since the diffusion time across the base is also short, the excess carriers will quickly be transferred to the external circuit and the transistor will recover quickly. The computer verified this behavior of the primary photocurrent for a 1-rad radiation pulse, as shown in Figure 24.

When the same transistor is connected in a common-emitter circuit with a large resistance in the base circuit, the current is expected to be prolonged. This means that the minority carriers (electrons) injected into

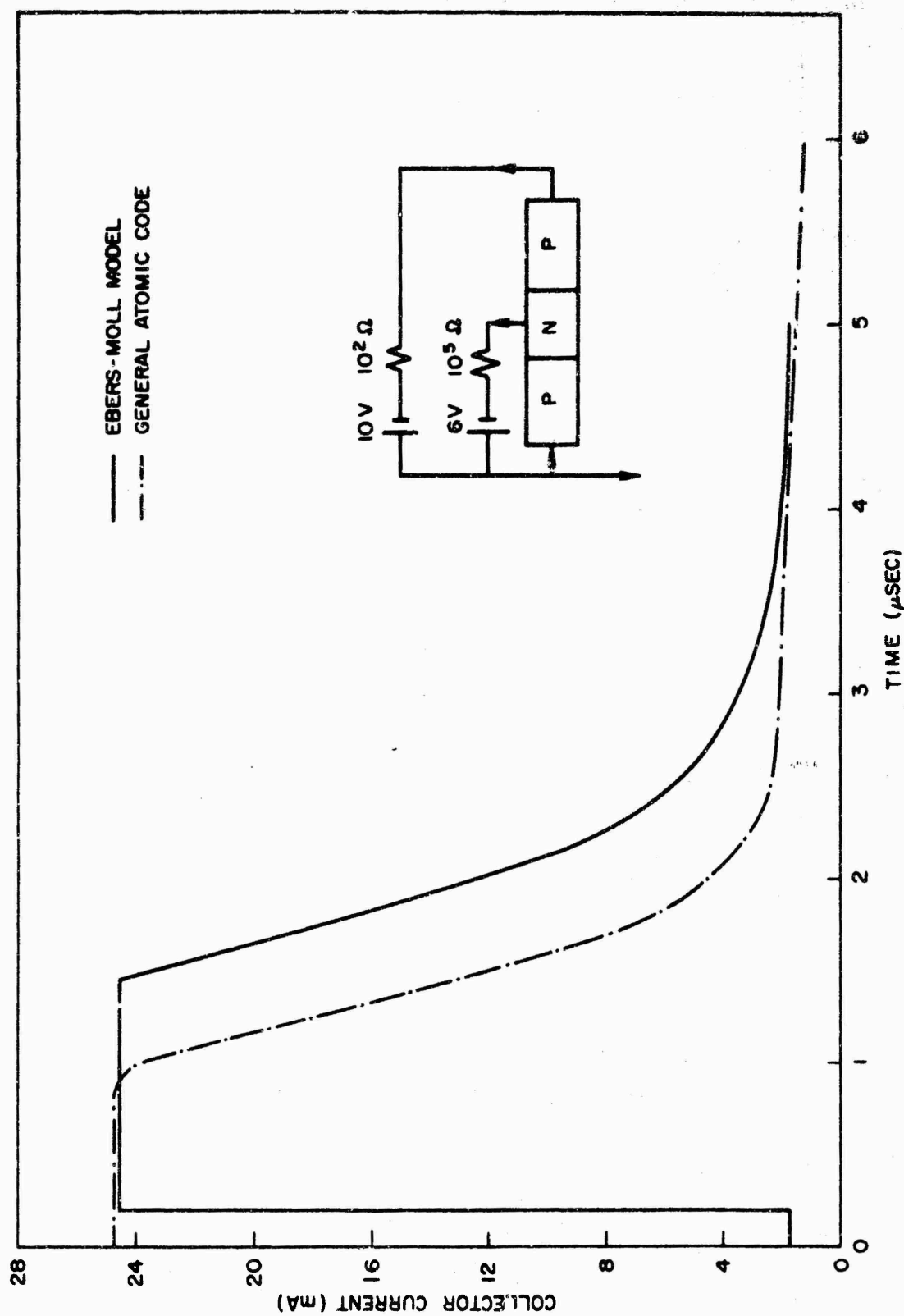


Figure 23. Collector current of reference transistor

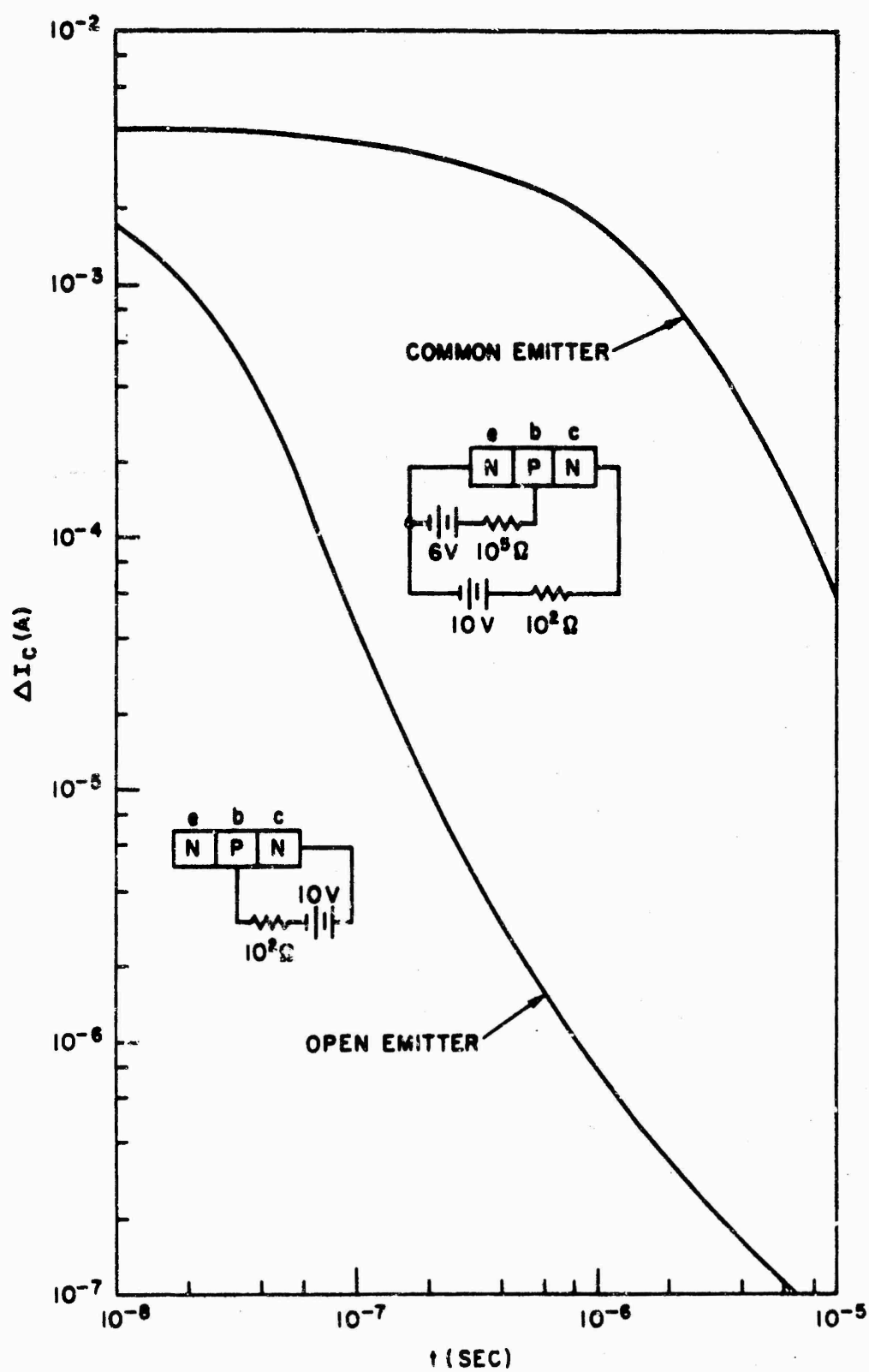


Figure 24. Transistor 2N396A primary and secondary photocurrent, dose = 1 rad

Table V

2N396A TRANSISTOR PARAMETERS

$n_0 = 2.4 \times 10^{13} / \text{cm}^3$	$\tau_{pc} = 10^{-9} \text{ sec}$
$\mu_n = 3800 \text{ cm}^2 / \text{V-sec}$	$n'_e = 2.4 \times 10^{13} / \text{cm}^3$
$\mu_p = 1820 \text{ cm}^2 / \text{V-sec}$	$p'_e = 2.4 \times 10^{13} / \text{cm}^3$
$N_e = -10^{18} / \text{cm}^3$	$n'_b = 2.4 \times 10^{13} / \text{cm}^3$
$N_b = 10^{15} / \text{cm}^3$	$p'_b = 2.4 \times 10^{13} / \text{cm}^3$
$N_c = -10^{18} / \text{cm}^3$	$n'_c = 2.4 \times 10^{13} / \text{cm}^3$
$kT = 0.025 \text{ eV}$	$p'_c = 2.4 \times 10^{13} / \text{cm}^3$
$\kappa = 1.78 \times 10^{-11} \text{ (K = 16)}$	$a_0 = 0.001 \text{ cm}^2$
$\tau_{ne} = 10^{-8} \text{ sec}$	$x_e = -1.4 \times 10^{-3} \text{ cm}$
$\tau_{pe} = 10^{-9} \text{ sec}$	$x_{eb} = -0.9 \times 10^{-3} \text{ cm}$
$\tau_{nb} = 4.5 \times 10^{-6} \text{ sec}$	$x_{bc} = +0.9 \times 10^{-3} \text{ cm}$
$\tau_{pb} = 4.5 \times 10^{-5} \text{ sec}$	$x_c = +1.4 \times 10^{-3} \text{ cm}$
$\tau_{nc} = 10^{-8} \text{ sec}$	

the base cannot flow out through the base lead because they would develop too large a base-emitter voltage across the 10^5 -ohm base resistor. Therefore, they induce minority carriers (holes) to enter from the emitter, diffuse across the base, and exit the base at the collector junction. If the device does not saturate, the total charge delivered to the collector will be approximately h_{fe} times the majority-carrier charge injected into the base. The charge for the open-emitter case has been evaluated from the lower curve in Figure 24 to be $Q_p = 3.8 \times 10^{-4}$ coulomb. Similarly, the collector circuit has acquired $Q_s = 5.7 \times 10^{-9}$ coulomb in the common-emitter circuit. The ratio is 150.

The common-emitter current gain, h_{fe} , of this transistor should be given by (Reference 6)

$$h_{fe} = \frac{2\tau_b D}{W^2} = \frac{2 \times 4.5 \times 10^{-6} \times 95}{(1.8 \times 10^{-3})^2} = 260.$$

Considering the approximations made in the secondary-photocurrent argument, this agreement is satisfactory.

It should also be possible to estimate the magnitude of the charge flow in the open-emitter circuit. Since the charge flows out before it has a chance to recombine, it should be approximately equal to the charge of the carriers ionized in the base volume. Thus,

$$\begin{aligned} Q_p &\approx 1.6 \times 10^{-19} \text{ coulomb} \times 10^{14} \text{ carriers/cm}^3 \\ &\quad \times 10^{-3} \text{ cm}^2 \times 1.8 \times 10^{-3} \text{ cm} \\ &\approx 2.9 \times 10^{-11} \text{ coulomb}. \end{aligned}$$

Again, the agreement is very satisfactory.

2.3.5. Computer Results for High Field Effects

The effect of incorporating high field effects has been investigated using the 1N91 diode and reference diode configurations.

The electric field as a function of position in a reverse-biased 1N91 diode is shown in Figure 25. This result assumes the mobility to be constant (no velocity saturation). The sharp peak in field near the junction is not predicted by the simple diode model; it is due to the effect of the sizable mobile-carrier concentration on the heavily doped side of the junction. A finer scale presentation of this region is shown in the lower curve of Figure 26.

If the saturation of the drift velocity is introduced, the peak electric field increases, as shown in Figure 26. This follows because a decrease in carrier velocity implies that the mobile carriers are not removed from the junction by the electric field as rapidly, allowing them to build up a greater charge density. This phenomenon should be investi-

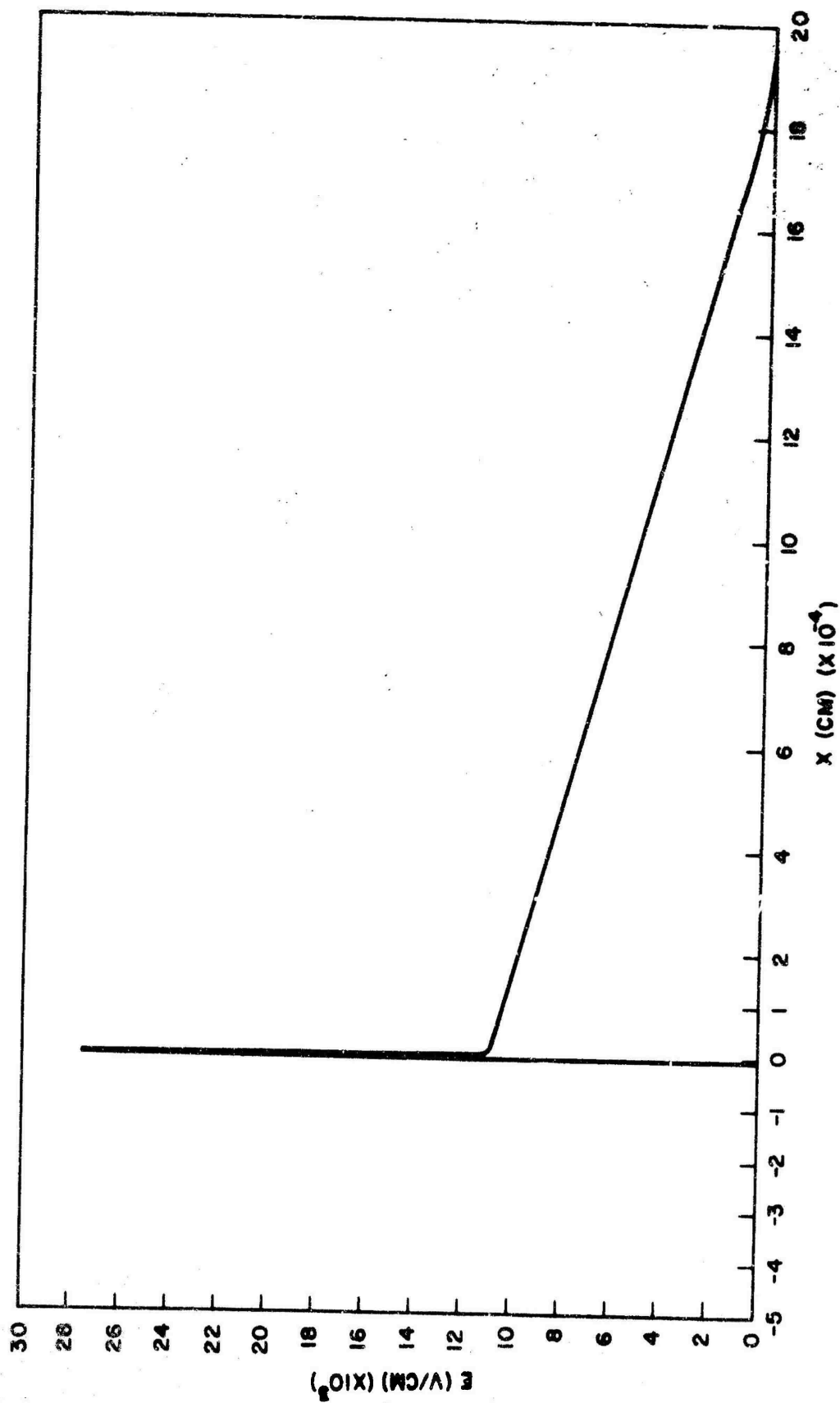


Figure 25. Electric-field profile

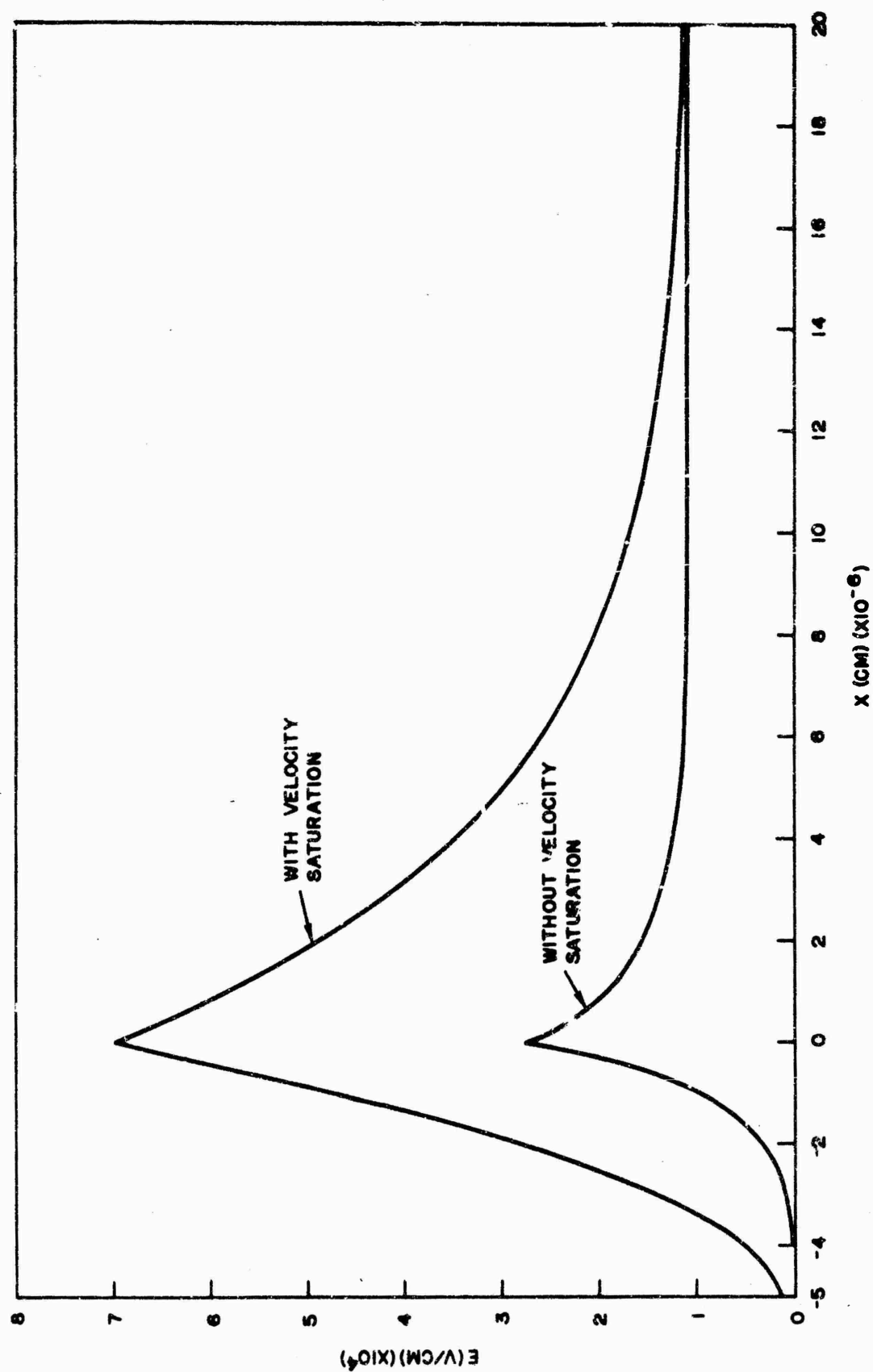


Figure 26. Electric-field profile (fine scale)

gated further, especially to evaluate the effect it may have on reverse breakdown.

The introduction of avalanche carrier generation at this voltage has no measurable effect on the electric-field profile or the reverse current, although carrier generation in the highest fields is evident in the R term of the computer printouts.

The reference diode was used to investigate avalanche in more detail. In a sense, the PND4 code takes account of avalanche in the calculation of the rate of generations of pairs of carriers. Specifically, the terms $n v_n \alpha_n(E) + p v_p \alpha_p(E)$, where v_j and α_j are, respectively, the drift velocity and the rate of generation of secondary pairs by avalanche per centimeter of drift of carriers of type j , for $j = n$ or p , occur in the formula that PND4 uses for computing the rate g of generation of pairs per cubic centimeter per second. Two algorithms for calculating α were tried. The first was

$$\begin{aligned} \alpha(E) &= e^{-P(|E|)} & \text{for } |E| > E_0, \\ \alpha(E) &= 0 & \text{for } |E| < E_0, \end{aligned}$$

where E_0 is an input threshold and p is an arbitrary quadratic function whose coefficients are input. The code performed in an entirely satisfactory manner when the parameters of the reference diode were used with $E_0 = 10^3 \text{ V cm}^{-1}$ and p was adjusted so that

$$\begin{aligned} \alpha(3 \times 10^4) &= 3 \times 10^3 \text{ cm}^{-1}, \\ \alpha(4 \times 10^4) &= 4 \times 10^4 \text{ cm}^{-1}, \\ \alpha(5 \times 10^4) &= 2 \times 10^5 \text{ cm}^{-1}, \end{aligned}$$

where the argument has as unit 1 V cm^{-1} . The second algorithm, the current version, which has a stronger theoretical basis (Reference 2), is $\alpha = c \exp(-b/E^2)$. It, too, was checked out, with the constants adjusted to give a strong effect with a reverse bias of 10 V. In the test problem for the diode code, for example, the assignments $c = 15.5 \text{ cm}^{-1}$, $b = 3 \times 10^9 \text{ V}^2 \text{ cm}^{-2}$ are made.

It has not been possible, however, to run realistic problems with a significant amount of avalanche. This fact is not very surprising because the devices that PND4 has been used to analyze would require a reverse bias of about 500 to 1000 V to produce an appreciable effect, and such biases take the device out of the regions of operation for which PND4 has so far been developed.

What happens when one runs a problem using the parameters of the reference diode and a bias of, say, -400 V with a resistance of 100 ohm, is that the time step required for convergence drops to below 10^{-12} sec. At the same time, the logarithmic derivatives of n and p become about 10^{12} sec^{-1} with perhaps 10 to 20 changes of n and p on a mesh of about 300 intervals.

There are several factors that have something to do with the observed behavior of the code in the regime in which avalanche is an important effect. Some of the more important factors are:

1. The fact that in the presence of the high electric fields required for a well-developed avalanche, the concentrations of the carriers have steeper gradients, so an extraordinary number of points are required in the spatial mesh if the distributions of carriers and fields are to be specified in sufficient detail. Increasing the number of mesh points increases the order of the system of linear equations in the quasi-linear scheme employed for solving the nonlinear difference equations, which, in turn, increases the number of figures lost through roundoff error.
2. The factor α in the avalanche term is a strong and very nonlinear function of the electric field, E . As a result, it might be necessary to calculate E much more accurately than would otherwise be the case and also a smaller time interval might be required in order to get the iterative scheme to converge.
3. The depletion layer of a reverse-biased diode that has been subjected to a heavy pulse of radiation is reestablished rather suddenly if the recombination process has reduced the concentration of excess

carriers to a certain low level. It may well be that this phenomenon is even more violent and takes place on an even shorter time scale when the bias is increased. Thus, it might be that the time steps must be shortened simply because the real time scale is shorter.

An investigation of the numerical phenomena that occur when the solution of a realistic avalanche problem is attempted has been started, but not enough has yet been done to determine which factors are the dominant ones or what it might be necessary to do in order to get around them. A good next step would be to run a realistic problem in double-precision arithmetic on a mesh of about 1000 points in order to get an accurate solution of the equations to provide a reliable reference point. Another possible tack is to run problems on more heavily doped structures, which more closely represent real avalanche diodes, so that the high fields are restricted to a smaller region near the junction.

SECTION III

EXPERIMENTAL PROGRAM

3.1. EXPERIMENTAL TECHNIQUES

The irradiation experiments used the General Atomic electron linear accelerator (Linac) as a source of 30-MeV or 5-MeV electrons. The samples were irradiated in a geometry designed to provide accurate monitoring of the beam intensity and to minimize radiation effects on the associated electronic equipment. The signals were transmitted via our standard radiation-effects amplifier system and recorded on an oscilloscope and camera at the remote control station.

3.1.1. Radiation Facility

The Linac is an L-band microwave linear accelerator with an energy range of 3 to 45 MeV and peak currents up to 700 mA. Pulse widths are variable from 0.01 to 14 μ sec with possible repetition rates varying from a single pulse to $7\frac{1}{2}$, 15, 30, 60, 120, 180, 360, or 720 pulses per second, depending on the pulse width used. Most of the irradiation work was done with single pulses. The exposure rate was varied by varying the beam current and by using scatterers of different thickness. The various pulse widths also allowed a wide range in total exposure per pulse.

The experimental setups at the linear accelerator were similar for most experiments. Figure 27 shows a typical setup. Electrons coming from the beam tube were collimated in a 3/8-in.-diameter hole in a 4-in.-long aluminum collimator. This was followed by a 0.0008-in.-thick titanium foil in an evacuated chamber used for beam monitoring. The scatterer was an aluminum plate of about 1/8 in. thickness to ensure uniform irradiation of our sample. Following the scatterer was a 2-in.-thick aluminum collimator block with a 1-in.-diameter hole. When the 1-in.-diameter hole was in line with the beam, the sample was irradiated primarily with electrons at the maximum exposure rate.

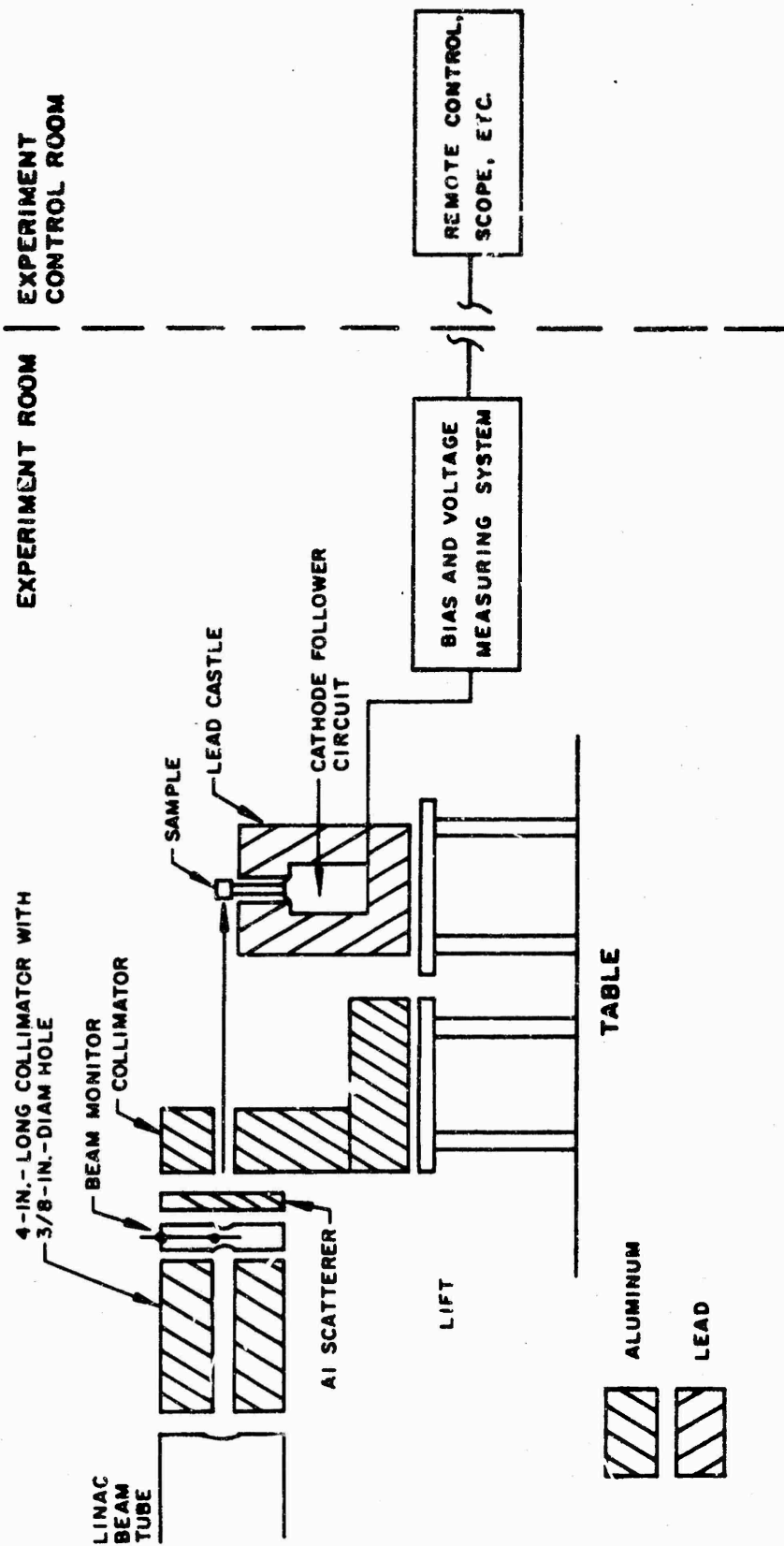


Figure 27. Typical experimental setup

The transistor and diode were placed directly behind the collimator block atop a lead castle, the walls of which were about 2 in. thick, as shown in Figure 27. The lead castle minimized radiation-induced transient effects in the two cathode-follower circuits which it housed. This shielding was effective; the radiation-induced signals from the cathode followers were well below the signals generated in the samples being irradiated.

For the tunnel-diode tests, a simpler circuit was possible and a more finely collimated beam was required. The electron beam was collimated by a 4-in. -long, $3/16$ or $5/8$ in. ID aluminum collimator up to within 1 in. of the diode. The tunnel diodes were mounted in an aluminum box 2 by 4 by 4 in. to shield rf noise. Two $3/8$ -in. holes were bored on opposite sides of the box to allow sight alignment within the Linac beam of the unit under test. BNC connectors provided patching to an adjacent aluminum box housing a remotely controlled Ledex switch capable of switching to the various load resistors.

3.1.2. Circuitry

Figure 28 shows a block diagram of the circuit setup used for transistor and diode measurements. Figure 29 shows a circuit diagram of the cathode-follower circuit. The cathode follower on the base circuit has the input shield driven by the output of the first tube to decrease the input capacitance as seen by the transistor. This technique was used mainly to look at the open-circuit photovoltage of diodes in which the impedance of the diodes is very high after irradiation. The dc-measuring system was controlled by a relay mounted inside the cathode-follower circuit box. This relay removed the dc-measuring cables from the transistor circuit when measuring transient effects to eliminate any noise which might be induced by the dc cables. These cables measured the voltages and currents at the base and collector of the sample. Two Hewlett-Packard 425A dc voltmeters with 10^8 -ohm input impedance were used to measure the dc voltages and currents.

The base and collector resistors mounted in the cathode follower circuit box were remotely selected by a Ledex system energized from the

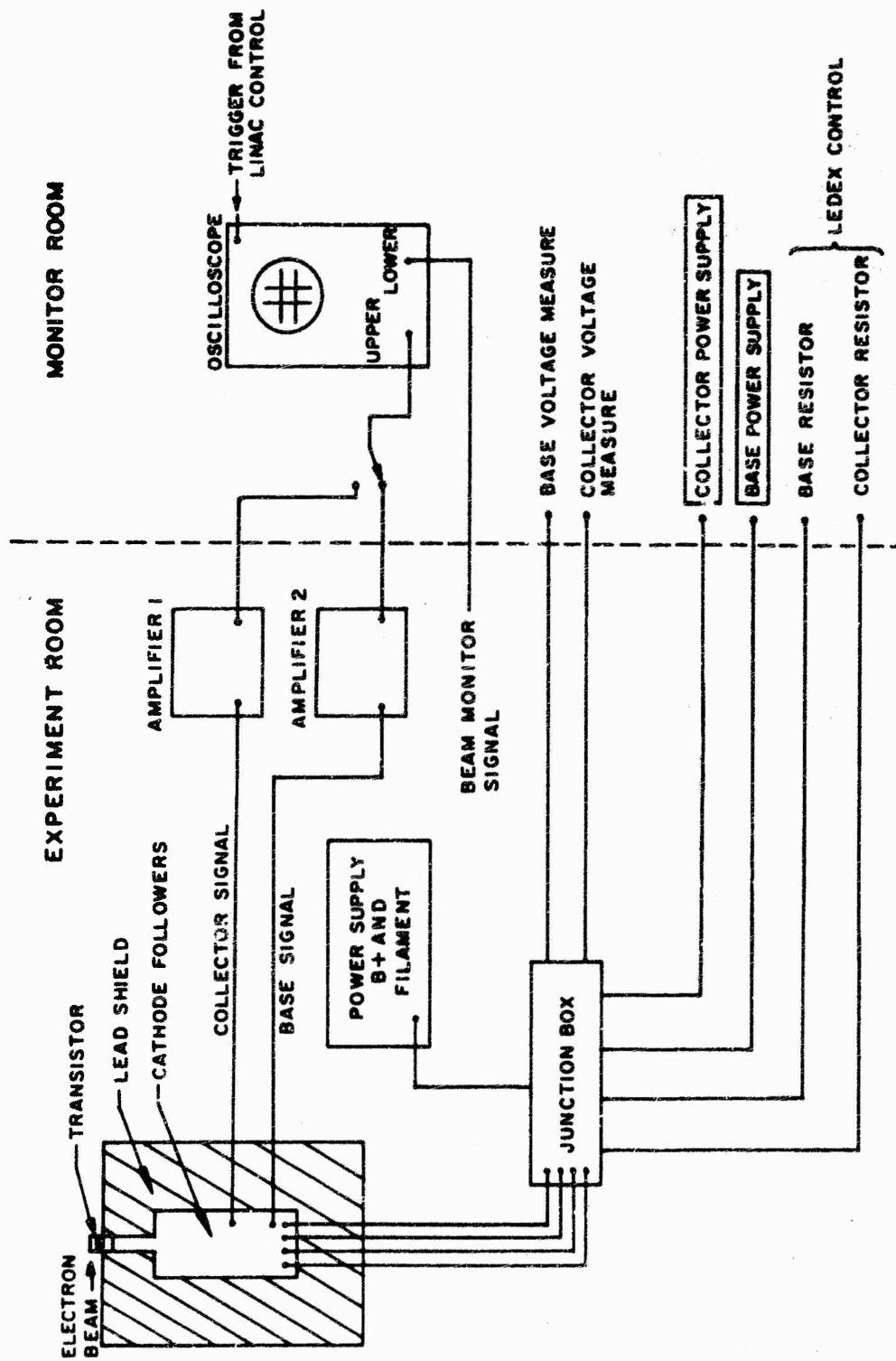


Figure 28. Block diagram of transistor test system

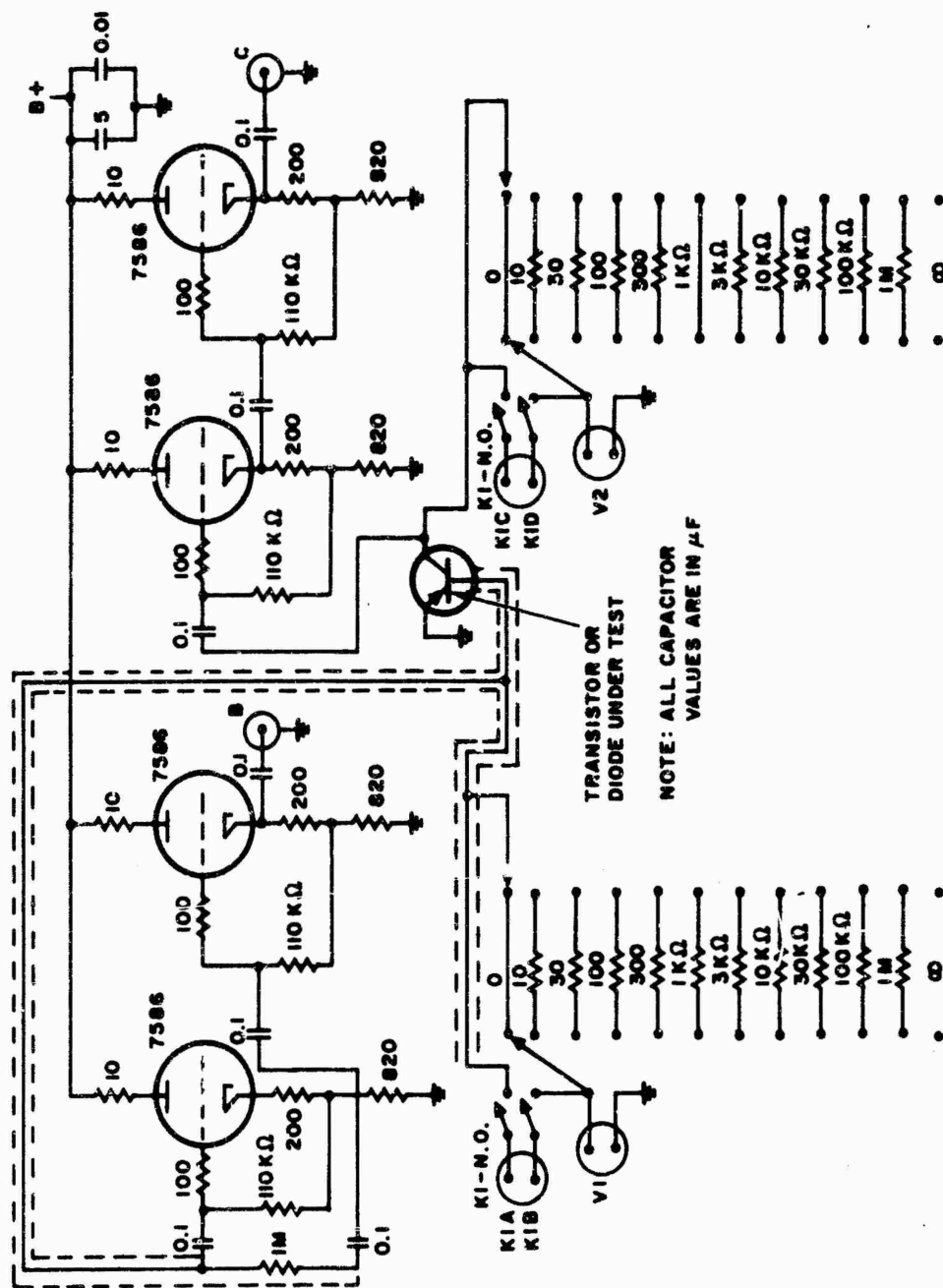


Figure 29. Dual cathode-follower circuit

control room. The Hewlett-Packard bias supplies for the base and collector of the transistors were remotely located in the Monitor Room. These supplies were connected through filters to eliminate any noise induced by the power-supply cables to the cathode-follower circuit box. Figure 30 shows the test-circuit schematics and how the diode was placed in the transistor test socket. Figure 31 shows the schematic of the tunnel-diode test circuit.

The outputs of the cathode followers on tunnel-diode test circuits were connected to our main amplifier system, as illustrated in Figure 32. The main amplifier system consists of a vacuum-tube amplifier with an output stage driving a 93-ohm cable extending 150 ft from the irradiation area to the experiment control room. The main amplifier consists of a Tektronix Type G oscilloscope preamplifier followed by a replacement vertical amplifier for a Tektronix Type 545 oscilloscope. The output stage is a specially designed direct-coupled cathode-follower stage. The output from the cathode follower is fed into a Tektronix Type G preamplifier to drive the upper beam of a Tektronix 551 dual-beam oscilloscope. The waveforms obtained were recorded on Tri-X 70-mm film at a magnification of 0.8 using a semiautomatic camera system.

Subsidiary data not recorded on the oscilloscope film, such as the part being tested, amplifier and oscilloscope gains, sweep speeds, etc., are recorded by dictating into a Stenorette tape recorder located next to the oscilloscope. The experimenter need only press a foot switch to activate a microphone, thereby leaving his hands free for other necessary adjustments.

The data from an accelerator experiment are recorded in two forms: (a) oscilloscope photographs on transparent negative film, and (b) tape-recorder records of dictated information.

The film is developed commercially. The tape-recording is transcribed onto special data sheets which provide a format presenting standard information on each picture taken, as well as additional comments. Parti-

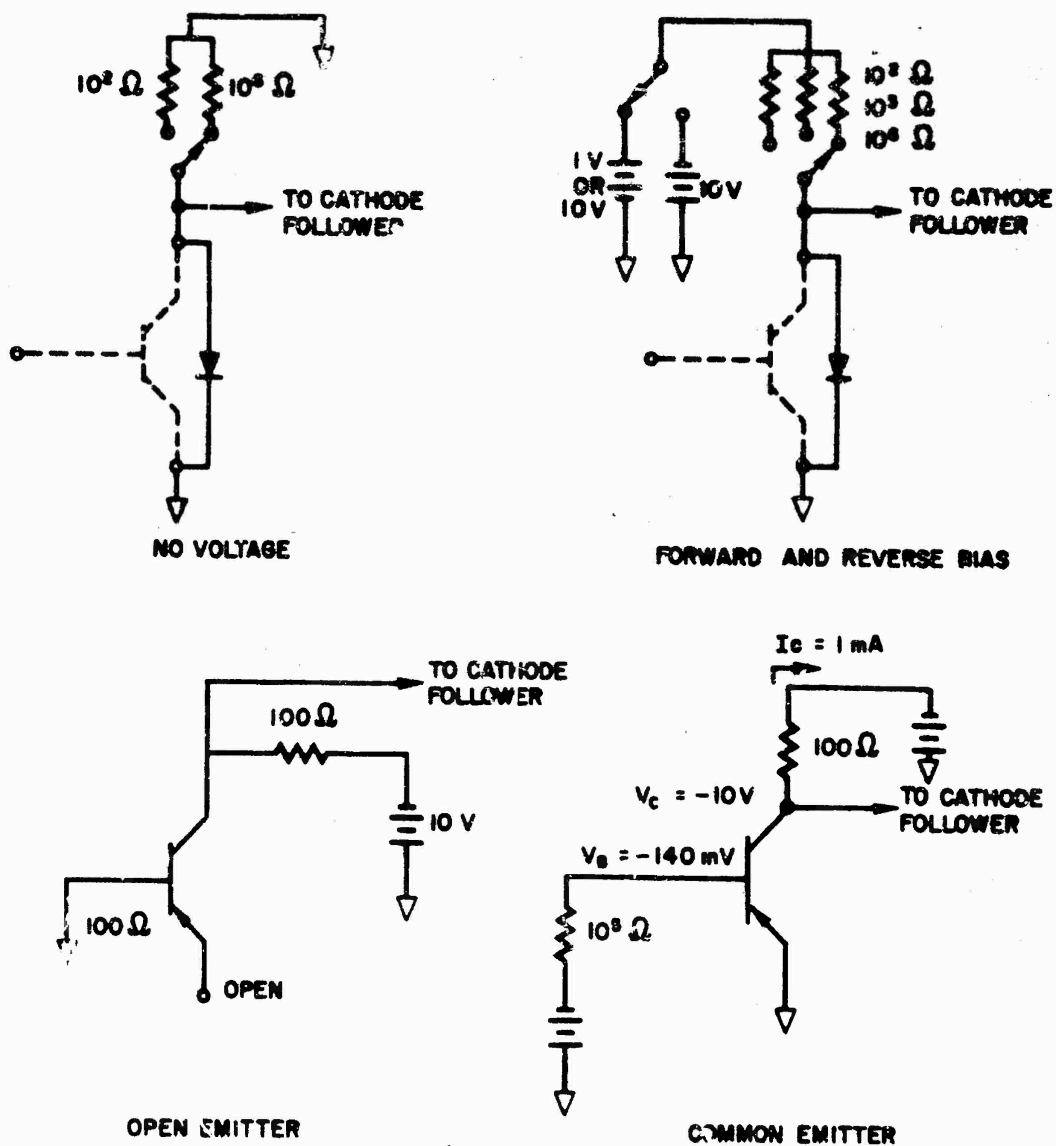


Figure 30. Transistor-diode test schematics

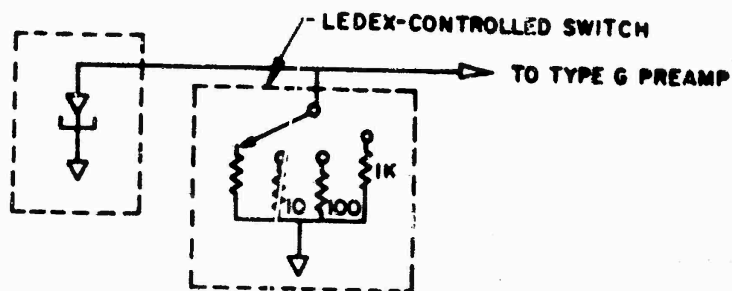


Figure 31. Tunnel diode test schematic

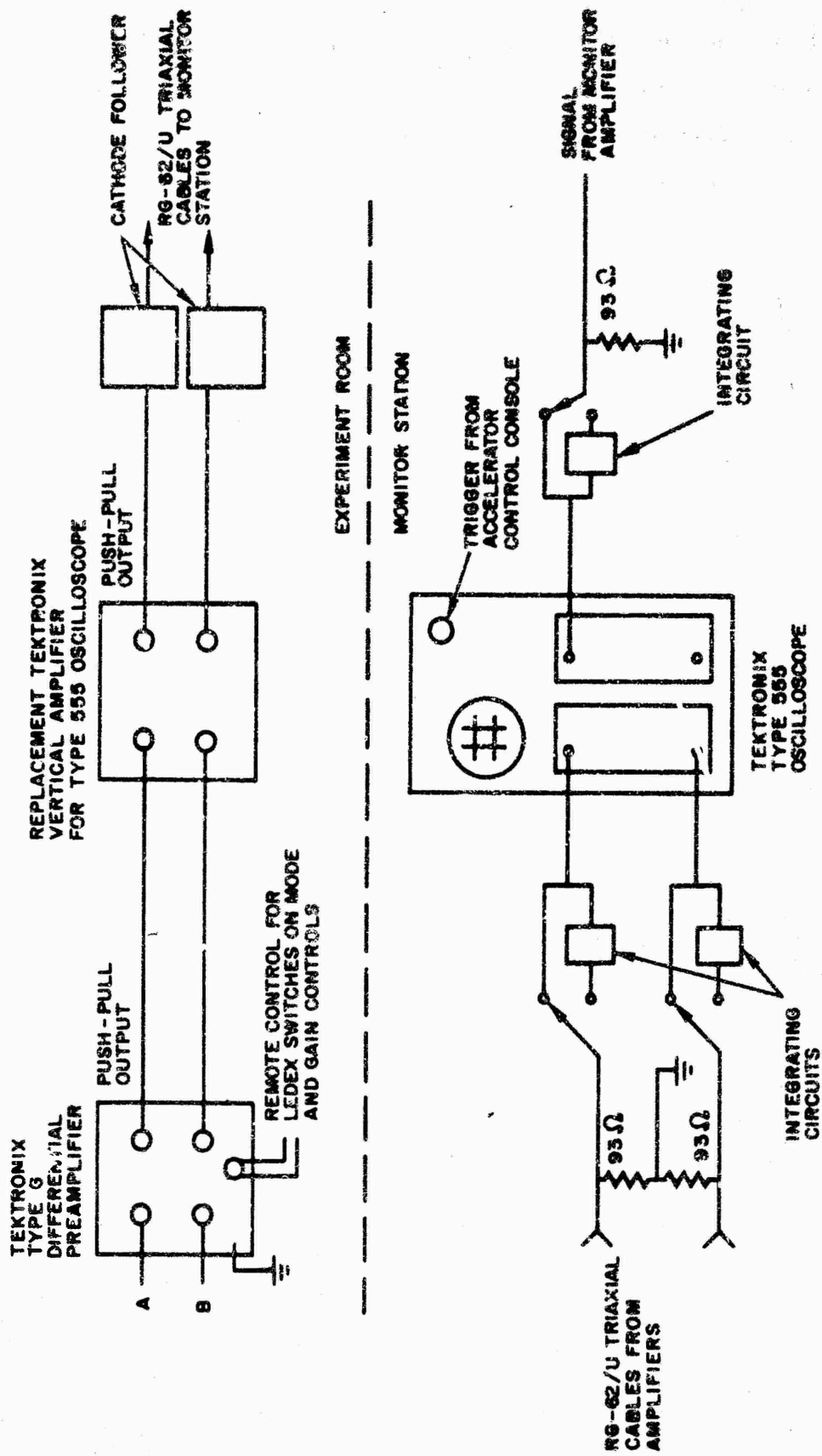


Figure 32. Signal monitoring system

ment coordinates on the film are measured by superposing an accurately ruled graph paper over the image. For computer data analysis, the coordinates are determined by a flying spot scan over the film, and these coordinates are then automatically coded onto punched tape for direct use by the computer.

3.1.3. Dosimetry

A titanium-foil secondary-electron emitter, $3/4$ in. diameter and 0.0006 in. thick in an evacuated chamber, was used for beam monitoring. The scatterer was varied from $1/32$ to $3/8$ -in. -aluminum plate used to spread and homogenize the electron beam.

On each picture of the dual-beam oscilloscope, the lower beam indicated the amplified output of the secondary-electron-emission titanium foil.

The dose level for each test period was established in the following manner. A thermistor, mounted in an evacuated, water-cooled chamber with a 1-mil Mylar window, as shown in Figure 33, was placed in the same

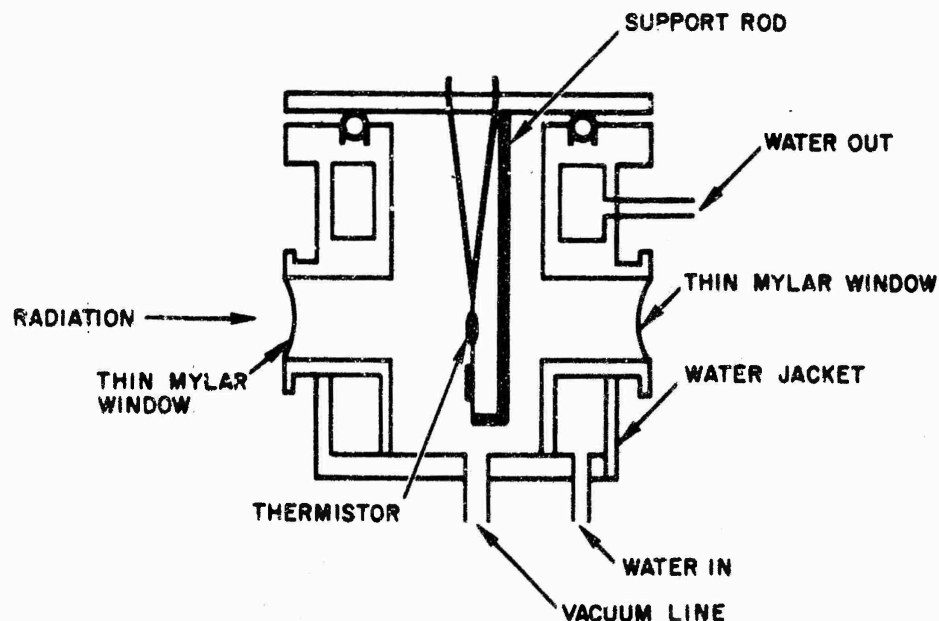


Figure 33. Thermistor calorimeter used in dosimetry in Linac tests

position that the unit under test would occupy. The thermistor was connected to one arm of a Wheatstone-bridge circuit, and the bridge was then balanced. When the thermistor was exposed to a pulse of radiation, the resulting heating caused a voltage unbalance of the bridge circuit that was a measure of the radiation dose delivered in the pulse. The unbalanced voltage of the bridge circuit had been calibrated against the heating of a thin copper-block calorimeter, which in turn had been cross-calibrated with a Faraday cup. The thermistor-Wheatstone-bridge circuit was used in preference to the copper-block calorimeter since it has a sensitivity approximately 400 times greater, and this additional sensitivity was needed for monitoring the doses delivered in these pulses. Defocusing magnets at the injector of the Linac permit adjustment of beam current.

Before impinging on the thermistor, the Linac beam also passed through a secondary-emission foil-monitor chamber mounted on a collimator, as shown in Figure 27. This monitor consists of a 0.0006-in.-thick titanium foil mounted in an evacuated chamber with 0.001-in.-thick titanium windows. The high-energy electron beam was not attenuated as it passed through the foil; however, in traversing the foil, it did knock secondary electrons from the foil, thereby creating a current as the secondary electrons were replaced. The current signal was amplified, and the resulting signal was integrated and displayed on the lower beam of the Tektronix Type 555 dual-beam oscilloscope. The amplitude of this integrated monitor signal was proportional to the Linac beam current and, consequently, to the dose delivered to the test specimen. This monitor signal was correlated with the dosimetry data collected, and since each photograph contains the signal from the device test circuit as well as the monitor signal, an accurate measure of the dose delivered in each pulse was obtained.

3.2. EXPERIMENTAL RESULTS AND DISCUSSION

3.2.1. Tunnel Diodes

3.2.1.1. Summary of Theory. A theory of transient effects in tunnel

diodes was developed previously. So that the experimental results to be presented are understood, the essence of the theory will be summarized.

Since carrier lifetimes in tunnel diodes are much smaller than the radiation pulse widths to be used, a steady-state theory is invoked; i. e., carrier generation and removal are in equilibrium at any time. We will assume that circuit rc time constants are also small compared to relevant radiation response times.

Under these conditions, the current flowing across the junction of a tunnel diode under irradiation can be treated as the superposition of four terms:

1. A reverse current, i_{rad} , due to diffusion of radiation-induced minority carriers toward the junction and generation of carriers within the depletion layer, i. e.,

$$i_{rad} = e a_0 g (L_n + W_d + L_p),$$

where a_0 is the junction area, g is the carrier generation rate, L_n and L_p are the diffusion lengths on the n and p side of the junction, and W_d is the width of the depletion layer.

2. A forward diffusion current, i_{diff} , due to the gradient of the carrier densities at the junction.
3. A reverse drift current, i_{drift} , due to the motion of carriers under the influence of the electric field in the depletion layer. A large portion of the electric field is usually the field due to the net donor/acceptor space charge left behind when the mobile charges attempt to diffuse across the junction.
4. A forward tunnel current, i_{tun} , due to carriers which are able to perform the quantum mechanically allowed transition from filled states to spatially nearby empty states in spite of an absence of available states in between.

In a tunnel diode without radiation or bias voltage, the forward diffusion current balances out the reverse drift current. There is no net tunnel current since the same fraction of the available states are occupied on both sides of the junction. The integral of the electric field across the depletion layer under these conditions is called the built-in voltage, V_{bi} .

As an external forward bias, V_0 , is applied, the built-in electric field is decreased, resulting in a decrease of the reverse drift current. The tunnel current becomes finite, because the occupancy of majority carriers in states on one side of the junction is greater than the occupancy of the corresponding minority carriers on the other side. A second-order effect is that the depletion layer width decreases, causing a slight enhancement of the normal diffusion current.

Under irradiation, i_{rad} is also present. In an actual circuit, the balance between these currents is established by the external circuit bias voltage and resistance. Hence, in general,

$$V_0 - IR = V_a,$$

$$i = i_{diff} + i_{tun} - i_{rad} - i_{drift}.$$

Note that i_{tun} and i_{drift} and to a lesser extent i_{diff} and i_{rad} , are functions of V_a , the voltage drop across the diode.

The results of the previous analysis were a calculation of i_{rad} as a function of dose rate under short-circuit conditions ($R = 0$); i. e., V_a is constant, and hence i_{diff} , i_{tun} , and i_{drift} are constant. A second calculation assumed i_{rad} to be independent of V_a (a good assumption, since $W_d \ll L_n + L_p$) and evaluated the magnitude of V_a required to produce a forward current $-i_{drift} + i_{tun}$ equal to the reverse current i_{rad} . Under these conditions, V_a is the open-circuit voltage (no change in total circuit current). The results are summarized in Figure 34.

Figure 35 can be used to apply these results to a variety of external circuit resistances. For a low-enough resistance, the voltage change required to push i_{rad} through the circuit is small enough that the change in $i_{tun} - i_{drift}$ is negligible. At large R , the current required to establish V_a across the diode is a negligible fraction of i_{rad} . At intermediate R , a part of i_{rad} flowing through the external circuit establishes sufficient V_a to cause $i_{tun} - i_{drift}$ to increase in order to cancel the rest of i_{rad} .

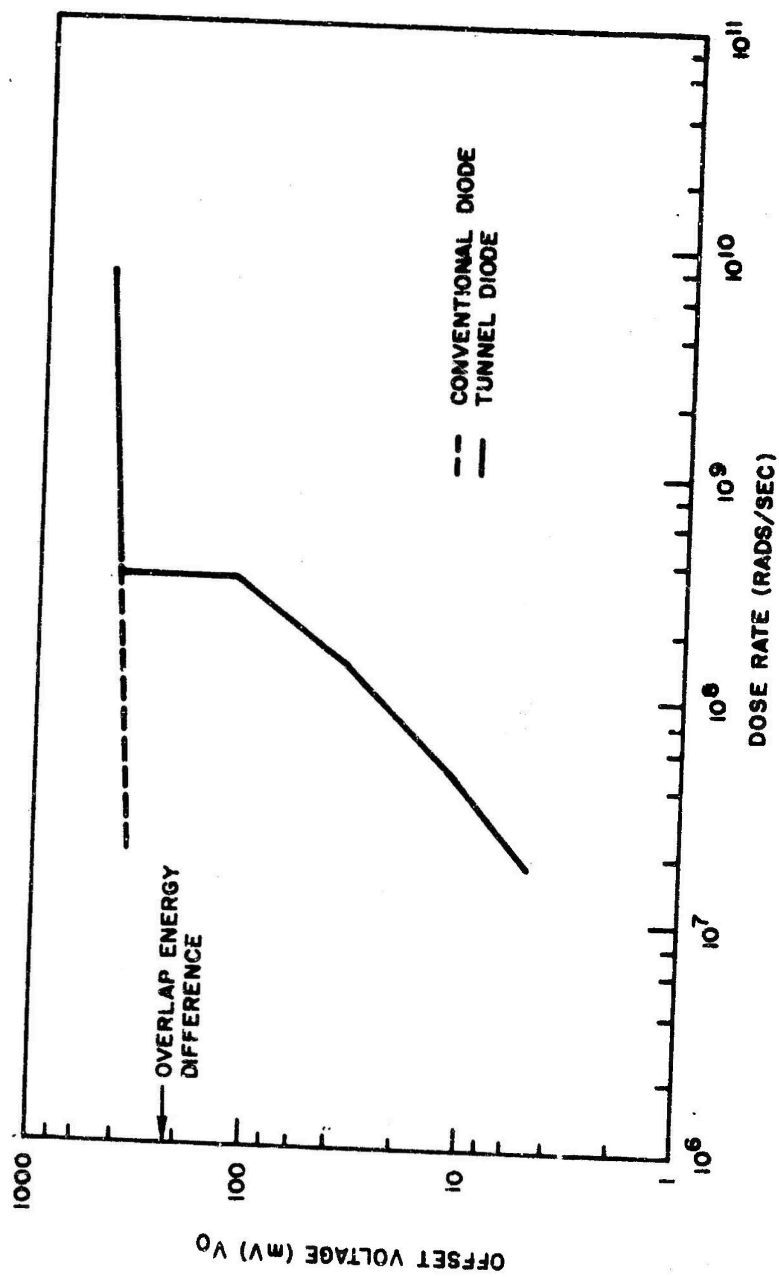


Figure 34. Offset voltage vs dose rate (theoretical)

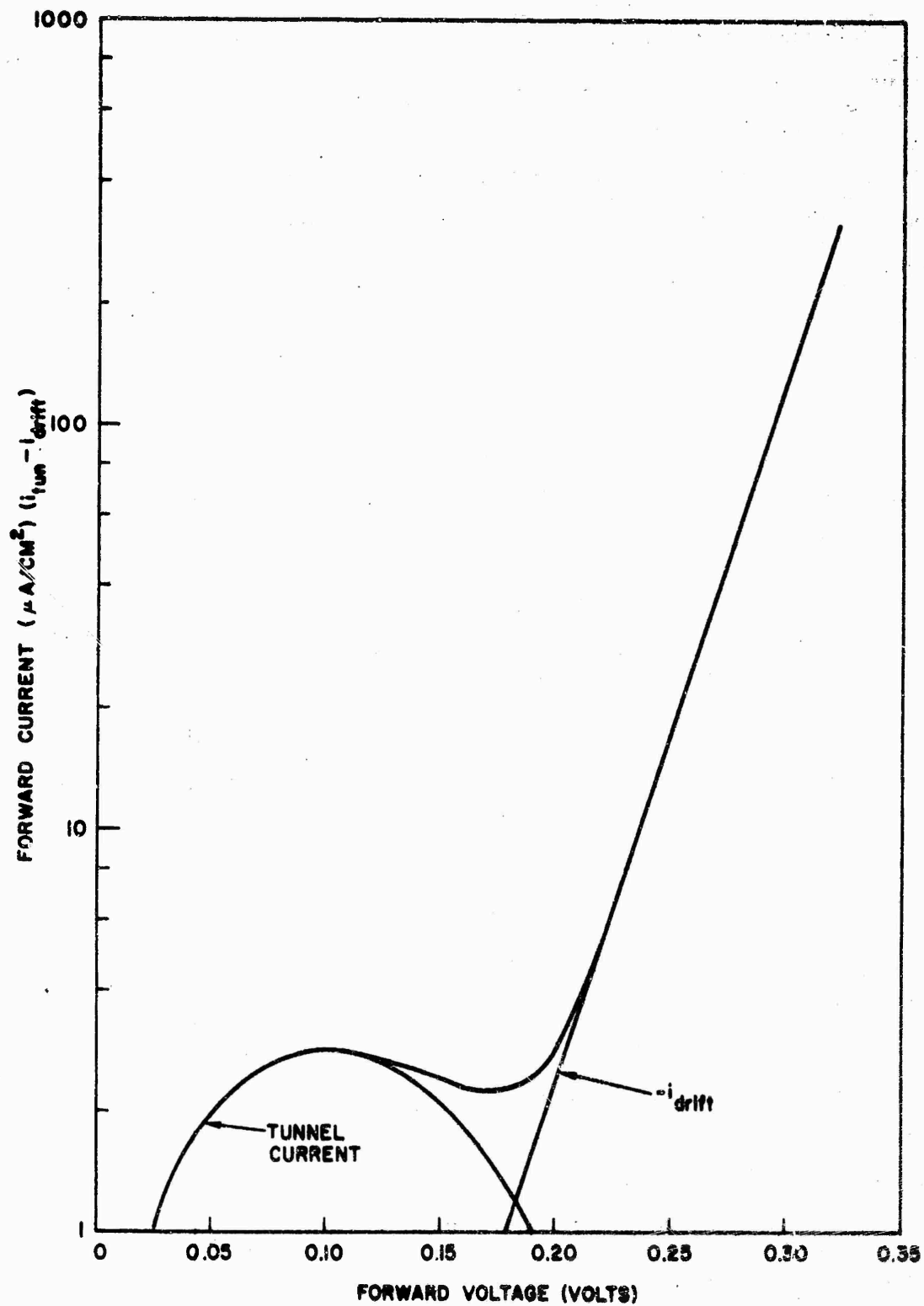


Figure 35. Energy-band overlap = 0.21 eV

An important feature of this discussion is that the tunnel-diode circuit will respond in an identical fashion to any source of extra current. i_{rad} is simply a current source proportional to dose rate. If any other current source were placed in series with the tunnel diode, the circuit would exhibit V_a versus i_{source} characteristics identical to those in Figure 35.

Note that the foregoing discussion is equally applicable to an ordinary diode by setting $i_{\text{tun}} = 0$, as long as the duration of the radiation pulse is long compared to the carrier and circuit relaxation times.

3.2.1.2. Experimental Results. Previous experiments on a tunnel diode (Reference 12) revealed a curve of voltage versus dose rate in reasonable agreement with the theory, if a carrier lifetime as long as 10^{-9} sec was assumed. However, suggestions that other diodes exhibited much less response prompted reexamination of the experimental technique and some tests of other diodes.

The primary source of interfering noise was assumed to be secondary-electron emission from associated measuring circuits and the tunnel-diode case. An upper limit to this noise was established by breaking the grounded lead to the tunnel diode so that all the secondary-emission current had to flow through the external-circuit resistance. In this way it was shown that the secondary-emission current was small compared to the measured radiation-induced current.

Nevertheless, some apparent contradictions appeared in the resultant data. For example, data taken at two different irradiation positions to achieve a wide range of dose rates did not agree at the same dose rate. The beam calibration technique was the same at both positions, and the only variation appeared to be the size of the irradiated area. A second background experiment revealed a further anomaly. If instead of disconnecting the ground lead of the diode, one simply moved it laterally out of a finely collimated electron beam, the signal did not decrease as expected! Scattered radiation could not account for the signal, as verified by dosimetry.

Finally, it was established that the signal could be eliminated by interposing a conducting plate between the electron beam and the tunnel diode.

Thus, it was established that the signal previously observed was not due to particulate radiation impinging on the tunnel diode but was due to electromagnetic radiation emitted by the pulsating electron beam from the L-band electron linear accelerator being rectified by the diode.

The moral of this story is that care must be taken when irradiating nonlinear electronic devices capable of operating at very high frequencies (> 1 kMc) with electrons from linear accelerators. The lack of validity in the simulation of a nuclear weapons gamma burst in this case was not the use of electrons instead of gammas, but in the L-band modulation superimposed on the ionization pulse. A bremsstrahlung beam from an L-band accelerator would produce the same problem since the secondary electrons would be directional and would have the same modulation frequency. For such very high frequency, it appears to be necessary to use a flash x-ray machine for such tests or else to investigate the feasibility of providing sufficient symmetry and electromagnetic shielding to cancel the electromagnetically induced signal.

3.2.2. Experimental Results and Discussion for the 1N91 Diode

Experimental data were obtained for the 1N91 diode and the 2N396A transistor for comparison with the computer solutions given in Section 2.3. Because of the finite length of the experimental radiation pulse (~ 20 nsec) and a comparable delay in the external circuit response, the zero time for the experimental data is of the order of $0.1 \mu\text{sec}$ rather than of the order of 10^{-11} sec given by the code for an instantaneous radiation pulse.

3.2.2.1. Zero Bias. Figure 36 presents the experimental data on the time dependence of the photovoltage from a 1N91 diode irradiated in a 10^2 -ohm circuit. The theoretical curves have been shortened in time by a factor of 7, since the apparent lifetime appears to be closer to $7 \mu\text{sec}$ than the $50 \mu\text{sec}$ used by the computer. It can be seen that there is qualitative agreement in the data and hence that the discrepancies could be due to inadequate knowledge of diode parameters.

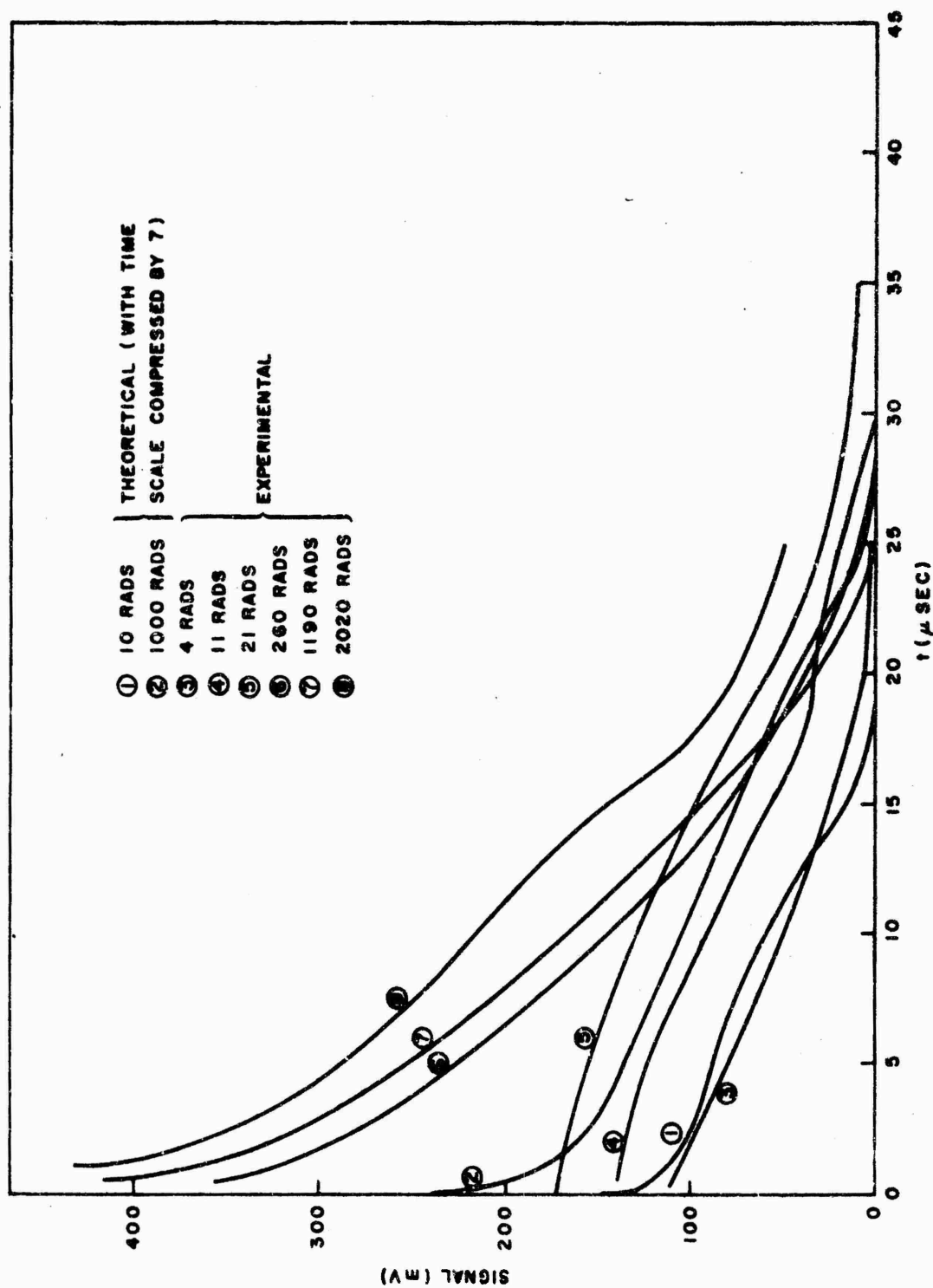


Figure 36. No bias on IN91 diode with 100-ohm load in series

Figure 37 presents a similar set of data for a circuit having an impedance of 2.5×10^5 ohms. Some lengthening of the decays over the 10^2 -ohm decays is obvious.

The computer curves have been shortened by a factor of 28; a factor of 7 for the lifetime error and a factor of 4 in the circuit impedance. The validity of this procedure is questionable and should be checked with further computer runs.

It would be particularly interesting to explore the validity of the long-lifetime theory for the few excess majority carriers in the edges of the depletion layer. It is possible to perform a definitive experiment on this feature by using a high-impedance measuring circuit and by adding to the computer calculation a realistic circuit capacitance. If the long decay does not appear experimentally, there must be an unidentified mechanism for removal of these carriers.

3.2.2.2. Forward Bias. The forward-biased diode signals for a 0.9-mA diode current are shown in Figures 38 and 39. Similarly, for a 10-mA diode current, the signals are shown in Figures 40 and 41. The theoretical curves have again been shortened by a factor of 7, although this procedure is particularly suspect when current transports many of the excess carriers.

Again the agreement is qualitatively good. Experimentally and theoretically, the signal decreases with increasing bias current. Most of the discrepancies can be accounted for by the uncertainty in actual device parameters.

3.2.2.3. Reverse Bias. The experimental data for a reverse-biased 1N91 diode are shown in Figures 42 and 43. Again, the theoretical time scale has been compressed by a factor of 7. This correction is probably too large for saturation conditions, such as those at the 10^3 -rad datum. A computer run with the correct 7- μ sec lifetime is obviously required.

The dose at which saturation is achieved is slightly underestimated by the computer. This is probably also a consequence of the long lifetime,

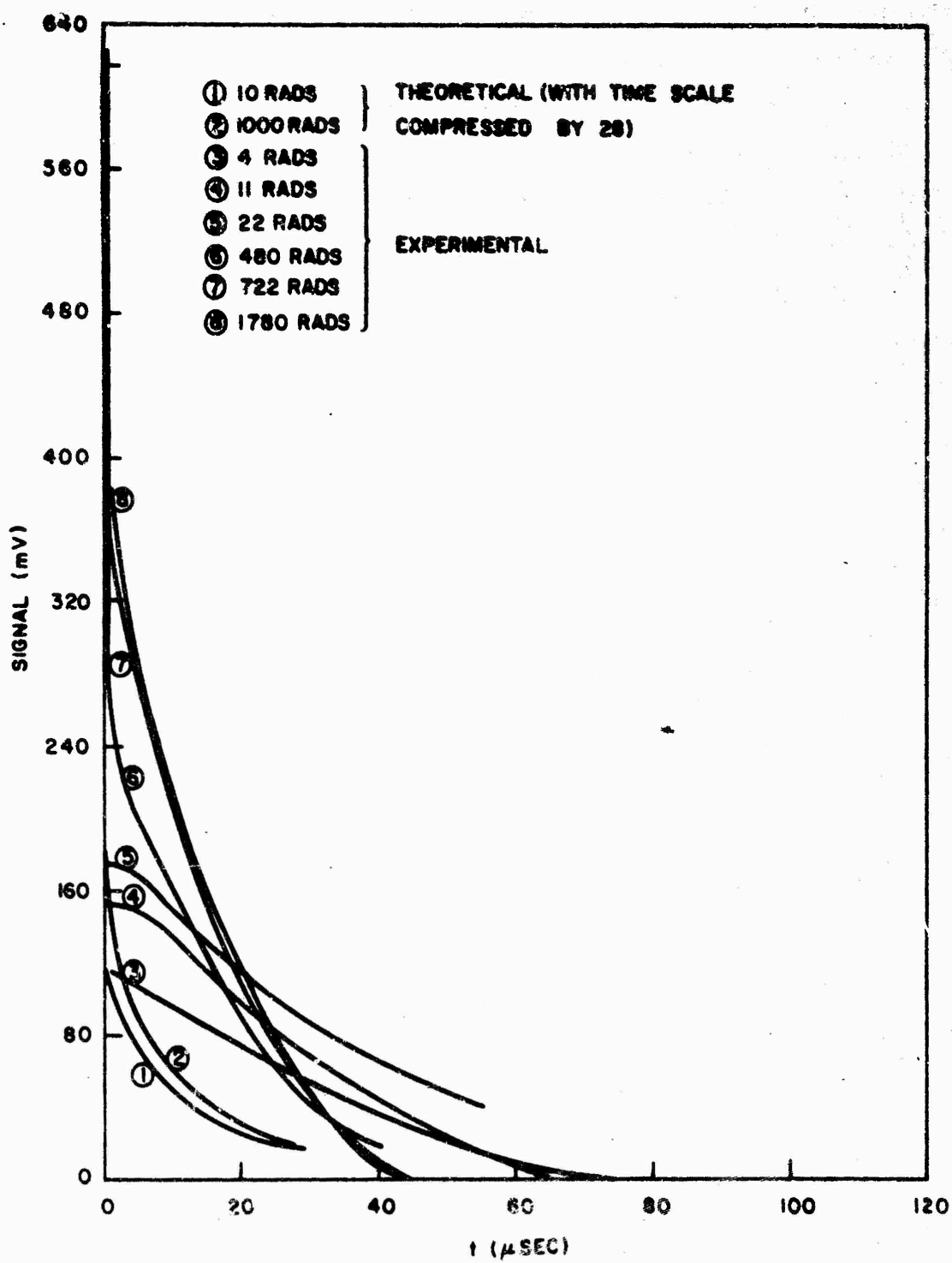


Figure 37. No bias on 1N91 diode with 10^6 -ohm load in series

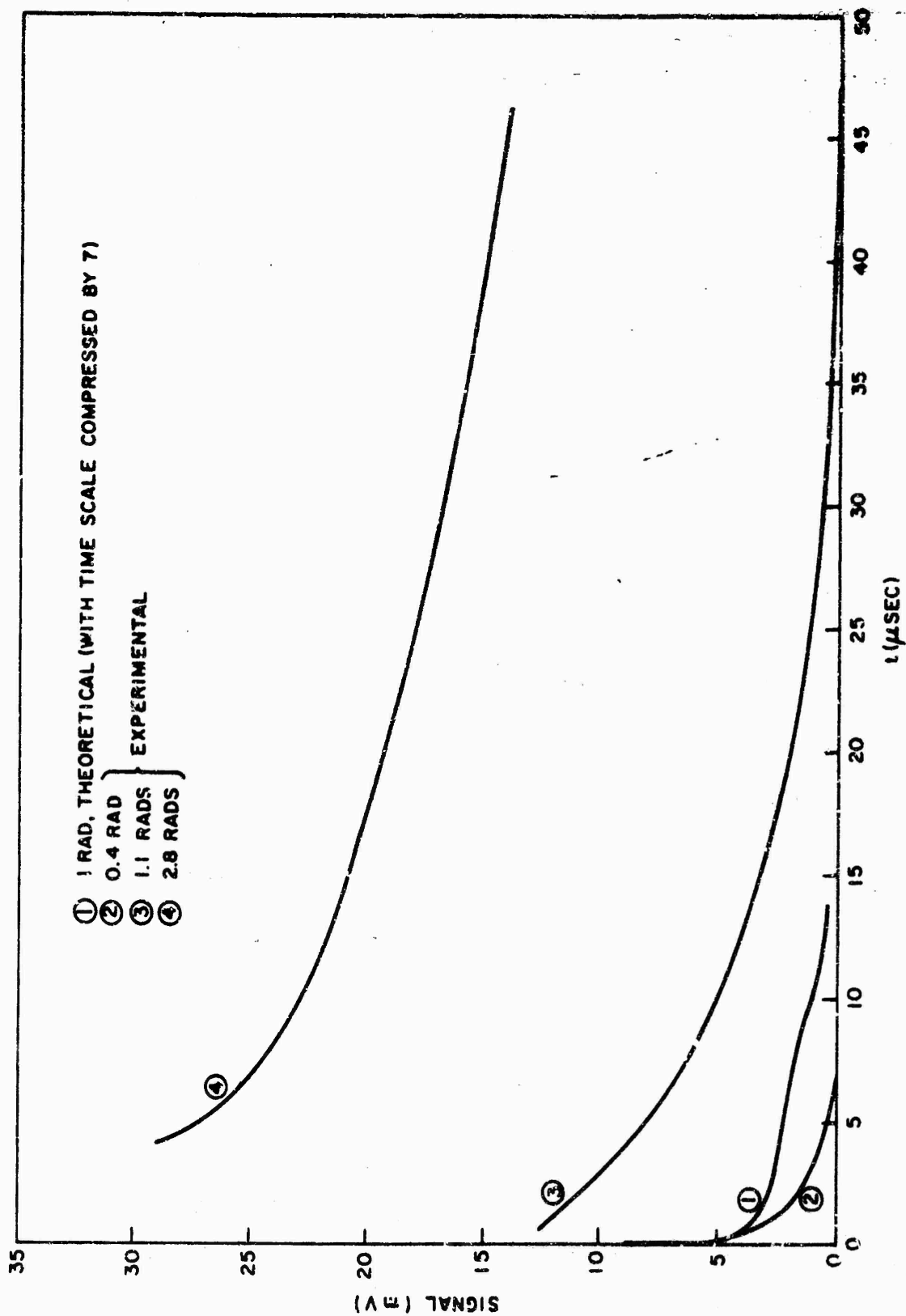


Figure 38. +1-V forward bias on 1N91 diode with 1000-ohm load in series

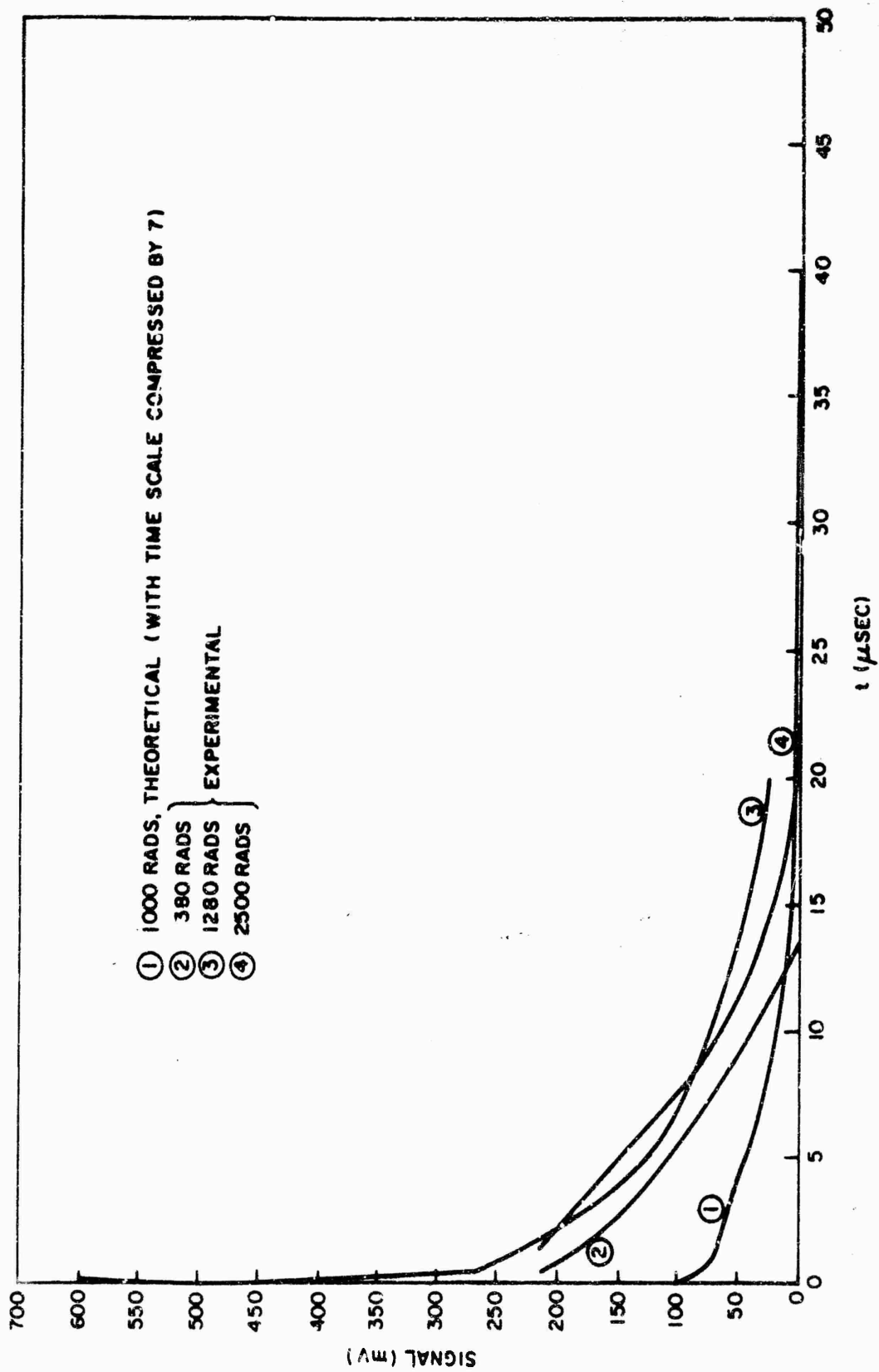


Figure 39. +1-V forward bias on LN91 diode with 1000-ohm load in series

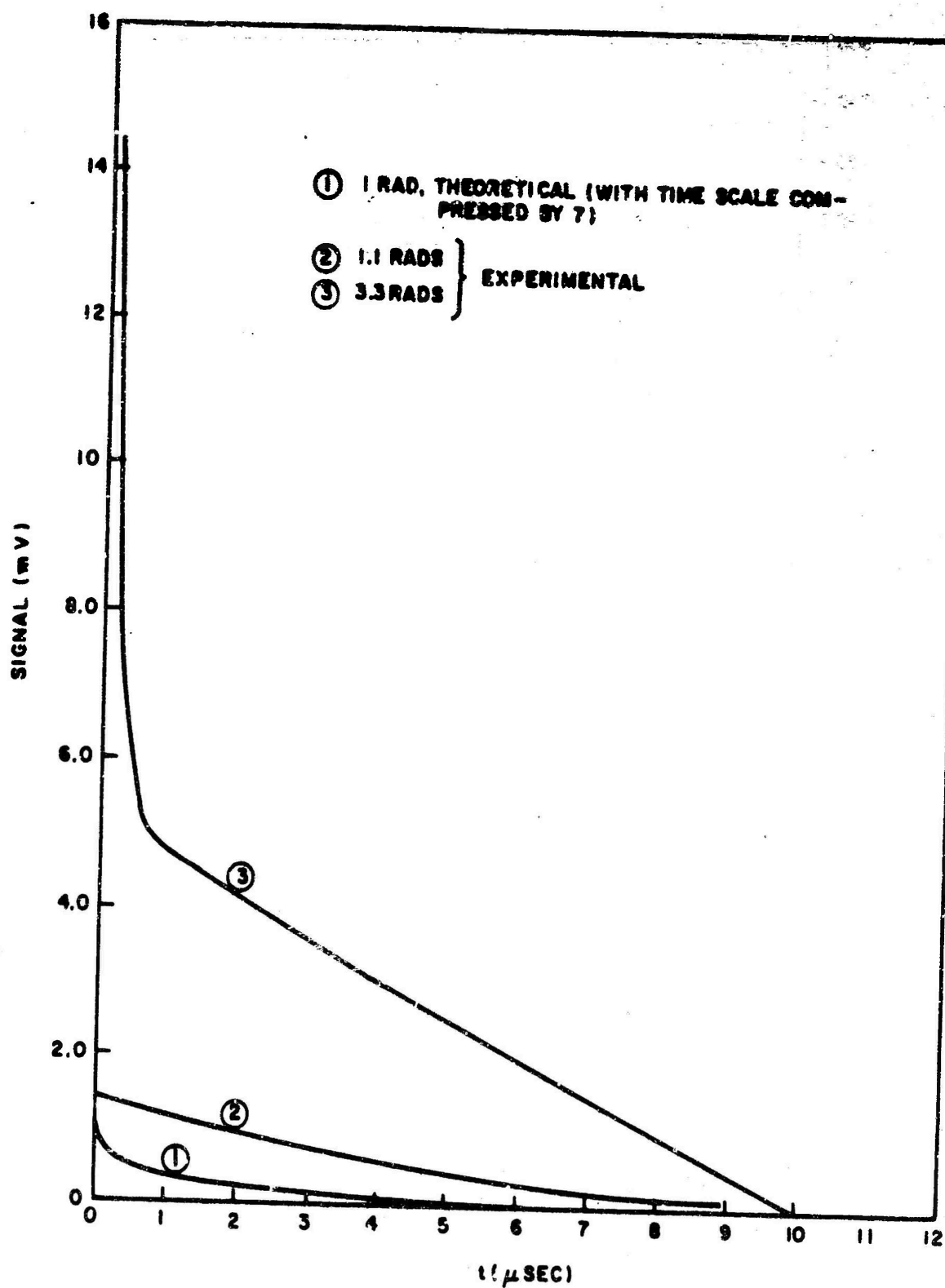


Figure 40. +10-V forward bias on 1N91 diode with 1000-ohm load in series

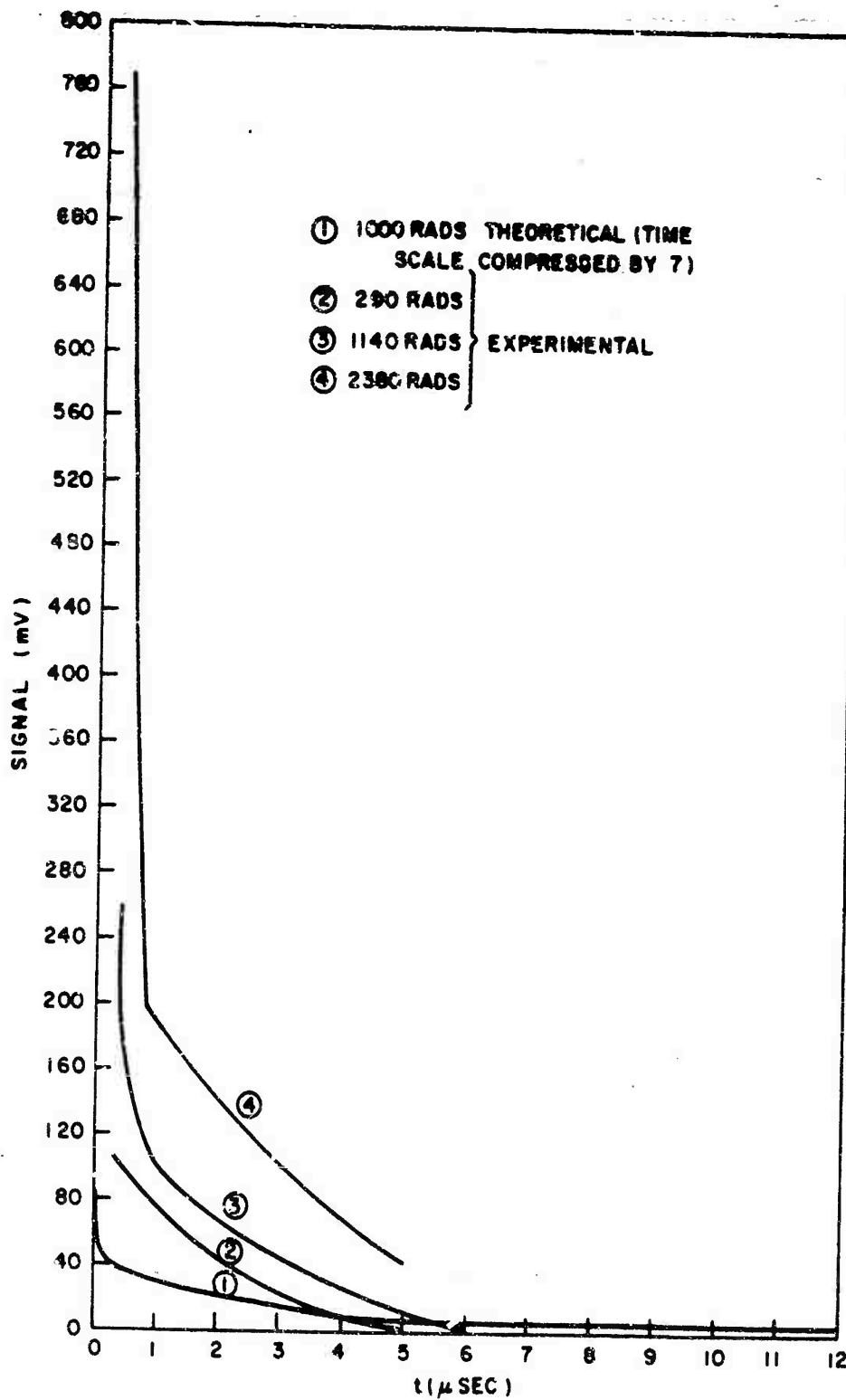


Figure 41. +10-V forward bias on LN91 diode with 1000-ohm load in series

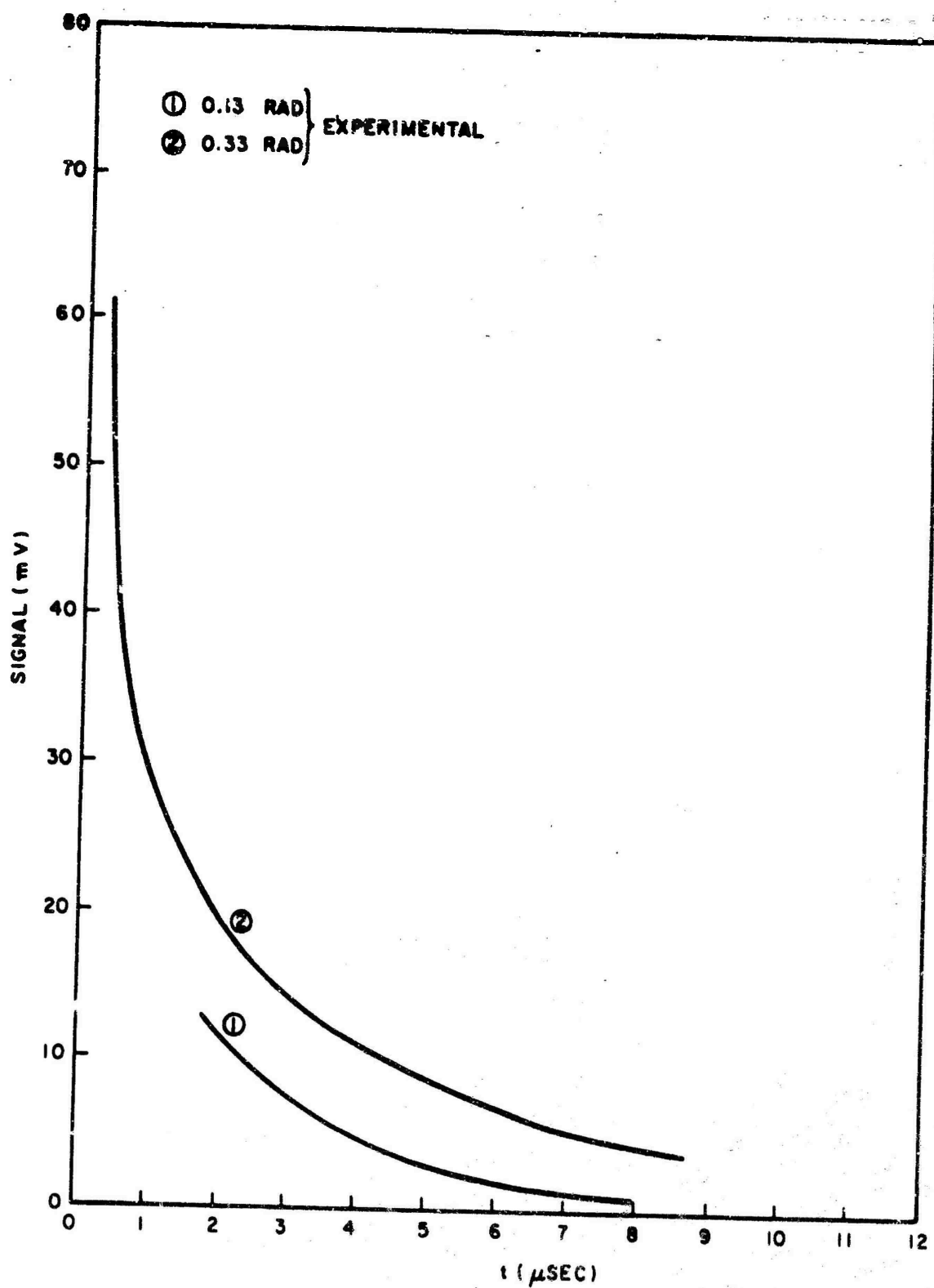


Figure 42. 10-V reverse bias on 1N91 diode with 100-ohm load in series

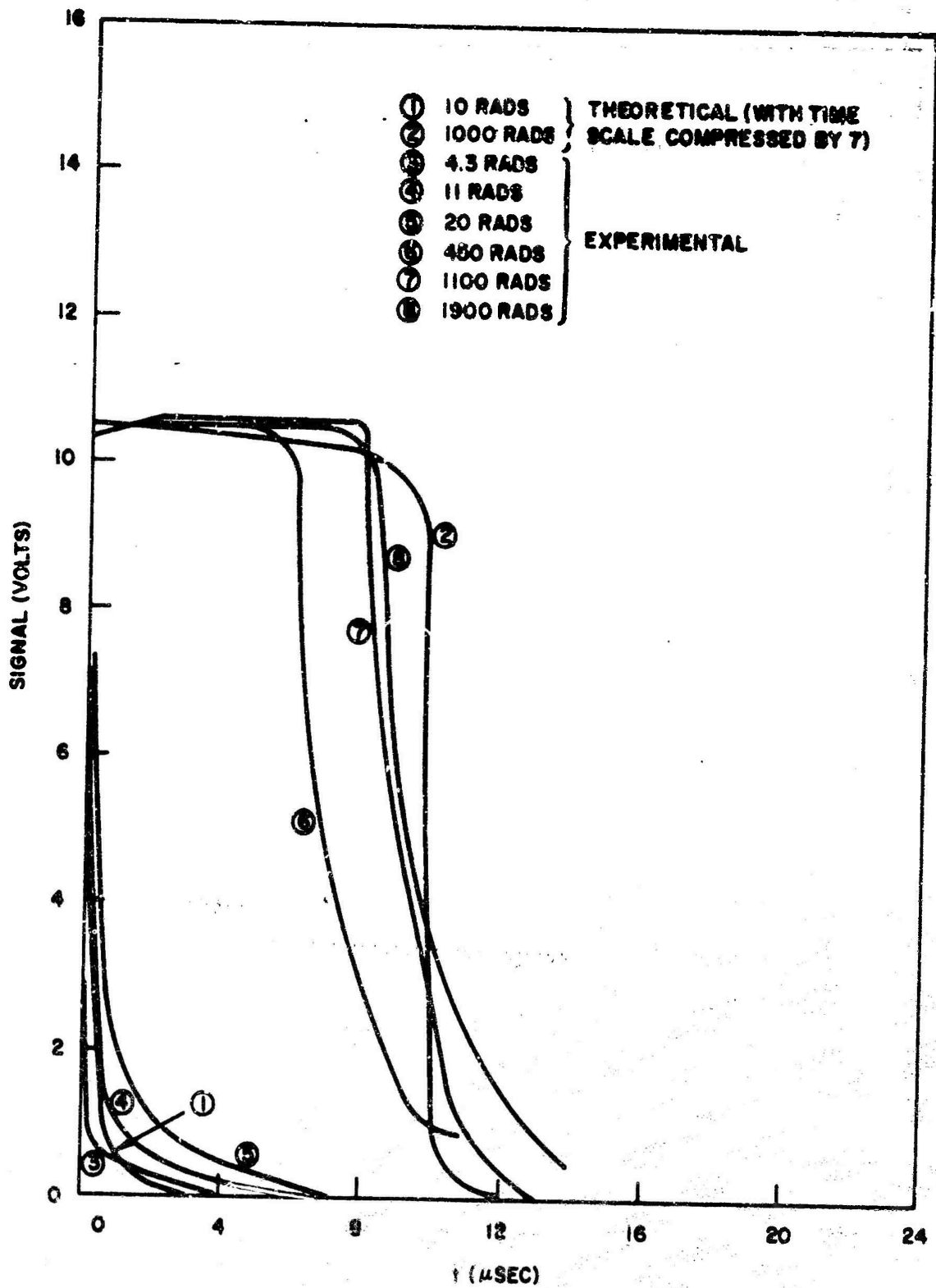


Figure 43. 10-V reverse bias on LN91 diode with 100-ohm load in series

since it implies a larger diffusion volume from which to collect carriers.

3.2.3. Experimental Results and Discussion for 2N396A Transistor

Figure 44 compares the observed secondary photocurrent in a 2N396A transistor with the computer result. Figure 45 is a tracing of oscilloscope photos of the primary photocurrent. The time dependence is primarily determined by circuit response and radiation pulse width. The total charge has been estimated to be 8×10^{-11} coulomb at 1 rad and 3×10^{-12} coulomb at 3.6 rads. These values are larger by a factor of 2 than the computer value, suggesting a factor of 2 error in the base volume. This error could easily be due to charge collection from the peripheral base volume outside the alloy dots. The charge collected by the collector in the common-emitter circuit was 8×10^{-9} coulomb at 1 rad, indicating that h_{fe} for this transistor was 100. The measured value was $h_{fe} = 93$. Again, agreement is as good as the device data allow.

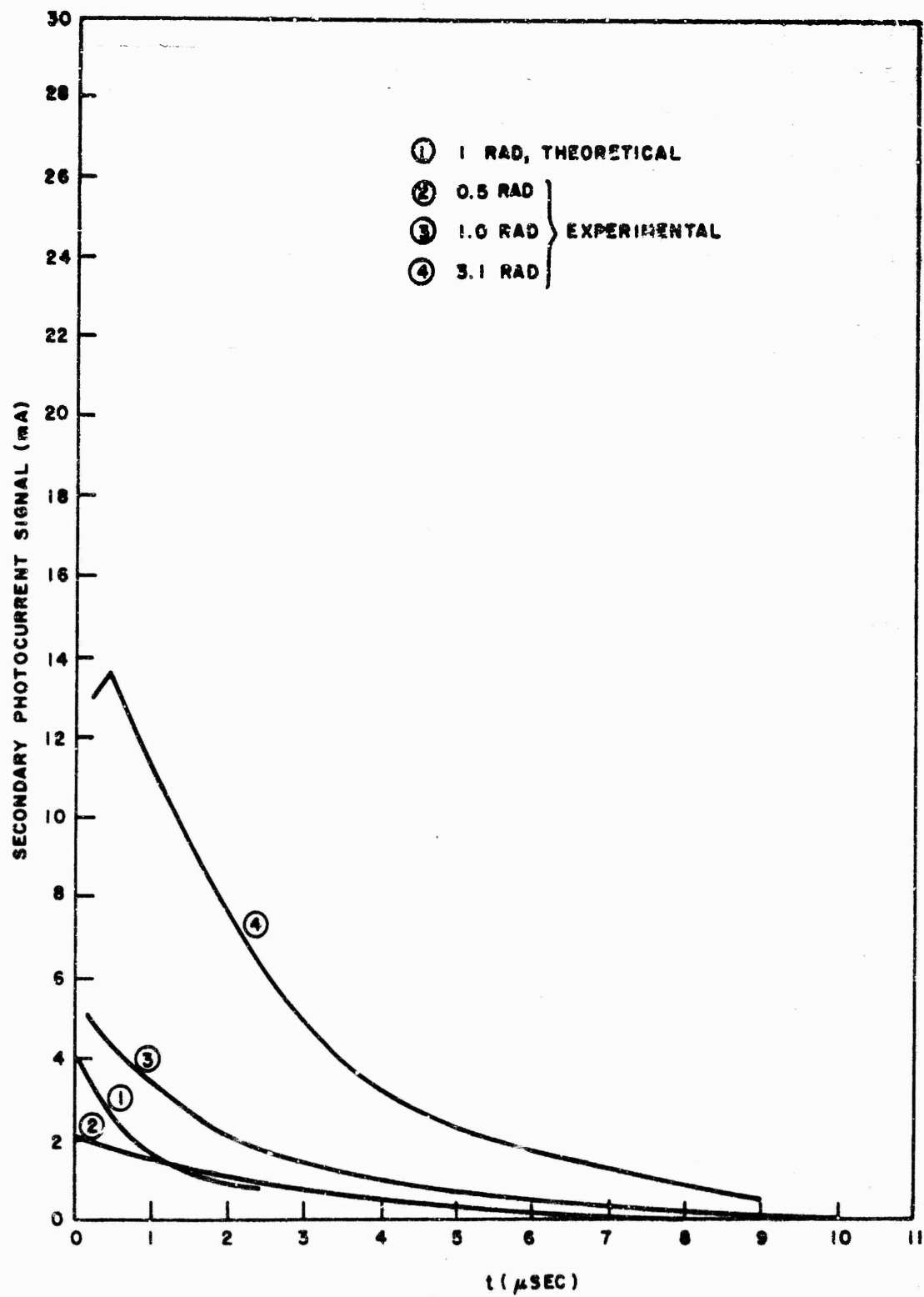
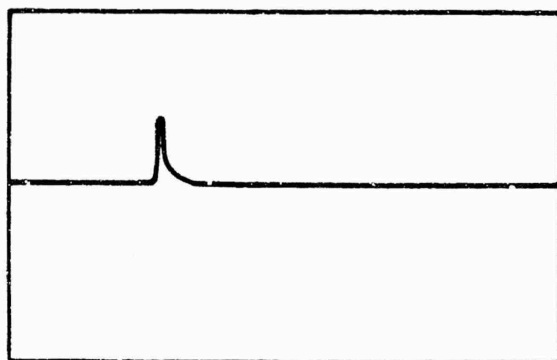


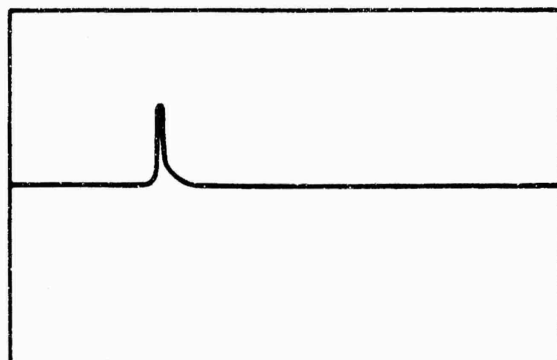
Figure 44. 2N396A transistor common-emitter collector-current signal above 1 mA quiescent state



Vertical: 690 mV/Div
(across: 100 ohms)

Horizontal: 0.5 μ sec/Div

Integrated Linac dose = 3.6 rads



Vertical: 15 mV/Div
(across: 100 ohms)

Horizontal: 0.5 μ sec/Div

Integrated Linac dose = 0.1 rad

Figure 45. Primary photocurrent for 2N396A transistor (emitter open)

SECTION IV

SUMMARY AND CONCLUSIONS

The computer code for calculating relaxation of carriers in semiconducting devices is working well. The automatic spatial meshing and time-step routines are necessary and have performed reliably on such difficult problems as the saturation transition of a reverse-biased diode.

The code has been exercised on some problems for a reference diode, a 1N91 diode, a reference transistor, and a 2N396A transistor. Previously unappreciated phenomena have been uncovered, such as

1. Long effective lifetime for some carriers when the diode is in a high-impedance circuit.
2. Carrier ambipolar diffusion toward the junction in alloy devices.
3. Increase in peak electric fields in alloy devices when velocity saturation is introduced.

Comparison of the results with experimental data on a 1N91 diode and a 2N396A transistor is satisfactory and is limited by knowledge of actual transistor parameters.

The code has performed satisfactory calculations, including velocity saturation, time-dependent carrier lifetimes, graded structures (four-layer PNPP⁺ configurations such as in epitaxial transistors), and avalanche generation of carriers with a pseudo weak avalanche relation. Some further investigation will be required to enable the code to contend with the high electric fields under true avalanche conditions.

A new artifact in the use of microwave electron accelerators to irradiate high-frequency devices, such as tunnel diodes, has been identified as rectification of electromagnetic radiation from the electron beam by the diode.

REFERENCES

1. van Lint, V. A. J., J. Alexander, and D. K. Nichols, Short-pulsed Gamma Radiation Effect on Dynamic Electronic Components, Final Report, Contract AF29(601)-6374, Air Force Weapons Laboratory, Report AFWL TR-65-44, May 21, 1965.
2. Gunn, J. B., Progress in Semiconductors, Vol. 2, A. F. Gibson, ed., John Wiley and Sons, New York, 1957, pp. 213-247.
3. Chynoweth, A. G., and K. G. McKay, Phys. Rev., Vol. 106, 1957, p. 418.
4. McAfee, K. B., E. J. Ryder, W. Shockley, and M. Sparks, Phys. Rev., Vol. 83, 1951, p. 650.
5. Esaki, L., Phys. Rev., 1958, p. 603.
6. Hunter, L. P., Handbook of Semiconductor Electronics, 2d ed., McGraw-Hill Book Co., New York, 1962, pp. 4-22.
7. Hamilton, D. J. Lindholm, F. A., and J. A. Narud, Proc. IEEE, Vol. 52, 1964, p. 239.
8. Study for Generalized Model of Semiconductor Radiation Response Prediction, Northrup Corporation, Ventura Division, Technical Report ECOM-00-432-1, 1965.
9. Choy, S. C., Computer Program Description of Short-pulsed Gamma Radiation Effects on Dynamic Electronics Components, General Atomic Division, General Dynamics Corporation, Report GA-6217 Supplement.
10. Richtmyer, R. D., Difference Methods for Initial-value Problem, Interscience, New York, 1957.
11. Shockley, W., and W. T. Read, Jr., Phys. Rev., Vol. 87, 1952, p. 835.
12. van Lint, V. A. J., H. Horiye, D. K. Nichols, R. A. Poll, and B. W. Roos, The Effects of Pulsed Gamma Radiation on Dynamic Electronic Components, Final Report, Contract AF29(601)-5685, RTD TDR-63-3110, January 1964.

Appendix A

PNPP⁺ CODE

The following printout is a list of change cards for modifying the PNPMN program as it exists on the tape AFWLT in order to treat general doping profiles. A specific case for the PNPP⁺ epitaxial transistor is illustrated as a modification of the 2N396A transistor doping profile with a P⁺ region ($p = 10^{19}/\text{cm}^3$) located at the right-hand edge of the collector region ($x = 1.35 \times 10^{-3} \text{ cm}$).

```

A      654      5      DOPING PROFILE      CFFPNP
C      CHANGE CARDS FOR TREATING MORE GENERAL DOPING
C      PROFILES. INPUT IS MADE BY WAY OF DATA STATEMENTS.

      DIMENSION ENP(8),XBK(8)
      DATA ENP/2*-10.,2*.01,2*-10.,2*-100./,XBK/-1.,-.900001E-3,--.9E-3,
      . . .9E-3,.900001E-3,1.35E-3,1.39E-3,1./

C      669      14      DOPING PROFILE      CFFPNP
C      CALCULATE EN IN EACH INTERVAL

      I=1
      K=2
      DRV=(ENP(2)-ENP(1))/(XBK(2)-XBK(1))
      H2=ENP(1)+DRV*(XH(1)-XBK(1))
      DTN=0.
      H1=H2
      XS=XH(I)
      I=I+1
      IF(I.GE.MI) GO TO 15
      IF(XBK(K).LT.XH(I)) GO TO 13
      H2=H1 + DRV*(XH(I)-XS)
      EN(I)=(DTN+(H2+H1)*(XH(I)-XS))/(X(I+1)-X(I-1))
      GO TO 12

      12      DTN=DTN+(ENP(K)+H1)*(XBK(K)-XS)
      XS=XBK(K)
      H1=ENP(K)
      DRV=(ENP(K+1)-ENP(K))/(XBK(K+1)-XBK(K))
      K=K+1
      GO TO 121

      15      EN(MI)=EN(MIM)
      EN(1)=EN(2)
END OF BLOCK

C      763      4      4      DOPING PROFILE      CNSPNP
C      CALCULATE BUILT-IN VOLTAGES
      VBCC=ZKT*ALOG(SQRT(4.*ZNOSQ + EN(IOP)*EN(IOP))+EN(IOP))
      VEBC=-ZKT*ALOG(SQRT(4.*ZNOSQ + EN(1)*EN(1))+EN(1))+VBCC
      VBCC=ZKT*ALOG(SQRT(4.*ZNOSQ + EN(MI)*EN(MI))+EN(MI))-VBCC

C      820      32      7      DOPING PROFILE      IZPNP
C      CALCULATE INITIAL CONCENTRATIONS

      DO 12 I=1,MI
      EFD(I)=0.
      GAM=SQRT(4.*ZNOSQ+EN(I)*EN(I))
      HD(I)=.5*(GAM-EN(I))+DEIR
      ED(I)=HD(I)+EN(I)

```

Appendix B

THE DIODE CODE

B.1. ORGANIZATION

The PND4 code is divided into a number of subroutines. The functions of the subroutines are described below.

1. The Main Program controls the flow of the calculation. The principal phases of the calculation are

- a. Reading the input, which is done by PNDIN*.[†]
- b. Initialization. When starting from scratch, XCAL* builds the initial mesh and PNDCI* sets up an initial distribution of carriers. When starting from a distribution obtained from a restart dump, READ* reads the dump tape and places it in position to receive additional blocks. In either case, PNDCI* computes constants derived from the input data and COPF* calculates the geometrical factors that occur in the coefficients of the difference equations.
- c. Taking one step in time, which is an operation performed by PNDCAL* in conjunction with VICAL*, which calculates the voltage across the diode, and with COPCAL*, which finds the crossover point.
- d. Checking for the appearance of negative densities.
- e. Backing up and reducing the time step either when negative densities occur or when the iterative procedure for solving the nonlinear difference equations fails.
- f. Printing results, which is done by PNDOUT* and INTCAL*.
- g. Dumping blocks of restart data, which is done by PUNCH*.
- h. Checking the rate of progress and terminating when it falls too low (Section 2.2.3).

[†] When reference is made to a subroutine that is called by the subroutine under discussion, the name of the former subroutine, i.e., the subroutine that is called, is starred.

i. Checking elapsed Central Processor time and terminating when the time limit is exceeded.

j. Controlling the time step (Section 2.2.3).

k. Comparing changes of densities and field strength with remesh criterion. When the critical ratio is exceeded, REMESH* builds a new mesh, after which ADJUST* calculates what the densities should be at the new mesh points. Then COEFF recalculates geometrical factors, and VICAL recalculates the voltage across the diode.

l. Terminating the run.

2. PNDIN is the input routine. It is called by the Main Program. Its function is to read the input cards. A separate section, Section B.3, INPUT, is devoted to explaining what goes into the input deck. PNDIN edits and prints all the input data.

3. COPCAL finds the crossover point (see Section 2.2.1.4), which is the last point i in the mesh at which $n_i > p_i$. COPCAL is called from a number of places in the Main Program.

4. PNDCAL is called by the Main Program. Its function is to advance the calculation one step in time. The procedure it uses (see Section 2.2.1.5) is to

a. Call RCAL* to obtain the denominators d_i of the recombination term;

b. Call HJKCAL* to obtain H_i^{l-1} , J_i^{l-1} , and K_i^{l-1} ;

c. Calculate $g(t^l)$ using the (FORTRAN) function G*; and then, in the iterative loop,

d. Have HJKCAL and ABCAL* form the coefficients of the linearized equations;

e. Have EXSCAL* solve the linearized equations;

f. Have NPECAL* update the estimates of n^l , p^l , and E^l and check for convergence;

g. Go back to (d) if the iteration limit has not been exceeded

nor the convergence criterion met; otherwise,

h. Have PNCAL* calculate the densities of the majority carriers, and

i. Return.

5. PNDOUT is called by the Main Program. There are two print modes: a short print, consisting of one line of important quantities, including the time, voltage, and current, and a long print, in which all available information of physical interest is printed. A complete tabulation of the printout is contained in Section B.4.

6. EXSCAL is called by the subroutine PND CAL. First, it calculates those coefficients of the linearized equations that depend on the current. To do this, it needs the voltage which it obtains by calling VICAL*. Next, the elimination procedure is performed upon the matrix \mathcal{Q} of coefficients of the linearized equations. Finally, the corrections ι , ν , π , and ϵ are calculated (see Section 2.2.1.5).

7. REMESH is called by the Main Program when a new set of mesh points is to be constructed (see Section 2.2.3.2). REMESH uses RTSCH* for optimizing the parameter p .

8. RTSCH is a general-purpose root-searching routine called by REMESH. It is designed for use by a calling program that contains within it the evaluation of a function f of one variable X , one of whose roots is to be located. The standard form of call is,

CALL RTSCH (IND, Y, X, DY, EPSX, EPSY, ITX).

The standard procedure is first to command RTSCH to initialize itself, which is done by calling it after having set $IND = 0$, $X = X_0$, a first estimate of a root of f , and $DY = DY_0$, an estimate of $f'(X_0)$. Note: $DY = 0$ is prohibited. When RTSCH returns, IND is an output indicating the status of the searching process. When RTSCH returns with $IND = 1$, it is requesting an evaluation of $f(X)$, so after the calling routine sets $Y = f(X)$, it reenters

RTSCH with IND unchanged, ITX set equal to a bound on the number of steps to take, and EPSX and EPSY set to tolerances on X and Y. When RTSCH returns with IND = 2, it is indicating that either $|Y| < \text{EPSY}$ or else that both positive and negative values of f have been observed in the interval between $X \pm \text{EPSX}$. When RTSCH returns with IND = 3, the iteration limit ITX has been exceeded.

†
List of arguments:

- ** (1) IND, integral input and output
 - IND = 0 on input is a command to initialize
 - IND = 1 on output requests $Y = f(X)$
 - = 2 on output indicates convergence
 - = 3 on output indicates nonconvergence
- (2) Y, real input. $Y = f(X)$
- ** (3) X, real input and output. X is to be used as the argument of f .
- ** (4) DY, real input and output. DY is an estimate of $f'(X)$ used to estimate by how much X should be changed.
- (5) EPSX, real input, tolerance on X
- (6) EPSY, real input, tolerance on Y
- (7) ITX, integral input, bounds number of trials

The method used for searching is the rule of false position (also called regula falsi and ROFP) combined with interval halving. ROFP is used until a point, X_i , is found at which the sign of f differs from that of $f(X_{i-1})$. The points X_i and X_{i-1} are then set up as bounds on the interval in which the search is to be continued. These bounds are updated after every evaluation of f , and when ROFP recommends an X outside the bounds, the point midway between them is selected instead.

† A double-starred argument is an input parameter which, because it is also an output parameter, may not be a literal constant but only a variable name.

Sample Application

```
.  
. .  
X = 0.5  
DY = 1.  
IND = 0  
13 CALL RTSCH (IND, Y, X, DY, -1., 1.E-6, 20)  
GO TO (14, 16, 15), IND  
14 Y = 0.333  
IF (X.EQ.0.) GO TO 13  
Y = (TAN(X)/X - 1.)/(X * X)  
GO TO 13  
15 Print error message  
CALL EXIT  
16 CONTINUE  
. . .
```

9. ADJUST is called by the main routine after remeshing (REMESH). It calculates the carrier densities at the new mesh points and then recalculates the electric field (see Section 2.2.3.2).

10. PUNCH is called by the Main Program for dumping the arrays X, ED, HD, and EFD at a rate prescribed by an input parameter to provide data for restarting. The data are dumped in two records called a block. The first record is a short one of fixed length containing the time, t^l , the latest time interval, Δt , the number of intervals (called I in Section 2.2) in the current mesh, and a few other numbers that are not essential. Details of the procedure for restarting are to be found in Section B.2.

11. READ is called by the Main Program to read the dump tape. Blocks dumped in various problems may be stacked one after another on one tape. When this is to be done, the input quantity IOPT(1) tells how many

restarting blocks already on the tape are to be preserved. If $IOPT(1) > 0$, READ prints a catalog of the first $IOPT(1)$ blocks on the tape and leaves the tape positioned so that the first block dumped (by PUNCH) will be the $IOPT(1) + 1$ th block on the tape. All this is done for scratch starts as well as restarts. The input quantity $IOPT(2) (\leq IOPT(1))$ is the number of the block containing the data to be used for restarting.

12. XCAL is the routine that the Main Program calls in order to obtain an initial mesh for starting from scratch. The procedure for generating the mesh is to select points by taking steps of constant length until some limit $XDX(K)$ is passed, at which point the length of the step is multiplied by the quantity $XDXM(K)$ and K is advanced. The process starts at the center, $x = 0$, with an interval of length $DELXI$, and is carried out independently in both directions until the end of the diode is reached. The pairs $XDX(K)$, $XDXM(K)$ are read off cards by XCAL. Two sets of data are read: the first for the left side of the diode and the second for the right side. Restrictions: left side, $XM < XDX(K + 1) < XDX(K) < 0$, $XDXM > 0$; right side, $0 < XDX(K) < XDX(K + 1) < XP$, $XDXM > 0$.

13. PNDCI is called by the Main Program just once near the beginning of each run. It calculates much used constants and, when starting from scratch, the initial distribution of electric field and carriers (see Section 2.2.1.6).

14. INTCAL is called by the Main Program for calculating conservation integrals (Section 2.2.4).

15. NPECAL is called by PNDCAL after it calls EXSCAL. It adds corrections to the old estimates of n , p , and E to get new ones in the iterative procedure for solving the nonlinear difference equations (Section 2.2.1.5). NPECAL also increments the iteration counter and checks to see if the convergence criterion has been met.

16. VICAL is called by the Main Program and EXSCAL. It calculates the voltage across the diode.

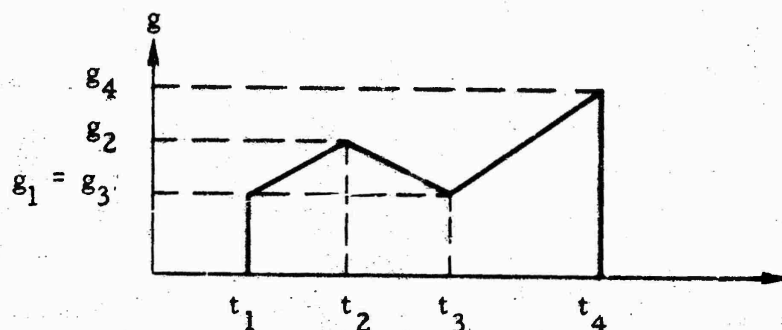
17. COEFF is called by the Main Program whenever the mesh is changed. It calculates all the geometrical constants in the coefficients of the difference equations.

18. G is the FORTRAN name for the dose rate as a function of time (Section 2.2.2.1). Actually, the function subprogram G, which is called by PNDGAL, calculates not only $g(t)$ but also the dose $GINT = \int_0^t g \, dt$. The input routine PNDIN reads the specification of the function g as a set of pairs g_k, t_k , $1 \leq k \leq k_{\max}$, where $g_k \geq 0$ and $t_k < t_{k+1}$. Then,

$$g(t) = 0 \quad \text{for } t < t_1, t_{k_{\max}} < t,$$

$$g(t) = g_{k+1} \frac{t - t_k}{t_{k+1} - t_k} + g_k \frac{t_{k+1} - t}{t_{k+1} - t_k} \quad \text{for } t_k \leq t \leq t_{k+1},$$

or graphically,



When G is called, it is not actually $g(t)$ that is returned but

$$\bar{g} = \frac{1}{\Delta t} \int_{t}^{t+\Delta t} g(t') \, dt'.$$

At the same time, $\bar{g} \Delta t$ is added to GINT. Thus, use is made of the fact that G is called only once for each time step. Whenever GINT is updated, its previous value is saved in GINTO so that GINT can be restored in the event of a back-step procedure.

19. GAVAL is called by HJKCAL. It calculates

$$\begin{aligned} \text{HELP}(i) &= 1/\bar{E}_i^3 \\ \text{GNFN}(i) &= n_i \alpha_n(\bar{E}_i) & n_i < p_i \\ \text{GNFP}(i) &= n_i \alpha_n(\bar{E}_i) & p_i \leq n_i \\ \text{GPFN}(i) &= p_i \alpha_p(\bar{E}_i) & n_i < p_i \\ \text{GPFP}(i) &= p_i \alpha_p(\bar{E}_i) & p_i \leq n_i \end{aligned}$$

which are the contributions of avalanche to the rate of generation of pairs of carriers (see Section 2.2.2.1).

20. RCAL is called by PNDCAL. It calculates the denominator d_i of the recombination term (Section 2.2.2.1). In the process, it calculates the lifetimes as a function of total dose (Section 2.2.2.3).

21. HJKCAL is called by PNDCAL. It calculates the H, J, K of Section 2.2.1.5.

22. ABCAL is called by PNDCAL. It calculates the matrix of coefficients of the linearized equations.

23. PNCAL is called by PNDCAL. It calculates the densities of the majority carriers and also

$$\begin{aligned} \Delta N / \Delta t &= \frac{N^l - N^{l-1}}{t^l - t^{l-1}}, & \Delta P / \Delta t &= \frac{P^l - P^{l-1}}{t^l - t^{l-1}}, \\ H_i^V &= - \frac{\delta \bar{n}_i^V}{\delta x_i}, & J_i^V &= - \frac{\delta \bar{p}_i^V}{\delta x_i}, \\ H_i^D &= \frac{\delta \bar{n}_i}{\delta x_i}, & J_i^D &= \frac{\delta \bar{p}_i}{\delta x_i}, \end{aligned}$$

$$-G_i = R_i - g - A_i, \quad H_i = G_i + H_i^V + H_i^D, \quad \text{and} \quad J_i = G_i + J_i^V + J_i^D.$$

The latter quantities are all listed in the long form of printout (see Section B.4 and Section 2.2.4).

B.2. SETTING UP A RUN ON PND4

The code PND4 refers to three files: INPUT, OUTPUT, and TAPE7. The INPUT and OUTPUT files are the standard ones. The other file, TAPE7, is for storing restart points. The code was designed so that when one run uses data from a previous run as a source of input values, the restart points dumped by the new run are added to the tape from which the initial values were read.

The differences between starting from scratch and restarting are:

1. When starting from scratch, IOPT(2) = 0, and when restarting, IOPT(2) is the number of the block containing the initial distribution for the new run.
2. When restarting, the input deck need not contain the cards that XCAL reads to obtain specifications for an initial mesh.
3. When starting from scratch, any tape may be REQUESTed for receiving blocks of restart data. If the tape contains no restart data to be preserved, IOPT(1) = IOPT(2) = 0 and dumping begins at the load point. Indeed, it is not necessary to submit any tape when starting from scratch. Setting the number of time steps per dump, IOPT(4), to an absurdly high value will suppress all dumps but that of the initial data, which may be allowed to fail on the disk.

B.3. INPUT

The input deck for PND4 is divided into three sets. Strictly speaking, all three sets are of variable length, but in practice, the first, Set I, always contains a title card followed by 13 cards (Card 2 through Card 14) of basic parameters. Set II contains specifications for the pulse of radiation. It usually contains just one card but it may contain as many as seven, depending on how complicated the shape of the pulse is. Set III is needed when starting from scratch in order to specify how the initial mesh is to be generated.

Three formats are used in preparing the cards. The title card is in format E12.8, 10A6, the first field holding a problem number and the

second, the title itself. The other cards are either in a 12I6 or 6E12.8 format, depending on whether they contain interger or real parameters.

Input Cards

Set I. Basic Parameters

Card 1 (E12.8, 10A6)

PROBNC Problem number.
PROBNM(I) Problem title.

Card 2 (12I6)

IOPT(1) Number of blocks to be preserved on the dump
file TAPE7. IOPT(1) = 0 when a new tape is
used or when no tape is desired.

IOPT(2) Block number of block from which to obtain
initial data. IOPT(2) = 0 when starting from
scratch. Restriction: IOPT(2) \leq IOPT(1).

IOPT(3) Maximum number of iterations per time step
(see Section 2.2.1). Usually IOPT(3) = 5.

IOPT(4) Restart dumps are recorded every IOPT(4) time
steps.

IOPT(5) Print control. An extensive printout showing the
state of the diode is printed every IOPT(5) time
steps or after each dump, whichever is oftener.

IOPT(6) Number of input parameters in array IEXTRA.
Set IOPT(6) = 5.

IOPT(7) Number of input parameters in array EXTRA.
Set IOPT(7) = 16.

IOPT(8) When restarting, t and Δt are normally (IOPT(8) = 0)
picked up off TAPE7. If IOPT(8) \neq 0, then t and Δt
are read from Card 6 as when starting from scratch.

IOPT(9) INFLEC, the number of points in the specification
of g. (See description of function G in Section B.1;

see also Section 2.2.2.1). Restriction: $2 \leq \text{IOPT}(9) \leq 20$.

IOPT(10) Not used.

IOPT(11) Not used.

IOPT(12) Not used.

Card 3 (6E12.8) (See Sections 2.1.1 and 2.2.1.)

DELN(1) ΔN_p , the difference between concentration of donors and concentration of acceptors in p region.

DELN(2) ΔN_n , the difference between concentration of donors and concentration of acceptors in n region.

D(1) D_n , the diffusion constant of electrons.

D(2) D_p , the diffusion constant of holes.

XMU(1) μ_n , the mobility of electrons.

XMU(2) μ_p , the mobility of holes.

Note: Ordinarily, $D(1)/D(2) = \text{XMU}(1)/\text{XMU}(2)$.

Card 4 (6E12.8)

XM -a, the x coordinate of the boundary of the p region.

XP b, the x coordinate of the boundary of the n region.

TAU0(1) τ_{p0} , the lifetime of electrons in the p region before damage (see Section 2.2.2.3).

TAU0(2) τ_{n0} , the lifetime of holes in the n region before damage (see Section 2.2.2.3).

VS(1) v_{ns} , saturated drift velocity of electrons.

VS(2) v_{ps} , saturated drift velocity of holes.

Card 5 (6E12.8)

CNP	n_{0p} , equilibrium concentration of electrons in the p region.
CNN	n_{0n} , equilibrium concentration of electrons in the n region.
CPP	p_{0p} , equilibrium concentration of holes in the p region.
CPN	p_{0n} , equilibrium concentration of holes in the n region. (Usually, $CNP * CPP = CNN * CPN = n_0^2$, where n_0 is the intrinsic concentration of electrons. $CNP - CPP = DELN(1)$ and $CPP - CPN = DELN(2)$.)
XE	q , the magnitude of the charge on an electron (usually, $XE = 1.6E - 19$).
SKAPPA	K , the dielectric constant (usually SKAPPA = $1.78E - 11$ for Ge, $1.33E - 11$ for Si, and $1.11E - 12$ in vacuo).

Card 6 (6E12.8)

TB	t^0 , the starting time.
TEND	Ending time. Run is discontinued if $t^l > TEND$.
DELTI	$t^1 - t^0$, the duration of the first time step (usually, $DELTI = 1.E - 14$).
DL	w_0 , used in controlling the time step. ($w_0 = 10$ works well; see Section 2.2.3.1.)
DELR	$r = C * DELR$ is the density of pairs due to ionization at $t = t^0$ (see Section 2.2.1.6).
RTL	Run time limit. No time steps are begun if the elapsed CP time exceeds RTL sec.

Card 7 (6E12.8)

ERROR	ϵ_{max} , the convergence criterion in the iterative procedure for solving the difference equations (see Section 2.2.1.5).
-------	---

DELX The length of the interval at $x = 0$ (see Subroutine XCAL in Section B. 1).

OMEGA ω , a weighting factor used in the time integration. Set $\omega = 1$ (see Section 2.2.1.3).

C The scale factor for concentrations. CNP, CNN, CPP, CPN, DELN(1), DELN(2), and DELR multiplied by C give the true values of the quantities they represent (usually, $C = 1.E + 17$).

AN i , the initial current in the external circuit. AN is used in subroutine PNDCI to compute the initial conditions when starting from scratch.

RN Not used.

Card 8 (6E12.8)

EPS(1) V_0 , the bias voltage (see Section 2.1.2).

EPS(2) R , the resistance in the external circuit (see Section 2.1.2).

EPS(3) a_0 , the effective area of the diode (see Section 2.2.1.1).

EPS(4) Not used.

EPS(5) n' } are used by subroutine RCAL for calculating the
 EPS(6) p' } denominator of the recombination term.

Card 9 (12I6)

IEXTRA(1) I_{\max} , the maximum number of points in the spatial mesh (see Section 2.2.3.2). Restriction: IEXTRA(1) < 300.

IEXTRA(2) I_{\min} , the minimum number of points in the mesh (Section 2.2.3.2). Usually, IEXTRA(2) = IEXTRA(1) - 15.

IEXTRA(3) n_2 in the control of the time step (see Section 2.2.3.1). IEXTRA(3) = 3 is reasonable.

IEXTRA(4) n_1 in the control of the time step (Section 2.2.3.1). IEXTRA(4) = 3 is reasonable.

IEXTRA(5) n_3 in the control of the time step (Section 2.2.3.1).
IEXTRA(5) = 3 is good.

IEXTRA(6)
through IEXTRA(12) Not used.

Card 10 (6E12.8)

EXTRA(1) Criterion for remeshing. When the ratio of concentrations or fields at consecutive points exceeds EXTRA(1), a new mesh is built (see Section 2.2.3.2). EXTRA(1) = 30. works well with IEXTRA(1) = 150.

EXTRA(2) Not used.

EXTRA(3) In calculating the spatial mesh, the ratio of the lengths of successive intervals is required to be no more than EXTRA(3) (Section 2.2.3.2). Usually, EXTRA(3) = 1.6. Restriction: EXTRA(3) > 1.

EXTRA(4) ρ , an initial estimate of the magnitude of the log of the ratio of concentrations or fields at consecutive mesh points (Section 2.2.3.2). EXTRA(4) = 0.2 is reasonable. Restriction: EXTRA(4) > 0.

EXTRA(5) An estimate of $dI/d\rho$. (Section 2.2.3.2.) EXTRA(5) = 200. is reasonable. Restriction: EXTRA(5) > 0.

EXTRA(6) E_M . The restriction on the mesh that pertains to the field is that

$$\rho < |\log ((|E_i| + E_M) / (|E_{i-1}| + E_M))|.$$

(Section 2.2.3.2) EXTRA(6) = 2. works well.

Card 11 (6E12.8)

EXTRA(7) w_1 , the amount that is added to w_0 by the time step control (see Section 2.2.3.1 and DL on Card 6). EXTRA(7) - 5 is reasonable.

EXTRA(8) w_2 , an amount that is subtracted from w_0 in the event of failure to converge or convergence to negative concentrations (Section 2.2.3.1). EXTRA(8) = 5 is reasonable.

- EXTRA(9) w_{\max} , the upper limit on w_0 (Section 2.2.3.1).
EXTRA(9) = 10. is reasonable.
- EXTRA(10) w_{\min} , the lower limit on w_0 (Section 2.2.3.1).
EXTRA(10) = 1. is reasonable.
- EXTRA(11) Multiplies Δt in the event of failure to converge or convergence to negative concentrations (Section 2.2.3.1). Usually, EXTRA(11) = 0.2.
- EXTRA(12) ϵ_w , used in the criterion for bogging down (Section 2.2.3.1). EXTRA(12) = 0.001 seems to do a good job.

Card 12 (6E12.8)

- EXTRA(13) Not used.
- EXTRA(14) On restarts, if EXTRA(14) $\neq 0$, then the code sets $\Delta t = \text{EXTRA}(14)$ rather than using the value on the dump tape. It is an alternative to IOPT(8), which also resets time.
- EXTRA(15) } When $t < \text{EXTRA}(15)$, then $E_M = \text{EXTRA}(16)$ instead of
EXTRA(16) } EXTRA(6). Usually, EXTRA(16) = EXTRA(6).
- EXTRA(17) Not used.
- EXTRA(18) Not used.

Card 13 (6E12.8)

- | | | |
|-------|-------|---|
| CB(1) | b_n | } Constants used to describe multiplication caused by avalanche (see Section 2.2.2.1). Set $k = b = 0$ for suppressing avalanche. |
| CK(1) | k_n | |
| CB(2) | b_p | |
| CK(2) | k_p | |
- Fields 5, 6 Not used.

Card 14 (6E12.8)

TK(1)	K_p	} Used in calculation of effect of flux on lifetimes (see Section 2. 2. 2. 3).
TK(2)	K_n	
GINT	$\int_{-\infty}^0 g(t) dt$	

Fields 4, 5, 6 Not used.

Set II. Specification of $g(t)$

The function of g is determined from a set of pairs t_k, g_k for $1 \leq k \leq \text{IOPT}(9)$, where $t_k < t_{k+1}$. In the interval $t_k \leq t \leq t_{k+1}$, g is assumed to vary linearly from g_k to g_{k+1} , and unless $t_1 \leq t \leq t_{\text{IOPT}(9)}$, g is assumed to vanish. Each card of Set II contains three pairs of t_k, g_k , so there are $(\text{IOPT}(9) + 2)/3 \equiv \text{NSET2}$ cards in the set, i.e., just enough to hold all the data. Since $2 \leq \text{IOPT}(9) \leq 20$, it follows that $1 \leq \text{NSET2} \leq 7$.

Card 14+n (6E12.8)

$1 \leq n \leq \text{NSET2}$

TIM(3n - 2)	t_{3n-2}	} Restriction: $\text{TIM}(K) < \text{TIM}(K + 1)$ If $g \equiv 0$, set $\text{IOPT}(9) = 2$, $H(1) = H(2) = 0$, $\text{TIM}(1) = -2$, and $\text{TIM}(2) = -1$.
H(3n - 2)	g_{3n-2}	
TIM(3n - 1)	t_{3n-1}	
H(3n - 1)	g_{3n-1}	
TIM(3n)	t_{3n}	
H(3n)	g_{3n}	

Set III. Specification of the Initial Mesh

The cards of this set contain specifications for the initial mesh, and so the whole set is usually absent for restarts ($\text{IOPT}(2) > 0$). The cards of this set are read by subroutine XCAL. The set is divided into two subsets, the first for specifying the mesh in the p region ($x < 0$) and the second for specifying the mesh in the n region ($0 < x$). The first card of each subset

contains an interger NDX_j , $j = 1$ or 2 , and the following cards of each subset contain the NDX_j pairs of specifications on $(NDX_j + 2)/3$ cards, i. e., just enough cards to hold the data, as in Set II.

Card 15 + NSET2 (I6)

NDX_1 The number of pairs in the specification of the mesh in the p region.

Card 15 + NSET2 + M (6E12.8) $1 \leq M \leq (NDX_1 + 2)/3 \equiv NSET31$

$XDX(3M - 2)$	}	See XCAL in Section B. 1. Restriction: $XM < XDX(K + 1) < XDX(K) < 0$.
$XDXM(3M - 2)$		
$XDX(3M - 1)$		
$XDXM(3M - 1)$		
$XDX(3MO)$		
$XDXM(3M)$		

Card 16 + NSET2 + NSET31 (I6) (Where $NSET31 \equiv (NDX_1 + 2)/3$.)

NDX_2 The number of pairs in the specification of the mesh in the n region.

Card 16 + NSET2 + NSET31 + M (6E12.8) $1 \leq M \leq (NDX_2 + 2)/3$

Same as Card 15 + NSET2 + M except for the Restriction: $0 < XDX(K) < XDX(K + 1) < XP$.

B. 4. PRINTOUT

At the beginning of the output for each problem, MAIN prints C. P. time (Central Processor time) charged to the run at that point (including compilation time, if any). PNDIN prints the input data contained on input Card 1 through Card 15 (or more) and, in addition, prints EPNI, where

$$EPNI = \frac{4\pi qC}{K}$$

If there are any blocks to be saved on the dump tape, a map of these blocks is printed by READ. If the problem is a restart, the restarting block is noted and the time at which the problem is actually restarted is printed by READ. If the problem is an initial start, PNDCI prints VSUBC, A1, and A2, where

$$VSUBC = V_C = \frac{1}{40} \log \left(\frac{P_{0p}}{P_{0n}} \right), \text{ the equilibrium voltage,}$$

$$\begin{aligned} A1 &= \alpha \\ A2 &= \beta \end{aligned} \left\{ \begin{array}{l} \text{The } \alpha \text{ and } \beta \text{ of Eqs. (10) and (11) of the Supplement} \\ \text{to General Atomic Report GA-6217 by S. C. Choy.} \end{array} \right.$$

After each converged cycle, the following variables are always printed by either PNDOUT or INTCAL:

<u>OUTPUT TITLE</u>	<u>FORTTRAN VARIABLE NAME</u>	<u>DESCRIPTION</u>
TIME	TIME	t, problem time.
DELT	DELT	Δt , time step from previously converged cycle.
DL	DL	w_0 , constant used in time calculation.
V(T)	VT	Voltage across diode.
NUMBER OF ITERATIONS		Number of iterations to obtain converged cycle.
C-O-P	X(I0)	X coordinate of crossover point.
TAU(1)	TAU(1) (τ_p)	Electron lifetime in the p region for previously converged cycle.
TAU(2)	TAU(2) (τ_n)	Hole lifetime in the n region for previously converged cycle.
GINT	GINT ($\int_0^t g(t') dt'$)	Unscaled by C (the scaling factor).
GINTO	GINTO ($\int_0^{t-\Delta t} g(t') dt'$)	Unscaled by C.
G	GTCCC ($\int_{t-\Delta t}^t g(t') dt'$)	Scaled by C; thus, actual integral = C · G.

After remeshing, the following variables are always printed by
REMESH:

MI		I, number of mesh points generated by REMESH.
RO		ρ , remesh parameter.
RODEL	$RODEL \left(- \frac{dI}{d\rho} \right)$	Derivative of remesh parameter.

After every IOPT(5) converged cycles, the following variables are printed by PNDOUT or INTCAL:

BLOCK NO.	IBLOCK	(This is only printed on the IOPT(4)th converged cycle.) Block (record) number in which the cycle is recorded.
X	X(I)	X coordinate of integral mesh point.
	XH(I)	X coordinate of half-integral mesh point.
N	ED(I)	n_i , electron density at integral mesh point.
P	HD(I)	p_i , hole density at integral mesh point.
DN/DT	OUT(I, 1)	$\partial n / \partial t$ at integral mesh point (in line of output with X(I)).
	OUT(I, 8)	$\frac{n_i^l - n_i^{l-1}}{\Delta t} = \frac{\Delta n}{\Delta t}$ (in line of output with XH(I)).
D(N)	OUT(I, 2)	$D_n \frac{\partial^2 n}{\partial x^2}$ at integral mesh point.
MU(N)	OUT(I, 3)	$\mu_n \frac{\partial}{\partial x} (E \cdot n)$ at integral mesh point.
DP/DT	OUT(I, 4)	$\frac{\partial \rho}{\partial t}$ at integral mesh point (in line of output with X(I)).
	OUT(I, 9)	$\frac{p_i^l - p_i^{l-1}}{\Delta t} = \frac{\Delta \rho}{\Delta t}$ (in line of output with XH(I)).

D(P)	OUT(I, 5)	$D_p \frac{\partial^2 p}{\partial x^2}$ at integral mesh point.
MU(P)	OUT(I, 6)	$-\mu_0 \frac{\partial}{\partial x} (E \cdot p)$ at integral mesh point.
R	OUT(I, 7)	$-G_i$ term at integral mesh point.
E	EFD(I)	Electric field at half-integral mesh point (in line of output with XH(I)).
INTEGRAL OF N	SUME	$\int n \, dx$
INTEGRAL OF P	SUMH	$\int p \, dx$
INTEGRAL OF R	SUMR	$-\int G \, dx$
INTEGRAL OF DN/DT	SUMEDT	$\int (\partial n / \partial t) \, dx$
INTEGRAL OF DP/DT	SUMHDT	$\int (\partial p / \partial t) \, dx$
INTEGRAL OF RIGHT(N)	SUMRET	$\int (\Delta n / \Delta t) \, dx$
INTEGRAL OF RIGHT(P)	SUMPHT	$\int (\Delta p / \Delta t) \, dx$

ERROR MESSAGES

<u>SUBROUTINE</u>	<u>MESSAGE PRINTED</u>	<u>COMMENT</u>
MAIN	"CHGMAX IS LESS THAN OR EQUAL TO (CHGMAX) CONSECUTIVELY FOR (KICK) TIMES"	The problem is terminated after printing and writing on dump tape. See Section 2.2.3.1 for further discussion.
MAIN	"SOME ELECTRON- OR HOLE-DENSITIES ARE ZERO OR NEGATIVE, BUT REMESHING IS NOT POSSIBLE"	This message should not be encountered; it indicates a programming error.
COPCAL	"CROSS-OVER-POINT IS OUTSIDE OF ALLOWED RANGE"	The problem is terminated immediately.
REMESH	"REMESH IS UNABLE TO CALCULATE RO"	The problem is terminated immediately.

<u>SUBROUTINE</u>	<u>MESSAGE PRINTED</u>	<u>COMMENT</u>
READ	ERROR--IOPT(2) IS GREATER THAN IOPT(1)--READ	Input error--the problem is terminated immediately.
XCAL	"ONE OF XDXM(I) IS ZERO OR NEGATIVE--XCAL"	Input error--the problem is terminated immediately.
XCAL	"MAXIMUM NUMBER OF X-POINTS ALLOWED (300) IS EXCEEDED (MI) POINTS GENERATED-XCAL"	The problem is terminated immediately.
XCAL	"NDX IS GREATER THAN 60 -XCAL"	Input error--the problem is terminated immediately.
PNDCl	"ERROR TMP12 = "	Error in calculation of initial densities and fields. Problem is terminated immediately. See Section 2.2.1.6 for further discussion.
PNDCl	"ERROR TMP13 = "	
PNDCl	"ERROR A2 = "	
NPECAL	"(DID NOT YIELD CONVERGENCE) MAXIMUM RELATIVE ERROR = (ERMAX) AT X = (XMAX)"	Problem is not terminated. The time is backed up to that of the previous time step, Δt is reduced by EXTRA(11), and the densities and field values at each mesh point are restored to those of the previous time step.

B.5. GLOSSARY

The variables in COMMON storage are defined. Notation developed in Section 2.2 is used freely. A variable marked "obs." is no longer used, although it may still be computed. The address of each variable relative to the first word in its block is given in the form "/LAB/ + n" where LAB is the label of the block and n is expressed in octal.

AA(300) / / + 4313 $1/(\delta x_i \delta x_{i-\frac{1}{2}})$, for $1 \leq i \leq I$, the coefficient of n_{i-1} in $\delta(\delta n_i / \delta x_i) / \delta x_i$.

AED		obs.
AEFD		obs.
AEX(2)	/ / + 16743	Exceptional elements, $A_{2i+1\pm 1}^{2i+1\mp 2}$, of the matrix \hat{Q} near the crossover point.
AHD(300)		obs.
AMI(600)	/ / + 12203	The diagonal of \hat{Q} just below the main diagonal. A_k^{k-1} for $1 \leq k \leq 2I - 1$.
AM2(600)	/ / + 11053	The diagonal of \hat{Q} two below the main diagonal. A_k^{k-2} for $1 \leq k \leq 2I - 1$.
AN	/ / + 34	(Input, Card 7) The initial current.
APA(300)	/ / + 6573	$2/\delta x_i$ for $1 \leq i \leq I$.
API(600)	/ / + 14463	The diagonal of \hat{Q} just above the main diagonal. A_k^{k+1} for $1 \leq k \leq 2I - 2$.
AP2(600)	/ / + 15613	The diagonal of \hat{Q} two above the main diagonal. A_k^{k+2} for $1 \leq k \leq 2I - 3$.
AR	/ / + 20077	$a_0 R = \text{EPS}(2) * \text{EPS}(3) = A_1^1$ in the matrix \hat{Q} .
AZR(600)	/ / + 1332	The main diagonal of \hat{Q} . A_k^k for $1 \leq k \leq 2I - 1$.
B(600)	/ / + 16745	The RHS of the linearized equations.
BB(300)	/ / + 4767	$-2/\delta x_i / \delta x_i$ for $1 \leq i \leq I$, which is the coefficient of n_i in $\delta(\delta n_i / \delta x_i) / \delta x_i$.
BTA(300)	/ / + 7247	$1/\delta x_{i+2}$ for $1 \leq i \leq I$.
C	/ / + 33	(Input, Card 7) A scale factor by which input and printed concentrations are to be multiplied.
CB(2)	/COM10/+ 2735	(Input, Card 13) b_n and b_p in the avalanche term.
CC(300)	/ / + 5443	$1/\delta x_i / \delta x_{i+2}$ for $1 \leq i \leq I$, the coefficient of n_{i+1} in

		$\delta(\delta n_i / \delta x_i) / \delta x_i$.
CK(2)	/COM10/ + 2737	(Input, Card 13) k_n and k_p in the avalanche term.
CNN	/ / + 16	(Input, Card 5) n_{0n} , the equilibrium concentration of electrons in the n region.
CNP	/ / + 15	(Input, Card 5) n_{0p} , the equilibrium concentration of electrons in the p region.
CPN	/ / + 20	(Input, Card 5) p_{0n} , the equilibrium concentration of holes in the n region.
CPP	/ / + 17	(Input, Card 5) p_{0p} , the equilibrium concentration of holes in the p region.
CRR(2)	/ / + 1321	CRR(1) = CNP * CPP and CRR(2) = CNN*CPN. They should both be equal to n_0^2 in ordinary applications.
CSS(2)		obs.
D(2)	/ / + 5	(Input, Card 3) $D(1) = D_n$ and $D(2) = D_p$, the diffusion constants.
DELN(2)	/ / + 3	(Input, Card 3) $DELN(1) = \Delta N_p$ and $DELN(2) = \Delta N_n$, the doping levels of the p- and n-regions, respectively.
DELNN(2)		obs.
DELR	/ / + 27	(Input, Card 6) r , the initial concentration of pairs caused by radiation.
DELTA	/ / + 1347	$t^l - t^{l-1}$, the time interval.
DELTI	/ / + 25	(Input, Card 6) $t^1 - t^0$, the initial DELT.
DELX	/ / + 31	(Input, Card 7) The length of the interval in which the junction lies in the initial mesh.
DELXX		obs.
DENS	/ / + 4313	Used in subroutine REMESH. For each interval I,

RO/DENS(I) is the optimum interval length.

DEPN	/ / + 1340	A much used constant, $4\pi qC(D_p - D_n)/\kappa$, occurring in $K_{i+\frac{1}{2}}$ and calculated in subroutine PNDCL.
DL	/ / + 26	(Input, Card 6) The initial value of w_0 , used to compute the time step.
DNDIF		obs.
DNMU(2)	/ / + 1341	A pair of constants calculated by subroutine PNDCL. $DNMU(1) = 4\pi qC\mu_n \Delta N_p / \kappa$ and $DNMU(2) = 4\pi qC\mu_p \Delta N_n / \kappa$.
DNMUZ		obs.
DNSUM		obs.
DTCHG		obs.
ED(300)	/ / + 1354	n_i for $1 \leq i \leq I$, the electron density.
EDN(300)	/ / + 13333	A temporary storage for new n_i as they are computed by subroutine ADJUST on a new mesh.
EDO(300)	/ / + 21241	n_i^{l-1} for $1 \leq i \leq I$, the electron density at $t = t^{l-1}$.
EFD(300)	/ / + 2504	$E_{i+\frac{1}{2}}$ for $1 \leq i \leq I - 1$, the electric field.
EFDN		obs.
EFDO(300) /CMMNY/	+ 0	$E_{i+\frac{1}{2}}^{l-1}$ for $1 \leq i \leq I$, the electric field at $t = t^{l-1}$.
EN(300)	/ / + 3163	ΔN_i for $1 \leq i \leq I - 1$, the excess concentration of donors.
EPN	/ / + 143	A constant $\kappa/4\pi qC$ occurring in Poisson's equation.
EPNE	/ / + 20075	A factor $\kappa/4\pi$ occurring in some elements of Q .
EPNI	/ / + 144	A constant $4\pi qC/\kappa$ computed by PNDIN. $EPN = 1./EPNI$.
EPNMU		obs.
EPS(6)	/ / + 36	(Input, Card 8) An input array.

I EPS(I)

- 1 V_0 , the bias voltage.
- 2 R, the external resistance.
- 3 a_0 , the effective area of the diode.
- 4 Not used.
- 5 n' , concentrations when Fermi level is at energy.
- 6 p' , level of recombination centers.

ERROR / / + 30

(Input, Card 7) ϵ_{\max} , used in the convergence criterion.

EXS(600) / / + 7723

Y_k for $1 \leq k \leq 2I - 1$, the solution of the linearized equations.

EXTRA(20) / / + 70

(Input, Cards 10 through 12)

J EXTRA (J)

- 1 Criterion for remeshing.
- 2 obs.
- 3 ROX, the maximum ratio of abutting intervals.
- 4 $\rho = RO$, remeshing parameters. This quantity is updated.
- 5 $-dI/d\rho$. It is updated.
- 6 E_M . Electric fields weaker than E_M are ignored in remeshing.
- 7 w_1 . An increment to the time-control parameter w_0 .
- 8 w_2 . A decrement of the time-control parameter w_0 .
- 9 w_{\max} . The upper limit on w_0 .

		10 w_{\min} . The lower limit on w_0 .
		11 The factor by which Δt is multiplied when convergence fails, or negative concentrations appear.
		12 ϵ_w . When the fractional change in the concentrations is less than ϵ_w for $n_3 = \text{IEXTRA}(5)$ consecutive time steps, the run is halted.
GG(300)	/ / + 6117	$-4/\delta x_{i+1/2}/\delta x_{i+1/2}$, a factor in the formula for $K_{i+1/2}$ when its dependence on majority carriers is eliminated.
GINT	/COM20/ + 2	$\text{GINT} = \int_0^t g(t) dt.$
GINTO	/COM20/ + 3	$\text{GINTO} = \int_0^t g(t) dt.$
GNFN(300)	/COM10/ + 1130	$\alpha_n(\bar{E}_i)n_i$, the avalanche due to electrons in the p region.
GNFP(300)	/COM10/ + 0	$\alpha_n(\bar{E}_i)n_i$, the avalanche due to electrons in the n region.
GPFN(300)	/COM10/ + 1604	$\alpha_p(\bar{E}_i)p_i$, the avalanche due to holes in the p region.
GPFP(300)	/COM10/ + 454	$\alpha_p(\bar{E}_i)p_i$, the avalanche due to holes in the n region.
GTC	/ / + 20107	$g(t)$, the rate of production of pairs.
H(20)	/COM9/ + 24	(Input, Set II) g_k for $1 \leq k \leq \text{IOPT}(9)$. The pairs t_k, g_k serve to define $g(t)$.
HD(300)	/ / + 2030	p_i for $1 \leq i \leq I$ is the density of holes.
HDN(300)	/ / + 14070	A temporary storage for new p_i as they are computed by subroutine ADJUST on a new mesh.
HDO	/ / + 21715	p_i^{l-1} for $1 \leq i \leq I$, the density of holes at $t = t^{l-1}$.
HELP(300)	/COM10/ + 2260	$1/\bar{E}_i^3$ for $1 \leq i \leq I$, a factor in $d\alpha_n(\bar{E}_i)/d\bar{E}_i$.

HJK(300)	/ / + 2011	$HJK_{2i} = H_i$ when $n_i < p_i$, $HJK_{2i} = J_i$ when $n_i \geq p_i$, and $HJK_{2i+1} = K_{i+\frac{1}{2}}$ for $1 \leq i \leq I$.
IBLOCK	/ / + 0	IBLOCK is the block number of the latest restart point written on TAPE7.
IEXTRA(20)	/ / + 44	(Input, Card 10) J IEXTRA(J) 1 I_{\max} , the maximum number of points in the spatial mesh. 2 I_{\min} , the minimum number of points in the mesh. 3 n_2 , used in controlling the time step. When fewer than n_2 iterations are required on n_1 consecutive time steps, the parameter w_0 is incremented. 4 n_1 , defined above. 5 n_3 . When n_3 consecutive time steps produce relative changes in concentration of no more than ϵ_w , the run is terminated. 6-20 Not used.
II0		obs.
IND	/ / + 3162	IND = -1 indicates either failure to converge or presence of negative densities. IND = 0 is normal.
INFLEC	/COM9/ + 50	INFLEC = IOPT(9), the number of points in the specification of $g(t)$.
IOPT(12)	/ / + 127	(Input, Card 2) J IOPT(J) 1 The number of blocks of restart data on TAPE7 to be saved.

2 Number of blocks on TAPE7 from which to get initial distribution.

3 Maximum number of iterations per time step.

4 Number of steps per restart dump.

5 Number of steps per long printout.

6 Number of parameters to be read into IEXTRA.

7 Number of parameters to be read into EXTRA.

8 When IOPT(12) $\neq 0$, use TB and DELTI from cards, even when restarting.

9 INFLEC, length of g(t) specification.

10-12 Not used.

IPRINT	/ / + 2	Number of time steps since previous long printout.
IPUNCH	/ / + 1	Number of time steps since previous restart dump.
ISSET		obs.
ISUBI		obs.
ITER	/ / + 3161	The iteration counter.
IO	/ / + 1307	The index of the interval in which the junction lies.
IOM	/ / + 1310	$IOM = IO - 1$.
IOP	/ / + 1311	$IOP = IO + 1$.
MAXT		obs.
MI	/ / + 1302	The number of points in the mesh.

MIM	/ / + 1303	$MIM = MI - 1.$
MIMOLD	/ / + 1311	In subroutine ADJUST, the old value of MIM.
MIM2	/ / + 1305	$MIM2 = MI - 2.$
MIM3	/ / + 1306	$MIM3 = MI - 3.$
MIP	/ / + 1304	$MIP = MI + 1.$
MX	/ / + 1313	$MX = 2 * MI.$
MXM	/ / + 1314	$MXM = MX - 1 = 2 * MI - 1.$
MXM2	/ / + 1316	$MXM2 = MX - 2 = 2 * MI - 2.$
MXM3	/ / + 1317	$MXM3 = MX - 3 = 2 * MI - 3.$
MXP	/ / + 1315	$MXP = MX + 1 = 2 * MI + 1.$
NT	/ / + 3160	A counter for the number of consecutive time steps using fewer than n_2 iterations. ($n_2 = IEXTRA(3).$) Used in controlling the time steps.
OMEGA	/ / + 32	(Input, Card 7) The weighting factor ω used in estimating time derivations, $\omega = 1$ almost always.
OMEGAV	/ / + 1320	$OMEGAV = 1. / OMEGA - 1. = (1 - \omega) / \omega.$ Usually, $OMEGAV = 0.$
OUT(300,10)	/ / + 11053	An array for holding quantities for the long printout.

K OUT(I,K)

- 1 H_i , which is printed under "DN/DT".
- 2 $D \delta(\delta n_i / \delta x_i) / \delta x_i$, which is printed under " $\bar{D}(N)_i$ ".
- 3 $-\delta \bar{n}_{i,n} / \delta x_i$, under "MU(N)".
- 4 J_i , under "DP/DT".

- 5 $D_p \delta(\delta p_i / \delta x_i) / \delta x_i$, under "D(P)."
- 6 $-\delta \bar{p}_i u_i / \delta x_i$, under "MU(P)."
- 7 $-G_i$, under "R."
- 8 $(N^\ell - N^{\ell-1}) / (t^\ell - t^{\ell-1})$, under "DN/DT."
- 9 $(P^\ell - P^{\ell-1}) / (t^\ell - t^{\ell-1})$, under "DP/DT."
- 10 Not used.

PI	/ / + 1301	PI = 3.1415927.
PROBNM(10)	/ / + 115	(Input, Card 1) The title of the run.
PROBNO	/ / + 114	(Input, Card 1) An identifying number for the run.
QD(2)		obs.
QPN		obs.
QRR(2)		obs.
Q2	/ / + 1331	A constant. $Q2 = \kappa / 2\pi qC$.
R(300)	/ / + 3637	d_i for $1 \leq i \leq I$, the denominator of the recombination term.
RN		obs.
RPN		obs.
RTL	/ / + 20110	The run is discontinued when the elapsed C.P. time exceeds RTL sec.
SKAPPA	/ / + 22	(Input, Card 5) κ , the dielectric constant.
SUMMU	/ / + 1336	A constant. $SUMMU = XMU(1) + XMU(2) = \mu_n + \mu_p$.
TAU2	/ / + 13	The lifetimes of the carriers. $TAU(1) = \tau_p$, the lifetime of electrons in the p region, and $TAU(2) = \tau_n$, the lifetime of holes in the n region.

TAU0(2) /COM20/ + 4 (Input, Card 4) The lifetimes of the carriers before irradiation. See TAU.

TB / / + 23 (Input, Card 6) The time t^0 at which the problem starts.

TCHG obs.

TEND / / + 24 (Input, Card 6) Time at which problem ends.

TIM(20) /COM9/ + 0 (Input, Card 15) Times t_k at which $g(t_k) = g_k$ are given in order to specify $g(t)$.

TIME / / + 1346 The current value t^l of the independent variable, time.

TIME1 obs.

TIME2 obs.

TK(2) /COM20/ + 0 (Input, Card 14) Constants in the equation for flux-dependent lifetime:

$$\frac{1}{\tau_j} = \frac{1}{\tau_j^0} + K_j \int_0^{t^l} g(t) dt,$$

where $K_p = TK(1)$ and $K_n = TK(2)$.

VBAR obs.

VBAR1 obs.

VBAR2 obs.

VND(300) /COM11/ + 1130 v_i for $1 \leq i \leq I$, the drift velocity of electrons in interval i .

VOJT / / + 20076 The bias voltage plus the built-in voltage,
 $V_{OUT} = V_0 - .025 \log p_{0p}/p_{0n}$

VPD(300) /COM11/ + 1604 u_i for $1 \leq i \leq I$, the drift velocity of holes in interval i .

VSUBC Negative of the built-in voltage, $.025 \log p_{0p}/p_{0n}$ (in PNDCI)

VT	/ / + 1352	$V = \sum_{i=1}^{I-1} E_{i+\frac{1}{2}} \delta x_{i+\frac{1}{2}}$, the voltage across the diode less the built-in voltage, VSUBC.
WDT	/ / + 1350	$\omega(t^l - t^{l-1})$
WDTI	/ / + 1351	$1/\omega(t^l - t^{l-1})$
X(300)	/ / + 147	x_i for $1 \leq i \leq I$, the coordinate of the mesh points.
XB	/ / + 7723	A provisional mesh constructed by the sub-routine REMESH.
XE	/ / + 21	q , the magnitude of the charge of the electron.
XEE	/ / + 21	A synonym for XE.
XH(300)	/ / + 623	$x_{i+\frac{1}{2}}$ for $1 \leq i < I$, the coordinates of the midpoints of the intervals.
XHN(300)	/ / + 12203	$XHN(I) = .5 * (XN(I) + XN(I + 1))$, the midpoints of the new intervals.
XIT		obs.
XJ	/ / + 20105	i/a_0 , the current density at the ends of the diode.
XJV	/ / + 20106	$4\pi i/Ka_0$, a term of K.
XM	/ / + 11	(Input, Card 4) $-a$, the coordinate of the left boundary of the diode.
XMU(2)	/ / + 7	(Input, Card 3) The mobilities of the carriers. $XMU(1) = \mu_n$, $XMU(2) = \mu_p$.
XMUU(2, 300)	/COM11) + 0	$dv_j(E_{i+\frac{1}{2}})/dE_{i+\frac{1}{2}}$ for $j = n, p$ and $1 \leq i < I$. It is the derivative of the drift velocity with respect to the field strength. $XMUU = \mu$ below saturation and 0 above.
XMU4		obs.
XMU8		obs.

XN / / + 11053 A new set of mesh points.

XP / / + 12 (Input, Card 4) b, the coordinate of the
left boundary of the diode.

B. 6. LAYOUT OF COMMON VARIABLES

/ / + 0	IBLOCK	35	RN [†]	1313	MX	1354	ED
1	IPUNCH	36	EPS	1314	MXM	2030	HD
2	PRINT	44	IEXTRA	1315	MXP	2504	EFD
3	DELN	70	EXTRA	1316	MXM2	3160	NT
5	D	114	PROBNO	1317	MXM3	3161	ITER
7	XMU	115	PROBNM	1320	OMEGA	3162	IND
11	XM	127	IOPT	1321	CRR	3163	EN
12	XP	143	EPN	1323	CSS [†]	3637	R
13	TAU	144	EPNI	1325	Q2	4313	AA
15	CNP	145	RPN [†]	1326	QD [†]	4313	DENS
16	CNN	146	QPN [†]	1330	QRR [†]	4767	BB
17	CPP	147	X	1332	XMU4 [†]	5443	CC
20	CNP	623	XH	1334	XMU8 [†]	6117	GG
21	XE	1277	MAXT [†]	1336	SUMNU	6513	APA
21	XEE	1300	ISUBI [†]	1337	EPNMU [†]	7247	BTA
22	SKAPPA	1301	PI	1340	DEPN	7723	EXS
23	TB	1302	MI	1341	DNMU	7723	XB
24	TEND	1303	MIM	1343	DNSUM	11053	AM2
25	DELTI	1304	MIP	1344	DNMU2 [†]	11053	OUT
26	DL	1305	MIM2	1345	DNDIF [†]	11053	XN
27	DELR	1306	MIM3	1346	TIME	11527	OUT(1,2)
30	ERROR	1307	IO	1347	DELT	12203	AM1
31	DELX	1310	IO M	1350	WDT	12203	OUT(1,3)
32	OMEGA	1311	IO P	1351	WDTI	12203	XHN
33	C	1311	MIMOLD	1352	VT	12657	OUT(1,4)
34	AN	1312	II0 [†]	1353	XIT [†]	13333	AZR

13333 OUT(1, 5)	454 GNFN
13333 EDN	1130 GPFP
14007 OUT(1, 6)	1604 GPFN
14007 HDN	2260 HELP
14463 API	2734 ISET
14463 OUT(1, 7)	2735 CB
15137 OUT(1, 8)	2737 CK
15613 AP2	2741 VS
/ / + 15613 OUT(1, 9)	2743 last + 1
16267 OUT(1, 10) /COM11/ + 0 XMC	
16743 AEX	1130 VND
16745 B	1604 VPD
20075 EPNE	2260 last + 1
20076 VOUT /COM20/ + 0 TK	
20077 AR	2 GINT
20100 VBAR [†]	3 GINT0
20101 VBAR1 [†]	4 TAU
20102 VBAR2 [†]	6 last + 1
20103 TIME1 [†] /COM9/ + 0 TIM	
20104 TIME2 [†]	24 H
20105 XJ	50 INFLEC
20106 XJV	51 last + 1
20107 GTC	
20110 RTL	
20111 HJK	
20565 EDO	
21241 HDO	
21715 last + 1	

/CMMNY/ + 0 EFDO

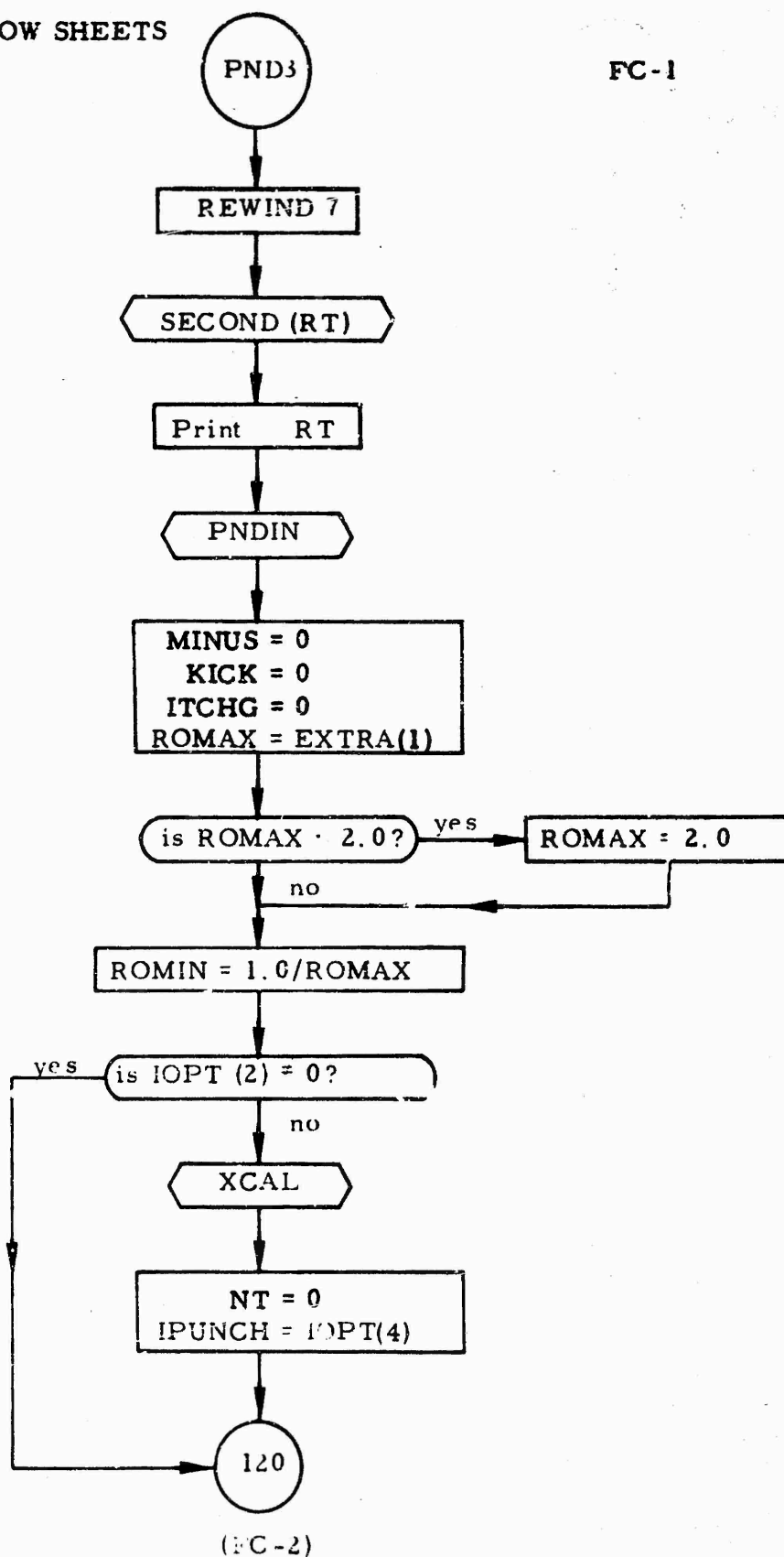
454 last + 1

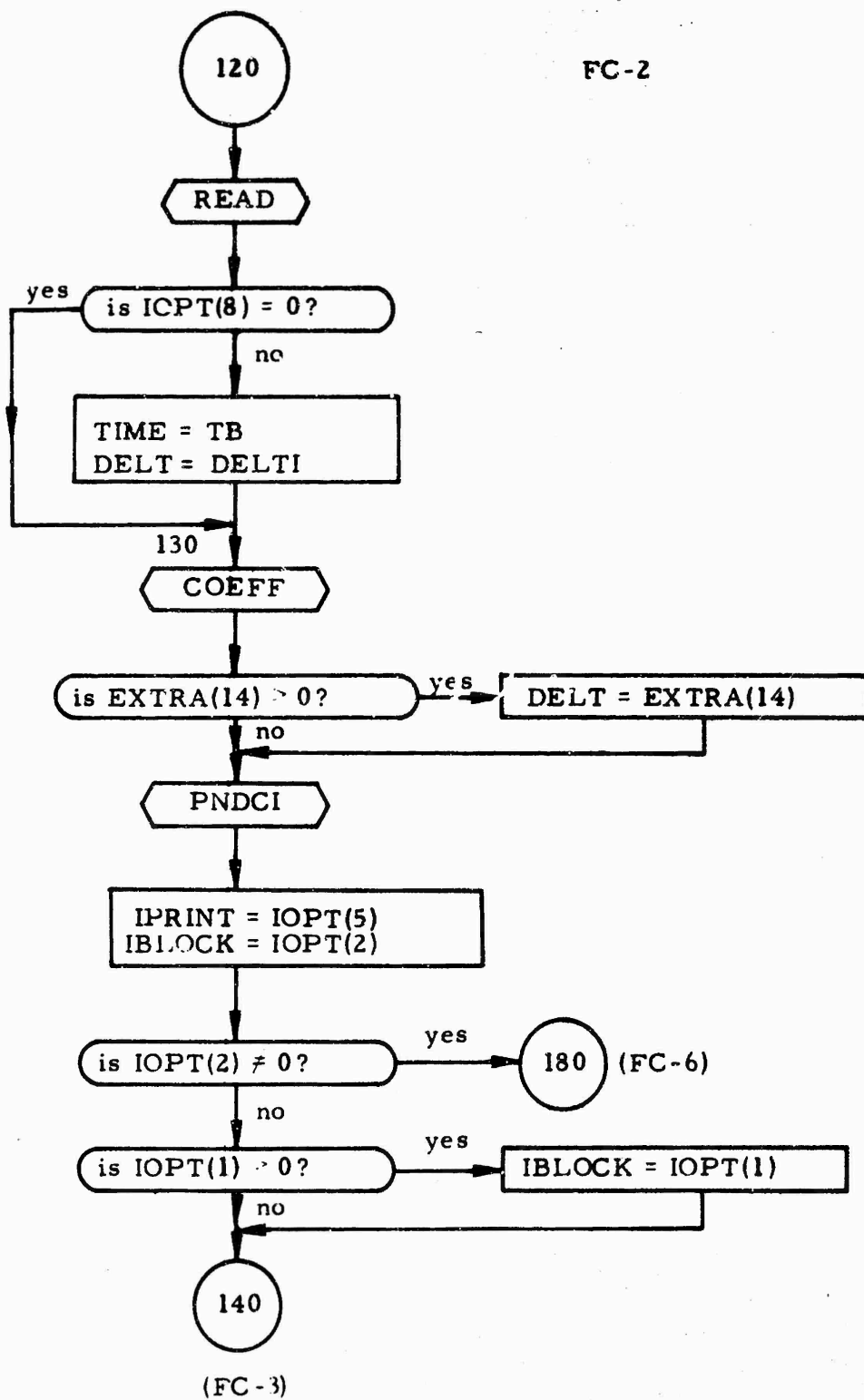
/COM10/ + 0 GNFP

[†]Obsolete.

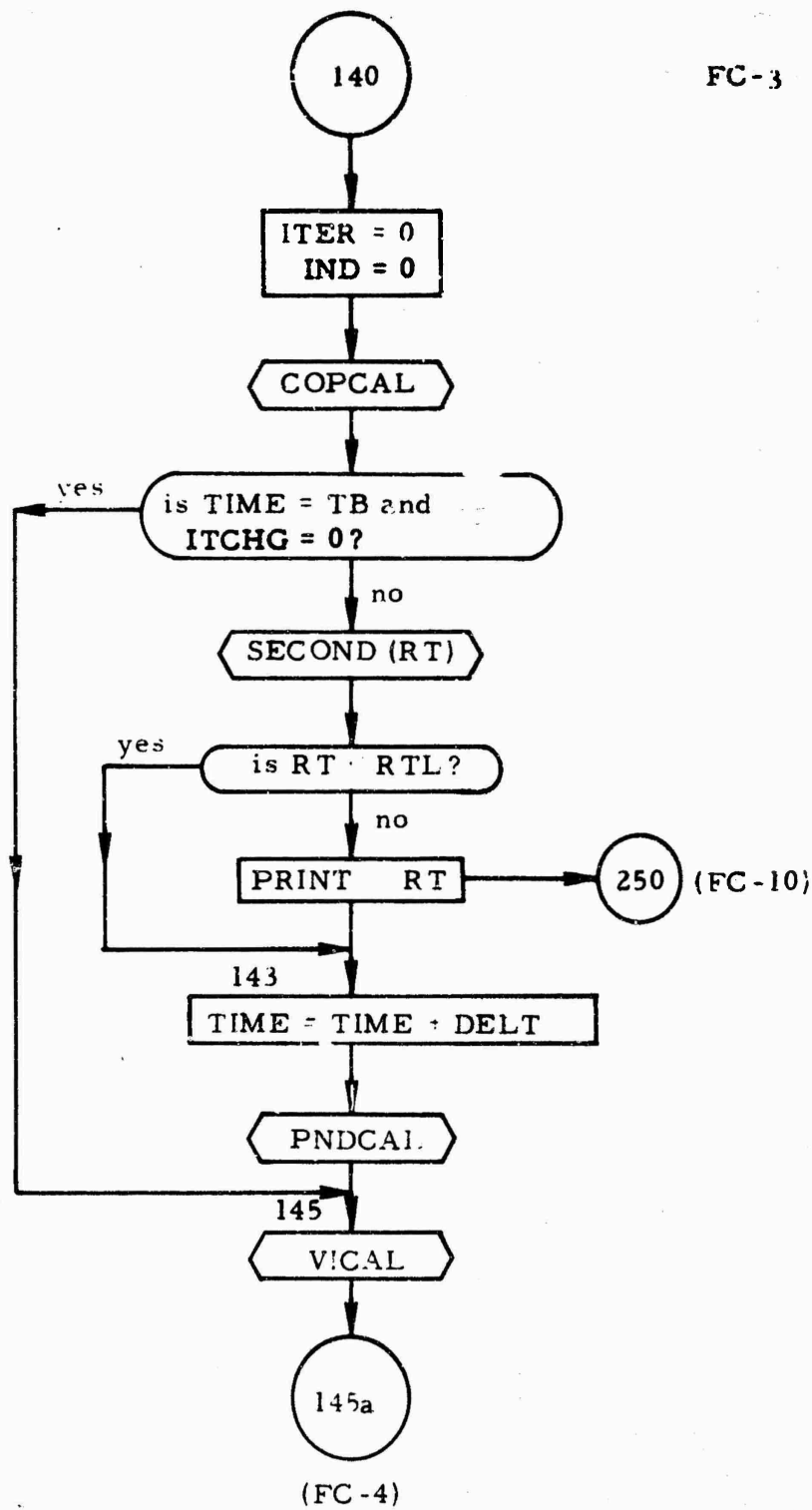
B. 7. FLOW SHEETS

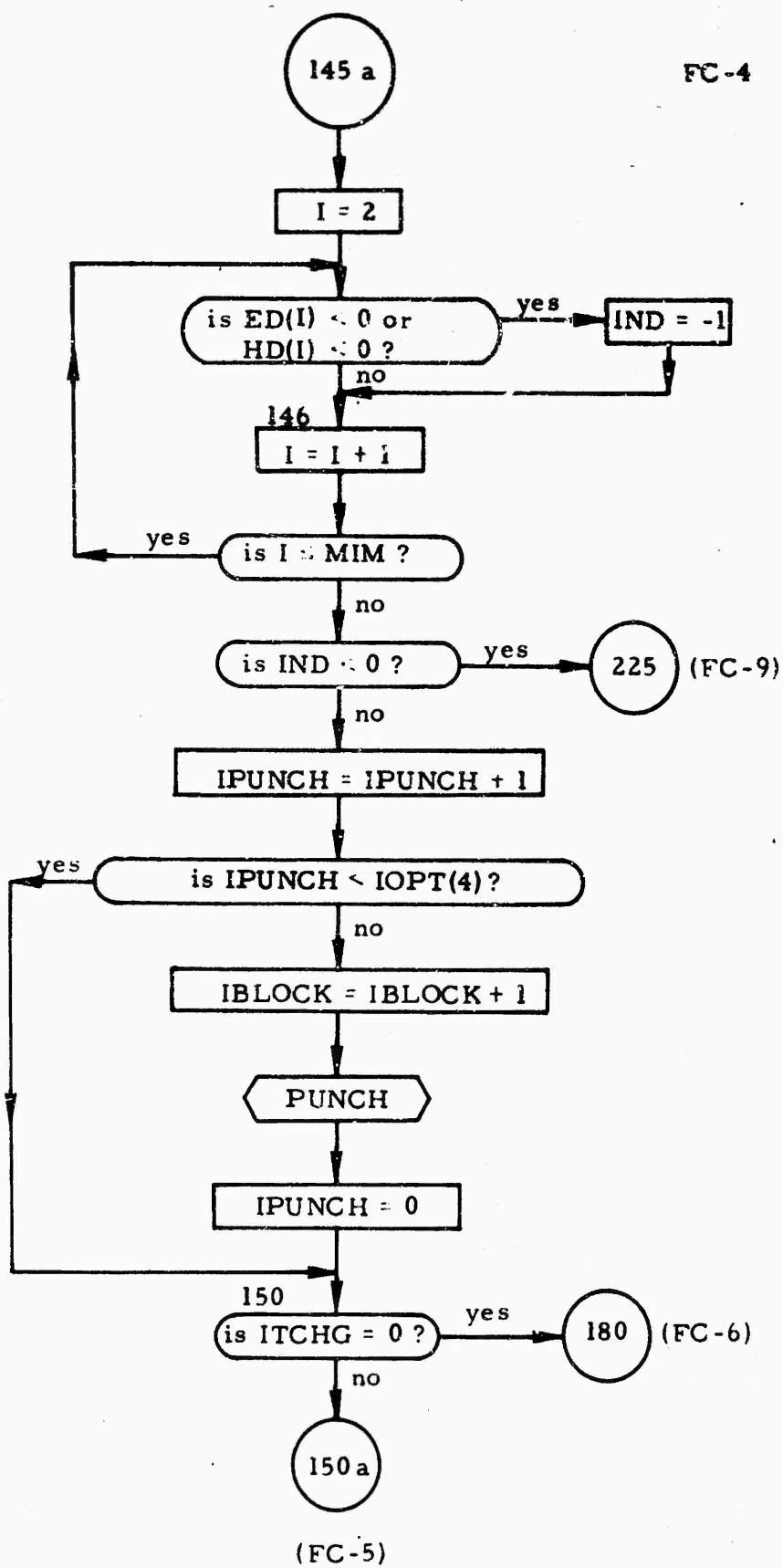
FC-1

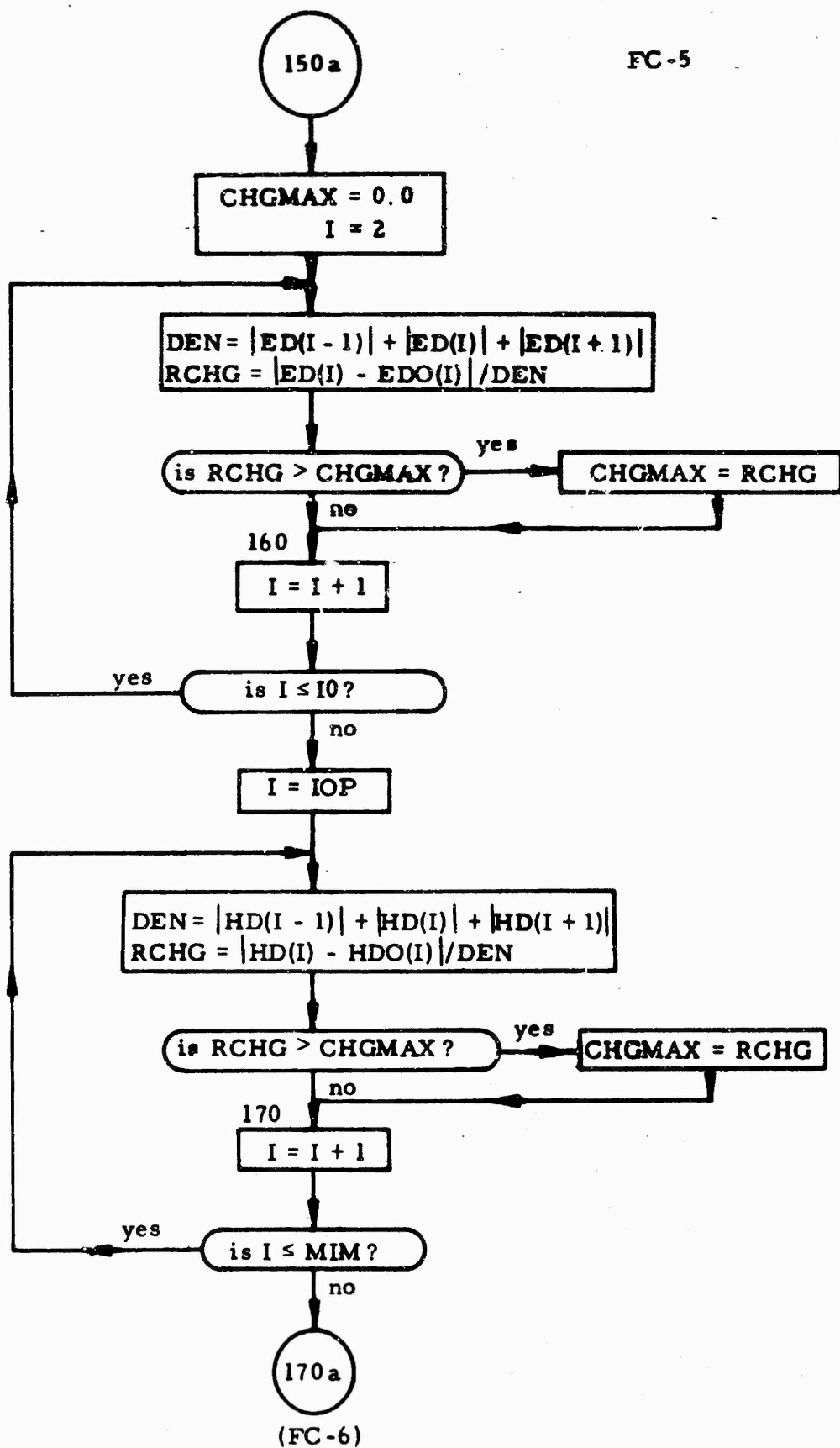


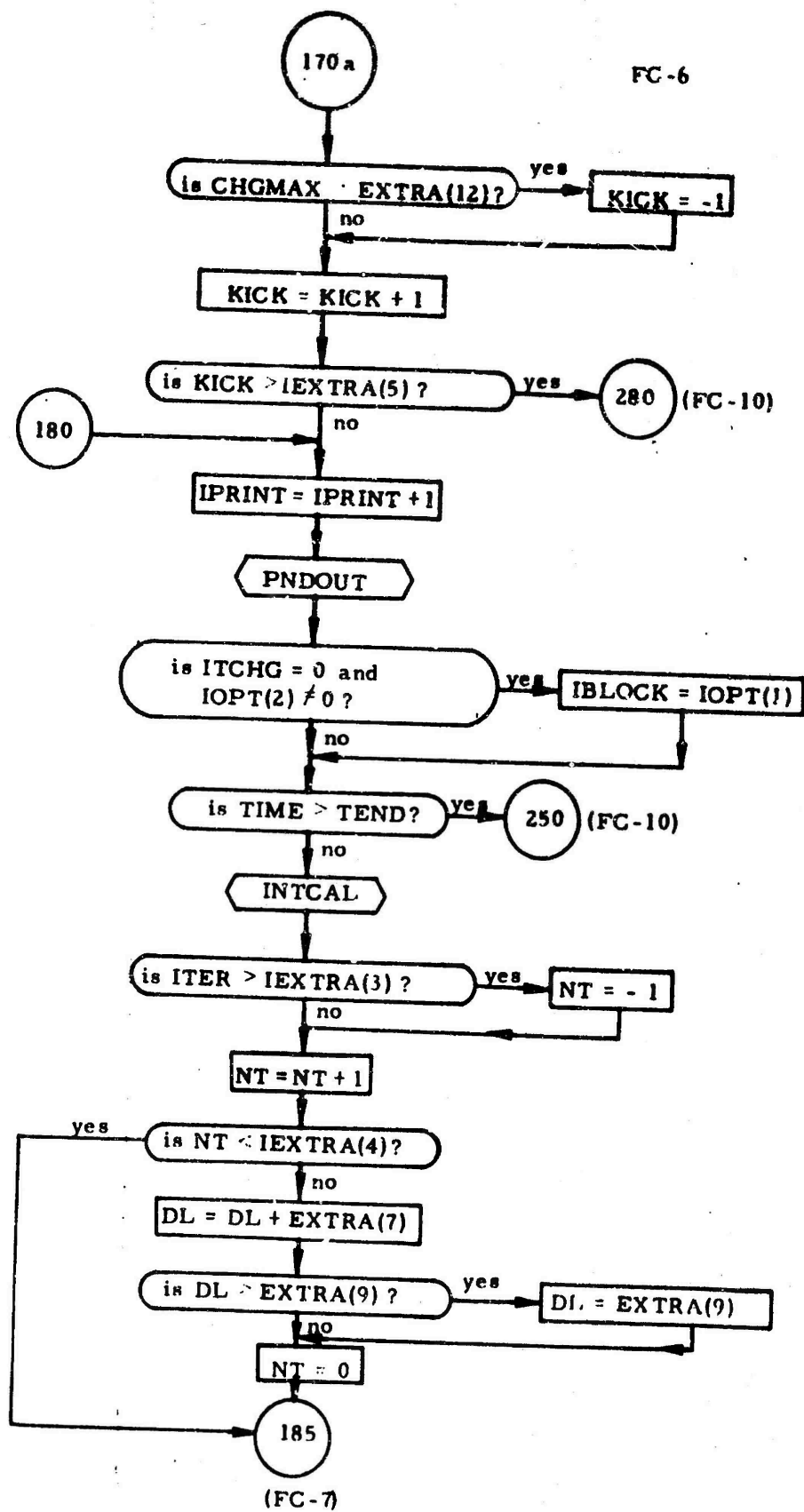


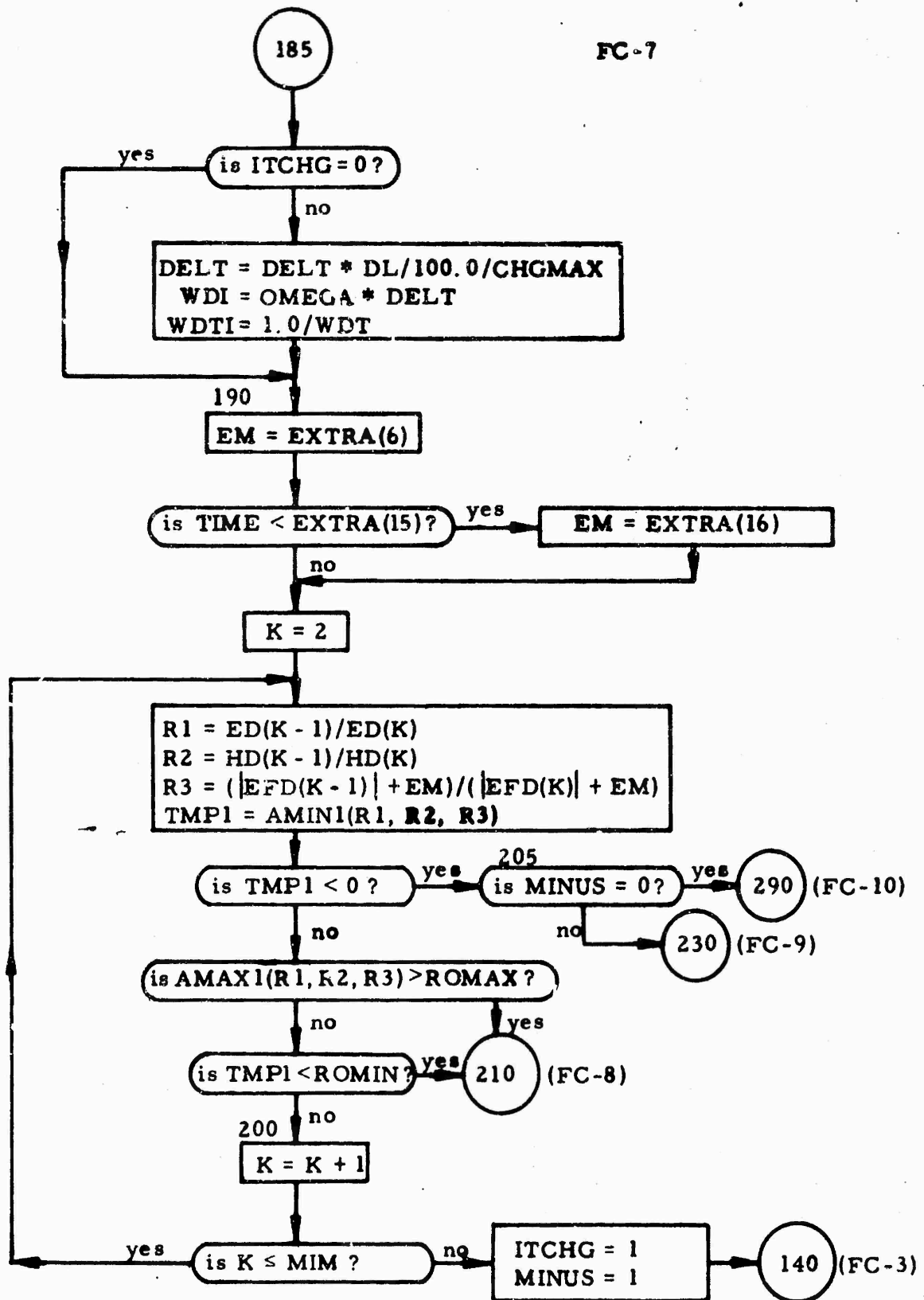
FC-3



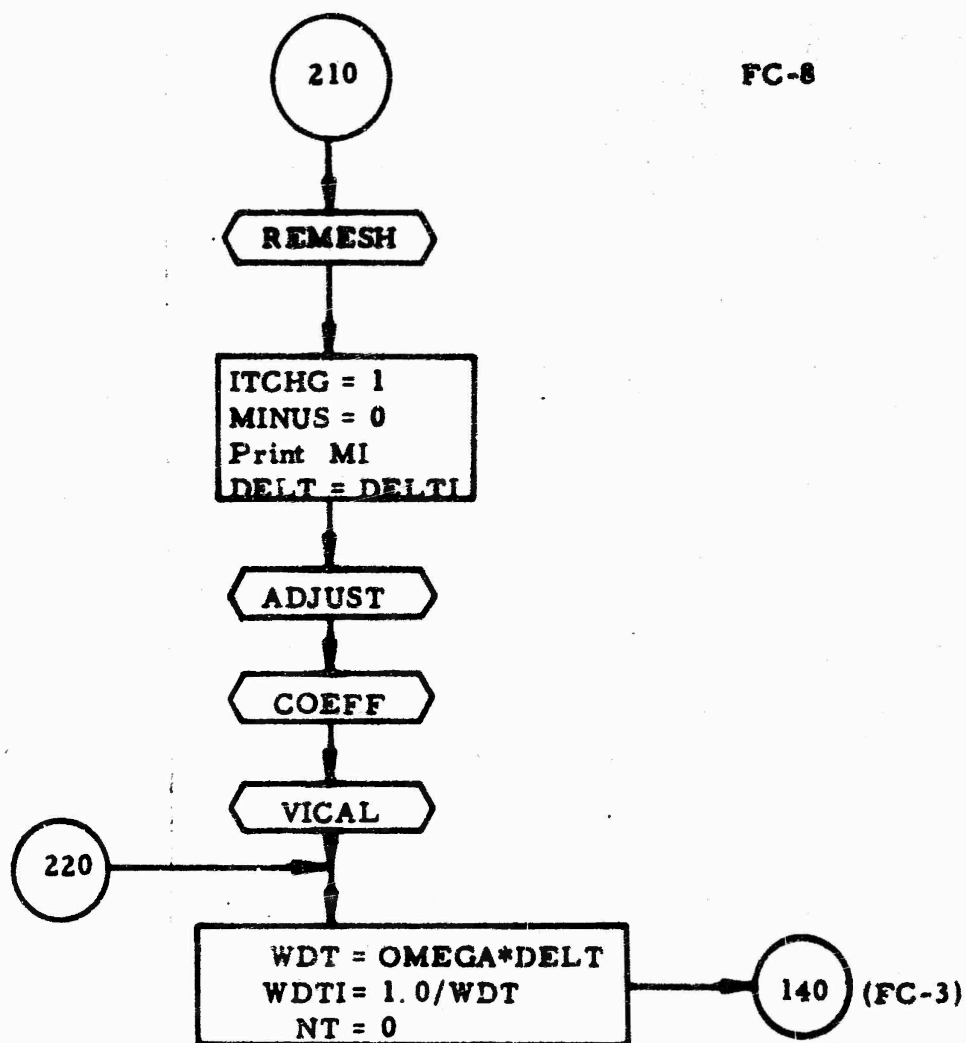




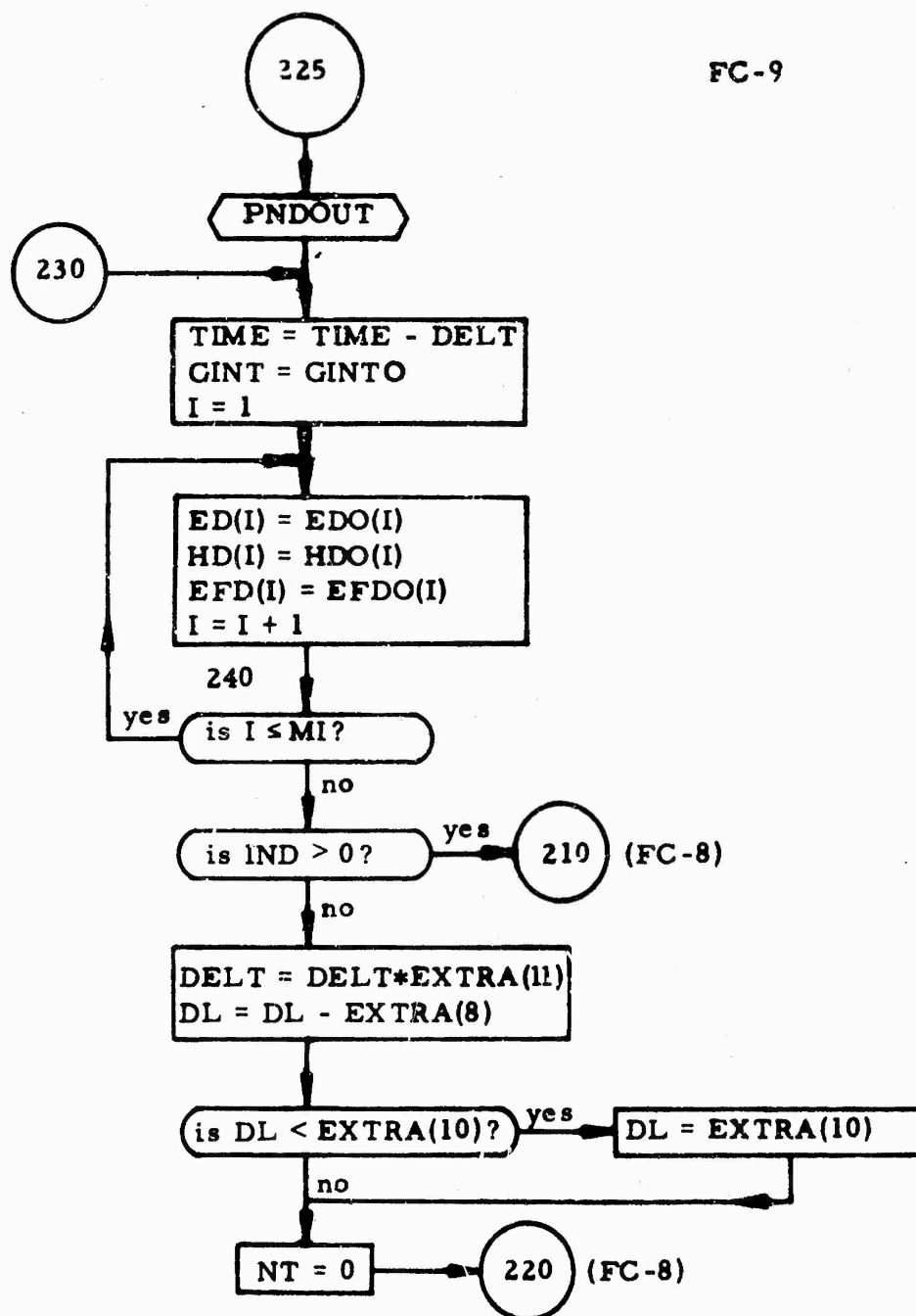


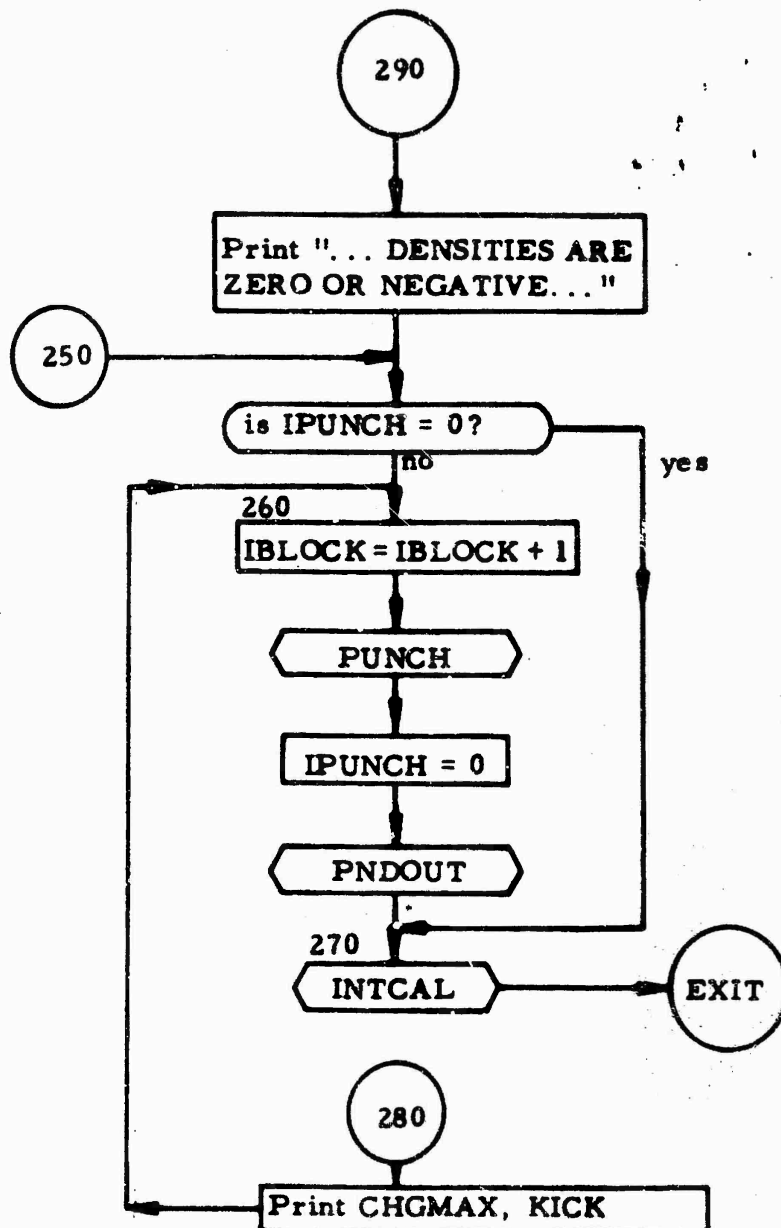


FC-8



FC-9





Appendix C

THE TRANSISTOR CODE

C.1. ORGANIZATION

The PNPMPN code consists of a main program and twenty-three subroutines. The functions of these routines are described below.

1. The Main Program controls the flow of the calculation. The principal phases of the calculation are

- a. Reading the input, which is done by INPNP*.[†]
- b. Initialization. When starting from scratch, XPNP* builds the initial mesh and IZPNP* sets up an initial distribution of carriers. When starting from a previously computed distribution contained in a restart dump, RDPNP* reads the dump tape and places it in position to receive additional blocks of restart data. Regardless of the source of the initial conditions, CNSPNP* computes constants derived from the input data and CFFPNP* calculates the geometrical factors that occur in the coefficients of the difference equations.
- c. Taking one step in time, which is the function of PNPCAL*. Also involved are VTPNP*, which calculates the voltages between the contacts, and COPPNP, which calculates the location of the crossover points.
- d. Checking for the appearance of negative densities.
- e. Backing up and reducing the time step when negative densities occur or the iterative procedure for solving the nonlinear difference equations fails.
- f. Printing results, which is done by OUTPNP*. INTPNP* is called for calculating conservation integrals just before OUTPNP is called.
- g. Dumping blocks of restart data, which is done by PCHPNP*.
- h. Checking the rate of progress and terminating when it drops too far. For this purpose, CHGCAL*, which calculates the maximum value of the relative change of the densities, is called.

[†] References to subroutines that are called by the subroutine under discussion are starred.

i. Checking elapsed Central Processor time and terminating when the input time limit, RTI , is exceeded.

j. Controlling the size of the time step (Section 2.2.3.1).

k. Comparing variations in densities and field strengths with remesh criterion. When the ratio of densities or field strengths at consecutive points exceeds a critical input value, $ROMESH$, $REMESH^*$ is called to build a new mesh, after which $ADJUST^*$ is called to calculate what the densities should be on the new mesh and to recalculate the geometrical factors. Then $VTPNP^*$ recalculates voltages.

1. Terminating the run.

2. $INPNP$ is the input routine. It is called by the Main Program. Its function is to read the input cards. Section 2.3 is devoted to the format of the input cards and to specifying what data they are to provide. $INPNP$ also edits and prints all the input data.

3. $XPNP$ is the subroutine that the Main Program calls in order to obtain an initial mesh when starting from scratch. The procedure for generating the mesh is to select points at intervals that increase in length by a constant ratio $XMLT(K)$ until some limit $XBRK(K)$ is passed at which point a new ratio $XMLT(K + 1)$ of interval lengths is used until a new limit $XBRK(K + 1)$ is passed, and so on. The process starts at $x = 0$ with an interval of length $DELX$ (input) and is carried out independently in both directions until the ends of the device are reached. The pairs $XMLT(K)$, $XBRK(K)$ are read off the input deck by $XPNP$ itself. Two sets of data are read: the first set is for the left (emitter) side and the second is for the right (collector) side. Restrictions: left side, $XE \leq XBRK(K + 1) < XBRK(K) < 0$; right side, $0 < XBRK(K) < XBRK(K + 1) \leq XC$; both sides, $0.5 < XMLT(K) < 2.0$ and no more than twenty pairs.

4. $XHPNP$ is called by the Main Program and by $ADJUST$. It calculates the array XH which contains the midpoints of the intervals, finds in which intervals the junctions and contacts lie, and calculates some indices derived from the indices of these special intervals.

5. CFFPNP is called by the Main Program and by ADJUST. It calculates the geometrical factors that occur in the difference equations and the excess concentration of donors in each interval.

6. CNSPNP is called by the Main Program shortly after the input subroutine INPNP is called. Its function is the calculation of several much-used constants.

7. IZPNP is called by the Main Program when starting from scratch for calculating an initial distribution of carriers. The distribution it selects is electrically neutral in every interval that is compatible with what it selects for the electric field, namely, zero everywhere.

8. COPPNP is called by the Main Program. It locates intervals containing crossover points, i. e., points at which the concentrations of holes and electrons are equal.

9. PNPCAL is called by the Main Program. Its function is to advance the calculation one step in time. The procedure it uses (see Section 2.2.1.5) is to

a. Calculate the denominator d_i of the recombination term in each interval;

b. Call HJKPNP* to obtain H_i^{l-1} , J_i^{l-1} , and K_i^{l-1} ; and then, in the iterative loop,

c. Have HJKPNP* and ABPNP* form the coefficients of the linearized equations;

d. Have EXSPNP* solve the linearized equations;

e. Have NPEPNP* update the estimates of n^l , p^l , and E^l , and check for convergence;

f. Go back to (c) if the iteration limit has not been exceeded nor the convergence criterion met; otherwise,

g. Have PNPNP* calculate the densities of the majority carriers; and

h. Return.

10. VTPNP is called by the Main Program and by EXSPNP. It calculates the voltages between pairs of contacts.

11. OUTPNP is called by the Main Program for editing and printing results. There are two print modes: a short print, consisting of one line of such important quantities as time, the voltages, and the currents, and a long print in which all available information of physical interest is printed. A complete tabulation of what the printout contains may be found in Section C.4. OUTPNP also saves n^l , p^l , and E^l to use as n^{l-1} , p^{l-1} , and E^{l-1} on the next step.

12. INTPNP is called by the Main Program just before OUTPNP for the purpose of calculating the conservation integrals (Section 2.2.4) that OUTPNP prints.

13. HJKPNP is called by PNPCAL. It evaluates the functions H, J, and K, which are defined in Section 2.2.1.5.

14. ABPNP is called by PNPCAL. It calculates the matrix of coefficients of the linearized equations.

15. EXSPNP is called by PNPCAL. First it calls VTCAL* to obtain the voltages which it uses to calculate the coefficients of the terms of the linearized equations that pertain to the current. Next, the elimination procedure is performed upon the matrix Q of coefficients of the linearized equations. Finally, the corrections u , v , π , and ϵ are calculated (see Section 2.2.1.5).

16. NPEPNP is called by PNPCAL after calling EXSPNP. It adds the corrections to the old estimates of n , p , and E to get new ones in the iterative procedure for solving the nonlinear difference equations (which is described in Section 2.2.1.5). NPEPNP also increments the iteration counter and checks to see if the convergence criterion is met.

17. PNPNP is called by PNPCAL just before returning to the Main Program. It calculates the densities of the majority carriers and also

$$\Delta N / \Delta t = \frac{N^l - N^{l-1}}{t^l - t^{l-1}}, \quad H_i^v = - \frac{\delta \bar{n}_i v_i}{\delta x_i}, \quad H_i^D = \frac{\delta (\delta n_i / \delta x_i)}{\delta x_i},$$

$$\Delta P / \Delta t = \frac{P^l - P^{l-1}}{t^l - t^{l-1}}, \quad J_i^V = - \frac{\bar{\sigma}_i u_i}{\delta x_i}, \quad J_i^D = \frac{\delta(\bar{\sigma}_i / \delta x_i)}{\delta x_i},$$

$$-G_i = R_i - g - A_i, \quad H_i = G_i + H_i^V + H_i^D, \quad \text{and} \quad J_i = G_i + J_i^V + J_i^D.$$

for the long form of printout.

18. RDPNP is called by the Main Program to read the restart tape. Blocks dumped in various problems may be stacked one after another on one tape. When this is done, the input quantity IOPT(1) tells how many restarting blocks already on the tape are to be preserved. If IOPT(1) > 0, RDPNP prints a catalog of the first IOPT(1) blocks on the tape and leaves the tape positioned so that the first block dumped (by PCHPNP) will be the IOPT(1) + 1th block on the tape. All this is done for scratch starts as well as restarts. The input quantity IOPT(2) (\leq IOPT(2)) is the number of the block containing the data to be used for restarting.

19. PCHPNP is called by the Main Program for dumping the arrays X, ED, HD, and EFD at various times to provide data for restarting. The data are dumped in a two-record unit called a block. The first record is a short one of fixed length containing the block number, the problem number, the time, the latest time interval, the voltages, the currents, a number of control parameters, and a set of 32 indices of such things as crossover points and intervals containing contacts and junctions. The second record contains the arrays.

20. CHGCAL is a subroutine of one parameter, an output, which is the maximum absolute value of the relative changes of the densities at the various points of the mesh over the preceding time step. It is called by the Main Program as a part of the time-step control, as described in Section 2.2.3.1.

21. REMESH is called by the Main Program when a new set of meshpoints is to be constructed, as described in Section 2.2.3.2. Searching for the optimum value of the remeshing parameter ρ is carried out by RTSCH*.

22. RTSCH is a general-purpose root-searching routine used by REMESH for optimizing the parameter ρ . It is described in detail in Appendix B.

23. ADJUST is called by the Main Routine after remeshing (REMESH). It calculates the carrier densities at the new mesh points and then recalculates the electric field, as described in Section 2.2.3.2. ADJUST then calls XHPNP* and CFFPNP* in order to update all other quantities that depend on the mesh.

24. G is a function called by HJKPNP for evaluating $g(t^{\frac{1}{2}})$, the rate of production of pairs by irradiation. The routine that is included in the current version of PNPMN simply sets $g = 0$.

C.2. SETTING UP A RUN ON PNPMN

The code PNPMN refers to three files: INPUT, OUTPUT, and TAPE16. The INPUT and OUTPUT files are the standard ones. The other file, TAPE16, is for storing restart points. The code was designed so that when one run uses data from a previous run as a source of input values, the restart points dumped by the new run are added to the tape from which the initial values were read.

The differences between starting from scratch and restarting are:

1. When starting from scratch, IOPT(2) = 0, and when restarting, IOPT(2) is the number of the block containing the initial distribution for the new run.

2. When restarting, the input deck need not contain the cards that XCAL reads to obtain specifications for an initial mesh.

3. When starting from scratch, any tape may be REQUESTed for receiving blocks of restart data. If the tape contains no restart data to be preserved, IOPT(1) = IOPT(2) = 0, and dumping begins at the load point. Indeed, it is not necessary to submit any tape when starting from scratch. Setting the number of time steps per dump, IOPT(5), to an absurdly high

5. UTILIZATION OF TEMPORARY/SUMMER HIRE PERSONNEL: Supervisors and office chiefs are reminded that personnel employed as summer help, or in other type temporary positions, have been appointed to non-sensitive positions; therefore are not eligible for security clearances. Since such appointments are not subject to the normal Civil Service Commission investigative requirements for applicants, no investigations are initiated; consequently, no basis exists upon which security clearance can be granted. In scheduling summer leave for regular personnel, do not plan to utilize temporary personnel to fill in during such absences, unless the position involved does not require access to classified information nor place the incumbent in a position whereby he/she may be exposed to such information. (DSA Bulletin No. 74, 28 Jun 67)

6. DDC REGULATORY PUBLICATIONS: DDCR 7730.2, Work Measurement Reporting, 12 February 1965 is superseded by DDCM 1125.1, DDC Work Measurement Manual, 1 July 1967. (Mrs. Dunbar, DDC-EA, 81975)

BY ORDER OF THE ADMINISTRATOR, DEFENSE DOCUMENTATION CENTER

OFFICIAL

H. C. Clark
HERBERT D. CLARK
Lt. Col., USA
Executive Officer

U N O F F I C I A L

DDC PICNIC: Hurry and buy your tickets to the DDC Picnic! Bring your family and friends. \$1.00 per adult, children under 16 free. We will have lots of fun. Be sure to come.

DATE: Saturday, 15 July 1967

TIME: 1200 to 1700

PLACE: Near the rear gate at Cameron Station

(Lt. Col. Clark, DDC-E, 81885)

THE FOLLOWING ARE NEW DDC EMPLOYEES:

Dix, Saranne, DDC-RPS, 5C368, 88206

Hatton, Thelma J., DDC-TSR-1, 5A317, 81813

Holloway, Ward N., Jr., DDC-PPS, 5A473, 81931

Kobonis, Louis P., DDC-TAA, 5A272, 81823

Yerger, Donald J., DDC-PPR, 5D523, 81963



HEADQUARTERS

Defense Documentation Center

CAMERON STATION, ALEXANDRIA, VIRGINIA

STAFF BULLETIN

DDC-E

No. 24

7 July 1967

OFFICIAL

1. EMPLOYEE ARRIVAL AND DEPARTURE: DDCR 1422.1 provides for a basic day shift from 0745 to 1615. Employees working the day shift are expected to be at their post of duty ready to commence work when the 0745 buzzer sounds and to remain at their post of duty until the buzzer sounds at 1615. (Lt. Col. Clark, DDC-E, 81885)
2. CHANGE IN MOTOR VEHICLE REGISTRATION REQUIREMENTS: Seat belts are no longer required in order to register vehicles at Cameron Station. Reference: Ch 1, Cam Sta Reg 190-1, 26 June 1967. (Lt. Col. Clark, DDC-E, 81885)
3. EMPLOYEE RIGHTS TO COMMUNICATE: It is the policy of the Defense Supply Agency that employees have the right to communicate with:

Members of the Civilian Personnel Division (DSASC-Z).

The DSA Equal Employment Opportunity Officer or Deputy Equal Employment Opportunity Officer.

A supervisory or management official of higher rank than his immediate supervisor.

When an employee wishes to visit the personnel office or talk with any of the management personnel shown above, the employee should ask his immediate supervisor to indicate a convenient time for him to do this which would not unduly disrupt the work schedule. The employee is not required to explain his reasons for wishing to talk to any of the above officials. (DSA Bulletin No. 76, 3 Jul 67)

4. PROMOTION OF EMPLOYEES WHILE SERVING IN ARMED FORCES: Supervisors are reminded that employees who are called, or who volunteer for duty with the Armed Forces (for periods of up to four years) are often entitled to promotions which they would have received if they were still employees and not serving with the Armed Forces. That is, employees who ~~were~~ serving in "trainee" positions and who would have been promoted upon completion of a prescribed period of training should be promoted when that period is completed even though the employee is temporarily off the rolls fulfilling his military obligation. Supervisors who have employees on military furlough should check with their Personnel Management Specialist to determine in each case whether or not a Request for Personnel Action (SF-52) should be initiated. (DSA Bulletin No. 76, 3 Jul 67)

value (say, 1000) will suppress all dumps but that of the initial data, which may be allowed to fall on the disk.

C.3. INPUT

The input deck for PNPMN consists of 14 cards of parameters followed, when starting from scratch, by a deck of from 3 to 15 cards specifying how the initial mesh is to be generated.

Three formats are used for reading cards. The first card is a title card in format E12.8, 10A6, the first field holding the problem number and the second, the title itself. The cards following the title card are either in a 12I6 or 6E12.8 format, depending on whether they contain integer or real parameters.

Input Cards

Card 1 (E12.8, 10A6)

PROBNO	Problem number.
PROBNM	Problem title.

Card 2 (12I6)

IOPT(1)	Number of blocks to be preserved on TAPE16. IOPT(1) = 0 when new tape or no tape is used.
IOPT(2)	Block number of block from which to obtain initial data. IOPT(2) = 0 when starting from scratch. Restriction: IOPT(2) ≤ IOPT(1).
IOPT(3)	Maximum number of iterations per time step. (See Section 2.2.1.3) Usually, IOPT(3) = 5.
IOPT(4)	IOPT(4) = 0 is normal and allows the program to compute the time step. IOPT(4) ≠ 0 forces $\Delta t = \text{DELTI}$ (Card 11) on every time step.
IOPT(5)	Restart dumps are recorded every IOPT(5) time steps.
IOPT(6)	Print control. An extensive printout showing the state of the device occurs every IOPT(6) time steps, or after each dump, whichever is more frequent. There is a short printout for every time step attempted.

IOPT(7)	Number of data of integral type. Set IOPT(7) = 5.
IOPT(8)	Number of data of real type. Set IOPT(8) = 64.
IOPT(9)	Set IOPT(9) = 2. This option is being reserved for controlling input of specifications of pulse form.
IOPT(10)	When restarting, t and Δt are normally (IOPT(10) = 0) picked up off TAPE16. If IOPT(10) \neq 0, then t and Δt are read from Card 11, as when starting from scratch.
IOPT(11, 12)	Not used.

Card 3 (12I6)

IDATA(1)	n_2 in the control of the time step (see Section 2.2.3.1). IDATA(1) = 3 is reasonable.
IDATA(2)	n_1 in the control of the time step (Section 2.2.3.1). IDATA(2) = 4 is reasonable.
IDATA(3)	n_3 in the control of the time step (Section 2.2.3.1). IDATA(3) = 3 is usual.
MAXPT	I_{\max} , the maximum number of intervals in the mesh. If subroutine REMESH generates a mesh with more than I_{\max} points in it, a less restrictive (i.e., larger) value of the parameter ρ is chosen for the next trial. MAXPT \leq 150.
MINPT	I_{\min} , the minimum number of points in an acceptable mesh. MINPT = MAXPT - 15 is usual.
Fields 6-12	Not used.

Cards 4 through 14 are read into a buffer (DATA(J), J = 1, 64). The data on these cards are listed below in the order in which they appear in the buffer.

Card 4 (6E12.8)

1	ZNO	n_0 , the intrinsic concentration of electrons.
2	ZMUN	μ_n , the mobility of electrons.
3	ZMUP	μ_p , the mobility of holes.
4	ENE	ΔN , the concentration of donors minus that of acceptors in the emitter.

5 ENB ΔN in the base.

6 ENC ΔN in the collector.

Card 5 (6E12.8)

7 ZKT θ , the temperature in volts.

8 ZE q , the magnitude of the charge of the electron.

9 ZKAPPA κ , the dielectric constant.

10-12 Not used.

Card 6 (6E12.8)

13 TAUNE τ_n in the emitter (see Section 2.2.2.1).

14 TAUPE τ_p in the emitter.

15 TAUNB τ_n in the base.

16 TAUPB τ_p in the base.

17 TAUNC τ_n in the collector.

18 TAUPC τ_p in the collector.

Card 7 (6E12.8)

19 ZNSE n' in the emitter (Section 2.2.2.1).

20 ZPSE p' in the emitter.

21 ZNSB n' in the base

22 ZPSB p' in the base.

23 ZNSC n' in the collector.

24 ZPSC p' in the collector.

Card 8 (6E12.8)

25 VEBO V_{EBO} , the supply voltage in the base circuit.

- 26 VECO V_{ECO} ; the supply voltage in the collector circuit.
- 27 REB R_1 , the resistance in the base circuit.
- 28 REC R_2 , the resistance in the collector circuit.
- 29 A0 a_0 , the effective area of the device.
- 30 RTL The CP time limit, in seconds.

Card 9 (6E12.8)

- 31 XE The coordinate of the emitter contact relative to the base contact.
- 32 XEB The coordinate of the emitter-base junction relative to the base contact.
- 33 XBC The coordinate of the base-collector junction relative to the base contact.
- 34 XC The coordinate of the collector contact relative to the base contact. Restriction: $XE < XEB < 0 < XBC < XC$.
- 35 DELX The length of the interval containing the base contact.
- 36 Not used.

Card 10 (6E12.8)

- 37 ERROR ϵ_{max} . The criterion for convergence of the iterative process for calculating new concentrations and fields is that the relative magnitudes of the corrections to the concentrations of the minority carriers be less than ϵ_{max} at all points (see Section 2.2.1.5).
- 38 OMEGA ω , a weighting factor used in the time integration. Set $\omega = 1$. (See Section 2.2.1.3.)
- 39 C The scale factor of concentrations. The values of concentrations in the input, the printout, and in storage must be multiplied by C to give their true values. Usually, $C = 1.0 E + 17$.
- 40 DELR r , the density of pairs due to irradiation at time $t = t_0$. (See Section 2.2.1.6.)

41,42

Not used.

Card 11 (6E12.8)

- 43 TBEGIN t^0 , the starting time.
- 44 TEND When $t^l > \text{TEND}$, the run is terminated.
- 45 DELTI $t^1 - t^0$, the length of the first time step. Usually, $\text{DELT I} = 1.0 \text{ E} - 14$.
- 46 DELTN When restarting, the first Δt is usually ($\text{DELT N} = 0$) read off TAPE16. But if $\text{DELT N} > 0$, then it is used as the initial Δt .
- 47 DELTM A factor that Δt is multiplied by in case of failure to converge and when negative densities appear. $\text{DELT M} = 0.2$ works well.
- 48 PERCHG w_0 , the parameter that controls the time step (see Section 2.2.3.1). $\text{PERCHG} = 10$ is good.

Card 12 (6E12.8)

- 49 PERMAX w_{max} , an upper bound on w_0 (Section 2.2.3.1). $\text{PERMAX} = 10.0$ is reasonable.
- 50 PERMIN w_{min} , a lower bound on w_0 (Section 2.2.3.1). $\text{PERMIN} = 1.0$ is reasonable.
- 51 PERADD w_1 , an increment to w_0 (Section 2.2.3.1). $\text{PERADD} = 5.0$ is reasonable.
- 52 PERSUB w_2 , a multiplier for w_0 when a back step must be taken (Section 2.2.3.1). $w_2 = 0.5$ is good.
- 53 RKICK ϵ_w , used in the criterion for bogging down (Section 2.2.3.1). Usually, $\text{RKICK} = 0.001$.
- 54 Not used.

Card 13 (6E12.8)

- 55 ROMESH Criterion for remeshing. When the ratio of concentrations or fields at consecutive points exceeds ROMESH , a new mesh is generated (see Section 2.2.3.2). Usually, $\text{ROMESH} = 30$.
- 56 ROX ρ_x , the maximum allowable ratio of lengths of consecutive intervals (Section 2.2.3.2). Usually, $\text{ROX} = 1.6$.

57 RO ρ , the remesh parameter. The log of the ratio of the concentrations and fields at consecutive points must be less than ρ (Section 2.2.3.2). The input estimate is automatically adjusted. RO = 0.2 is a good guess.

58 RODEL $-dI/d\rho$, the sensitivity of the remesh parameter (Section 2.2.3.2). The input estimate is automatically adjusted. Usually, RODEL = 100.

59,60 Not used.

Card 14

61 DELTR Δt to be used after remeshing. DELTR = 1.0×10^{-14} is reasonable.

62-64 $E_M = \begin{cases} \text{DATA}(64), & \text{if } t^b < \text{DATA}(63), \\ \text{DATA}(62), & \text{if } t^b \geq \text{DATA}(63). \end{cases}$
 E_M is added to the magnitude of the electric field in the remeshing criteria, so weak fields are ignored. $E_M = 1$ V seems to work well at all times.

65,66 Not used.

Card 15 Blank. Reserved for specifying the pulse $g(t)$ of radiation.

The following cards are required only when starting from scratch:

Card 15 (12I6)

NMLT(1) The number of pairs XMLT(K), XBRK(K) to specify the initial mesh left and right of the base contact, respectively. See description of XPNP
 NMLT(2) Restriction: NMLT \leq 20.

Fields 3-12 Not used.

Cards 17, 18 Consist of two sets of pairs (XMLT, XBRK), three pairs to a card in the format (6E12.8). The first set specifies the mesh to the left of $x = 0$ and the second set specifies the mesh to the right. Each set has just enough cards to hold the data it contains, and XMLT(1) begins in the first field (columns 1 through 12) in the first card of each set. The method used to generate the mesh is described with subroutine XPNP in Section C.1.

C.4. PRINTOUT

OUTPUT FOR PNPMN

At the beginning of every problem, MAIN prints C. P. time (Central Processor time) charged to the run at that point (including compilation time, if any). INPNP prints the input data contained on input Card 1 through Card 15 (or more). If there are blocks (records) to be saved on the dump tape, a map of these blocks is printed by RDPNP. CNSPNP prints out the following variables:

<u>OUTPUT TITLE</u>	<u>FORTTRAN VARIABLE NAME</u>	<u>DESCRIPTION</u>
N(0, E)	ZN0E	Equilibrium concentration of electrons in the emitter region.
N(0, B)	ZN0B	Equilibrium concentration of electrons in the base region.
N(0, C)	ZN0C	Equilibrium concentration of electrons in the collector region.
P(0, E)	ZP0E	Equilibrium concentration of holes in the emitter region.
P(0, B)	ZP0B	Equilibrium concentration of holes in the base region.
P(0, C)	ZP0C	Equilibrium concentration of holes in the collector region.
Q	Q	$4\pi qC/K$.
D(N)	DN	D_n , electron diffusion constant.
D(P)	DP	D_p , hole diffusion constant.
VC(EB)	VEBC	$V_B - V_E$, built-in voltage between emitter and base contacts.
VC(BC)	VBCC	$V_C - V_B$, built-in voltage between base and collector contacts.

VC(EC)

VECC

 $V_C - V_E$, built-in voltage between emitter and collector contacts.

If the problem is a restart, the restarting block is noted in the map dump-tape blocks and the time (TIME) at which the problem is actually restarted is printed.

After each cycle, the following variables are always printed by OUTPNP:

ITER	ITER	Number of iterations required to complete cycle.
TIME	TIME	t, problem time.
DELT	DELT	Δt , time step from previous cycle.
V(E, B)	VEBT	V_{EB} , voltage between emitter and base at time t.
V(E, C)	VBCT	V_{BC} , voltage between emitter and collector at time t.
J(B)	ZJB	i_B/a_0 , base current density.
J(C)	ZJC	i_C/a_0 , collector current density.
PERCENT	PERCHG	Percent change associated with cycle.
R. T.	RT	Run time (C.P. seconds).
IND	IND	Convergence indicator (not printed on IOPT(6)th converged cycle). IND = 1, continue iteration; IND = 0, converged; IND = - 1, failed to converge.

After remeshing, the following variables are always printed by REMESH:

MI	MI	I, number of mesh points generated by REMESH.
RO	RO	ρ , remesh parameter.
RODEL	RODEL	$dI/d\rho$, derivative of remesh parameter.

After every IOPT(6) converged cycles, the following variables are printed by OUTPNP:

BLOCK NO	IBLOCK	Block number (record number) in which the cycle is recorded (only printed on IOPT(5)th converged cycle).
X	X(I)	X_i , x coordinate of integral mesh point.
	XH(I)	$X_{i+\frac{1}{2}}$, x coordinate of half-integral mesh point.
N	ED(I)	n_i , electron density at integral mesh point.
P	HD(I)	p_i , hole density at integral mesh point.
DN/DT	OUT(I, 1)	H_i , $\partial n / \partial t$ at integral mesh point (in line with X(I)).
	OUT(I, 8)	$n_i^\ell - n_i^{\ell-1} / dt = dn/dt$ (in line with XH(I)).
D(N)	OUT(I, 2)	H_i^D , $D_n (\partial^2 n / \partial x^2)$ at integral mesh point.
MU(N)	OUT(I, 3)	H_i^V , $\mu n (\partial / \partial n) (E \cdot n)$ at integral mesh point.
DP/DT	OUT(I, 4)	J_i , $\partial p / \partial t$ at integral mesh point (in line with X(I)).
	OUT(I, 9)	$p_i^\ell - p_i^{\ell-1} / dt = dp/dt$ (in line with XH(I)).
DP	OUT(I, 5)	J_i^D , $D_p (\partial^2 p / \partial x^2)$ at integral mesh point.
MU(P)	OUT(I, 6)	J_i^V , $-\mu p (\partial / \partial x) (E \cdot p)$ at integral mesh point.
R	OUT(I, 7)	$-G_i$, $-G_i$ term at integral mesh point.

E	EFD(I)	$E_{i+\frac{1}{2}}$, electric field at half-integral mesh point.
INTEGRAL OF N	SUME	$N, \int n dx$
P	SUMH	$P, \int p dx$
R	SUMR	$R, -\int G dx$
DN/DT	SUMEDT	$\int (\partial n / \partial t) dx$
DP/DT	SUMHDT	$\int (\partial p / \partial t) dx$
RIGHT(N)	SUMRET	$\int (\Delta n / \Delta t) dx$
RIGHT(P)	SUMRHT	$\int (\Delta p / \Delta t) dx$
INDEX OF CROSS- OVER-POINTS	ICOP(I)	
X-VALUE OF CROSS- OVER-POINTS	XH(ICOP(I))	x coordinate of midpoint of interval in which the electron concentration equals the hole concentration.

ERROR MESSAGES

<u>SUBROUTINE</u>	<u>MESSAGE PRINTED</u>	<u>COMMENT</u>
MAIN	"CHGMAX IS LESS THAN OR EQUAL TO (RKICK) CONSEC- UTIVELY FOR (KICK) TIMES"	The problem is terminated after printing and writing on the dump tape. See Section 2.2.3.) for further discussion.
MAIN	"SOME ELECTRON- OR HOLE- DENSITIES ARE ZERO OR NEGATIVE, BUT REMESHING IS NOT POSSIBLE"	This message should not be encountered; it indi- cates a programming error.
INPNP	"EITHER IOPT(7) IS GREATER THAN 60 OR IOPT(8) IS GREAT- ER THAN 180"	Input error-problem is terminated immediately.

XPNP	"NMLT(I) MUST BE LESS THAN OR EQUAL TO 20 NMULT(1) = NMULT(2) =	Input error--problem is terminated immediately.
XPNP	"XMLT(I) MUST BE GREATER THAN 0.5"	Input error--problem is terminated immediately.
XPNP	"MAXIMUM NUMBER OF X-POINTS ALLOWED (150) IS EXCEEDED (MI) POINTS GENERATED-XCAL"	The problem is terminated immediately.
XHPNP	"ERROR IN INDEX OF INTER-FACE CALCULATION"	Input error; "base contact" must be in base region. The problem is terminated immediately.
COPPNP	"CROSS-OVER-POINT IS OUTSIDE OF ALLOWED RANGE"	The problem is terminated immediately.
COPPNP	"MAXIMUM NUMBER OF CROSS-OVER-POINTS ALLOWED IS 10"	The problem is terminated immediately.
NPEPNP	"(DID NOT YIELD CONVERGENCE) MAXIMUM RELATIVE ERROR = (ERMAX), AT X = (XMAX)"	Problem is not terminated. The time is backed up to that of the previous time step, Δt is reduced by DELTM, and the densities and field values at each mesh point are restored to those of the previous time step.
RDPNP	"ERROR-IOPT(2) IS GREATER THAN IOPT(1)-READ"	Input error--problem is terminated immediately.
REMESH	"REMESH IS UNABLE TO CALCULATE RO."	The problem is terminated immediately.

C.5. GLOSSARY

The variables in COMMON storage are defined. Notation developed

in Section 2.2 is freely used. A variable marked "obs." is obsolete and no longer used, although it still may be computed. The address of each variable in COMMON blocks are given in the form "/LAB/ + nnnnn" where LAB is the label of the block (LAB is omitted for blank COMMON) in which the variable is stored and nnnnn is the address of the variable in octal relative to the beginning of the block.

AA(150)	/ / + 3105	$1/(\delta x_i \delta x_{i-1})$, for $1 \leq i \leq I$, the coefficient of n_{i-1} in $\delta(\delta n_i / \delta x_i) / \delta x_i$.
AEX(10, 2)	/ / + 12125	AEX(K, 1) and AEX(K, 2) are the two exceptional elements, $A_{2i+1+2, 2i+1+1}$ of the matrix \hat{Q} , where i is the K th cross-over point.
ALOGX		obs.
AM1(300)	/ / + 7645	A_k^{k-1} , for $1 \leq k \leq 2I - 1$, the elements of the matrix \hat{Q} just below the main diagonal.
AM2(300)	/ / + 7171	A_k^{k-2} , for $1 \leq k \leq 2I - 1$, the elements of the matrix \hat{Q} in the second diagonal below the main diagonal.
APA(150)	/ / + 4235	$2/\delta x_i$, for $1 \leq i \leq I$.
AP1(300)	/ / + 10775	A_k^{k+1} , for $1 \leq k \leq 2I - 2$, the elements of \hat{Q} just above the main diagonal.
AP2(300)	/ / + 11451	A_k^{k+2} , for $1 \leq k \leq 2I - 3$, the elements of \hat{Q} in the diagonal two above the principal diagonal.
AREB	/ / + 573	$a_0 R_1$, a constant used in EXSPNP.
AREC	/ / + 574	$a_0 R_2$, a constant used in EXSPNP.
AZR(300)	/ / + 19321	A_k^k , for $1 \leq k \leq 2I - 1$, the elements of \hat{Q} on the main diagonal.

A0	/ / + 453	a_0 , the effective cross-sectional area of the device.
B(300)	/ / + 6515	The RHS of the linearized equations.
BB(300)	/ / + 3333	$-(2/\delta x_i)/\delta x_i$, for $1 \leq i \leq I$, the coefficient of n_i in $\delta(\delta n_i/\delta x_i)/\delta x_i$.
BTA(150)	/ / + 4453	(Input, Card 10) A scale factor by which input and printed concentrations are to be multiplied.
CC(150)	/ / + 3561	$(1/\delta x_i)\delta x_{i+1}$, for $1 \leq i \leq I$, the coefficient of n_{i+1} in $\delta(\delta n_i/\delta x_i)/\delta x_i$.
DATA(180)	/ / + 136	The array of input parameters of real type.
DELN		obs.
DELR	/ / + 464	(Input, Card 10) r , the initial concentration of pairs caused by irradiation.
DEL T	/ / + 2157	$t^{\ell} - t^{\ell-1}$, the time step.
DEL TI	/ / + 467	(Input, Card 11) $t^1 - t^0$, the initial time step.
DEL TM	/ / + 471	(Input, Card 11) A factor, usually about 0.2, by which to reduce the time interval if negative fluxes appear or when convergence fails.
DEL TN	/ / + 470	(Input, Card 11) When restarting, if $DEL TN > 0$, it is used for the initial time interval instead of the one read off TAPE16.
DEL TR	/COM7/ + 6	(Input, Card 14) The time interval to use after remeshing.
DEL X	/ / + 460	(Input, Card 9) The length of the interval in which the base contact lies ($x = 0$) in the initial mesh.
DEL XR		obs.
DENS(150)	/ / + 3105	Used in subroutine REMESH. For each interval I , $RO/DENS(I)$ is the optimum interval length.

DN	/ / + 537	The diffusion constant for electrons.
DP	/ / + 540	The diffusion constant for holes.
ED(150)	/ / + 1254	n_i , for $1 \leq i \leq I$, the density of electrons.
EDN(150)	/ / + 7171	A temporary storage array for new n_i as they are computed by subroutine ADJUST.
EDO(150)	/ / + 2203	n_i^{l-1} , for $1 \leq i \leq I$, the electron density at $t = t^{l-1}$.
EFD(150)	/ / + 1730	$E_{i+\frac{1}{2}}$, for $1 \leq i < I$, the electric field.
EFDO	/ / + 2657	$E_{i+\frac{1}{2}}^{l-1}$, for $1 \leq i < I$, the electric field at $t = t^{l-1}$.
EM	/COM7/ + 7	E_M . The restriction on the mesh imposed by the field is that $\rho < \log ((E_i + E_M)/(E_{i-1} + E_M)) $ (see Section 2.2.3.2).
EN(150)	/ / + 4711	ΔN_i , for $1 \leq i \leq I$, the excess concentration of donors.
ENB	/ / + 426	(Input, Card 4) ΔN in the base region.
ENC	/ / + 427	(Input, Card 4) ΔN in the collector region.
ENE	/ / + 425	(Input, Card 4) ΔN in the emitter region.
ERROR	/ / + 461	(Input, Card 10) ϵ_{\max} , used in the convergence criterion (see Section 2.2.1.5).
EXS(300)	/ / + 5365	Y_k , for $1 \leq k < 2I$, unknowns in the linearized equations. $Y_{2i+\frac{1}{2}} = E_{i+\frac{1}{2}} - E_{i+\frac{1}{2}}^*$, the correction to the field and $Y_{2i} = \begin{cases} n_i - n_i^* & \text{if } n_i^{l-1} < p_i^{l-1} \\ p_i - p_i^* & \text{if } p_i^{l-1} \leq n_i^{l-1} \end{cases},$ the correction to the minority-carrier density.

GG(150)	/ / + 4007	- $(4/\delta x_{i+\frac{1}{2}})/\delta x_{i+\frac{1}{2}}$, for $1 \leq i \leq I$, a factor that occurs in $K_{i+\frac{1}{2}}$ when the majority-carrier concentration is eliminated.
H(20)	/COM9/ + 24	Not used. Reserved for specifying $g(t)$.
HD(150)	/ / + 1502	p_i , for $1 \leq i \leq I$, the density of holes.
HDN	/ / + 7645	A temporary storage array for new p_i as they are computed by subroutine ADJUST.
HDO(150)	/ / + 2431	p_i^{l-1} , for $1 \leq i \leq I$, the density of holes at $t = t^{l-1}$.
HJK(150)	/ / + 6041	$HJK_{2i+1} = K_{i+\frac{1}{2}}$ and $HJK_{2i} = \begin{cases} H_{2i} & \text{when } n_i < p_i, \\ J_{2i} & \text{when } p_i \leq n_i. \end{cases}$
IBC	/ / + 520	The index of the interval in which the base-collector junction lies.
IBCM	/ / + 522	$IBCM = IBC - 1$.
IBCP	/ / + 521	$IBCP = IBC + 1$.
IBLOCK	/ / + 1	The number of the latest restart point written on TAPE16.
ICOP(10)	/ / + 525	The indices of intervals containing cross-over points.
IDATA(60)	/ / + 42	(Input, Card 3) An array of input data of integer type. See Section C.2.

K IDATA(K)

$\left. \begin{array}{l} 1 \ n_2 \\ 2 \ n_1 \\ 3 \ n_3 \end{array} \right\}$ used in time-step control.

$4 \ I_{\max}$
 $5 \ I_{\min}$

} used in remeshing.

6-60 Not used.

IEB	// + 515	The index of the interval in which the emitter-base junction lies.
IEBM	// + 517	IEB - 1.
IEBP	// + 516	IEB + 1.
IERROR	// + 0	IERROR = 0 is normal. When a subroutine returns to the Main Program with IERROR $\neq 0$, it indicates that an error has occurred and that execution of the current problem should be terminated.
IND	// + 3162	IND = 0 is normal. IND = - 1 indicates that negative densities have appeared or that the iterative procedure has failed to converge. In such cases, the time step is reduced.
INFLEC	// + 12	Not used. Reserved for specification of $g(k)$.
INOW		obs.
IOPT(12)	// + 26	(Input, Card 2)

J IOPT(J)

- 1 The number of blocks of restart data on TAPE16 to be saved.
- 2 Number of the block on TAPE16 from which the initial distribution is to be obtained.
- 3 Maximum number of iterations per time step.
- 4 Specified source of Δt when restarting.
- 5 Number of steps per restart dump.

6 Number of steps per long printout.

7 Number of parameters to be read into IDATA.

8 Number of parameters to be read into DATA.

9 Not used.

10 When IOPT(10) $\neq 0$, use TBEGIN AND DELTI from cards.

11, 12 Not used.

IPRINT	/ / + 3	Number of cycles since previous long print-out.
IPUNCH	/ / + 2	Number of cycles since previous restart dump.
ITCHG	/ / + 7	ITCHG = 0 indicates that the first time step of the current run has not yet been completed.
ITER	/ / + 4	The iteration counter.
I0	/ / + 477	I0 + 1 is the index of the interval containing the base contact.
I0M	/ / + 505	I0 - 1.
I0P	/ / + 506	I0 + 1.
I0P2	/ / + 507	I0 + 2.
KBGN		obs.
KICK	/ / + 10	A counter for the number of consecutive time steps with relative change less than ϵ_w . Used in controlling the time step (see Section 2.2.3.1).
MAXPT	/COM7/ + 10	I_{\max} , the maximum number of points in the mesh.
MI	/ / + 500	i, the number of intervals in the mesh.

MIM	// + 501	MI - 1.
MIMOLD	/COM8/ + 2	When remeshing, the previous value of MIM.
MIM2	// + 503	MI - 2.
MIM3	// + 504	MI - 3.
MINPT	/COM7/ + 11	L_{min} , the minimum number of points in the mesh.
MINUS		obs.
MIP	// + 502	MI + 1.
MX	// + 510	2*MI.
MXM	// + 511	MX - 1.
MXM2	// + 513	MX - 2.
MXM3	// + 514	MX - 3.
MXP	// + 512	MX + 1.
NCOP	// + 523	The number of crossover points.
NCCPP	// + 524	NCOP + 1.
NT	// + 11	A counter for the number of consecutive time steps requiring no more than n_2 (IDATA (1)) iterations (see Section 2.2.3.1).

OUT(150,10) // + 7171

An array for holding quantities listed in the long form of printout.

K OUT(I, K)

1 H_i printed under the label "DN/DT."

2 $D_n \delta(\delta n_i / \delta x_i) / \delta x_i$ under "D(N)."

3 $\mu_n \delta(n_i E_i) / \delta x_i$ under "MU(N)."

4 J_i under "DP/DT."

- 5 $D_p \delta(\delta p_i / \delta x_i) \delta x_i$ under "D(P)."
- 6 $-\mu_p \delta(p_i E_i) / \delta x_i$ under "MU(P)."
- 7 R_i under "R."
- 8 $(N^\ell - N^{\ell-1}) / (t^\ell - t^{\ell-1})$ under "DN/DT."
- 9 $(P^\ell - P^{\ell-1}) / (t^\ell - t^{\ell-1})$ under "DP/DT."

10 Not used.

PED		obs.
PEFD		obs.
PHD		obs.
PERADD	/ / + 474	(Input, Card 12) w_1 , an increment to the parameter w_0 that controls the time step (see Section 2.2.3.1).
PERCHG	/ / + 2160	(Input, Card 11) w_0 , the parameter that controls the time step (Section 2.2.3.1). The input value is automatically updated.
PERMAX	/ / + 472	(Input, Card 12) w_{\max} , the upper limit on w_0 (Section 2.2.3.1).
PEPMIN	/ / + 473	(Input, Card 12) w_{\min} , the lower limit on w_0 (Section 2.2.3.1).
PERSUB	/ / + 475	(Input, Card 12) w_2 , the quantity that multiplies (formerly: was subtracted from) w_0 in the event of failure to converge or appearance of negative densities (Section 2.2.3.1).
PROBNM(10)	/ / + 14	(Input, Card 1) The title of the problem.
PROBNO	/ / + 13	(Input, Card 1) The problem number.
Q	/ / + 553	$4\pi qC/k$, a much-used factor in Poisson's equation.
QD	/ / + 557	$Q*(DP - DN)$, a much-used constant.

QDN	/ / + 562	$Q \cdot DN$, a much-used constant.
QDP	/ / + 563	$Q \cdot DP$.
QEC	/ / + 564	$4\pi/\kappa$, a much-used constant.
QECN	/ / + 565	$-4\pi/\kappa$, a much-used constant.
QI2	/ / + 554	$2./Q = \kappa/(2\pi qC)$, a much-used constant.
QMU	/ / + 556	$Q \cdot (ZMUN + ZMUP)/2.$, a much-used constant.
QMUN	/ / + 560	$Q \cdot ZMUN$, a much-used constant.
QMUP	/ / + 561	$Q \cdot ZMUP$, a much-used constant.
R(150)	/ / + 5137	d_i , for $1 \leq i \leq I$, the denominator of the recombination term.
REB	/ / + 451	(Input, Card 8) R_1 , the resistance in the base circuit.
REC	/ / + 452	(Input, Card 8) R_2 , the resistance in the collector circuit.
RKICK	/ / + 476	(Input, Card 12) ϵ_w . When the fractional change in concentrations is less than ϵ_w for $K_3 = IDATA(3)$ consecutive steps, the run is terminated (see Section 2.2.3.1).
RO	/COM7/+ 2	(Input, Card 13) ρ , the remeshing parameter. The input estimate is automatically updated (see Section 2.2.3.2).
RODEL	/COM7/+ 3	(Input, Card 13) $-dI/d\rho$, the sensitivity of the remeshing parameter ρ . The input estimate is automatically updated (Section 2.2.3.2).
ROL		obs.
ROLI		obs.
ROMAX		obs.
ROMESH	/COM7/+ 0	(Input, Card 13) The criterion for remeshing.

The spatial mesh is revised unless $\rho_{\max}^{-1} < n_{i-1}/n_i < \rho_{\max}$, $\rho_{\max}^{-1} < p_{i-1}/p_i < \rho_{\max}$, and $\rho_{\max}^{-1} < (|E_{i-\frac{1}{2}}| + E_M)/(|E_{i+\frac{1}{2}}| + E_M)$, for $2 \leq i \leq I-1$, where $\rho_{\max} = \text{ROMESH}$.

ROX	/COM7/ + 1	(Input, Card 13) A parameter that is used in the restriction on the ratio of lengths of abutting intervals. Specifically, $\rho_x^{-1} \leq \delta x_{i-1}/\delta x_i \leq \rho_x$, for $2 \leq i \leq I-1$, where $\rho_x = \text{ROX}$.
ROXI		obs.
RTL	/COM7/ + 12	(Input, Card 8) The run is terminated when the elapsed CP time exceeds RTL sec.
SUME	/ / + 2166	$N = \sum n_i \delta x_i$, an estimate of $\int_{-a}^b ndx$. Appears at the end of the long form of printout labelled "INTEGRAL OF N" (Section 2.2.4).
SUMEDT	/ / + 2173	$(N^\ell - N^{\ell-1})/(t^\ell - t^{\ell-1})$, where $N = \sum n_i \delta x_i$. It is an estimate of $d/dt \int_{-a}^b ndx$ and appears at the end of the long form of printout labelled "INTEGRAL OF DN/DT" (Section 2.2.4).
SUMEO	/ / + 2177	$N^{\ell-1}$, the value of $N = \int_{-a}^b ndx$ at $t = t^{\ell-1}$.
SUMH	/ / + 2167	$P = \sum p_i \delta x_i$, an estimate of $\int_{-a}^b pdx$. It appears at the end of the long form of printout labelled "INTEGRAL OF P."
SUMHDT	/ / + 2174	$(P^\ell - P^{\ell-1})/(t^\ell - t^{\ell-1})$, where $P = \sum p_i \delta x_i$. It is an estimate of $d/dt \int_{-a}^b pdx$ and appears at the end of the long form of printout labelled "INTEGRAL OF DP/DT."
SUMHO	/ / + 2200	$P^{\ell-1}$, the value of $P = \int_{-a}^b pdx$ at $t = t^{\ell-1}$.
SUMMU	/ / + 555	$\mu_n + \mu_p$, a much-used constant.
SUMR	/ / + 2170	$R = \sum R_i \delta x_i$, an estimate of $\int_{-a}^b Rdx$. It appears in the long form of printout labelled "INTEGRAL OF R" (Section 2.2.4).

SUMRE	/ / + 2171	C_n , an estimate of $d/dt \int_{-a}^b n dx$ based on flow at contacts and recombination rates (Section 2.2.4).
SUMREO	/ / + 2201	$C_n^{\ell-1}$, the value of C_n at $t = t^{\ell-1}$ (Section 2.2.4).
SUMRET	/ / + 2175	$\omega C_n^{\ell} + (1 - \omega) C_n^{\ell-1}$, which appears in the long form of printout as "RIGHT(N)" (Section 2.2.4).
SUMRH	/ / + 2172	C_p , an estimate of $\int_{-a}^b p dx$, based on flow of holes at contacts and on recombination rates (Section 2.2.4).
SUMRHO	/ / + 2202	$C_p^{\ell-1}$, the value of C_p at $t = t^{\ell-1}$.
SUMRHT	/ / + 2202	$\omega C_p^{\ell} + (1 - \omega) C_p^{\ell-1}$, which appears in the long form of printout labelled "RIGHT(P)."
TAUNB	/ / + 435	(Input, Card 6) The lifetime τ_n in the base region.
TAUNC	/ / + 437	(Input, Card 6) The lifetime τ_n in the collector region.
TAUNE	/ / + 433	(Input, Card 6) The lifetime τ_n in the emitter region.
TAUPB	/ / + 436	(Input, Card 6) The lifetime τ_p in the base region.
TAUPC	/ / + 440	(Input, Card 6) The lifetime τ_p in the collector region.
TAUPE	/ / + 434	(Input, Card 6) The lifetime τ_p in the emitter region.
TBEGIN	/ / + 465	(Input, Card 11) t^0 , the starting time.
TEND	/ / + 466	(Input, Card 11) When $t^{\ell} > TEND$, the run is terminated.
TIM(20)	/COM9/+ 0	Not used. Reserved for specifying the pulse $g(t)$.

TIME	/ / + 2156	t^{ℓ} , the current time.
VBCC	/ / + 567	$V_C - V_B$, the difference in contact potentials between the base and the collector (see Section 2.2.1.2).
VBCT	/ / + 2163	V_{BC} , the internal rise of potential from base to collector (Section 2.2.1.2).
VEBC	/ / + 566	$V_B - V_E$, the difference in contact potentials between emitter and base (Section 2.2.1.2).
VEBO	/ / + 477	(Input, Card 8) V_{EBO} ; the supply voltage in the base circuit (Section 2.2.1.4).
VEBT	/ / + 2161	V_{EB} , the internal rise of potential from emitter to base (Section 2.2.1.2).
VECC	/ / + 570	$V_C - V_E$, the difference in contact potentials between the emitter and collector.
VECO	/ / + 450	(Input, Card 8) V_{ECO} ; the supply voltage in the collector circuit.
VECT	/ / + 2162	V_{EC} , the internal rise in potential from emitter to collector. $V_{EC} = V_{EB} + V_{BC}$.
VVB	/ / + 571	$VVB = VEBO - VEBC$.
VVC	/ / + 572	$VVC = VECO - VECC$.
WDT	/ / + 576	$\omega(t^{\ell} - t^{\ell-1})$ (see Section 2.2.1.3).
WDTI	/ / + 577	$WDTI = 1.0/WDT$ (Section 2.2.1.3).
WV1	/ / + 550	$1 - \omega$ (Section 2.2.1.3).
WV2	/ / + 551	$(1 - \omega)/\omega$ (Section 2.2.1.3).
X(150)	/ / + 600	x_i , for $1 \leq i \leq I$, the coordinates of the mesh points.
XB(300)	/ / + 5365	A provisional mesh constructed by the subroutine REMESH.
XBC	/ / + 456	(Input, Card 9) The coordinate of the base-

		collector junction relative to the base contact as origin.
XC	// + 457	(Input, Card 9) The coordinate of the collector contact relative to the base contact as origin.
XE	// + 454	(Input, Card 9) The coordinate of the emitter contact relative to the base contact as origin.
XEB	// + 455	(Input, Card 9) The coordinate of the emitter-base junction relative to the base contact as origin.
XH(150)	// + 1026	$x_{i+\frac{1}{2}}$, for $1 \leq i \leq I$. The midpoints of the spatial intervals.
XHN(300)	// + 1451	A temporary array for midpoints of intervals in a new mesh.
XN(300)	// + 10775	A temporary array for a new mesh.
ZE	// + 431	q , the magnitude of the electronic charge.
ZEC	// + 552	$ZE \cdot C$, a much-used constant.
ZJB	// + 2164	i_B/a_0 , the current density at the base contact.
ZJC	// + 2165	i_C/a_0 , the current density at the collector contact.
ZKAPPA	// + 432	(Input, Card 5) κ , the dielectric constant.
ZKT	// + 430	(Input, Card 5) θ , the temperature in electron volts.
ZMUN	// + 423	(Input, Card 4) μ_n , the mobility of electrons.
ZMUP	// + 424	(Input, Card 4) μ_p , the mobility of holes.
ZNSB	// + 443	(Input, Card 7) n' in the base region (see Section 2.2.2.1).
ZNSC	// + 445	(Input, Card 7) n' in the collector region (Section 2.2.2.1).

ZNSE	/ / + 441	(Input, Card 7) n' in the emitter region (Section 2.2.2.1).
ZN0	/ / + 442	(Input, Card 4) n_0 , the intrinsic concentration of free electrons.
ZN0B	/ / + 543	The equilibrium concentration of electrons in the base (see Section 2.2.1.6).
ZN0C	/ / + 544	The equilibrium concentration of electrons in the collector (Section 2.2.1.6).
ZN0E	/ / + 542	The equilibrium concentration of electrons in the emitter (Section 2.2.1.6).
ZN0SQ	/ / + 541	$n_0^2 = \text{ZN0}^{**2}$. A constant.
ZPSB	/ / + 444	(Input, Card 7) p' in the base region (see Section 2.2.2.1).
ZPSC	/ / + 446	(Input, Card 7) p' in the collector region (Section 2.2.2.1).
ZPSE	/ / + 442	(Input, Card 7) p' in the emitter region (Section 2.2.2.1).
ZP0B	/ / + 546	The equilibrium concentration of holes in the base (Section 2.2.1.6).
ZP0C	/ / + 547	The equilibrium concentration of holes in the collector (Section 2.2.1.6).
ZP0E	/ / + 545	The equilibrium concentration of holes in the emitter (Section 2.2.1.6).

C.6. LAYOUT OF COMMON VARIABLES

/ / + 0	ERROR	5	END	12	INFLEC	136	DATA
1	IBLOCK	6	MINUS	13	PROBNO	422	ZN0
2	IPUNCH	7	IPUNCH	14	PROBNM	423	ZMUN
3	IPRINT	10	KICK	26	IOPT	424	ZMUP
4	ITER	11	NT	42	IDATA	425	ENE

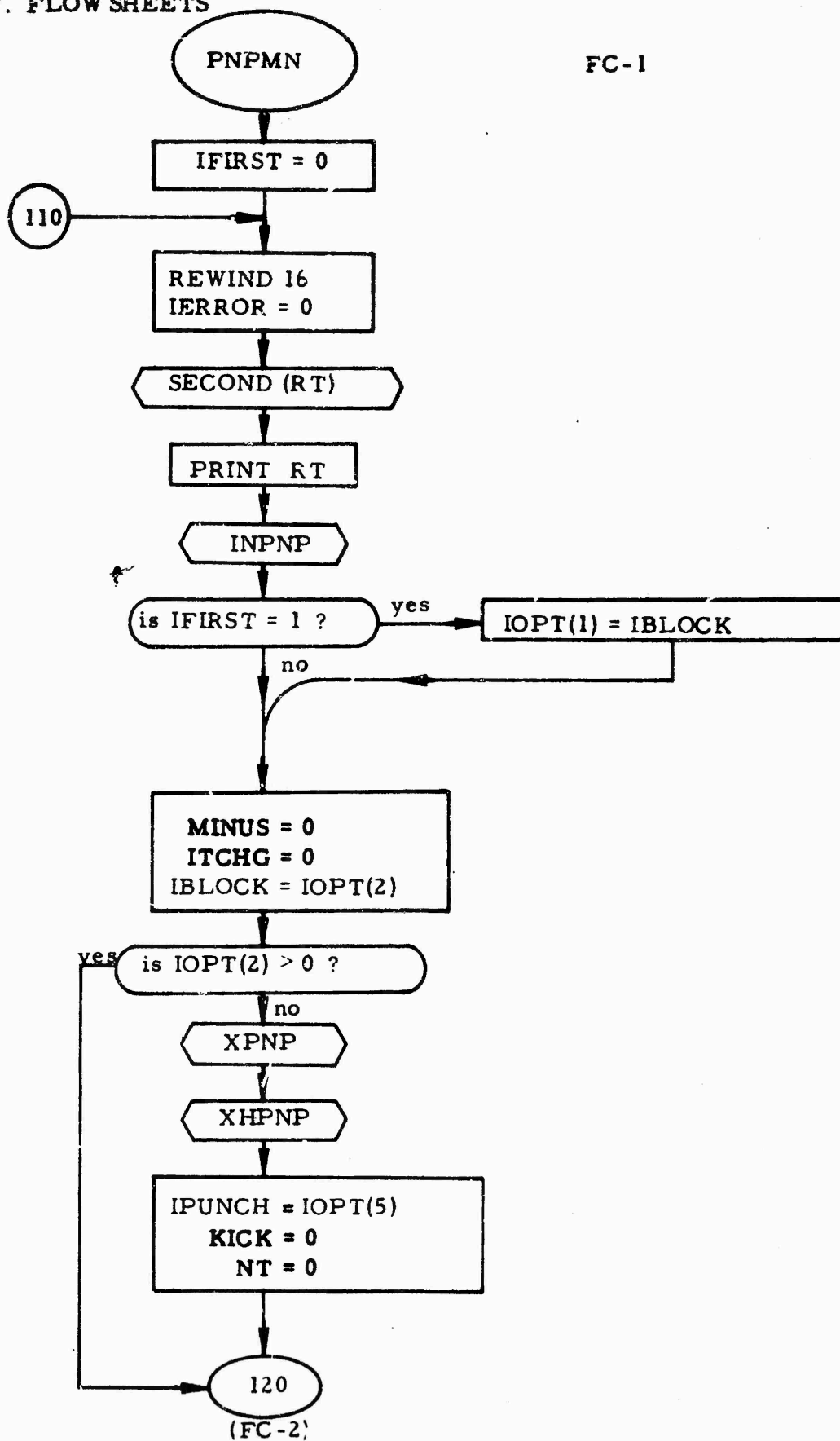
426 ENB	465 TBEGIN	524 NCOPP	574 AREC
427 ENC	466 TEND	525 ICOP	575 XBAR
430 ZKT	467 DELTI	537 DN	576 WDT
431 ZE	470 DELTN	540 DP	577 WDTI
432 ZKAPPA	471 DELTM	541 ZN0SQ	600 X
433 TAUNE	472 PERMAX	542 ZN0E	1026 XH
434 TAUPE	473 PERMIN	543 ZN0B	1254 ED
435 TAUNB	474 PERADD	544 ZN0C	1502 HD
436 TAUPB	475 PERSUB	545 ZP0E	1730 EFD
437 TAUNC	476 RKICK	546 ZP0B	2156 TIME
440 TAUPC	477 IO	547 ZP0C	2157 DELT
441 ZNSE	500 MI	550 WV1	2160 PERCHG
442 ZPSE	501 MIM	551 WV2	2161 VEBT
443 ZNSB	502 MIP	552 ZEC	2162 VECT
444 ZPSB	503 MIM2	553 Q	2163 VBCT
445 ZNSC	504 MIM3	554 QI2	2164 ZJB
446 ZPSC	505 IOM	555 SUMMU	2165 ZJC
447 VEBO	506 IOP	556 QMU	2166 SUME
450 VECO	507 IOP2	557 QD	2167 SUMH
451 REB	510 MX	560 QMUN	2170 SUMR
452 REC	511 MXM	561 QMUP	2171 SUMRE
453 A0	512 MXP	562 QDN	2172 SUMRH
454 XE	513 MXM2 / /	563 QDP	2173 SUMEDT
455 XEB	514 MXM3	564 QEC	2174 SUMHDT
456 XBC	515 IEB	565 QECN	2175 SUMRET
457 XC	516 IEBP	566 VEBC	2176 SUMRHT
460 DELX	517 IEBM	567 VBCC	2177 SUMEO
461 ERROR	520 IBC	570 VECC	2200 SUMHO
462 OMEGA	521 IBCP	571 VVB	2201 SUMREO
463 C	522 IBCM	572 VVC	2202 SUMRHO
464 DELR	523 NCOP	573 AREB	2203 EDO

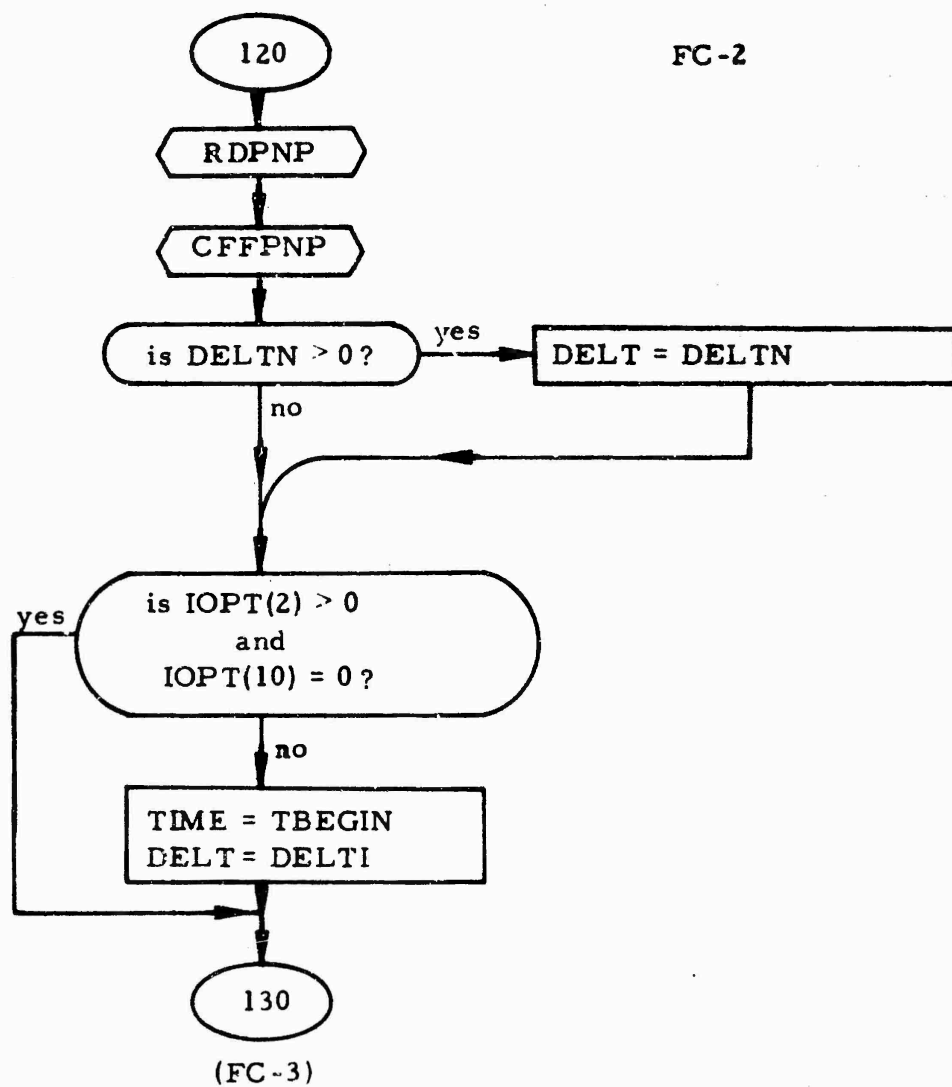
2431 HDO	12151 Last + 1
2657 EFDO	/COM7/ + 0 ROMESH
3105 AA	1 ROX
3105 DENS	2 RO
3333 BB	3 RODEL
3561 CC	4 ROMAX
4007 GG	5 oDELXR
4235 APA	6 DELTR
4463 BTA	7 EM
4711 EN	10 MAXPT
5137 R	11 MINPT
5365 EXS	12 RTL
5365 XB	/COM8/ + 0 INOW [†]
6041 HJK	1 KBGN [†]
6515 R	2 MIMOLD [†]
7171 AM2	/COM8/ + 3 ROXI [†]
7171 OUT	4 ALOGX [†]
7171 EDN	5 ROL [†]
7645 AM1	6 ROLI [†]
7645 OUT(1,3)	7 DELN [†]
7645 HDN	10 PED [†]
10321 AZR	11 PHD [†]
10321 OUT(1,5)	12 PEFD [†]
10775 AP1	13 XQ [†]
10775 OUT(1,7)	14 XP [†]
10775 XN	15 XR [†]
11451 AP2	/COM9/ + 0 TJM
11451 OUT(1,9)	24 H
11451 XHN	
12125 AEX	

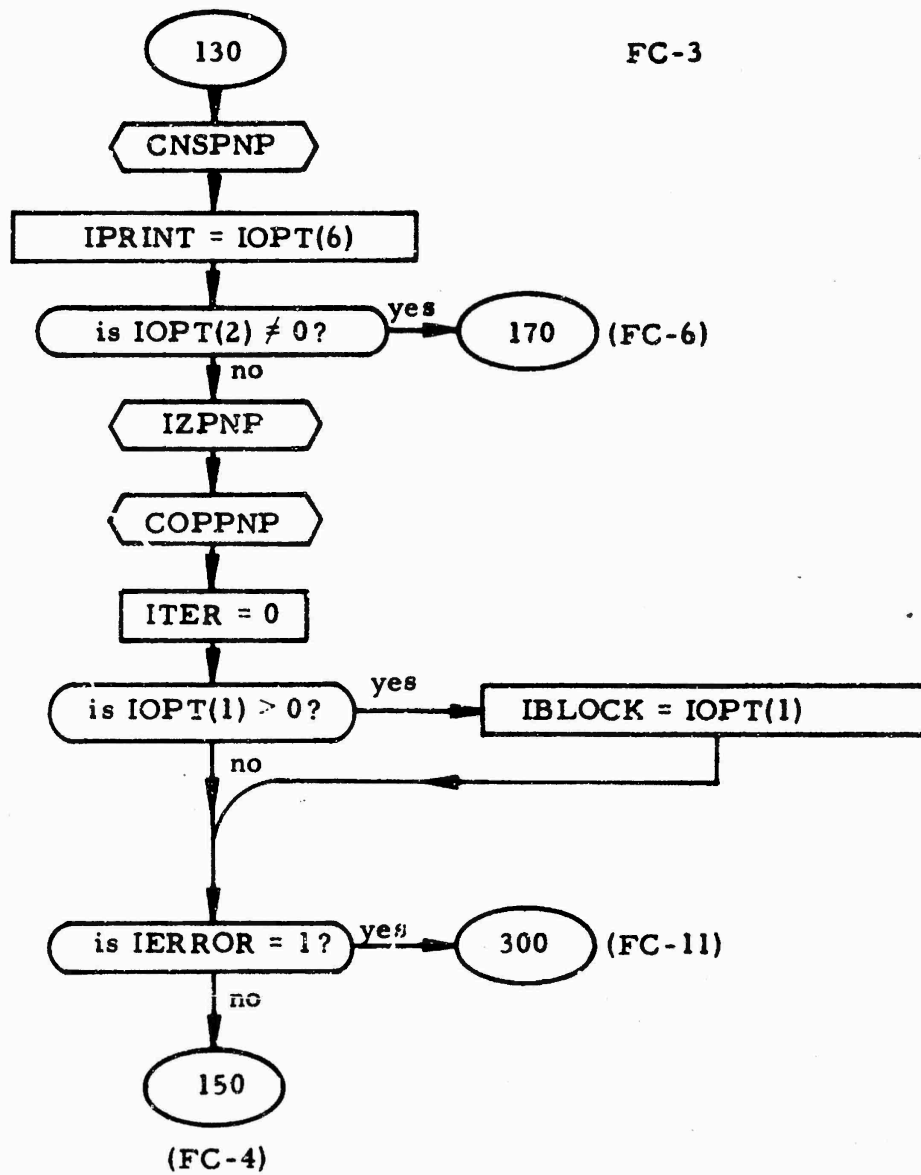
[†] Obsolete.

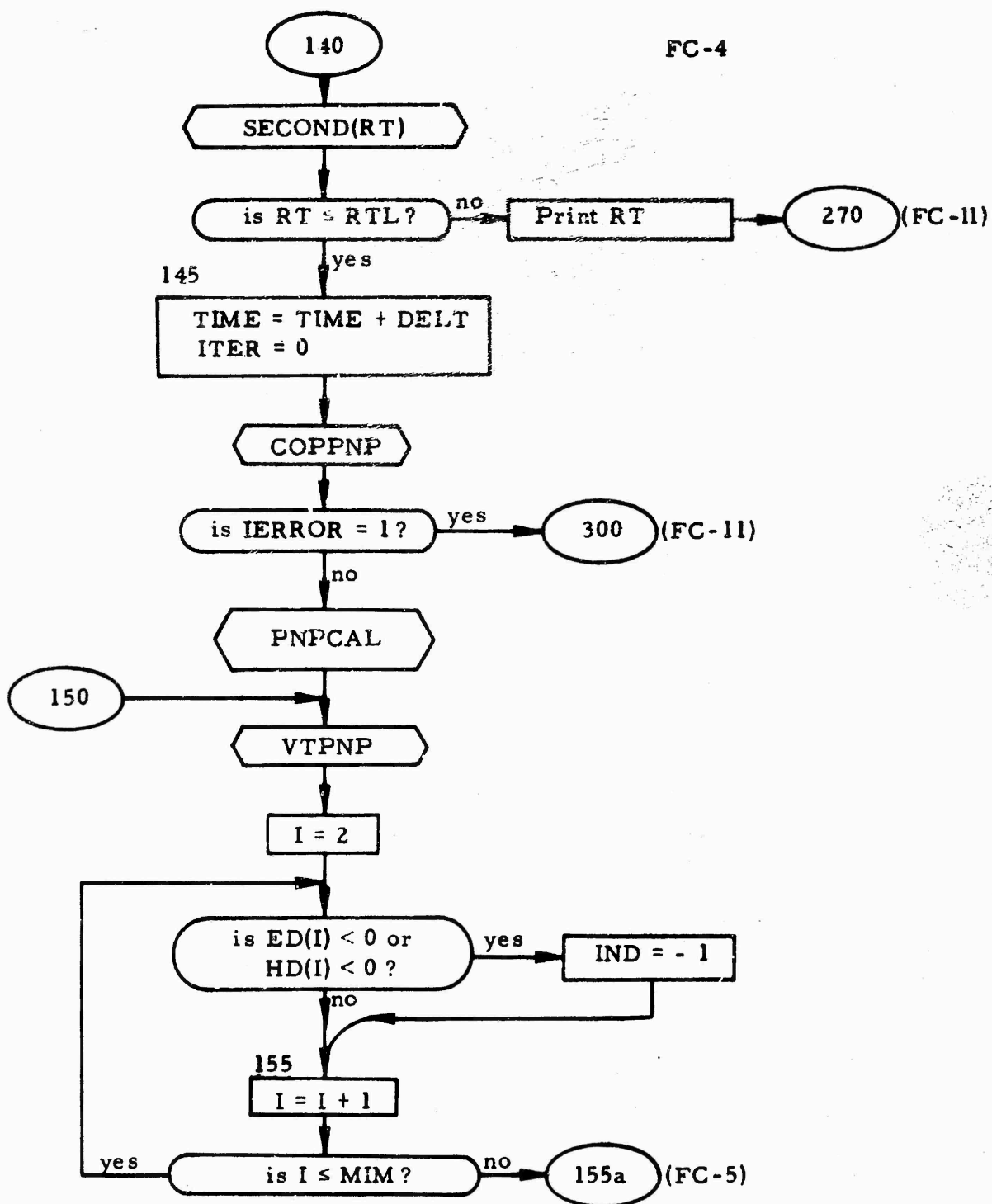
C.7. FLOW SHEETS

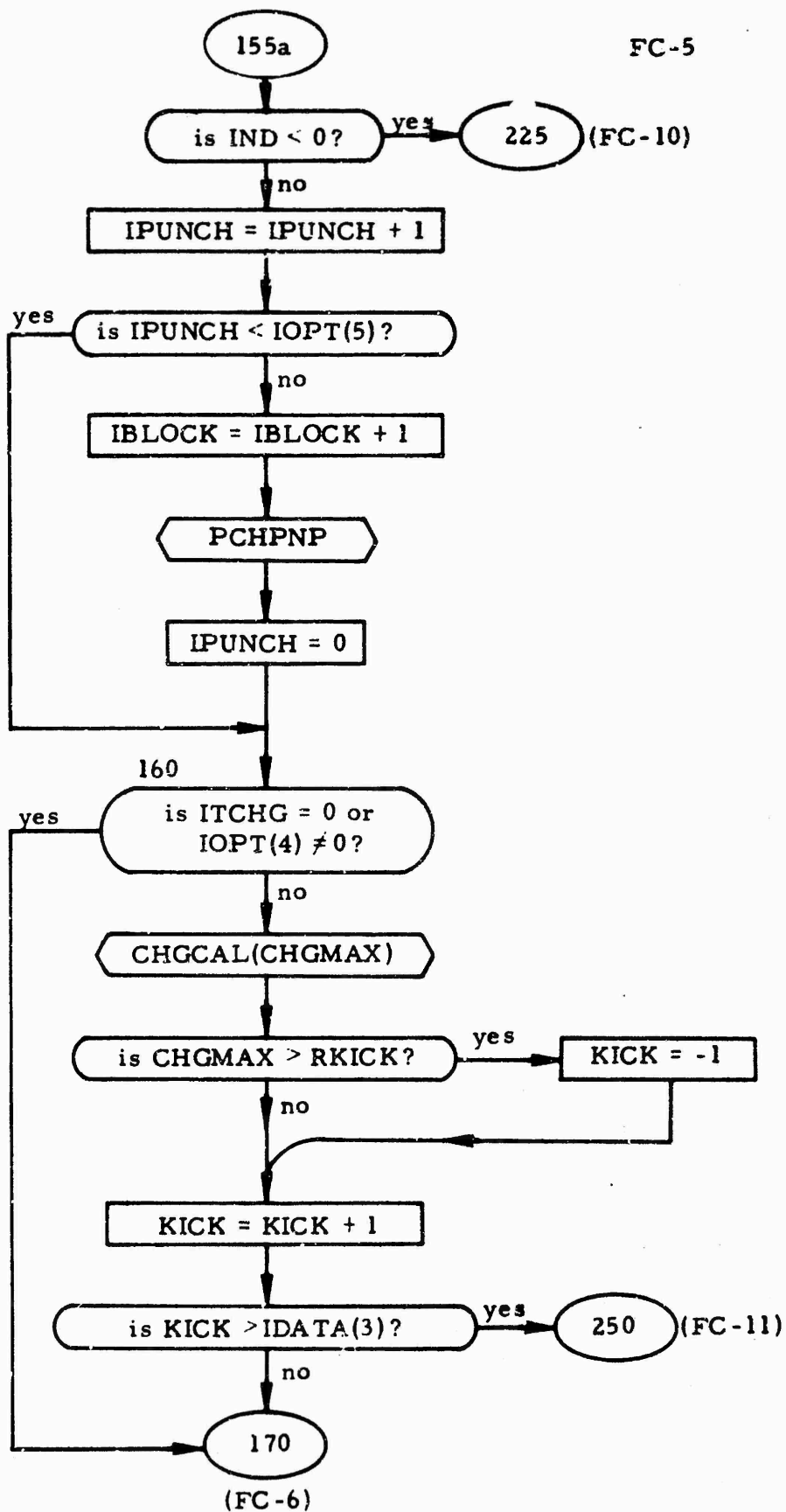
FC-1

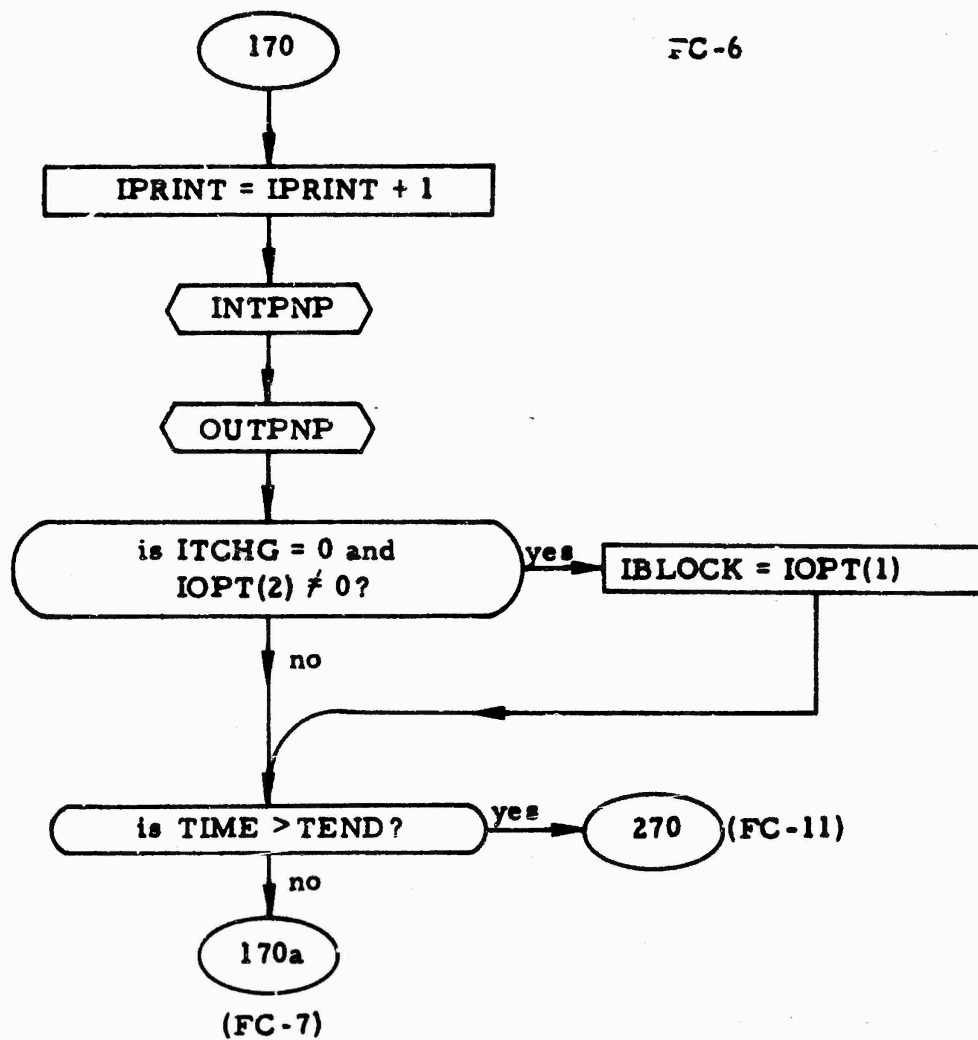


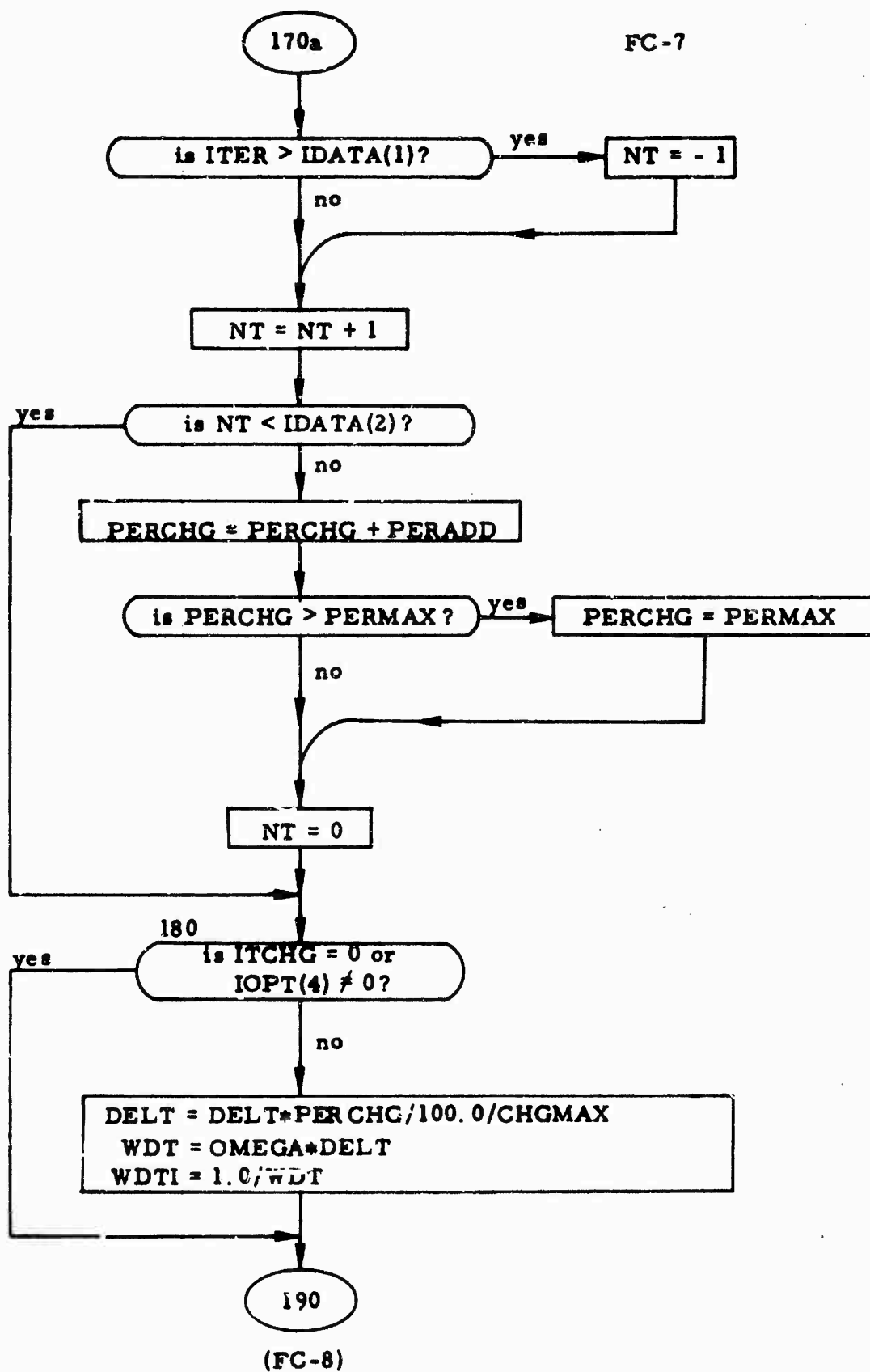




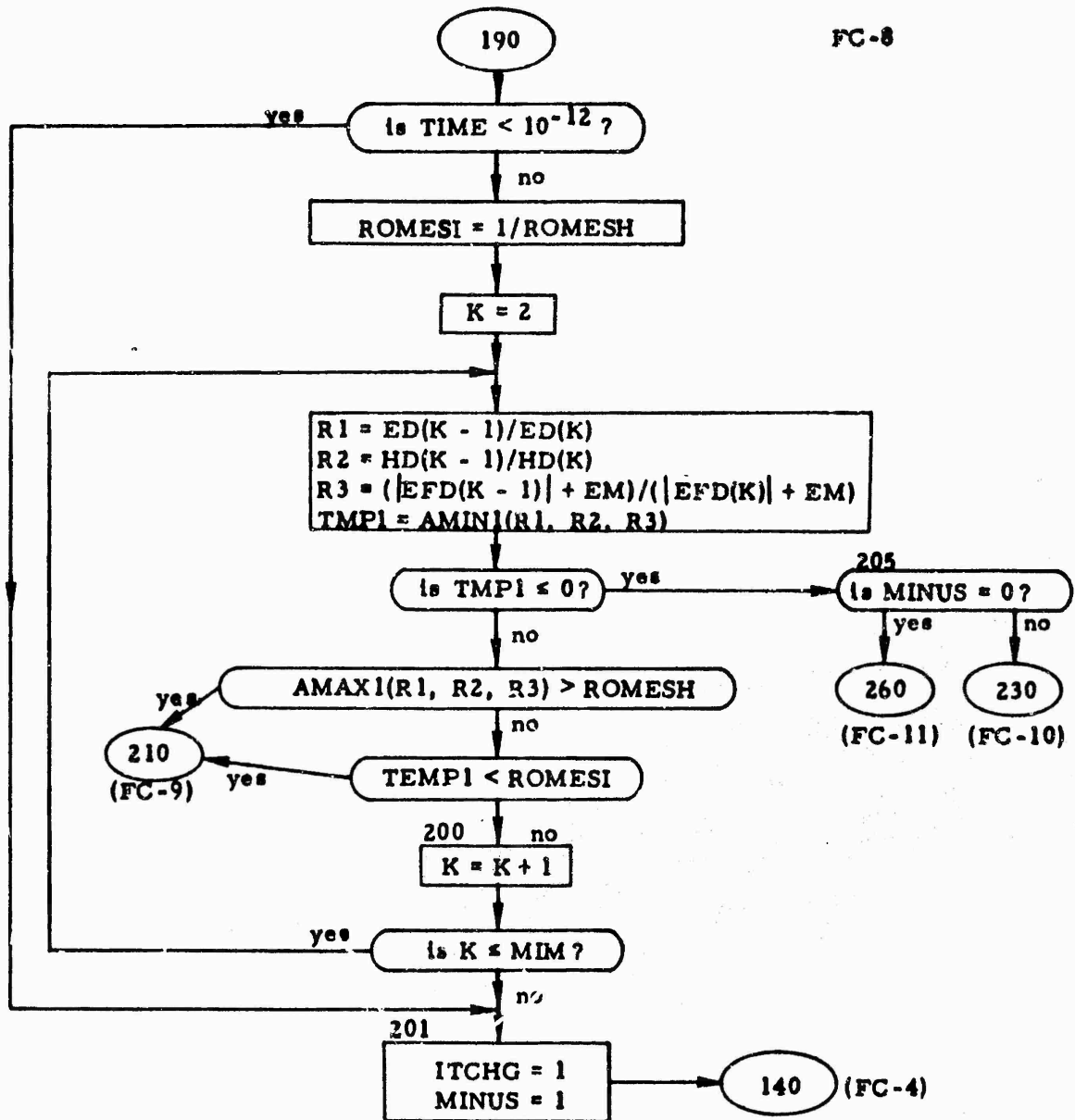




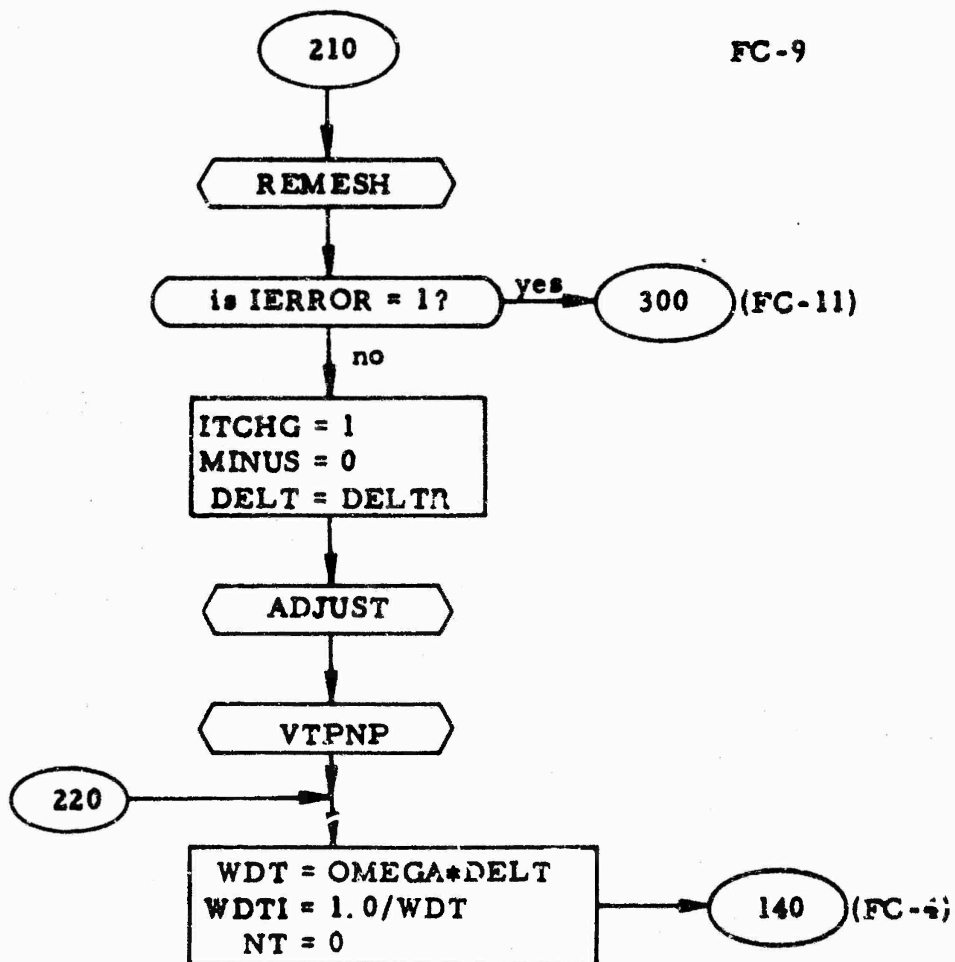


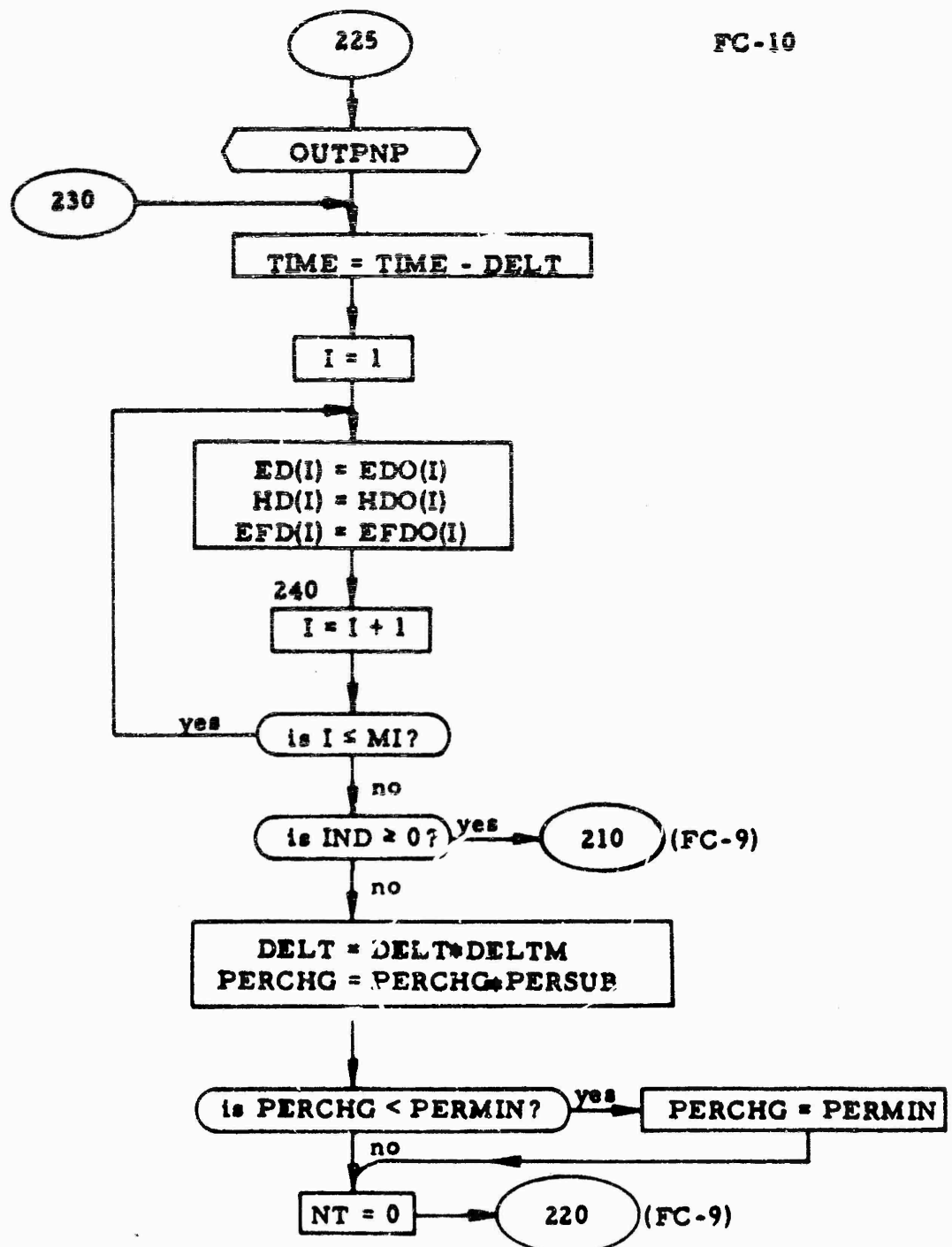


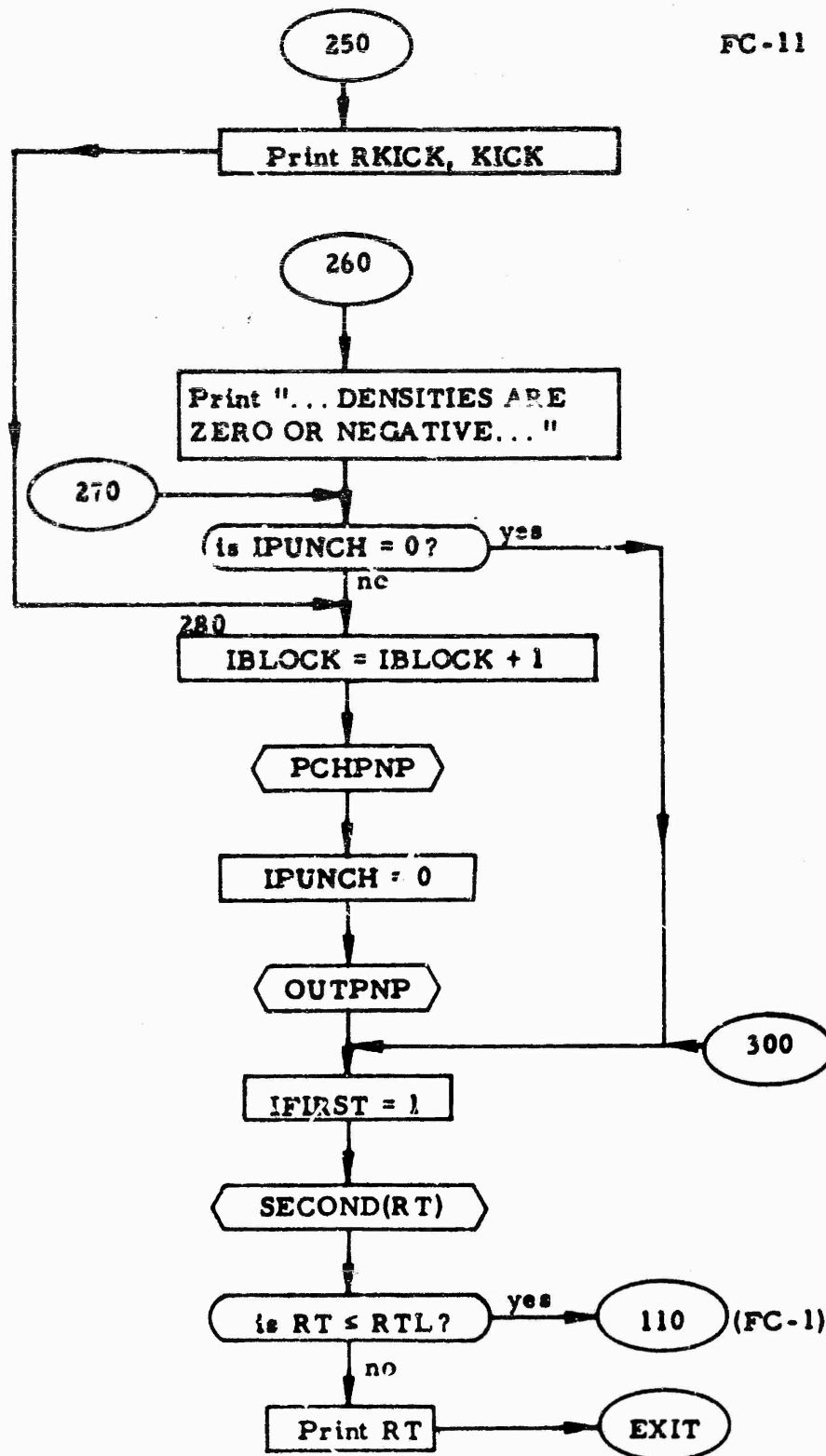
FC-8



FC-9







Appendix D

Computerized Model for Response of Devices to a Pulse of Ionizing Radiation*

D. K. NICHOLS, J. H. ALEXANDER, S. C. CHOY and V. A. J. VAN LINT
General Dynamics Corp., San Diego, California

Radiation Effects in Devices

Chairman: A. Chopra
Transistron, Wakefield, Mass.

WEDNESDAY, NOVEMBER 2, 1966, 10:00 A.M.
JEFFERSON ROOM ANNEX, SHERATON BOSTON

A COMPUTER CODE has been formulated and expressed to follow the flow of electrons and holes in a one-dimensional $P-N$ junction device. This work supplements the simple theory for the behavior of diodes which has to invoke the condition that the majority carrier is always much larger than the minority carrier in order to linearize the appropriate equations. By extending the calculations, it is possible to understand transient effects due to normal radiation environments. The equations which govern the flow of carriers in a semiconductor are the continuity equations:

$$\frac{\partial n}{\partial t} = g - R - \nabla \cdot j_e \quad (1)$$

for electrons and

$$\frac{\partial p}{\partial t} = g - R - \nabla \cdot j_h \quad (2)$$

for holes. Here n is the electron concentration, p is the hole concentration, j_e and j_h are the electron and hole particle currents, g is the rate of generation, and R is the rate of recombination which is assumed equal for each carrier (no trapping). The particle currents are given by the non-linear expressions:

$$j_e = -\mu_e n E - D_e \nabla n \quad (3)$$

$$j_h = \mu_h p E - D_h \nabla p \quad (4)$$

where μ is the appropriate mobility, D is the diffusion constant and E is the internal electric field. The first term is the drift current due to the field, and the second term is the diffusion current due to the gradient of the carriers. Equations (1) and (2), when coupled with Poisson's equation,

$$\nabla \cdot E = \frac{4\pi e}{K} (p - n + \Delta N),$$

completely describe the diode. A term, ΔN , is included for the excess of donors over acceptors for each region.

For customary analytical approximations, the first assumption that is made is that the two regions are separated by a depletion region where all of the voltage drop occurs. Then at thermal equilibrium, and for the open-circuit case, Eqs. (3) and (4) give the boundary condition for bridging each region as:

$$p_{on}/p_{op} = n_{op}/n_{on} = \exp(-eV/kT)$$

where the subscripts "o" refer to the equilibrium value of the concentration in the designated region using the fact that $j_e = j_h = 0$ and Einstein's relation between the mobility and diffusion constant. The built-in voltage V is then assumed to be modified by algebraic addition of an applied voltage, which must be smaller than V .

However, for non-equilibrium problems, there must exist a small field and carrier concentration gradient at the depletion-region boundaries. The magnitude of these quantities can be determined by assuming charge quasi-neutrality. This assumption states that the flow of current in the presence of non-uniform

carrier densities necessitates local variations of the electric field which are small enough to imply that the excess electron and hole concentrations are equal via Poisson's equation, but the electric field must now be calculated from Maxwell's requirement that $j_e + j_h = \text{constant}$. With this assumption it is possible to show that the excess carriers are given by the minority-carrier continuity equation in each region provided that the regions are fairly heavily doped and that the excess carriers (whether due to charge injection or irradiation) are small compared to the majority carrier.

Finally, in order to determine the total current it is necessary to assume that both the electron and hole currents taken separately are constant in passing through the depletion region and that generation and recombination is also negligible within this region. If such is the case, it can be shown that the magnitude of the total current is given by adding together the minority-carrier diffusion current of each carrier as evaluated at the depletion-region boundaries. The current at larger distances from the junction is due to both drift and diffusion currents but the value of E changes to assure that this value of the current is constant.

It is clear from the preceding comments that such an approximate model is not adaptable to a description of ionization radiation effects, since large excess-carrier concentrations are of great interest. What is perhaps less apparent is the critical nature of the form of the recombination term, R , in affecting the magnitude of the transient lifetime and reverse saturation current. A short comparison of the analytic outlook and numerical results for the thermal equilibrium calculation and the transient response under open-, forward-, and reverse-bias diode configurations is given for the following figures.

Figure 1 shows the computed electric field about the junction interface for the open-circuit steady-state diode. This is to be compared with a calculation using the simple theory that shows an asymmetric triangular field because of the assumption that

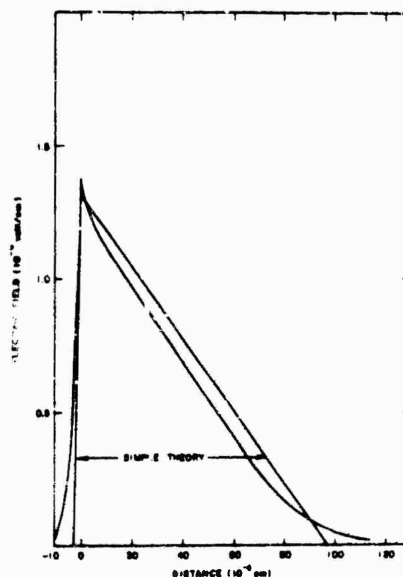


FIGURE 1 - Steady-state electric field

only the fixed concentration of donors or acceptors is present in the depletion region. Figure 2 shows the corresponding values for the carriers which are proportional to $\exp[\pm \int E dx]$. The steady-state approximate solutions are in excellent agreement with reality. Figure 3 shows the value of the built-in voltage in an open-circuit configuration after a pulse of radiation. The voltage approaches the equilibrium value of 0.63 V after 0.1 sec, and this long relaxation time is critically dependent on the form of R . The immediate rise at a time $t \sim 10^{-4}$ sec is consistent with the time expected for the assumed characteristic lifetimes. Figure 4 shows the forward-bias voltage with the small dip due to irradiation. This can be understood by recognizing that the irradiated diode acts as a voltage source which tends to push current through the external circuit in that direction corresponding to a reverse bias. The same conclusion can be derived from an argument based on carrier density gradients at the junction interface. At constant voltage, the carrier density at the junction is fixed. Under irradiation, the density in the bulk material is increased toward the value at the junction, so the gradient decreases.

Figure 5 shows the large instantaneous rise in the reverse

current after irradiation caused by those excess carriers within a diffusion length of the junction which are swept across the junction. The equilibrium value for the current is larger than that calculated on the assumption that only diffusion of minority carriers causes the reverse saturation current. The observed current is due primarily to generation of carriers in the depletion region when the correct Shockley-Read¹¹ recombination term is used. This result is in agreement with experiment.

With this computer code, it is also possible to construct a model of a transistor by use of suitable boundary conditions. In addition, the code is easily adapted to time-dependent values of the recombination lifetime from permanent radiation damage, field-dependent values of the mobility, or even avalanche processes.

*Work sponsored by Air Force Weapons Laboratory, Research and Technology Division, Air Force Systems Command, under Contract AF39 (601)-7048.

1. W. Shockley and W. T. Read, Jr., Phys. Rev. 87, 835 (1952).
Original Manuscript Received August 1, 1966.

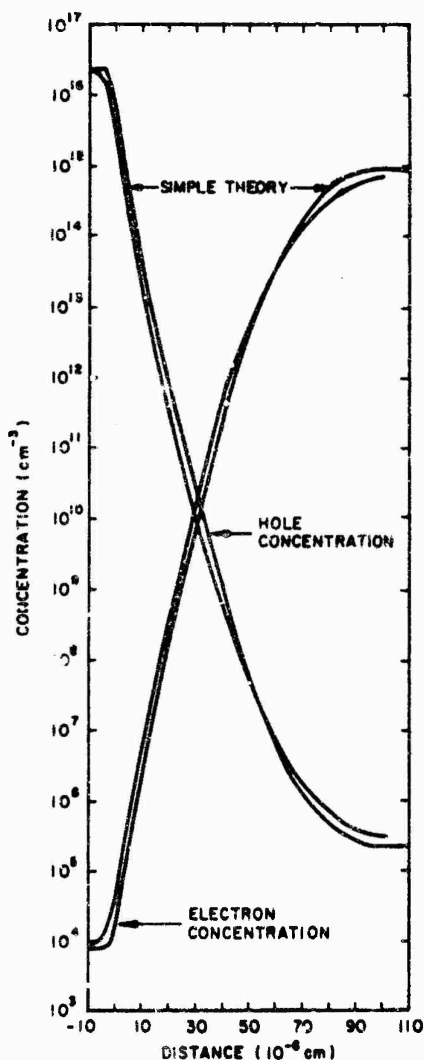


FIGURE 2—Steady-state carrier concentrations

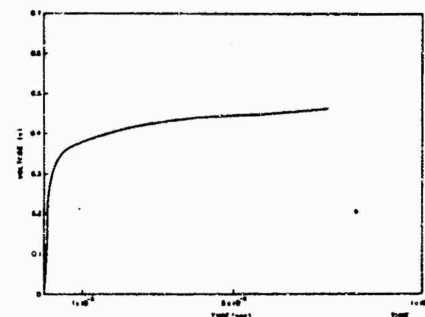


FIGURE 3—Voltage versus time of irradiated open-circuit diode

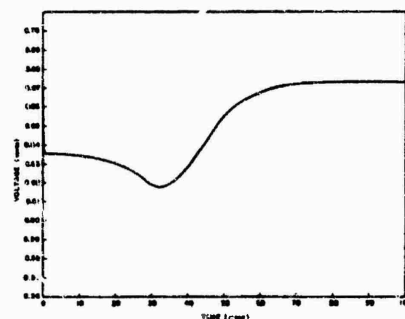


FIGURE 4—Forward-bias diode voltage (equilibrium voltage = 0.67 volts)

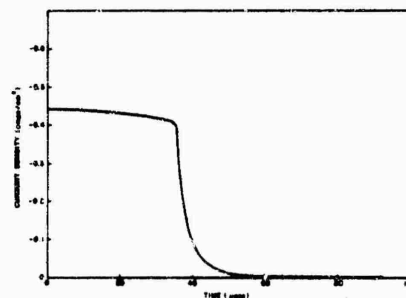


FIGURE 5—Reverse-bias current

UNCLASSIFIED

Security Classification

DOCUMENT CONTROL DATA - R&D		
(Security classification of title, body of abstract and indexing annotation must be entered when the overall report is classified)		
1. ORIGINATING ACTIVITY (Corporate author) General Atomic Division General Dynamics Corporation San Diego, California 92121		2a. REPORT SECURITY CLASSIFICATION UNCLASSIFIED
		2b. GROUP
3. REPORT TITLE SHORT-PULSED GAMMA-RADIATION EFFECTS ON DYNAMIC ELECTRONIC COMPONENTS		
4. DESCRIPTIVE NOTES (Type of report and inclusive dates) August 1965-February 1967		
5. AUTHOR(S) (Last name, first name, initials) van Lint, V. A. J.; Alexander, J. H.; Barkharc, D. J.; Nichols, D. K.; Ward, P. R.		
6. REPORT DATE May 1967	7a. TOTAL NO. OF PAGES 230	7b. NO. OF REFS 12
8a. CONTRACT OR GRANT NO. AF 29(601)-7048		8a. ORIGINATOR'S REPORT NUMBER(S) AFWL-TR-67-20
b. PROJECT NO. 5710		
c. Subtask No. 16.020	9b. OTHER REPORT NO(S) (Any other numbers that may be assigned to the report) General Atomic report number: GA-7651	
d.		
10. AVAILABILITY/LIMITATION NOTICES This document is subject to special export controls and each transmittal to foreign governments or foreign nationals may be made only with prior approval of AFWL (WLRE), Kirtland AFB, NM, 87117. Distribution is limited because of the technology discussed in the report.		
11. SUPPLEMENTARY NOTES		12. SPONSORING MILITARY ACTIVITY AFWL (WLRE) Kirtland AFB, NM 87117
13. ABSTRACT (Distribution Limitation Statement No. 2) A computer code has been developed for solving the nonlinear continuity equations and Poisson's equation which describe the response of electrons and holes in semiconductor devices to ionizing radiation. The ultimate goal of the research program was to incorporate the major second-order nonlinearities given by the output of the code (and observed by experiment) into simpler circuit models for active devices. The code is presently capable of obtaining solutions for two-region diodes and three-region transistors, which can be described by a one-dimensional geometry and discontinuous p-n junctions. Trivial changes in the program are described in detail for adapting the code to solutions for graded junctions and for the epitaxial four-region transistor ($N^+P^+NN^+$ or $PNPP^+$). Special features for representing avalanche effects, field-dependent mobility, and a recombination lifetime dependent on displacement radiation damage are included. Experiments were performed to provide data for comparison with the computer description of real diodes and transistors. The computer data are also compared with the Ebers-Moll transistor model, which is typical of simpler device representations.		

DD FORM 1473
1 JAN 64

UNCLASSIFIED

Security Classification

UNCLASSIFIED
Security Classification

14. KEY WORDS	LINK A		LINK B		LINK C	
	ROLE	WT	ROLE	WT	ROLE	WT
Transient radiation response Diode-radiation effects Transistor-radiation effects						

INSTRUCTIONS

1. ORIGINATING ACTIVITY: Enter the name and address of the contractor, subcontractor, grantee, Department of Defense activity or other organization (corporate author) issuing the report.

2a. REPORT SECURITY CLASSIFICATION: Enter the overall security classification of the report. Indicate whether "Restricted Data" is included. Marking is to be in accordance with appropriate security regulations.

2b. GROUP: Automatic downgrading is specified in DoD Directive 5200.10 and Armed Forces Industrial Manual. Enter the group number. Also, when applicable, show that optional markings have been used for Group 3 and Group 4 as authorized.

3. REPORT TITLE: Enter the complete report title in all capital letters. Titles in all cases should be unclassified. If a meaningful title cannot be selected without classification, show title classification in all capitals in parentheses immediately following the title.

4. DESCRIPTIVE NOTES: If appropriate, enter the type of report, e.g., interim, progress, summary, annual, or final. Give the inclusive dates when a specific reporting period is covered.

5. AUTHOR(S): Enter the name(s) of author(s) as shown on or in the report. Enter last name, first name, middle initial. If military, show rank and branch of service. The name of the principal author is an absolute minimum requirement.

6. REPORT DATE: Enter the date of the report as day, month, year, or month, year. If more than one date appears on the report, use date of publication.

7a. TOTAL NUMBER OF PAGES: The total page count should follow normal pagination procedures, i.e., enter the number of pages containing information.

7b. NUMBER OF REFERENCES: Enter the total number of references cited in the report.

8a. CONTRACT OR GRANT NUMBER: If appropriate, enter the applicable number of the contract or grant under which the report was written.

8b, 8c, & 8d. PROJECT NUMBER: Enter the appropriate military department identification, such as project number, subproject number, system numbers, task number, etc.

9a. ORIGINATOR'S REPORT NUMBER(S): Enter the official report number by which the document will be identified and controlled by the originating activity. This number must be unique to this report.

9b. OTHER REPORT NUMBER(S): If the report has been assigned any other report numbers (either by the originator or by the sponsor), also enter this number(s).

10. AVAILABILITY/LIMITATION NOTICES: Enter any limitations on further dissemination of the report, other than those

imposed by security classification, using standard statements such as:

- (1) "Qualified requesters may obtain copies of this report from DDC."
- (2) "Foreign announcement and dissemination of this report by DDC is not authorized."
- (3) "U. S. Government agencies may obtain copies of this report directly from DDC. Other qualified DDC users shall request through _____."
- (4) "U. S. military agencies may obtain copies of this report directly from DDC. Other qualified users shall request through _____."
- (5) "All distribution of this report is controlled. Qualified DDC users shall request through _____."

If the report has been furnished to the Office of Technical Services, Department of Commerce, for sale to the public, indicate this fact and enter the price, if known.

11. SUPPLEMENTARY NOTES: Use for additional explanatory notes.

12. SPONSORING MILITARY ACTIVITY: Enter the name of the departmental project office or laboratory sponsoring (paying for) the research and development. Include address.

13. ABSTRACT: Enter an abstract giving a brief and factual summary of the document indicative of the report, even though it may also appear elsewhere in the body of the technical report. If additional space is required, a continuation sheet shall be attached.

It is highly desirable that the abstract of classified reports be unclassified. Each paragraph of the abstract shall end with an indication of the military security classification of the information in the paragraph, represented as (TS), (S), (C), or (U).

There is no limitation on the length of the abstract. However, the suggested length is from 150 to 225 words.

14. KEY WORDS: Key words are technically meaningful terms or short phrases that characterize a report and may be used as index entries for cataloging the report. Key words must be selected so that no security classification is required. Identifiers, such as equipment model designation, trade name, military project code name, geographic location, may be used as key words but will be followed by an indication of technical context. The assignment of links, rules, and weights is optional.